The heteromeric 5-$HT_{3A/B}$ receptor: The effect of 5-HT_{3B} subunits on receptor structure and ligand recognition

Paul Herbert
Doctor of Philosophy

ASTON UNIVERSITY
January 2008

Thesis Summary

The 5-HT_3 receptors are members of the cys-loop family of ligand-gated ion channels. Two functional subtypes are known, the homomeric $5HT_{3A}$ and the heteromeric $5HT_{3A/B}$ receptors, which exhibit distinct biophysical characteristics but are difficult to differentiate pharmacologically.

Atomic force microscopy has been used to determine the stoichiometry and architecture of the heteromeric $5HT_{3A/B}$ receptor. Each subunit was engineered to express a unique C-terminal epitope tag, together with six sequential histidine residues to facilitate nickel affinity purification. The 5-HT_3 receptors, ectopically expressed in HEK293 cells, were solubilised, purified and decorated with antibodies to the subunit specific epitope tags. Imaging of individual receptors by atomic force microscopy revealed a pentameric arrangement of subunits in the order BBABA, reading anti-clockwise when viewed from the extracellular face.

Homology models for the heteromeric receptor were then constructed using both the electron microscopic structure of the nicotinic acetylcholine receptor, from *Torpedo marmorata,* and the X-ray crystallographic structure of the soluble acetylcholine binding protein, from *Lymnaea stagnalis,* as templates. These homology models were used, together with equivalent models constructed for the homomeric receptor, to interpret mutagenesis experiments designed to explore the minimal recognition differences of both the natural agonist, 5-HT, and the competitive antagonist, granisetron, for the two human receptor subtypes.

The results of this work revealed that the 5-HT_{3B} subunit residues within the ligand binding site, for both the agonist and antagonist, are accommodating to conservative mutations. They are consistent with the view that the 5-HT_{3A} subunit provides the principal and the 5-HT_{3B} subunit the complementary recognition interactions at the binding interface.

Key words/phrases: Atomic force microscopy, homology modeling, mutagenesis,

Acknowledgements

Collaborations

Three important collaborations contributed to the work of this thesis. Atomic force microscopy was performed by the research group of Mike Edwardson at Cambridge University. Images of the antibody-decorated 5-HT_3 receptors, presented in **Chapter 2** of this thesis, are the results from the work of this group.

The design, analysis and interpretation of the molecular modeling studies in **Chapter 3** were entirely my own work; however, the process of molecular modelling was performed by Dr John Simms.

The majority of two-electrode voltage clamp experiments were performed in the laboratory of Susan Dunn (University of Alberta, Canada), by Isabelle Paulsen and Delilah Roczkowski. This work was also performed by myself for certain 5-HT_{3B} subunit mutants expressed as 5-$HT_{3A/B(mut)}$ receptors in xenopus oocytes, detailed in **Chapter 5**.

Heartfelt thanks

From the start of my foray into pharmacology research, Professor Ian Martin has always been there to offer many pearls of wisdom from his vast experience and contacts in the field; he knows everybody. I am grateful for the opportunity afforded me to carry out this research and allow me to experience the wonders of academic endeavour. In spite of the constant frustration I must have caused my long suffering supervisor, he has stuck by me throughout, when others would surely have given me short shrift. Sliding down that rusty razorblade of life has been made a life-enriching experience, however painful at times.

From my initial start in the dust ridden MB442 laboratory, overlooking the scenic Aston Expressway, Dr Alex Conner took me under his wing, showed me the ropes, and let me know how easy it all was. His sharp mind and wit were something to behold, showing me that being erudite did not equate to boring. He is a one-off. The adjoining coffee room was a great source of lively banter; acting as a hub for the bringing together of biology research groups splintered across different levels of the main building. Among these groups were Sarah Aldridge and Melissa Grant, probably the most outdoor-type people I know, responsible for many team building excursions; be it camping, climbing, Halloween/fireworks parties or even running, which has now become a four times a week habit. They both remain a breath of fresh air.

Situated next door to the coffee room, I was conveniently able to consult with the ultimate knowledge of all matters pertaining to Aston University, Alan Richardson. A remarkable man, able to lay his hands on any piece of equipment, fixes virtually any piece of mistreated kit, and does not rest until the job is done. He is Aston University's dynamo; I hope the 'just do it' attitude has rubbed off on me. Alan's office space was later filled by the highlander, and chief technician, Derick Stirling. In moments of despair, Derick could always offer good cheer with his irony, talk of cycling and Star Trek, and, like a true Scot, general whinges about life. I hope we will engage in l'etape du Tour some time soon. Make it so, number one.

Somebody who I will always remember as providing a ray of light, whatever the conditions in the lab, was Karen Whitfield. Always smiling, always jovial, in spite of having a tragically sad job at the children's hospital, what a girl. I hope one day we can restart our cinema club.

A late arrival in the lab injected some much needed enthusiasm for world of molecular pharmacology: my mentor in molecular modelling, Dr John Simms. His passion for science, encyclopaedic knowledge of all things molecular, and unnerving interest and excitement in my own work, was an inspiration that made me persevere, like a squeaky wheel. Lab work etches many painful memories involving failed experiments, but, with the help of Big John's massive presence in the lab, these memories are overwritten by the atonal singing, 'fresh' moments, basketball skills, and i-sketch, to name but a few fondly remembered ways of passing the time and staying sane. It was a pleasure to have such a character as a colleague in the legendary lab 442. The buffet (all you can eat?) at Aston's 6th floor was never the same after John left. Thankfully my cholesterol shortly returned to normal levels, and John does not exert such an intense gravitational pull. .

My time in Canada was an amazing experience, not least attributable to the superb atmosphere within the laboratory of Susan Dunn. That was one efficient set up. Thanks to Isabelle for showing me the art of two-electrode voltage clamping, Delilah for introducing me to everything cultural that Edmonton has to offer, and Chris Carter for opening my eyes to Billy Talent and the perils of drinking whilst playing softball. My trip would not have been nearly as entertaining had it not been for the Edmonton Oilers and their gutsy performance in the Stanley Cup Finals. I can still hear the car horns and shouts of 'Lets Go Oilers' from Whyte Avenue.

In order to tear myself away from the lab at a reasonable hour, I was compelled to join a number of clubs that required my evening attendance. These groups of people require thanking for the provision of light-hearted entertainment, devoid of science. Of a dramatic ilk: the Stanley Players, Crossed-Keys, Drama13, BMOS and most importantly, Queensbridge

Musical Theatre Society. Of a sporting ilk: Aston's gym and sports hall; providing a great method of venting anger after a failed transfection, Birmingham rowing club, Astons Karate club, Coventry VISTA (Visually Impaired and Sighted Tandem Association); you guys put everything into perspective.

My family deserve a special prize for providing me with luxury hotel facilities at knock-down prices, and for putting up with years of abuse while waiting for me to get a 'proper job'. I promise to visit them more frequently from now on. If my parents are half as proud as me for finishing this thesis, then I am twice as proud of them for their achievements which have allowed me to get this far. My brother has been my best buddy throughout, who always managed to show me the lighter side of life, and let me play on his Playstation™ 3. I apologise to my Nan, Grandad, and Aunt, who never got to see me graduate. I dedicate this thesis to you. Sorry it took too long.

As for Dr Jennifer Griffiths, she is a marvel and a masterpiece of creation. I consider her a genius in her own right, and the reason I was finally able to say, it is done.

Table of Contents

List of Figures

List of Tables

List of Equations

List of Abbreviations

5-HT:	5-hydroxytryptamine
$5\text{-HT}_3\text{R}$:	5- hydroxytryptamine type 3 receptor
Ac:	*Aplysia californica*
ACh:	Acetylcholine
AChBP:	Acetylcholine binding protein
AFM:	Atomic force microscopy
AP:	Affinity Purified (receptor samples)
APC:	Affinity Purified and concentrated (receptor samples)
BES:	N,N-Bis(2-hydroxyethyl)-2-aminoethanesulfonic acid
B_{max}:	Binding Maximum
Bt:	*Bulinus truncates*
CAPS:	3-(cyclohexylamino)-1-propanesulfonic acid
cDNA:	Complimentary DNA
CDR:	Complimentarity determining region
CINV:	Chemotherapy induced nausea and vomiting
CNS:	Central nervous system
CSF:	Cerebro-spinal fluid
CTZ:	Chemoreceptor trigger zone
Cys-loop:	Cystein loop
DEPC:	Diethylpyrocarbonate
DMEM:	Dulbecco's modified Eagles medium
DNA:	Deoxyribonucleic acid
DPM:	Disintegrations per minute
EC:	Enterochromaffin (cells)
EC_{50}:	Effective concentration (50%)
ECL:	Enhanced chemiluminescence
EDTA:	Ethylenediaminetetraacetic acid
ER:	Endoplasmic reticulum
FA:	Fluctuation analysis
FR:	Framework region
GABA:	Gamma-amino butyric acid

$GABA_AR$:	Gamma-amino butyric acid type A receptor
glyR:	Glycine receptor
$h5\text{-}HT_3R$:	Human 5-hydroxytryptamine type 3 receptor
HA:	Amphipathic helix
HEK293:	Human embryonic kidney 293 cell line
HEPES:	4-(2-Hydroxyethyl)piperazine-1-ethanesulfonic acid
IBS:	Irritable bowel syndrome
IC50:	Inhibiting concentration (50%)
ICD:	Intracellular domain
K_d:	Equilibrium dissociation constant (determined directly)
K_i:	Equilibrium dissociation constant (determined by inhibition studies)
LBD:	Ligand binding domain
LGIC:	Ligand-gated ion channel
Ls:	*Lymnaea stagnalis*
$m5\text{-}HT_3R$:	Mouse 5- hydroxytryptamine type 3 receptor
mCPBG:	m-chlorophenylbiguanide
mRNA:	Messenger ribonucleic acid
nAChR:	Nicotinic acetylcholine receptor
NaCl:	Sodium chloride
NEB:	New England Biolabs
NG:	Nodose galnglion
NTS:	Nucleus tractus solitarius
OHP:	Overhead projection
PAGE:	Polyacrylamide gel electrophoresis
PCR:	Polymerase chain reaction
PBG:	Phenylbiguanide
PBS:	Phosphate buffered saline
PDB:	Protein database
PNS:	Peripheral nervous system
PONV:	Post-operative nausea and vomiting
PVDF:	Polyvinylidene Fluoride
RINV:	Radiotherapy induced nausea and vomiting
RLB:	Radioligand binding
RPM:	Revolutions per minute

RT-PCR:	Reverse transcription polymerase chain reaction
SC:	Single channel conductance
SCG:	Superior cervical ganglion
SE:	Standard error
SEM:	Standard error of means
SDS-PAGE:	Sodium dodecyl sulphate-polyacrylamide gel electrophoresis
TEMED:	N,N,N',N'-tetramethylethylenediamine
Tm:	*Torpedo marmorata*
T_m:	Melting temperature
TM1-4:	Transmembrane domains 1-4
TMD:	Transmembrane domain
VC:	Vomiting centre
WT:	Wild type

Chapter 1: General Introduction

1.1 5-HT Receptors

5-Hydroxytryptamine (5-HT) was first isolated and characterised from bovine serum nearly 60 years ago by Rapport, Green and Page (Rapport *et al.*, 1948). Serum had consistently demonstrated an ability to cause vasoconstriction and an increase in smooth muscle tone, hence the name 'serotonin' was coined. However, the pharmacology of this substance was to prove complex, especially concerning its diverse effects on the central nervous system (CNS): sleep (Adrien *et al.*, 1992; Portas *et al.*, 1998), appetite (Blundell, 1984), temperature regulation (Tricklebank *et al.*, 1985), blood pressure regulation (Merahi *et al.*, 1992), sexual behaviour (McIntosh & Barfield, 1984), aggression (Soubrie, 1986), pain (Roberts, 1984; Sawynok & Reid, 1991), neuroendocrine function (Fuller & Clemens, 1981) and several psychiatric conditions (Jones & Blackburn, 2002). These diverse effects pointed towards an elaborate array of receptor families that bind 5-HT.

The advent of molecular cloning techniques, together with the functional characterisation of receptors, has expedited the classification of receptors for which 5-HT is the natural agonist (Hoyer & Martin, 1997; Barnes & Sharp, 1999; Hoyer *et al.*, 2002). The most recent classification identifies seven classes of 5-HT receptor designated $5HT_1$-$5HT_7$, all of which are G-protein coupled receptors, with the exception of $5\text{-}HT_3$, which is a member of the ligand-gated ion channel family (LGIC) (Alexander *et al.*, 2006). The work presented in this thesis is to focus solely on the human $5\text{-}HT_3$ receptor, being expressed heterologously as homomeric $h5\text{-}HT_{3A}$ receptors ($5\text{-}HT_{3A}Rs$), or heteromeric $h5\text{-}HT_{3A/B}$ receptors ($5\text{-}HT_{3A/B}Rs$).

1.2 $5\text{-}HT_3$ Receptor Subunits

1.2.1 The 5-HT3A subunit

The mRNA coding for the mouse $5\text{-}HT_{3A}R$ ($m5\text{-}HT_{3A}R$) was first isolated by expression cloning with NCB-20 cells (a hybridoma cell line from mouse neuroblastoma cells and Chinese hamster embryonic brain cells) by Maricq *et al.* (1991). The open reading frame indicated that the mature peptide consisted of 487 amino acids. Subsequent studies have identified species orthologues from human (Belelli *et al.*, 1995; Miyake *et al.*, 1995; Bruss *et al.*, 1998), rat (Isenberg *et al.*, 1993; Miquel *et al.*, 1995), guinea-pig (Lankiewicz *et al.*, 1998) and dog (Jensen *et al.*, 2006). Comparison of the amino acid sequences between these

different species reveals a high level of sequence identity: human 5-HT_{3A} subunits (h5-HT_{3A}) respectively shares 85% and 84% sequence identity with mouse and rat 5-HT_{3A} subunits.

Two human splice variants of the h5-HT_{3A} subunit have been discovered, in addition to the 5-HT_{3A} transcript identified by Miyake *et al.* (1995). These are termed h5-HT_{3AL} (long) and h5-HT_{3AT} (truncated); neither of which can be heterologously expressed unless co-expressed with 5-HT_{3A} wildtype subunits (Bruss *et al.*, 2000). The h5-HT_{3AL} is not equivalent to the identically named rodent isoform that contains amino acid additions within a long intracellular loop (Hope *et al.*, 1993; Uetz *et al.*, 1994; Werner *et al.*, 1994; Emerit *et al.*, 1995; Miquel *et al.*, 1995), but instead contains additional amino acids within the extracellular M2-M3 loop (see **Figure 1**). Conversely, the h5-HT_{3AT} subunit is truncated to contain the 'normal' h5-HT_{3A} subunit extracellular N-terminus but only one transmembrane domain (TMD), distinct from any TMD found in 'normal' h5-HT_{3A} subunits. With such a strange topology, it is difficult to imagine how the 5-HT_{3AT} is incorporated into the 5-HT_3R heteromer; whether the single TMD forms part of the channel or has a unique function remains a question of some intrigue. Indeed, heterologous co-expression of h5-HT_{3AT} (with WT h5-HT_{3A}) in HEK293 cells is reported to cause an increase in cation flux by deceleration of receptor desensitisation, whereas h5-HT_{3AL} co-expression has the opposite effect (Bruss *et al.*, 2000). Although h5-HT_{3AL} and h5-HT_{3AT} mRNA has been detected by Southern blot of tissues from the hippocampus and amygdala, with placental tissue also showing h5-HT_{3AT} to be present (Bruss *et al.*, 2000), positive immunocytochemistry results have yet to be published.

Figure 1: Amino acid sequence comparison of h5-HT_{3A} (Miyake *et al.*, 1995) to h5-HT_{3AL} subunits. The h5-HT_{3AL} subunit contains 32 extra amino acids located between the α-helices (A) of transmembrane regions M2 and M3. *5-HT_{3A} SS* = secondary structure prediction.

1.2.2 The 5-HT_{3B} subunit

The rapid developments in molecular biology, the unravelling of the human genome sequence and the ability to search databases of various cDNA and chromosome vector libraries, eventually led to the discovery of a much anticipated homologue of the human 5-HT_{3A} subunit; aptly named the 5-HT_{3B} subunit (Davies *et al.*, 1999; Dubin *et al.*, 1999). The h5-HT_{3B} gene was assigned to the same location as 5-HT_{3A} (Weiss *et al.*, 1995) on chromosome 11, band 23.1 (Davies *et al.*, 1999), most likely representing a gene duplication event. Using standard polymerase chain reaction (PCR) techniques, flanking primers amplified encoding DNA from a human kidney cDNA library. The h5-HT_{3B} cDNA encodes a protein of 441 amino-acid residues, with 41% amino acid identity to h5-HT_{3A} and just 21-25% identity to subunits from the nAChR. Amino acid alignment of h5-HT_{3A} and h5-HT_{3B} demonstrates their sequence similarity (**Figure 2**). Shortly after the initial discovery of h5-HT_{3B}, orthologs from mouse and rat tissue sources were also described (Hanna *et al.*, 2000). In spite of this breakthrough, there is an absence of mutagenic data available regarding this subunit, particularly its extracellular domain.

Recently, the h5-HT_{3B} subunit has been found to express as two different transcripts due to alternative promoter regions (Tzvetkov *et al.*, 2007). In fact, the subunit discovered by Davies *et al.* (1999) is thought to be specific to the intestine or the peripheral nervous system (PNS). In the human brain, the DNA transcription start site is located some 4000bp downstream from that found in the intestine. The transcribed product has a new translational start site that may lead to isoforms of h5-HT_{3B} subunits being expressed that differ structurally at the N-terminus (Tzvetkov *et al.*, 2007).

1.2.3 h5-HT_{3C}, h5-HT_{3D}, h5-HT_{3E} subunits

Human 5-HT_3R genes have also been identified for a further three subunits, 5-HT_{3C} (Karnovsky *et al.*, 2003), 5-HT_{3D}, 5-HT_{3E} (Niesler *et al.*, 2003) and a recently discovered splice variant 5-HT_{3Ea} (Niesler *et al.*, unpublished), each located on chromosome 3q27. The 5-HT_{3C} and 5-HT_{3E} amino acid sequences have the characteristic features of a LGIC, whereas 5-HT_{3D} lacks a signal sequence and much of the typical N-terminus. These new subunits have recently been expressed in HEK293 cells, but like 5-HT_{3B} subunits, require co-transfection with 5-HT_{3A} subunit cDNA (Niesler *et al.*, 2007). The pharmacology of these novel heteromers is identical to 5-HT_{3A} homomers, and although the calcium permeability is suggested to be lower in 5-$HT_{3A/C}$ and 5-$HT_{3A/Ea}$ subtypes, more biophysical studies are needed to confirm this. Using reverse transcription PCR (RT-PCR), it has been shown that 5-

Figure 2: Alignment of the primary amino acid sequences of 5-HT_{3A} and 5-HT_{3B} subunits including their secondary structure (S.S.). Amino acid numbering (top) refers to the 5-HT_{3A} subunit, but includes gap penalties (after S231). Sequence identity is indicated by full stops (.) within the 5-HT_{3B} subunit sequence. Amino acids with similar properties are similar in colour, e.g. positively charged residues lysine (K) and arginine (R) are blue whereas negatively charged aspartate (D) and glutamate (E) residues are red. Putative binding loops are highlighted in different colours: loop-A, loop-B, loop-C, , loop-E, loop-F. Transmembrane domains are highlighted in grey, with the intervening amphipathic helix highlighted in a lighter grey. TM2 is also numbered below the sequence according to standard nomenclature. This labelling also contains the predicted location of the channel gate, intracellular region (IR) and the extracellular region (ER). Within the secondary structure sequences; A indicates an alpha helical region and B indicates a β-strand, with uppercase letters indicating the prediction scores with high reliability, whereas lowercase letters indicate the prediction is less reliable.

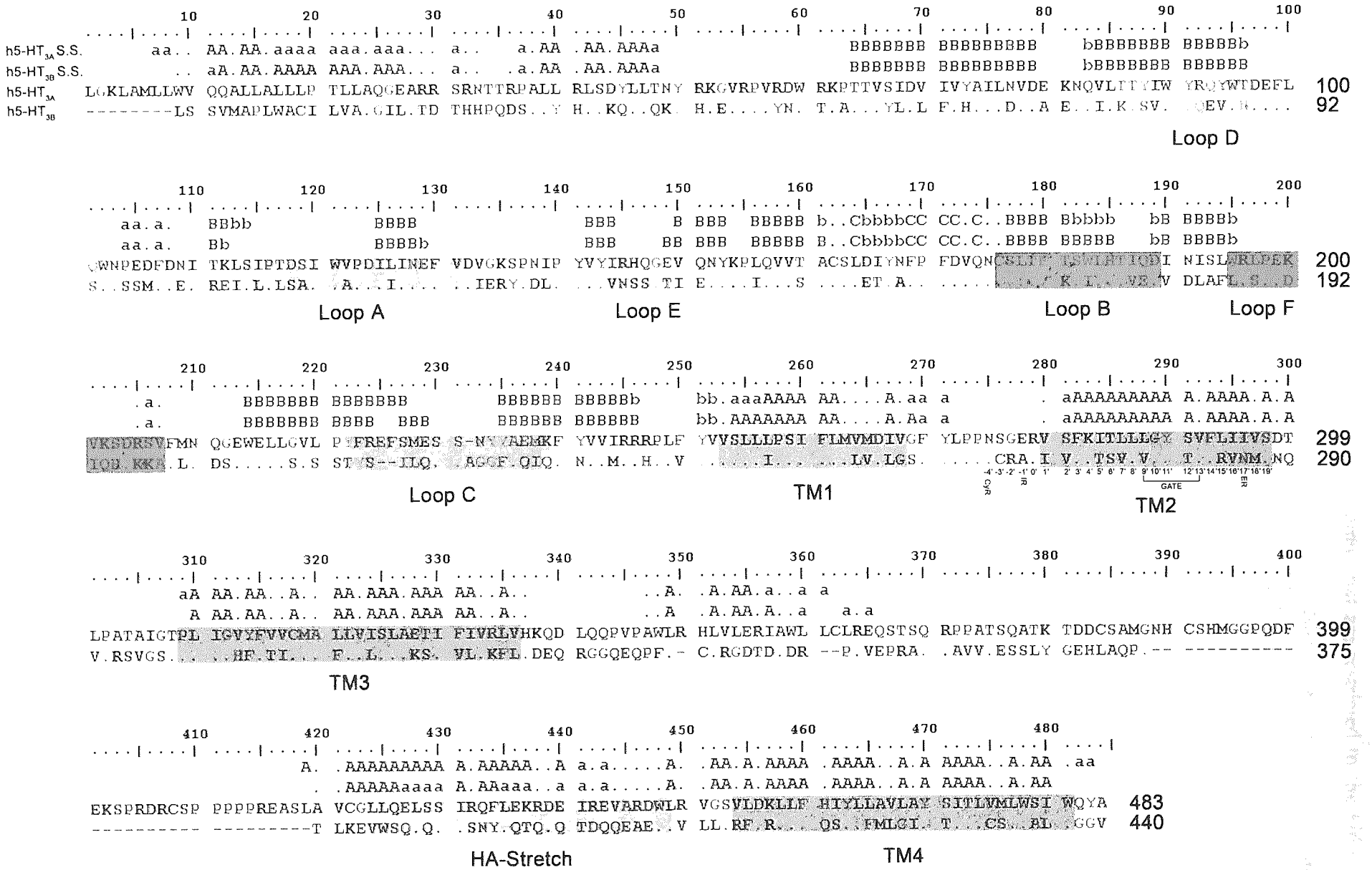
h5-HT3A S.S.
h5-HT3B S.S.
h5-HT3A
h5-HT3B
100
92
Loop D
200
192
Loop A
Loop E
Loop B
Loop F
299
290
Loop C
TM1
TM2
GATE
399
375
TM3
483
440
HA-Stretch
TM4

HT_{3D} and 5-HT_{3E} subunits are not expressed in the brain, but are restricted to the kidney, colon and liver or the kidney and intestine respectively (Niesler *et al.*, 2003). This gastrointestinal location identifies these subunits as possible targets for diseases such as irritable bowel syndrome.

1.3 Structural features of ligand-gated ion channels

The 5-HT_3 receptor belongs to the Cys-loop sub-family of ligand-gated ion channels, the archetypal member of which is the nicotinic acetylcholine receptor (nAChR). Each receptor is assembled from five polypeptide subunits (Boess *et al.*, 1995), arranged pseudosymetrically to create a central cavity, often described as a barrel formation (see **Figure 3**). When this pentameric receptor is inserted into the cell membrane, it traverses the whole lipid bilayer, creating a water-filled channel that is closed in its inactive state. Upon agonist binding, a rapid conformational change in the subunits causes the receptor to open, allowing the conduction of extracellular ions to the intracellular cytoplasm, changing the polarity of the cell. Both the nAChR and 5-HT_3R are cation specific. Other members of the family exhibit anion specificity: γ-aminobutyric acid (GABA) receptors $GABA_A$ and $GABA_C$, and the glycine receptor (GlyR).

Despite the apparently poor sequence identity between subunits from the Cys-loop subfamily of LGICs, it is generally believed that they share a common structural organisation (for example see Corringer *et al.*, 2000). Each of the subunits is 400-450 amino acid residues in length and exhibits: **i)** a long extracellular N-terminal region containing approximately half of the total amino acid residues, including amino acids important for ligand recognition located on six discontinuous 'binding loops' designated A-F (Corringer *et al.*, 2000); **ii)** a highly conserved extracellular cystine-bridged loop enclosing 13 residues: the eponymous Cys-loop; **iii)** four α-helical hydrophobic transmembrane domains (TMDs) designated TM1-TM4, and **iv)** a large cytoplasmic domain between TM3 and TM4. The location of these key features in the primary amino acid sequence of 5-HT_{3A} and 5-HT_{3B} subunits is shown in **Figure 3_{A+C}**.

Low resolution electronmicroscopic images of the $5HT_3$ receptor (Boess *et al.*, 1995) concur with much higher resolution images of the nAChR (Brisson & Unwin, 1985; Unwin, 1993) that functional 5-HT_{3A}Rs comprise five subunits arranged to enclose the integral ion channel (**Figure 3_B**). Within this pentameric arrangement, ligand recognition sites are located at the interface of two subunits (Brejc *et al.*, 2001), each subunit contributing three regions of contiguous amino acids called 'loops' that project into ligand binding site pocket. Loops A-C

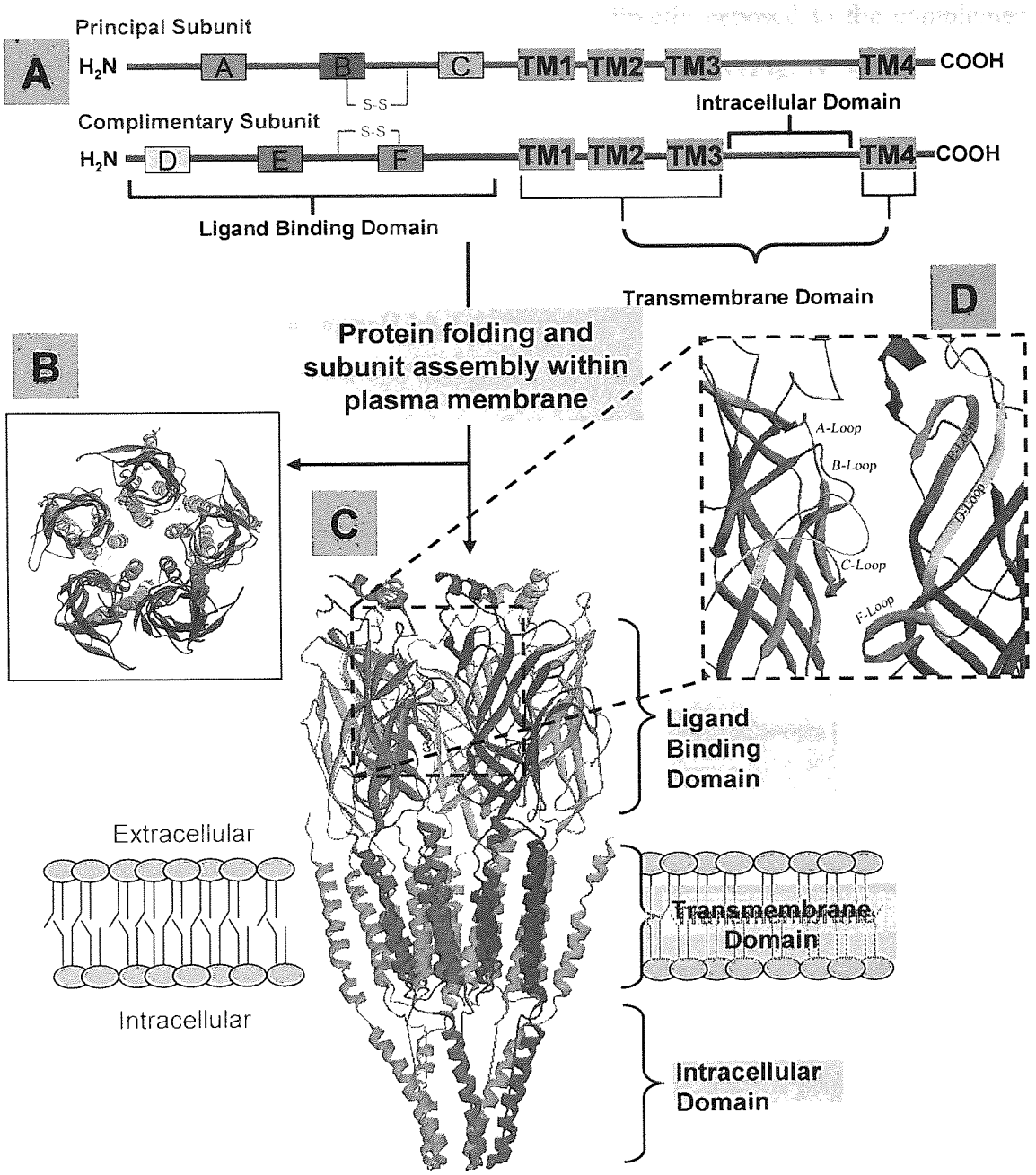

Figure 3: Schematic representation of LGIC subunits and their arrangement within the lipid bilayer. (A) General features of their primary sequence (B and C) their structure and pentameric arrangement within the plasma membrane, (B) viewed from the synapse and (C) perpendicular to the membrane plane. (A and C) Notable features include: a long extracellular N-terminal domain containing the ligand binding domain (LBD) and Cys-loop, four transmembrane domains (TM1-TM4), a long intracellular domain containing an amphipathic helix (or HA stretch), and a short extracellular C-terminus. (D) A zoomed image of the LBD and the interfacial binding loops (A-F) of the principal (red) and complimentary (blue) subunits.

from one subunit form the principal face, which is directly apposed to the complementary face residues provided by loops D-F on the neighbouring subunit (**Figure 3_D**).

1.4 Pharmacology of 5-HT_3Rs

Researchers of the 5-HT_3R are in the enviable position of having an arsenal of antagonists specific for their receptor, which have proved powerful tools for building a pharmacophore model, since their early discovery (Lloyd & Andrews, 1986; Schmidt & Peroutka, 1989). By comparing a selection of agonist and antagonist chemical structures (**Figure 4**), it is possible to identify key structural features of drugs that act at the 5-HT_3R: antagonists have larger, more space filling structures than agonists; all high affinity ligands have an aromatic ring; and antagonists require a large nitrogen-containing ring structure (typically tropane), whereas agonists have a cationic primary amine group. The size of the tropane ring (or equivalent) substitution (for example a methyl group), the distance of its nitrogen from the centre of the aromatic ring, and many other nuances that affect the flexibility and relative distances between integral binding components of the molecule, further influence the affinity of a drug at the 5-HT_3R binding site (Schmidt & Peroutka, 1989).

Quaternary ammonium and primary amine groups are integral for ligand binding via cation-π interactions (Zhong *et al.*, 1998; Beene *et al.*, 2002). These strong electrostatic interactions are responsible for much of the affinity demonstrated by ligands of the Cys-loop receptors (Dougherty, 1996). Both functional groups are contained within the chemical structures of ACh and 5-HT, which may explain reports of these agonists binding to each others target receptor (Gurley & Lanthorn, 1998; Blanton *et al.*, 2000). Such a property is found in *d*-tubocurarine (curare), active as an antagonist at both 5-HT_3Rs and AChRs (Hope *et al.*, 1996). The large ring structure of *d*-tubocurarine (**Figure 4**) will occupy a considerable proportion of the LGIC binding pocket, making many important ligand-receptor contacts, supportive of conclusions that AChRs and 5-HT_3Rs have a similar overall organisation to their binding pocket structures.

In the human 5-HT_3 receptor the major ligands have a rank order affinity of *S*-zacopride > granisetron > *Y*-25130 > BRL46470A > R-zacopride = ondansetron > m-chlorophenylbiguanide (mCPBG) > 5-HT > 2-methyl-5-HT > metoclopramide > phenylbiguanide (PBG) = cocaine > *d*-tubocurarine > morphine (Hope *et al.*, 1996; Brady *et al.*, 2001). These are the agonists and antagonists most commonly used for 5-HT_3R characterisation.

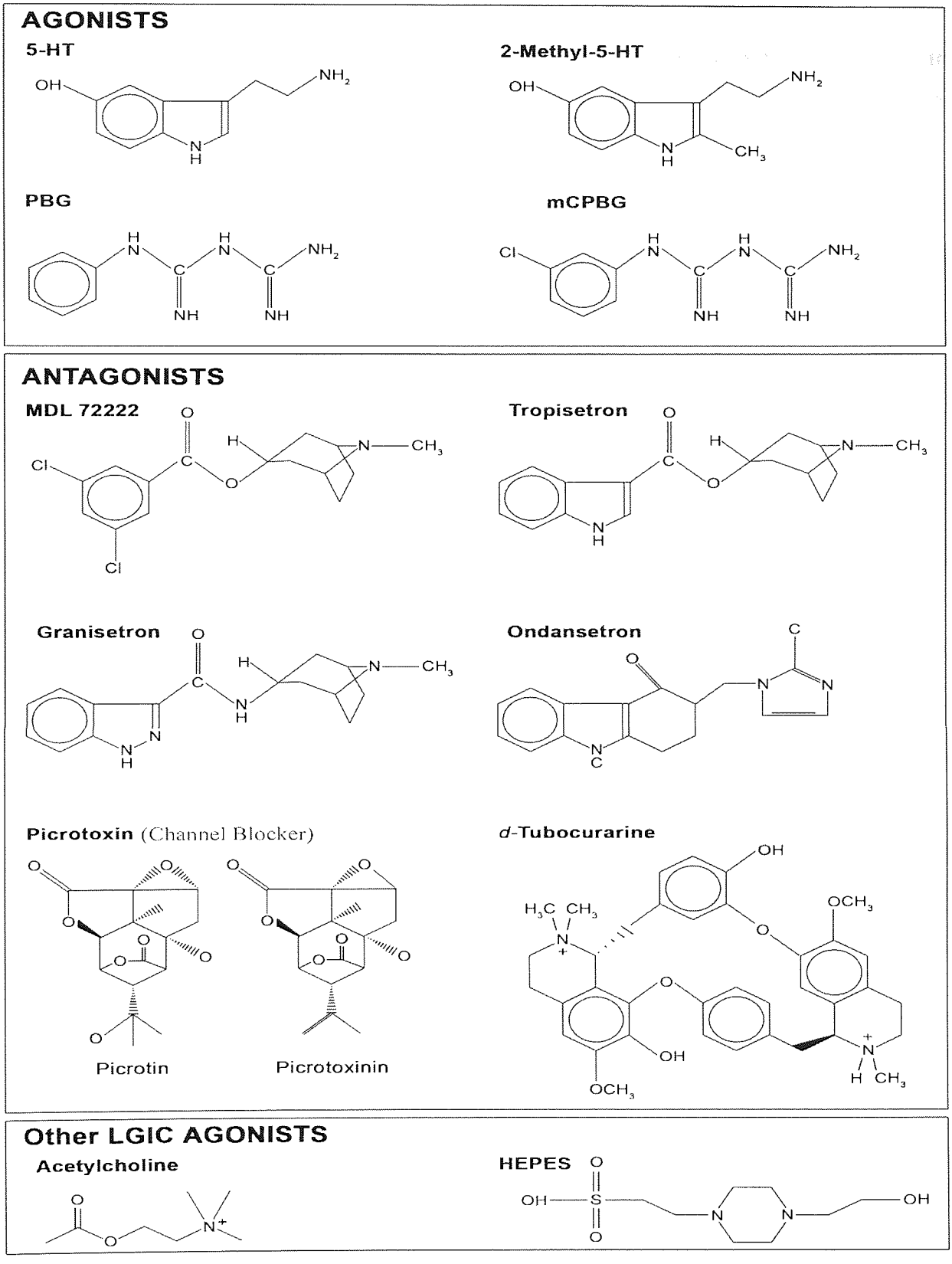

Figure 4: Chemical structures of agonists and antagonists commonly used for studying the 5-HT_3 receptor. These ligands all share structural commonalities, notably the aromatic ring and a positively charged nitrogen moiety. HEPES was the buffer molecule located within AChBP crystal structures.

1.4.1 Orthologs

5-HT_3Rs show marked pharmacological differences between species. Affinity constants for ligands acting on the human 5-HT_3R differ considerably from those found in other species, especially that of the guinea-pig, where mCPBG is much less potent, and PBG demonstrates neither agonistic or antagonistic properties (Butler *et al.*, 1990; Blier & Bouchard, 1993; Lankiewicz *et al.*, 1998). More pertinent to the work carried out in this thesis, d-tubocurarine also exhibits differential pharmacology between orthologs. It is a potent antagonist in the N1E-115 mouse neuroblastoma cell line (IC50 = 0.85 nM: Malone *et al.*, 1991), similar to heterologously expressed mouse 5-HT_{3A} subunits (IC50 = 12.99 nM: Zhang *et al.*, 2007). This potency is dramatically reduced in heterologously expressed human 5-HT_{3A} subunits, some 140-fold (IC50 = 1817 nM: Zhang *et al.*, 2007). These differences are not attributable to the incorporation of modifying subunits, but rather modifications to the primary amino acid sequence in the region of the binding pocket (for review see Peters *et al.*, 2005). These species specific modifications to the receptor pharmacology are useful models for interpreting mutagenic data.

1.4.2 5-HT_{3A}R and 5-$HT_{3A/B}$R

Expression of specific 5-HT_3R subunits in distinct regions of the CNS (see **Distribution of 5-HT_3Rs**) makes distinguishing homomeric (5-HT_{3A}) from heteromeric (5-$HT_{3A/B}$) h5-HT_3Rs pharmacologically advantageous, if specific brain regions can be targeted whilst others remain unaffected. Currently, the available ligands are making this task challenging. The pKi values for a range of common agonists and antagonists competing for [^{3}H]granisetron are almost indistinguishable between 5-HT_3R subtypes. The only significant divergence from this relationship has been shown for 5-HT (EC_{50} = 2.9 μM for 5-HT_{3A}, 6 μM for h5-$HT_{3A/B}$, Davies *et al.* (1999); EC_{50} = 1.4 μM for rat 5-HT_{3A}, 2.4 μM for rat 5-$HT_{3A/B}$, Hanna *et al.* 2000), generally implying that the 5-HT_{3B} subunit reduces 5-HT sensitivity. The magnitude of these differences varies between different species, but in humans, proves too small to discriminate between both receptor subtypes, using current techniques in electrophysiology and radioligand binding (Davies *et al.*, 1999; Dubin *et al.*, 1999; Hanna *et al.*, 2000; Brady *et al.*, 2001).

A more promising prospect in this regard, is the use of d-tubocurarine, which will be investigated in this thesis. This 5-HT_3 receptor antagonist demonstrates robust differences in potency at m5-HT_{3A}R, compared to h5-HT_{3A}R (Hope *et al.*, 1999; Zhang *et al.*, 2007). The components of this differential binding are contained within the amino acids of the C- and F-

loops of the extracellular N-terminus, which differ significantly between mouse and human 5-HT_3Rs. These loops also differ significantly between h5-HT_{3A} and h5-HT_{3B} subunits, and preliminary binding experiments suggest that d-tubocurarine has higher affinity for h5-HT_{3A}Rs over h5-$HT_{3A/B}$Rs (Davies *et al.*, 1999). Such discrimination of receptor subtypes is potentially invaluable for confirming the presence of a 5-$HT_{3A/B}$R population through simple binding experiments.

The $GABA_A$ receptor ($GABA_AR$) antagonist picrotoxin has previously been investigated for its ability to discriminate between 5-HT_{3A} and 5-$HT_{3A/B}$Rs (Das *et al.*, 2003; Das & Dillon, 2003, 2005). Indeed, it has been reported that picrotoxin has a 100-fold lower affinity for m5-$HT_{3A/B}$Rs than m5-HT_{3A}Rs. It remains untested in human 5-HT_3 receptors, but will be used in our experiments for the investigation of HEK293 cells transfected with 5-HT_{3A} and 5-HT_{3B} subunits.

1.5 Distribution of 5-HT_3Rs

The studies presented in this thesis are principally concerned with the role of the 5-HT_{3B} subunit and its ability to modify the properties of the homomeric 5-HT_{3A}R. It is therefore useful to establish the localisation and physiological contribution that the 5-$HT_{3A/B}$R makes in the peripheral (PNS) and central nervous systems (CNS). This will also help elucidate its function in health and disease, and rationalise observed responses to 5-HT_3R targeted drugs.

1.5.1 Central Nervous System

In early experiments on rodents and primates, the administration of ondansetron (GR38032F), MDL 72222 and ICS 205-930 was noted to induce behavioural effects (Costall *et al.*, 1989; Barnes *et al.*, 1990). These were clear indications that 5-HT_3Rs were present in the CNS. Radioligand binding by Kilpatrick *et al.* (1987) further showed that [^{3}H]GR65630 exhibits differentially distributed binding throughout the brain of rats, with high concentrations in cortical and limbic homogenates.

The presence of 5-HT_3Rs in the area postrema, nucleus tractus solitarius and dorsal motor nucleus of the vagus nerve is now well established (Pratt *et al.*, 1990). Autoradiography consistently shows binding in the dorso-vagal complex (including the area postrema and nucleus tractus solitarius) in different species (ferret, rat, mouse, marmoset and human), using [^{3}H]-(s)-zacopride (Barnes *et al.*, 1990a), [^{3}H]GR656030 (Kilpatrick *et al.*, 1988; Barnes *et al.*, 1990b; Jones *et al.*, 1992), [^{3}H]granisetron (Leslie *et al.*, 1990), [^{3}H]mCPBG (Steward *et al.*, 1993) and [^{125}I]-zacopride (Laporte *et al.*, 1992). Using *in situ* hybridisation, the dorsal

root ganglion tests positive for 5-HT_{3A} mRNA (Tecott *et al.*, 1993). In addition to the hindbrain regions discussed above, forebrain regions also express 5-HT_3Rs, although the level of expression in rodent and humans reveals interspecies variation. Rats have high 5-HT_3R expression levels in the amygdala, hippocampus, and cortical areas (primary olfactory cortex, entorhinal cortex: Barnes *et al.*, 1990a; Tecott *et al.*, 1993; Morales *et al.*, 1996a; Morales *et al.*, 1996b; Spier *et al.*, 1999). In the human forebrain, 5-HT_3R populations are relatively low compared to the hindbrain. The only significant concentrations are found in the amygdala (Kilpatrick *et al.*, 1989), hippocampus (Bufton *et al.*, 1993) and striatum (Barnes *et al.*, 1990a; Abi-Dargham *et al.*, 1993; Bufton *et al.*, 1993; Parker *et al.*, 1996a).

1.5.2 The gastrointestinal tract

A side-effect of 5-HT_3R antagonist treatment is the onset of constipation, which is another giveaway of a further distinct 5-HT_3R location. The presence of 5-HT_3R in the gastrointestinal tract is now well established (Pinkus *et al.*, 1989; Gordon *et al.*, 1990; Champaneria *et al.*, 1992; Hansen & Jaffe, 1994; Johnson *et al.*, 1994); *In situ* hybridisation has detected 5-HT_3R mRNA in both submucosal and myenteric ganglia of the duodenum, jejunum, and ileum (Johnson & Heinemann, 1995).

1.5.3 Distribution of 5-HT_{3B} subunits

The presence of 5-HT_{3B} subunits in the PNS is axiomatic because of its initial isolation from the intestine (Dubin *et al.*, 1999) and kidney (Davies *et al.*, 1999). Conversely, the presence of 5-HT_{3B} subunits in the CNS has been a contentious issue. Immunoprecipitation experiments on brain samples have, so far, been unable to co-precipitate the B subunit with the A subunit, which has previously been used as evidence to argue that the expression of 5-HT_{3B} subunits is functionally restricted to the PNS (Morales & Wang, 2002; van Hooft & Yakel, 2003). Furthermore, single-cell RT-PCR and patch-clamp recordings in rat hippocampal CA1 interneurons show expression of 5-HT_{3A} and α4-nAChR but not 5-HT_{3B} subunits (Sudweeks *et al.*, 2002). This has also been shown in neocortical interneurons (Ferezou *et al.*, 2002). It is of course possible that mRNA transcripts are found in cell bodies located outside of these hippocampal regions, whilst the nerve terminals containing 5-$HT_{3A/B}$Rs do extend to these hippocampal regions. Indeed, northern blot analysis shows 5-HT_{3B} subunit mRNA is present in brain regions occupied by 5-HT_{3A} subunits: amygdala, caudate nucleus, hippocampus and thalamus (Davies *et al.*, 1999). These data have been substantiated by other groups (Dubin *et al.*, 1999). Moreover, recent RT-PCR experiments have concurred with Davies *et al*, and show high levels of mRNA expression in the amygdala, caudate nucleus (half that of the

amygdala), and hippocampus (Brady *et al.*, 2007; Tzvetkov *et al.*, 2007). Interestingly, Tzvetkov *et al.* (2007) showed a 6-fold higher expression of the 5-HT_{3B} subunit mRNA in the amygdala, compared to the 5-HT_{3A} subunit. This is a possible indication that the 5-HT_{3B} subunit requires a greater number of transcripts for efficient expression *in vivo*.

Immunohistochemical localisation of 5-HT_{3B} subunits has been carried out in rodent brain tissue and transfected cells, using a polyclonal antibody raised against an epitope located in the first α-helix of the N-terminus (amino acid sequence PQDSA LYHLS KQLLQ KYHK: Reeves & Lummis, 2006). This antibody identified 5-HT_{3B} subunit immunolabeling in non–permeabilized and permeabilized preparations of HEK293/5-$HT_{3A/B}$ and rodent brain tissue. In HEK293/5-HT_{3B} preparations, only permeabilized cells were positively immunolabeled, demonstrating that the 5-HT_{3B} subunit was present, but could not be expressed at the cell surface, as expected. The most recent immunohistochemical evidence has detected 5-HT_{3B} subunits in hippocampal sections (Brady *et al.*, 2007). This wealth of data not only shows that both $5HT_{3A}$ and 5-HT_{3B} subunits are co-expressed in certain brain regions, peripheral neurons and cell lines, but also that their expression patterns are distinct. Approximately 50% of the cells in the rodent dorsal root ganglion have been shown to express only the $5HT_{3A}$ subunit, whereas over 90% of the cells expressing 5-HT_{3B} subunit mRNA were determined to co-express 5-HT_{3A} (Morales *et al.*, 2001; Morales & Wang, 2002). This is compelling evidence, not only for the existence of multiple subtypes, but also for each subtype having a distinct physiological function. It is therefore important to be able to distinguish between the two receptor subtypes; the homomer and the heteromer.

1.6 5-HT_3R Expression

In order to ensure safe passage of 5-HT_3Rs from the endoplasmic reticulum (ER) to the cell surface, individual 5-HT_3R subunits must fold correctly, make appropriate interactions with specific chaperones (RIC-3; Cheng *et al.*, 2005), and associate with other appropriate subunits, in order to prevent their proteolytic degradation.

During the process of assembly, the tertiary structure of the receptor may bear little resemblance that of the established crystallography models, due to the transient nature of protein folding before its insertion into the lipid bilayer. Consequently, certain distinct regions, normally considered part of the intracellular, transmembrane or extracellular domain, are predicted to interact, allowing cell surface expression, in spite of these interactions being implausible evidenced on crystal structures.

In contrast to the expression of 5-HT_{3A} subunits, it is evident that the 5-HT_{3B} subunit cannot be expressed as homomeric receptors, and is therefore lacking/containing specific amino acid motifs that would otherwise permit cell surface expression.

1.6.1 Endoplasmic reticulum retention signals

It has been demonstrated that 5-HT_3 subunit expression is partly due to an amino acid motif (CRAR) located in the TM1-TM2 intracellular loop, which causes the 5-HT_{3B} subunit to be retained within the endoplasmic reticulum (ER) (Boyd *et al.*, 2002; Boyd *et al.*, 2003). Similar motifs to that found in the 5-HT_{3B} subunit have previously been reported to cause ER retention or rescuing from this fate (Zerangue *et al.*, 1999; Standley *et al.*, 2000; Scott *et al.*, 2001). Replacing the 5-HT_{3B} subunit ER retention signal with the aligned 5-HT_{3A} subunit sequence (SGER) does not result in 5-HT_{3B} homomer expression unless the 5-HT_{3B} subunit is also truncated C-terminal to TM2 (Boyd *et al.*, 2003). This suggests that further sites exist downstream of TM2 that act to rescue/condemn the 5-HT_{3A}/5-HT_{3B} subunit. These regions have been alluded to in experiments by Peters *et al.* (2004). It should be noted that the amino acids that align with the 5-HT_{3B} subunit ER retention signal in 5-HT_{3C} (SENR), 5-HT_{3D} (SGNC) and 5-HT_{3E} (SGNR) subunits differ, but they are still unable to be expressed without rescue via 5-HT_{3A} subunit co-expression (Niesler *et al.*, 2007).

In addition to these ER retention signals, it is evident that the last two C-terminal amino acids, tyrosine and alanine, strongly affect the expression of subunits (Pons *et al.*, 2004). It is predicted that these residues interact with a hydrophobic motif within the Cys-loop (FPF) in such a way as to hide a retention signal within TM1 (PLFYVVS in h5-HT3A but discovered in nAChR; Wang *et al.*, 2002), preventing its degradation in the ER. Manipulation of the C-terminus using molecular biological techniques should obviously be performed with caution, to avoid possible loss of subunit expression.

The ability to express 5-HT_{3B} homomeric receptors would greatly enhance our knowledge of contributions this subunit makes to binding and function. However, the level of complexity demonstrated by ER retention signals, on top of other, possibly unknown factors that influence assembly and expression, suggest much more work will be required on this front.

1.6.2 Glycosylation

Both 5-HT_{3A} and 5-HT_{3B} subunits have a number of *N*-glycosylation sequence motifs within the ligand binding domain (LBD) with the amino acid sequence NXS/T (X is any amino acid except proline), which exhibit inter-species conservation within 5-HT_{3A} subunits. The glycosylation of asparagine residues within the LBD is thought to affect intersubunit

interactions critical for subunit folding, and assembly of intact pentameric 5-HT_3 subunit complexes (Monk *et al.*, 2004; Quirk *et al.*, 2004). Treatment of 5-HT_{3A} subunit transfected cells with the *N*-glycosylation inhibitor tunicamycin prevents the expression of 5-HT_3Rs to an extent that is dependant upon the tunicamycin incubation period (Monk *et al.*, 2004). More specifically, N109 glycosylation is a prerequisite for correct receptor assembly, and N175 and N191 are required for plasma membrane targeting and ligand binding (Quirk *et al.*, 2004).

In the nAChR, an *N*-glycosylation site exists that straddles the C-terminal cysteine within the Cys-loop. Interestingly, glycosylation of this site has been shown to enhance disulphide bond formation and promote incorporation of the *trans* isomer of proline, also located within the Cys-loop (Rickert & Imperiali, 1995). This glycosylation site corresponds to N175 in the 5-HT_{3A} subunit Cys-loop, and P170 is the equivalent proline residue. Proline isomerisation within the TM2-TM3 loop has recently been suggested as a possible mechanism for channel opening in the mouse 5-HT_{3A}R (see section 1.8.2.2, Lummis *et al.*, 2005). The close proximity of this glycosylation site and the TM2-TM3 proline may be coincidence, but requires further investigation.

1.7 Functional Properties of 5-HT_3Rs

1.7.1 Channel properties

5-HT_3Rs mediate 'fast' synaptic transmission (Derkach *et al.*, 1989). Whole-cell voltage clamp studies on the 5-HT_3R in the cultured rat neuroblastoma cell line N18, have demonstrated that 5-HT (10 μM) induces fast 'nicotinic like' depolarisations accompanied by large inward ionic currents (Yang, 1990). Similar results have been obtained from other neuronal sources such as mouse hippocampal cultures, rat NG108-15 cells and rat amygdala slices (Yakel & Jackson, 1988; Sugita *et al.*, 1992). This response can be blocked by the 5-HT_3R antagonists (see **Section 1.4 Pharmacology of 5-HT_3Rs**), but not by ligands specific for other classes of 5-HT receptor. Responses are seen within 10-40 ms of 5-HT delivery and rise to a peak in 34-130 ms. The agonist response involves channel opening and conductance of ions, with very little discrimination between small cations, showing high permeability for monovalent inorganic cations; Na^+, K^+, Cs^+, Li^+, and Rb^+, and lower permeability for divalent cations Ca^{2+}, Ba^{2+}, and Mg^{2+} (Yakel *et al.*, 1990; Yang, 1990; Yang *et al.*, 1992), decreasing as the extracellular concentration of divalent ions is increased. The channel is considered relatively impermeable to Cl^- (Lambert *et al.*, 1989), and although low level permeability has been recorded (Peters *et al.*, 1993), it is not thought to contribute to 5-HT evoked current.

1.7.2 Cellular calcium changes

It has been shown that 5-HT_3 receptors are the postsynaptic targets of 5-HT in fast synaptic transmission (Sugita *et al.*, 1992), where opening of the channel leads to increased intracellular calcium, subsequently inducing the release of neurotransmitter from synaptic vesicles by exocytosis. Binding of agonists to 5-HT_3Rs expressed in NG108-15 cells causes an increase in intracellular cytoplasmic calcium (Ca^{2+}), proportional to the measured response at varying agonist concentrations, and ablated by the addition of 5-HT_3R antagonists; EGTA chelation of extracellular Ca^{2+}; or inhibition of L-type calcium channels (Ronde & Nichols, 1997). In these cells, it is believed that the initial Na^+ and K^+ influx causes depolarisation of the cell, which leads to the opening of voltage sensitive Ca^{2+} channels. This rise in Ca^{2+} is then amplified by Ca^{2+}-induced intracellular Ca^{2+} release from ryanodine sensitive ER Ca^{2+} stores (Ronde & Nichols, 1997).

Not all 5-HT_3Rs mediate Ca^{2+} influx by the same mechanism or to the same extent. Within transfected HEK293/5-HT_{3A} cells (HEK293 cells transfected with 5-HT_{3A} cDNA) and N1E-115 cells, Ca^{2+} influx has been shown to occur even after intracellular calcium store depletion, and does not occur through voltage gated calcium channels (Hargreaves *et al.*, 1994). Similar results have also been obtained in presynaptic 5-HT_3Rs, studied in synaptosomes, confirming the absence of L-type calcium channels and a high permeability to Ca^{2+} (Ronde & Nichols, 1998). This highly Ca^{2+} permeable 5-HT_3R is in contrast to the heterologously expressed 5-$HT_{3A/B}$Rs that have a reduced permeability to Ca^{2+} (Davies *et al.*, 1999). The implication is that receptors observed for their high Ca^{2+} permeability are homomeric 5-HT_{3A}Rs, which have a different distribution in the brain and its neurones (presynaptic), compared to 5-$HT_{3A/B}$Rs.

1.7.3 Desensitisation

With prolonged application of 5-HT (10 μM), using a fast perfusion system, the 5-HT_3R response desensitizes rapidly in all cell types. Increases in extracellular calcium and/or magnesium, cause a decrease the current response and accelerate 5-HT_3R desensitization (Maricq *et al.*, 1991; Brown *et al.*, 1998). The desensitization kinetics can differ depending on the origin of the receptor being studied, but fall into one of two categories: i) biphasic (two exponential phases) in NG108-15 cells (Yakel *et al.*, 1991), hippocampal neurones (Yakel & Jackson, 1988), and cultured superior cervical ganglion cells (Yang *et al.*, 1992), and ii) single phase (one exponential phase) in N1E-115 (Neijt *et al.*, 1989) and most N18 cells

(Yang, 1990), which shortens the receptor response to continued agonist challenge compared to biphasic desensitisation.

It has now been demonstrated that heterologously expressed 5-$HT_{3A/B}$Rs have single-phase desensitisation kinetics, whereas 5-HT_{3A}R homomers are biphasic (Hapfelmeier *et al.*, 2003). It is tempting to conclude that, in vivo, the 5-HT_{3B} subunit is responsible for the observed dichotomy in desensitisation kinetics; however, the contribution of other subunits and factors are yet to be explored, and although the evidence is compelling, it is unlikely that the 5-HT_{3B} subunit provides a full explanation.

1.7.4 Conductance

Following the application of a 5-HT_3R agonist, certain cells demonstrate an ion conductance (γ) in the sub picosiemen (pS) range, only measurable by whole-cell fluctuation (noise) analysis (FA). Application of the same 5-HT_3R specific agonist can cause other cells to transmit ions with a conductance that can be resolved by outside-out membrane patch-clamp techniques, and demonstrate a single channel conductance measurable in the pS range. This dichotomy of 'high conductance' and 'low conductance' 5-HT_3Rs is highlighted in **Table 1**, and is exemplified by the mouse superior cervical ganglion, which demonstrates receptor conductances of 10-11pS determined by single channel measurements, but 2.5-3.5 pS when channel conductance is derived from whole-cell fluctuation analysis (Hussy *et al.*, 1994), an observation confirmed by Yang *et al.*(1992). Hussy *et al.* (1994) estimated that within the mouse superior cervical ganglion, high single channel conductance 5-HT_3Rs constitute 66% of the total 5-HT_3R population, with the rest being of the sub pS class, thus making the whole cell conductance an average of the two populations of 5-HT_3R.

1.7.4.1 The 'HA stretch'

It is now evident that differences in conductance are due to the inclusion of the 5-HT_{3B} subunit within the 5-HT_3R. 5-$HT_{3A/B}$Rs have a high single channel conductance and 5-HT_{3A}Rs have a sub-pS conductance (Davies *et al.*, 1999; Hanna *et al.*, 2000). Residues within the amphipathic helix (HA stretch) of the intracellular TM3-TM4 linker, have now been shown to contribute to this difference in conductance (Peters *et al.*, 2004). Ions that have been filtered through the hydrophobic girdle of the receptor channel are funnelled into the intracellular domain by five amphipathic helices; one from each subunit (Miyazawa *et al.*, 1999; Kelley *et al.*, 2003). The ions are thought to escape into the intracellular matrix through lateral openings between the helices, described as 'portals' (Miyazawa *et al.*, 1999). The residues which affect the passage of ions through these portals are different in 5-HT_{3A} and 5-

HT_{3B} subunits (see **Figure 5**). In the 5-HT_{3A} subunit, three arginine residues, R439, R443 and R445 (amino acid numbering refers to **Figure 2**), located in close proximity to the portals, play a pivotal role in dictating the level of conductance (Peters *et al.*, 2004). In the open channel state, the positively charged arginines found in 5-HT_{3A} subunits hinder the passage of cations through the portals into the intracellular matrix, whereas negatively charged and uncharged residues found in the 5-HT_{3B} subunit, permit freer passage of cations and thus increase the conductance. Replacing the arginine residues in 5-HT_{3A}Rs with those found in the aligned 5-HT_{3B} subunit sequence (Q394, D398, and A402), results in the expression of a 5-HT_{3A}R homomer with single channel conductance of 22.2 pS (Peters *et al.*, 2004). If this subunit is transfected in combination with WT 5-HT_{3A} subunit cDNA, a single channel conductance of ~13 pS is achieved, close to that measured for the WT 5-$HT_{3A/B}$ receptor.

Cell Type	Conductance (pS)	Reference
N1E-115 mouse neuroblastoma	140 (SC)	(Guharay *et al.*, 1985)
	0.31 (FA)	(Lambert *et al.*, 1989)
	0.4-0.6 (FA)	(Hussy *et al.*, 1994)
N18 mouse neuroblastoma	0.4-1 (FA)	(Yang, 1990)
NG108-15 (undifferentiated)	7.2-12 (FA)	(Shao *et al.*, 1991)
NG108-15 (differentiated)	3.6-4.4 (FA)	
rat SCG neurones	11.1 (SC)	(Yang *et al.*, 1992)
mouse SCG	10.0 (SC)	(Hussy *et al.*, 1994)
rabbit NG	16.6 (SC)	(Malone *et al.*, 1991)
	17.0 (SC)	(Peters *et al.*, 1993)
guinea pig submucus plexus	15 + 9 (SC)	(Derkach *et al.*, 1989)
rodent hippocampus	8.3 (SC)	(Jones & Surprenant, 1994)
Recombinant 5-HT_{3AS} (mouse)	0.4-0.6 pS (FA)	(Hussy *et al.*, 1994)
	0.42 (FA)	(Gill *et al.*, 1995)
Recombinant 5-HT_{3A} (human)	0.45 (FA)	(Brown *et al.*, 1998)
Recombinant 5-$HT_{3A/B}$ (human)	16.0 (SC)	(Davies *et al.*, 1999)

Table 1: Channel conductance measurements for 5-HT_3Rs from cells of different origin. Recordings were either by single channel conductance (SC) or fluctuation analysis (FA). SCG = superior cervical ganglion, NG = nodose ganglion.

Figure 5: A diagrammatic representation of the HA stretch (grey helix) in 5-HT_{3A} and 5-HT_{3B} subunits. Amino acids that affect ion conductance are drawn in ball and stick. (A and B) The space between two HA stretch regions, viewed parallel with the membrane plane, demonstrating the locations of 5-HT_{3B} and 5-HT_{3A} subunit residues that are important for conductance properties of 5-HT_3Rs (Kelley *et al.*, 2003; Peters *et al.*, 2004).

1.8 5-HT_3R Modeling

1.8.1 Acetylcholine binding protein

Much of the early work to characterise the LGICs has focused on the nAChR. Its abundance in the electric ray (*Torpedo marmorata)* has facilitated the production of tubular crystals for electron microscopic analysis (Brisson & Unwin, 1985; Miyazawa *et al.*, 2003). These low resolution electron micrograph images (Unwin, 1993; Boess *et al.*, 1995; Unwin, 1995; Miyazawa *et al.*, 1999) provided evidence for a pentameric arrangement, measurable dimensions and some indication of secondary structures, but provided little information about the composition of the binding site.

The new millennium heralded the atomic era for LGICs, with the publication of an atomic structure (2.7 Å resolution) for a soluble protein called acetylcholine binding protein (AChBP), isolated from the freshwater snail *Lymnaea stagnalis* (Brejc *et al.*, 2001). In nature, AChBP is released from glial cells to modulate cholinergic synaptic transmission by binding and sequestering acetylcholine, effectively acting as a 'decoy receptor' (Brejc *et al.*, 2001; Smit *et al.*, 2001). This is possible because AChBP is homologous to the major extracellular domain of the α7-nAChR, comprising subunits of 210 amino acids arranged as a homopentamer. In contrast to previously published structures of proteins that bind acetylcholine, such as acetylcholinesterase (Sussman *et al.*, 1991; Sussman *et al.*, 1993), AChBP is able to bind all known nAChR agonists and competitive antagonists of α7-nAChR (Smit *et al.*, 2001; Hansen *et al.*, 2002). Indeed, AChBP only differs from a functional LGIC by its truncation, as evidenced by the construction of an AChBP/5-HT_{3A} chimera. This chimera, composed of the AChBP LBD joined to the 5-HT_3 TM and intracellular domains, functioned as a 5-HT_3R channel with α7-nAChR ligand-binding properties, after a minimal number of select point mutations (Bouzat *et al.*, 2004).

1.8.2 Homology modeling

Inevitably, as with the entry of any structural coordinates into the protein database (PDB), sequence similarities between AChBP and other members of the LGIC family are utilised to validate homology models. This is because the atomic structure of AChBP (Brejc et al., 2001) potentially provides an invaluable template, upon which, aligned residues of other LGICs can be substituted, to create a molecular model. A typical homology model has ~2 Å agreement between the matched α-carbon atoms at 70% sequence identity, but only 4-5 Å agreement at

25% sequence identity. However, this relatively low sequence identity can still lead to 80% accuracy in secondary structure estimations (Saqi *et al.*, 1998).

Figure 6 is a sequence alignment, to demonstrate the sequence similarity between AChBP and subunits of the nAChR and 5-HT_3R. The AChBP shares 24% sequence identity with the LBD of LGICs, which includes the 5-HT_3R subunits (Brejc *et al.*, 2001). The secondary structure similarity between α7-nAChR and AChBP is ~80% (Le Novere et al., 2002). The 5-HT_{3A} subunit has a 31% amino acid sequence identity with α7-nAChR (55% including conservative substitutions). Indeed, 5-HT_3 receptor chimeras have been constructed to contain the N-terminal LBD of the α7-nAChR subunit. Not surprisingly the result is a receptor that is activated by acetylcholine (Eisele *et al.*, 1993).

Since the initial AChBP crystal structure publication by Brejc *et al.* (2001), further AChBP crystal structures, from three other species, have been published (see **Table 2**): *Lymnaea stagnalis* (Ls-AChBP), *Aplysia californica* (Ac-AChBP, 33% sequence similarity to *Ls*-AChBP) and *Bulinus truncatus* (Bt-AChPB, 41% sequence identity to *Ls*-AChBP, 29% to Ac-AChBP). The sequence similarities between the different AChBPs are marginally better than the sequence similarity between the LGICs and Ls-AChBP. Despite this fact, all three AChBPs have been shown to have the same structural scaffold, which has preserved the binding site characteristics (see references in **Table 2**). This further validates the use of AChBP as a suitable model of LGICs.

1.8.3 Current homology models

Homology models have now been generated for the $GABA_AR$ (Cromer *et al.*, 2002), α7-nAChR (Le Novere *et al.*, 2002; Schapira *et al.*, 2002; Law *et al.*, 2005) and glycine receptor (Laube *et al.*, 2002; Bertaccini *et al.*, 2005; Cheng *et al.*, 2007; Speranskiy *et al.*, 2007). The next step in homology modeling is to predict the whereabouts of different ligand binding sites and their orientation, as exemplified by the ligand-docked models of Le Novere *et al.* (2002) and Schapira *et al.* (2002). Later crystallographic data of ligand-bound AChBP (Celie *et al.*, 2004) did not embarrass these earlier predictions, although a major limitation of predictions based on single homology models was highlighted: conformational rearrangements of the protein, caused by the process of ligand binding, are not accounted for, detrimentally affecting the predictions of ligand-receptor interactions. Ligands are computationally docked into the most energetically favourable positions within the receptor, those that do not support the current data are disregarded, and those that remain valid are tested. Therefore, the predictive value of models can be tested by mutating residues that are proposed to interact with a ligand.

Figure 6 (overleaf): ClustalX protein sequence alignment of human 5-HT_3 subunit isoforms to those of other members of the Cys-loop family of LGICs. Amino acid numbering (top) is that of 5-HT_{3A} and accounts for gap penalties. Secondary structure elements such as alpha helices (A) and β-strands (B) are indicated above the amino acid sequences. Amino acids with similar properties are similar in colour, e.g. positively charged residues lysine (K) and arginine (R) are blue whereas negatively charged aspartate (D) and glutamate (E) residues are red. This allows highly conserved residues to be more easily noticed. Putative binding loops are highlighted in different colours: loop-A, loop-B, , , loop-E, loop-F. **Species abbreviations use: *h* is *Homo sapiens*, *r* is rat, *m* is mouse, *t* is *Torpedo californica, Ls* is *Lymnaea stagnalis*, *Bs* is *Bulinus truncatus* and *Ac* is *Aplysia californica***

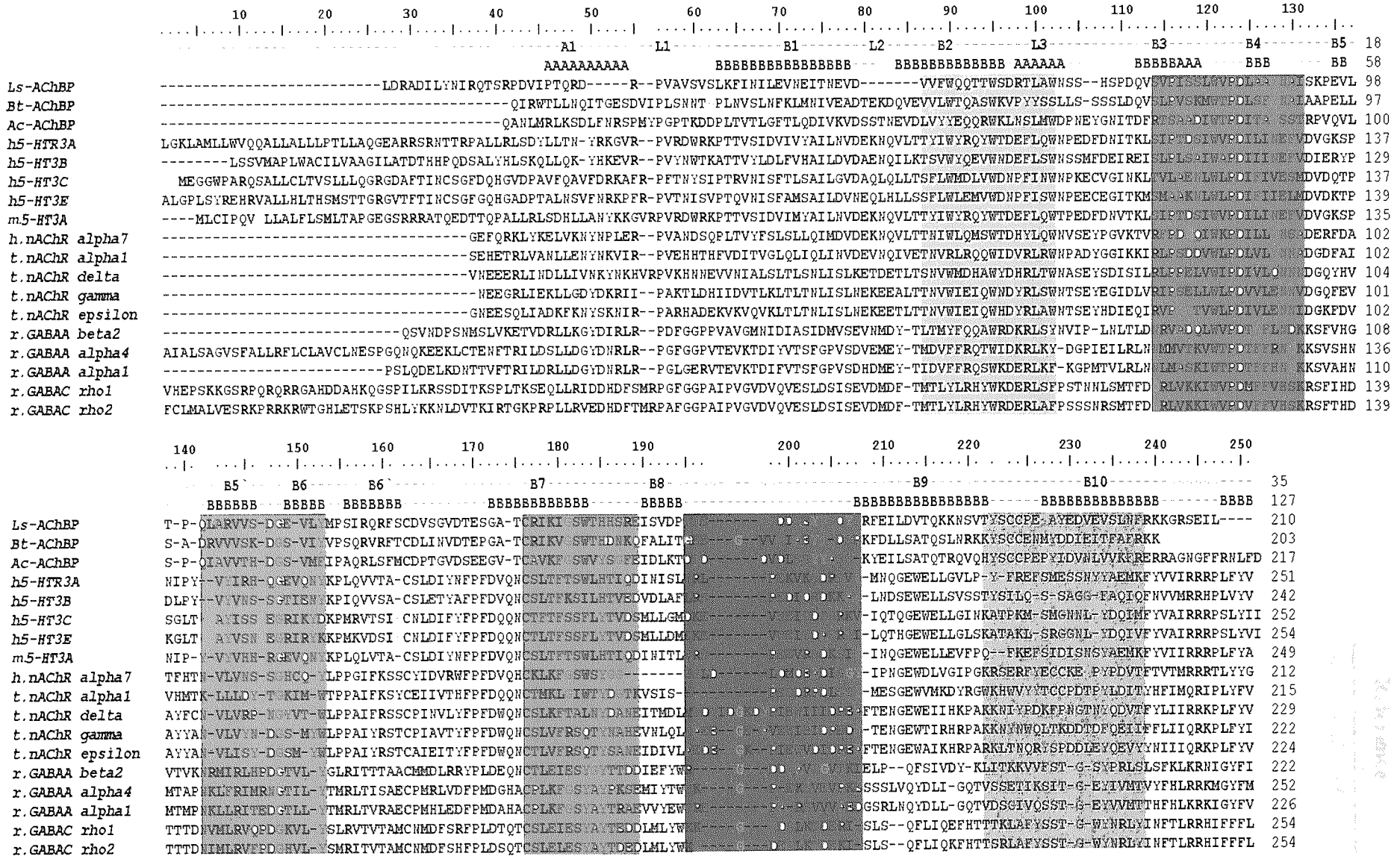
Ls-AChBP
Bt-AChBP
Ac-AChBP
h5-HTR3A
h5-HT3B
h5-HT3C
h5-HT3E
m5-HT3A
h.nAChR alpha7
t.nAChR alpha1
t.nAChR delta
t.nAChR gamma
t.nAChR epsilon
r.GABAA beta2
r.GABAA alpha4
r.GABAA alpha1
r.GABAC rho1
r.GABAC rho2

AChBP Origin	Molecule in Binding Domain	Reference
Ls	HEPES (+)	(Brejc *et al.*, 2001)
Ls	Nicotine (+), Carbamoylcholine (+)	(Celie *et al.*, 2004)
Ls	α-cobratoxin (-)	(Bourne *et al.*, 2005)
Ac	None (apo conformation)	(Hansen *et al.*, 2005)
Ac	α-conotoxin (-)	(Celie *et al.*, 2005a)
Bt	CAPS (+)	(Celie *et al.*, 2005b)

Table 2: Resolved crystal structures of AChBP and the molecules co-crystallised within the ligand binding domain. Lymnaea stagnalis = Ls, Aplysia californica = Ac and Bulinus truncatus = Bt. Agonist = (+) and antagonist = (-). HEPES and CAPS are denoted as agonists due to the primary amine interactions within the binding domain and the similarity of its structure to the desensitised state. Apo conformation = no ligand or amine buffer present in crystallisation process. CAPS = 3-(cyclohexylamino)-1-propanesulfonic acid.

For example, multiple 5-HT docking positions suggested for 5-HT_3R models based on AChBP, need to satisfy the mutagenic data regarding residues W90, W183, Y143, Y153 and Y234, which are known to affect ligand binding (Reeves *et al.*, 2003).

Using the 5-HT_3R for agonist docking simulations has a major advantage over other Cys-loop receptors such as the nAChR, $GABA_A$R and GlyR. This is by virtue of its natural agonist, 5-HT, being a comparatively large and inflexible molecule. Smaller ligands are much more challenging and will be computationally docked in multitudinous positions, generating more artefacts that need to be discounted.

1.8.4 The ligand binding domain

The length of the extracellular N-terminus reflects the importance of this region in providing a robust mechanism that allows specific ligands to bind and activate the receptor. It is thus known as the ligand binding domain (LBD). It consists largely of β-strands, now clearly apparent from the highest resolution images currently available (Unwin, 2005). The arrangement of these β-strands in all LGICs has commonalities with that of immunoglobulin domains (Bork *et al.*, 1994; Brejc *et al.*, 2001), as previously predicted for the nAChR before the publication of the AChBP structure (Le Novere *et al.*, 1999; Corringer *et al.*, 2000). In total there are 10 β-strands (two more than immunoglobulin domains), which fold to form two twisted β-sheets packed into a β-sandwich that is joined by a disulphide bridge. The inner β-sheet, which faces the lumen of the channel, is composed of long β-strands β1, β2, and β6 (β3,

β5, and β8 are also part of the inner sheet, but are much shorter). The outer β-sheet, facing the exterior, is composed of long β-strands β7, β9 and β10, and smaller β-strand, β4 (Unwin, 2005).

These structural details become more enlightening once the aligned 5-HT_{3A} and 5-HT_{3B} subunit residues are superimposed onto these AChBP structural details, allowing the relative positioning of amino acids to be seen (**Figure 7**). This is the basis of homology modelling. The arrangement of binding loops in the LBD (discussed in **Section 1.3 Structural features of LGICs**) allows specific amino acid residues between β-strands, or in the β-strands themselves, to be juxtaposed in the tertiary structure, providing the exquisite recognition characteristics of the individual members for their specific ligands (Changeux *et al.*, 1992; Karlin & Akabas, 1995). Residues within many of the β-strands exhibit high levels of sequence homology within the family; their mutation usually has severe consequences for ligand binding. The β-sheets create a specific LBD scaffold (or framework regions), which permits residues within the putative binding loops to be altered without deleterious effects upon the conserved folding pattern, maintaining the binding pocket shape. The binding loops and framework regions are homologous to the complementarity determining regions (CDRs) and framework regions (FRs) found in immunoglobulins respectively. Antibodies can enhance their epitope affinity (affinity maturation) by restricting mutations to within CDRs, whilst maintaining the composition of their FRs (Goldsby *et al.*, 2003). Both LGICs and immunoglobulin mechanisms allow ligand/paratope affinities to be altered without detriment to the robust tertiary structure.

1.8.5 Conformational changes

1.8.6 Rotations

Electron micrograph images of nAChRs, frozen within milliseconds of being sprayed with ACh, are thought to be the best images of an open channel conformation for the nAChR (Unwin, 1995). Compare these images to those of the closed channel conformation (Unwin, 1993), and it is apparent that structural rearrangements occur in the region of the LBDs and TM2 domains, causing rotations in the α-nAChR subunit (principal subunit), though not as a rigid body (Purohit & Auerbach, 2007). This general movement was confirmed by superimposing the structural coordinates of electron micrograph imaging (4 Å resolution) of the closed channel nAChR structure onto that of AChBP, thought to represent the ligand bound state.

Figure 7 (overleaf): Schematic representation of the tertiary structure for h5-HT_{3A} and h5-HT_{3B} subunits, based on the nAChR structure determined by Unwin (2005). Standard single letter abbreviations are used to represent the approximate region that residues are located. The β-strands (β1-β10; draw as arrows) form antiparallel interactions with neighbouring β-strands, to create two antiparallel β-sheets, termed the inner (purple arrows) and outer sheets (orange arrows). Two cysteines, present at opposing ends of the β_6-β_7 linker, form a disulphide bond, connecting the two β-sheets. The amino acids between the two cysteines form the Cys-loop, highlighted in blue. Amino acids contained within putative binding loops A-F are highlighted in green. For clarity, only loops A-C in 5-HT_{3A} and D-F in 5-HT_{3B} are shown. Linking regions of particular importance are β1-β2, β8-β9, β6-β7 (cys loop) and M2-M3. C-terminal to the β10 strand are the membrane spanning alpha helices (red coils) TM1-TM4.

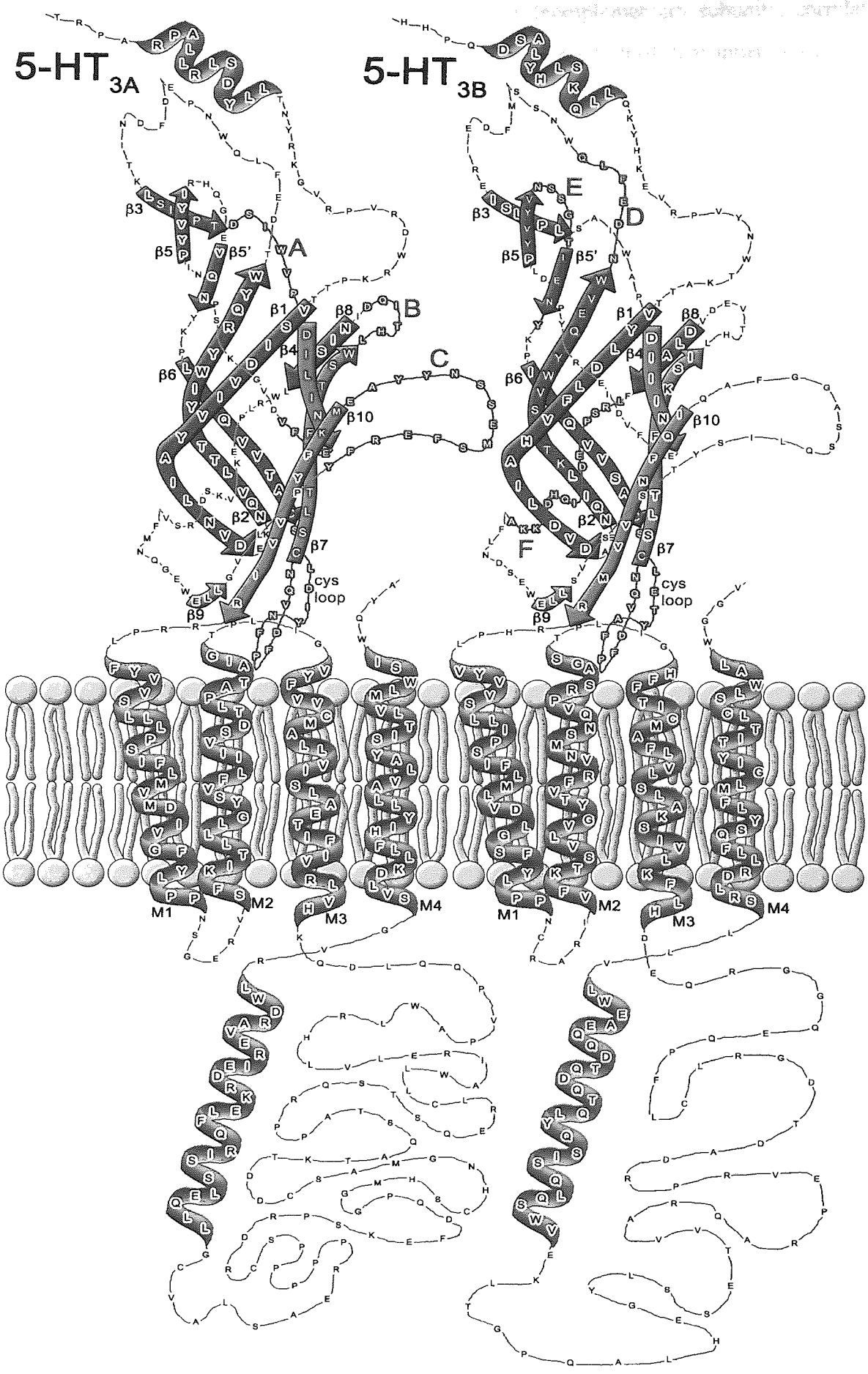
5-HT3A
5-HT3B
β3
β5
β5'
β1
β8
β4
β6
β10
β2
β7
β9
cys loop
A
B
C
D
E
F
M1
M2
M3
M4

Although structural coordinates of the non α-subunits (complementary subunits) correlated well with those of AChBP, the α-subunits required a ~10° rotation of their inner β-sheets and ~11° tilting of their outer β-strands to align with the α-carbon backbone of AChBP (Unwin *et al.*, 2002; Unwin, 2005). This suggests that, in the ground state receptor, the inner β-sheet of α-subunits is held under tension, in an anticlockwise twisted conformation, relative to non-α subunits. The binding of the agonist must instigate a change in α-subunit conformation, involving clockwise rotations of the inner β-sheet, until a conformation resembling that of non α-subunits is adopted.

The AChBP structure publications, detailed in **Table 2**, have related the extent of subunit rotations to the type of ligand entering the LBD. When an agonist enters the LBD, it causes the outer β-sheet β-strands in both principal and complementary subunits to translocate towards the LBD and each other, ultimately contracting around the agonist (Henchman *et al.*, 2005) and reducing the binding pocket volume (Celie *et al.*, 2004; Hansen *et al.*, 2005). Due to its much larger molecular structure, the binding of an antagonist prevents the LBD from contracting, which maintains the channel in a closed state, with a more open LBD conformation (Bourne *et al.*, 2005).

1.8.7 C-loop and F-loop movements

The described β-sheet movements impact upon residues within the binding loops by altering their position relative to the ligand as it enters and exits the binding pocket. The C-loop (β9-β10) and F-loop (β8-β9) of the respective principal and complementary subunits are prominently situated at the binding pocket entrance, on the extracellular side of the receptor. It is from above or below the C-loop that ligands are thought to access the ligand binding site. These loops appear to 'wrap around' the agonist as it enters the LBD, the C-loop moving a distance of ~30 Å due to rotations, compared to its position when antagonists are bound (Celie *et al.*, 2004; Bourne *et al.*, 2005; Hansen *et al.*, 2005). These C-loop movements have also been demonstrated by molecular dynamics simulations, homology modelling with subunit rotations, and tryptophan fluorescence (Maksay *et al.*, 2004; Gao *et al.*, 2005). The movements of the C- and F- loops correspond to movements of strands β10 and β9, proposed by Unwin (2005).

The structure and position of the C-loop mean that it is greatly affected by rigid body movements of the outer β-sheet. In addition, it is the most independently dynamic loop of the LBD, playing an integral role from ligand binding to channel opening. Electron micrograph imaging of the ligand free nAChR has had difficulty resolving the C-loop (Unwin, 2005),

which is assumed to reflect its flexibility when agonists or antagonists are not present in the binding site to stabilise it. Other crystal structures have indicated multiple positions for the C-loop, but only at interfaces that do not bind ligand or buffer molecules (Celie *et al.*, 2004; Celie *et al.*, 2005b). Indeed, for antagonists to gain access to the binding pocket, the AChBP structural data indicates that movement of the C-loop from its resolved position would be a prerequisite (Brejc *et al.*, 2001).

Compared to agonist bound conformations (Brejc *et al.*, 2001; Celie *et al.*, 2004), the C-loop in ligand free (Hansen *et al.*, 2005) or antagonist bound conformations (Bourne *et al.*, 2005; Celie *et al.*, 2005a) protrudes from the relatively well-packed rosette arrangement (see **Figure 8**). In fact, the type of ligand within the binding site influences the extent of C-loop movement, within a range of ~11 Å (Hansen *et al.*, 2005); large antagonists cause large outward movements, small agonists cause large inward movements. The functional consequence of this was demonstrated years previously by incorporating 6 Å and 12 Å moieties into the tip of the nAChR C-loop (by utilising the two reducible cysteine residues present here), mimicking agonists and antagonists respectively (Silman & Karlin, 1969). Moieties that spanned 12 Å caused the receptor to remain in the inactive state, whilst those spanning 6 Å activated the receptor like agonists. Furthermore, these vicinal cysteines could not be reduced when agonist was bound (Damle & Karlin, 1980), indicating that these residues make intimate contacts with the agonist in the binding pocket, effectively covering it. When the ligand is covered in such a way, the binding site is said to be 'capped'. This capping has implications for the binding kinetics, potentially slowing the off-rate (Karlin, 2002; Joshi *et al.*, 2006). All AChBP crystal structures have difficulty resolving the F-loop. This not only makes homology modelling a challenge, but also complicates predictions regarding the involvement of its amino residues in ligand binding events. Perhaps for this reason, it is one of the last loops to undergo detailed mutagenic analysis in the 5-HT_3R (Thompson *et al.*, 2006). The F-loop was sufficiently resolved by Bourne *et al.* (2005) to show its outward movement (towards the extracellular side) by ~8 Å when comparing the HEPES bound Ls-AChBP to α-cobratoxin bound Ls-AChBP. Hansen *et al.* (2005) also noted conformational flexibility of the F-loop. It is likely that upon agonist binding, the F-loop moves towards the binding pocket, reciprocating the inward rotation shown by the C-loop of the principal subunit, and causing the partial occlusion of the binding pocket (Hansen *et al.*, 2005).

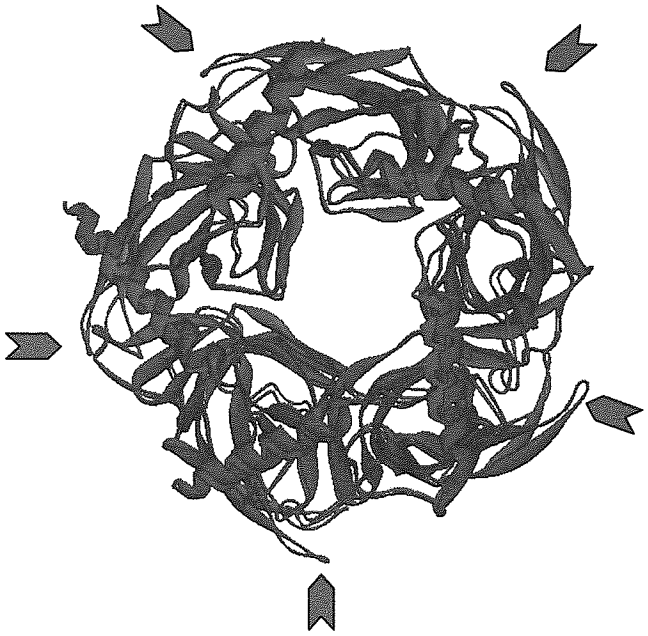

Figure 8: Positioning of C-loops in agonist-bound and ligand-free (apo) states. Crystal structures of AChBP in the ligand-free (blue) and ligand-bound (red) conformations have been superimposed. The C-loops (indicated by black arrows) are tightly packed within the rosette in the ligand-bound state, but assume an open conformation in the ligand-free state, protruding from the rosette.

1.9 Ligand Binding Interactions

1.9.1 The binding pocket

Although biochemical data identifies residues essential for ligand binding interactions, it was not until the first publication of AChBP (Brejc *et al.*, 2001) that the relative positioning of these residues within the binding pocket was known. The first AChBP structure was crystallized in 100 mM HEPES, a buffer molecule that has two protonated nitrogens in a piperazine ring, equivalent to the positively charged quaternary ammonium of ACh (see **Figure 4**). This molecule located itself at all subunit interfaces. **Table 3** shows all the residues identified by Brejc *et al.* (2001) to be within the binding pocket and in close proximity to the HEPES molecule. Particular residues within the binding pocket will affect the affinity of some ligands more than others, depending on the structure of the ligand. Indeed, considerable amounts of data have discerned different binding interactions for different ligands within the same receptor, as well as the same ligands within different species of the same subtype, reflecting that subtle alterations to certain residues can modulate binding characteristics. This data will be drawn upon in later chapters.

Table 3: Amino acid residues identified by Brejc *et al.* (2001) as forming the binding pocket of Ls-AChBP and potentially interacting with HEPES, including the aligned residues of other LGICs. Those residues identified as making contact with HEPES are in bold. Residues marked (*) have also been identified by Celie *et al.* (2004). Residues marked (#) have been identified by Celie *et al.* (2004) only. F226 has been identified as an important aromatic residue for binding and function in 5-HT_3Rs, but due to a low fidelity alignment in this region, is difficult to assign to homologous residues.

1.9.2 The LGIC aromatic box

The structural data provided by the AChBP drew attention to an 'aromatic box' of residues that surround the HEPES molecule, provided by both principal and complementary subunits. Subsequent alignments and biochemical testing has identified homologous aromatic residues within other members of the receptor family (see **Table 4**). Due to the universal nature of this aromatic box within the LGIC family, it is likely that these aromatic residues form a core set

of amino acids integral to the binding of all ligands. Indeed, even before the AChBP crystal structure, biochemical experiments on aromatic residues of LGICs had discerned that these residues were important components of the binding pocket: of the 9 tryptophan residues in the 5-HT_{3A}R LBD, only W60 was found to be inconsequential to ligand binding or expression (Spier & Lummis, 2000), the remainder were determined to be essential for correct subunit folding/assembly or play an integral role in ligand binding.

Aromatic residues can make very strong non-covalent interactions by virtue of their delocalised cloud of π-electrons, as well as making hydrophobic interactions with the hydrophobic groups of ligands, such as the methyl groups of a quaternary ammonium. The electrostatic interactions include π-π and cation-π (Dougherty, 1996). For a π-π interaction to occur, two aromatic residues are stacked so that their π electron clouds interact. Cation-π interactions occur when a positively charged group, such as that of a quaternary ammonium, interacts with the π electrons of the aromatic residue. Within all LGICs, an aromatic residue exists, normally adopting a central location within the binding pocket, which forms a strong cation-π interaction, integral to all ligand binding (see **Table 4**). Non-conservative mutagenesis of this residue will ablate binding (Yan *et al.*, 1999) and unnatural mutagenesis can reduce ligand affinity relative to the extent of disturbance to the π-electron cloud; a finding, so far, consistent for all LGICs.

			Loop		
Receptor	**A**	**B**	**C1**	**C2**	**D**
nAChR	Y93	**W149**	Y190	Y198	W55
Ls-AChBP	Y89	**W143**	Y185	Y192	W53
5-$HT_{3A/B}$R	E129	**W183**	F226	Y234	W90
MOD-1	C120	Y180	Y221	**W226**	F83
$GABA_A$	**Y97**	Y157	F200	Y205	F65
$GABA_C$	F138	**Y198**	Y241	Y247	Y102

Table 4: Amino acid residues comprising the aromatic box of Cys-loop receptor family members. The C1 and C2 loop refer to residues within the C-loop with their α-carbon positioned either closest to the channel lumen (C1) or extracellular matrix (C2). Residues in bold type are those identified as contributing the to main cation-π interaction.

1.9.3 The 5-HT_3R aromatic box

In the principal subunit of the 5-HT_3R, the major cation-π interaction corresponds to W183 (Yan *et al.*, 1999; Beene *et al.*, 2002), which is located centrally in the B-loop, and is considered as the strongest of all molecular interactions within receptor-ligand complexes (Beene *et al.*, 2002). Although W183 has this central role in the ligand binding aromatic box, other aromatic residues contribute major interactions with the ligands, to affect either their affinity or the subsequent opening of the channel.

Residue Y234, within the C-loop, also has the potential to make cation-π interactions. Indeed the equivalent residue of MOD-1 has demonstrated such an interaction (see **Table 4**). However, because this cation-π interaction is attributable to W183 (Beene *et al.*, 2002), Y234 is more likely to make aromatic stabilising interactions, and no hydrogen bonding contributions to binding (Beene *et al.*, 2004; Price & Lummis, 2004). D-loop residue W90 (Spier *et al.*, 1999; Yan *et al.*, 1999) and F-loop residue W195 (Spier & Lummis, 2000) have proven to be essential for binding; as are tyrosine residues Y141, Y143, Y153 (E-loop, Venkataraman *et al.*, 2002) and Y234 (C-loop) (Beene *et al.*, 2004).

Mutagenesis of the E-loop tyrosine residues (Venkataraman *et al.*, 2002) highlights the role of hydrogen bond formation and dissolution, orchestrated by numerous residues of the complementary subunit. These transient hydrogen bonding opportunities are the predominant interaction of the complementary subunit (Celie *et al.*, 2004), compared to the π-π, cation-π and hydrophobic interactions of the principal subunit, probably reflecting a more functional role for complementary subunits, as has been demonstrated for the AChR (Ohno *et al.*, 1996) and the $GABA_AR$ (Mihic *et al.*, 1994). Significantly, movement of the E-loop is likely to impact upon the adjacent Cys-loop (of the same subunit), which plays a role in communicating conformational changes of the LBD to the channel (Chakrapani *et al.*, 2004; Jha *et al.*, 2007).

1.9.4 A general binding mechanism

Using the multitude of AChBP crystallography structures, homology modelling, ligand docking and molecular dynamics simulations, it has been possible to piece together a list of most likely binding events occurring at the 5-HT_{3A} homomeric receptor. The current consensus regarding the binding mechanism involves the attraction of the 5-HT primary amine group to the relatively static W183 residue, located centrally in the binding pocket, to form a cation-π interaction. This part of the mechanism has been described as a 'wedge' (Mu *et al.*, 2003), referring to the lack of multiple, specifically placed residue interactions seen in

the familiar lock and key mechanism of enzymes. Antagonists, specifically granisetron, are believed to make π-π interactions with Y234 and W183 via its aromatic group, while its tropane ring makes other significant interactions with W90 and F226 (Beene *et al.*, 2004; Maksay *et al.*, 2004; Price & Lummis, 2004). Such a comprehensive set of data regarding the binding mechanism does not yet exist for the heteromeric 5-$HT_{3A/B}$ receptor, and although it is assumed to share commonalities with the homomer, variation to this proposed mechanism remain to be examined.

1.10 Channel Opening Mechanism

The 5-HT_3 receptor has been shown to maintain its cation conducting function equally well when expressed as a chimera containing the N-terminal LBD of either AChBP (Bouzat *et al.*, 2004) or α7-nAChR (Eisele *et al.*, 1993). These chimeras not only demonstrate the presence of the binding site in the extracellular domain by having the pharmacological profile pertaining to the N-terminal receptor portion, but also show that a common circuitry exists between ligand binding and channel opening. The rapid opening of the receptor channel, 40 Å from the ligand binding event, involves the movement of the TM2 channel-lining helix, causing a disruption in the electrostatic interactions that maintain the hydrophobic girdle. Disregarding whether the TM2 helix is pushed, pulled or twisted (Unwin *et al.*, 2002; Kash *et al.*, 2003; Miyazawa *et al.*, 2003; Reeves *et al.*, 2005; Cheng *et al.*, 2006), it ultimately requires the efficient communication from the LBD to TM2.

1.10.1 The LBD, Cys-loop, β1-β2 and β8-β9

Figure 9a shows how the TM2 α-helix protrudes from the plasma membrane by two turns (Bera *et al.*, 2002; Miyazawa *et al.*, 2003) and the TM2-TM3 linker region comes tantalisingly close to certain residues of the LBD, which makes this complex of loops a potential site of LBD-ICD communication. The β1-β2 and Cys-loop residues straddle the TM2-TM3 linker (**Figure 9b**), making rotations of these LBD loops likely to impinge upon TM2 and ultimately the channel gate (Reeves *et al.*, 2005). Unlike the β1-β2 loop and Cys-loop, the β8-β9 loop does not interdigitate with the TM2-TM3, though some of its hydrophobic core facing residues can contact amino acid side chains from the Cys-loop, β1-β2 loop and possibly M2-M3 (**Figure 9b**). It is also possible for the β8-β9 loop to make contact with β1-β2 loop from the neighbouring subunit (**Figure 9c**). In the AChBP/5-HT_{3A} chimeric receptor, all three of these loops required amino acid exchanges for those residues aligned in the 5-HT_{3A} subunit in order to create a functional receptor (Bouzat *et al.*, 2004),

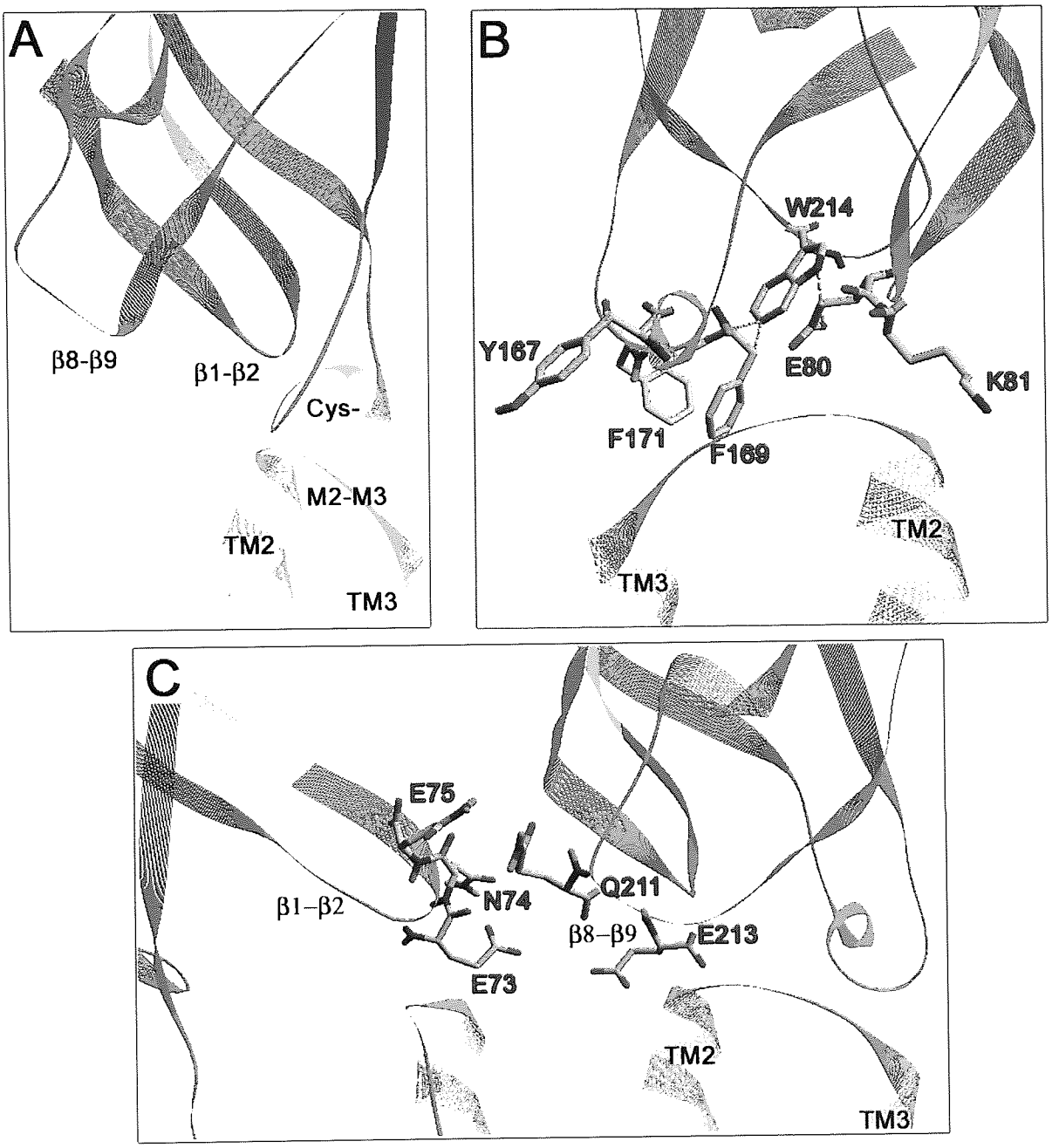

Figure 9: The location of amino acids of the LBD descending loops that are closely associated with residues of the TM2-TM3 loop. Colours indicate putative binding-loop regions, as described in Figure 2 (Yellow = D-loop, Pink = B loop, and Blue = F loop). *(A)* The Cys-loop (Cys) is shown closest to TM3, β1-β2 is closest to TM2, and β8-β9 is the loop furthest away from both TM3 and TM2, as viewed parallel to the lipid bilayer from the extracellular side. *(B)* Amino acid residues of the loops, predicted to extend towards the M2-M3, as viewed parallel to the lipid bilayer, from the luminal side. Residues of β1-β2 and the Cys-loop appear to straddle TM2-TM3. *(C)* The β8-β9 loop residues which are predicted to interact with residues from the β1-β2 loop.

thus demonstrating the compatibility required between the LBD and the TM2-TM3 loop of different receptors.

1.10.2 The TM2-TM3 linker

There is a high degree of sequence similarity in the TM2-TM3 linker, between 5-HT_3R and nAChR. Extensive studies of this region have demonstrated its involvement in the opening of the channel in 5-HT_{3A}R homomers (Deane & Lummis, 2001), glyR (Lynch *et al.*, 1997), nAChRs composed of different subunits (Campos-Caro *et al.*, 1996; Rovira *et al.*, 1998; Rovira *et al.*, 1999), and $GABA_A$R (Davies *et al.*, 2001; Kash *et al.*, 2003). Movement of the α-carbon backbone in this region could be responsible for modulating the orientation of TM2. Indeed, the *cis/trans* isomerisation state of P308, a conserved proline in the TM2-TM3 linker of the mouse 5-HT_{3A}R homomer, has been shown to affect the opening rate of the channel (Lummis *et al.*, 2005). It was concluded that P308 made receptors non-functional when in the *trans* conformation, thus making *cis/trans* isomerisation a mechanism for modulating the opening of the ion channel. However, the low sequence identity with other LGICs, particularly $GABA_A$R subunits, in the TM2-TM3 and LBD loops (β1-β2 and Cys), make this specific mechanism unlikely to be universal throughout the LGIC family. Furthermore, the isomerisation of proline is thought to be a slow process (Lummis *et al.*, 2005), and would not be compatible with the much faster gating kinetics of nAChRs, unless a further mechanism exists to catalyse the *cis/trans* isomerisation process.

1.11 Clinical implications of 5-HT_3Rs

As previously discussed, 5-HT_3Rs are located in a number of distinct brain regions. In addition, their presynaptic location in different neurones also enables the regulation/modulation of different neurotranmitters being released: dopamine in rat striatum (Blandina *et al.*, 1989), nucleus accumbens (Carboni *et al.*, 1989; Chen *et al.*, 1991; De Deurwaerdere *et al.*, 1998), olfactory tubercle (Zazpe *et al.*, 1994); ACh in the hippocampus (Consolo *et al.*, 1994), cerebral cortex (Maura *et al.*, 1992); cholecystokinin from nucleus accumbens and cerebral cortex (Paudice & Raiteri, 1991); GABA in hippocampal interneurones and synaptosomes (McMahon & Kauer, 1997; Katsurabayashi *et al.*, 2003; Turner *et al.*, 2004), and the denatate gyrus (Kawa, 1994); and glutamate in the nucleus tractus solitarius (Glaum *et al.*, 1992). Such diversity actually obfuscates the therapeutic uses of drugs targeting the 5-HT_3R. The exhaustive list of potentially treatable illnesses, based on 5-HT_3R location and behavioural studies, is outside the scope of this thesis, but usually

includes: anxiety (Costall *et al.*, 1993), psychosis (Zoldan *et al.*, 1995), memory dysfunction (Domeney *et al.*, 1991; Staubli & Xu, 1995), fibromyalgia (Spath, 2002; Seidel *et al.*, 2007) and alcoholism (Sellers *et al.*, 1992; Jones & Blackburn, 2002; Costall & Naylor, 2004). Contrary to this list, the universal clinical use of 5-HT_3R antagonists remains the same as 17 years ago; treating chemotherapy/radiotherapy induced nausea and vomiting (CINV/RINV) or post-operative nausea and vomiting (PONV). The treatment of irritable bowel syndrome (IBS) is also becoming an established clinical use of potent 5-HT_3R inhibitor (Houghton *et al.*, 2000; De Ponti & Tonini, 2001).

1.11.1 Antiemetic drugs

Nausea and vomiting are a conferred evolutionary advantage, designed to minimise damage caused by exposure to toxic substances, usually ingested. This is achieved by evacuating the stomach of its contents, often preceded by a nauseous feeling and retching, which prevents further ingestion of toxins. This mechanism becomes a disease when it is involuntarily activated in response to therapeutic drugs. Nausea and vomiting are still clinically significant side-effects of cancer chemotherapy and radiotherapy (Gan *et al.*, 2003). Chemotherapy regimens often have to be tapered to reduce side effects (reduced appetite and dehydration), often at the cost of their therapeutic benefit. The debilitating effects of CINV mean that compliance to chemotherapy regimens is also affected. Anticipatory nausea and vomiting alone, are thought to result in up to 25% of patients refusing chemotherapy treatment (Morrow *et al.*, 1996).

The peripheral mechanism of emesis begins in the stomach, jejunum and ileum, which contain mechano- and chemoreceptors that respond to problems with gastrointestinal motility (mechanical distortion, blockages, tears etc.) and presence of toxic substances respectively. The activation of these receptors triggers the release of 5-HT from enterochromaffin (EC) cells in a positive feedback mechanism. Chemotherapeutic agents damage the mucosa of the small intestine, causing EC cells to release 5-HT (Schworer *et al.*, 1991). Whatever the mechanism of 5-HT release, its function is the same: to activate enteric neuron action potentials in vagal afferent neuronal pathways, including 5-HT_3Rs involved in the emetogenic response (Balfour & Goa, 1997). These neurones terminate in the chemoreceptor trigger zone (CTZ) of the brainstem, located in the area postrema of the 4th ventricle. Its location outside the blood-brain barrier means that it too can respond to toxins, in addition to vagal afferent input, either from the cerebral spinal fluid (CSF) or the blood (Habib & Gan, 2003). It is believed that stimulation of the CTZ by anaesthetics, narcotics and reversal agents (drugs that

accelerate the recovery from anaesthesia) is responsible for PONV. The efferent part of the emetic reflex is initiated in the medulla oblongata, within a non-distinct anatomical site known as the vomiting centre (VC), due to this region containing many converging neuronal pathways transducing vomiting impulses. When activated, the VC induces vomiting via stimulation of the abdominal, pharyngeal, and gastrointestinal muscles, as well as the pre-emptive stimulation of salivary and respiratory centres. Inputs to the VC are not only from vagal sensory pathways and CTZ, but also from the vestibular apparatus, higher centres of the cortex and intracranial pressure receptors. The multiplicity of neuronal inputs means that preventing emesis cannot be achieved by simple 5-HT_3Rs blockade. Indeed, it has been shown that receptor antagonists of histamine, acetylcholine, dopamine, adrenaline and substance P, all have varying degrees of anti-emetic effect (Herrstedt, 2004).

Granisetron, ondansetron, dolasetron and tropisetron are known as the first generation 5-HT_3 receptor antagonists. These have long formed the first-line antiemetic therapy for moderately to highly emetogenic chemotherapy (Costall & Naylor, 2004). Prior to 5-HT_3R antagonists, drugs such as the benzamides (metoclopramide), antihistamines (diphenhydramine), anticholinergics (scopolamine), phenothiazines (promethazine and perphenazine) and butyrophenones (droperidol) were used as antiemetic treatments, producing significant side effects, most notably sedation and hypotension. Contrastingly, granisetron is highly selective for 5-HT_3Rs, having little or no affinity for dopaminergic, adrenergic, benzodiazepine, histaminic, or opioid receptors (Blower, 1995). This specificity affords fewer reported side effects (headache, dizziness and constipation), when compared to the other classes of drugs mentioned. However, 5-HT_3R antagonists are by no means a panacea; one in three patients are still reported to suffer from CINV or PONV, despite taking antiemetics (Rubenstein, 2004). This is because, in spite of 5-HT_3R antagonists being supremely efficacious at preventing acute CINV (nausea and vomiting occurring within 24 hours of chemotherapy), they are disappointingly poor at preventing delayed CINV (occurring between 24 and 72 hours after chemotherapy) caused by cyclophosphamide chemotherapy treatment (Tavorath & Hesketh, 1996). Experiments on a variety of animal models has confirmed this limitation (Bountra *et al.*, 1996; Tavorath & Hesketh, 1996; Hickok *et al.*, 2005). New 5-HT_3R antagonists such as palonosetron have been developed to address this problem (Hesketh, 2004), and show signs of improvement over those drugs of the first generation (Eisenberg *et al.*, 2003; Gralla *et al.*, 2003). However, due to the multifactorial nature of CINV/PONV previously discussed, combination therapy is preferred to the sole use of 5-HT_3R antagonists (Gan *et al.*, 2003). Combination therapy with any of the first generation 5-HT_3R antagonist

and dexamethasone (a corticosteroid) has consistently shown better control of acute emesis from CINV and PONV (*TIGfAR*, 2000; Navari, 2003), as well as modest improvements in delayed emesis compared to the use of a 5-HT_3R antagonist alone, although the improvement was no better than dexamethasone therapy alone (Navari, 2003). A new line of defence against CINV and PONV is the drug aprepitant. It is an antagonist to the neurokinin-1 (NK-1) receptor, for which substance P is its natural agonist. Where 5-HT_3R antagonists fail, aprepitant succeeds, by being effective at preventing delayed emesis (Dando & Perry, 2004; Navari, 2004). Aprepitant is now recommended for use in triple therapy antiemetic regimens, combined with dexamethasone and a 5-HT_3R antagonist.

1.11.2 Irritable bowel syndrome

5-HT_3Rs are implicated in the peristaltic reflex in the small intestine (Neya *et al.*, 1993; Yuan *et al.*, 1994) and colon (Kadowaki *et al.*, 1996), and are thought to work synergistically with nicotinic and 5-HT_4 receptors. Also, increased luminal pressure probably activates 5-HT_3Rs, which modulate 5-HT secretion by EC cells (Gebauer *et al.*, 1993).

Serotonin has long been implicated in influencing gut motility, with more recent evidence suggesting it is the 5-HT_3R that specifically alters bowel movements (Humphrey *et al.*, 1999). As such, 5-HT_3Rs have become a clinical target for the treatment regimes of irritable bowel syndrome (IBS, Gershon, 1999; Hansen, 2003). Compared to their use as antiemetics, it has taken much longer to harness the properties of 5-HT_3R antagonists for the treatment of gastrointestinal problems. The complication in this respect has been the initial lack of a clearly defined disease. Even though work on irritable bowel syndrome dates back to the early 1970s (Edmonds, 1970; McHardy, 1971; Campobasso, 1972), its aetiology has remained an enigma. IBS sufferers present symptoms of irregular bowel movements that can fluctuate from constipated to diarrhoeal, generally experiencing abdominal pain and bloating, which is often relieved after defecation. IBS is classified as a functional disorder of the gut, which means there is no organic or structural cause. Although guidelines have been introduced (Rome III guidelines) that characterise the symptoms of IBS (Vanner *et al.*, 1999), a diagnosis requires all other aetiologies, such as inflammatory bowel disease, Crohns disease, cancer, intolerances and allergies, to be eliminated. These are known as 'red flags' and alert the physician to an alternate diagnosis. IBS is further subdivided into various clinical forms which depend upon predominant symptoms: diarrhoea predominant IBS (IBS-D), constipation predominant IBS (IBS-C), alternating stool pattern IBS (IBS-A), and IBS caused by an infectious agent (IBS-I).

So far, 5-HT_3R antagonists such as ondansetron and alosetron have only been clinically effective at treating IBS-D in women. Such drugs do not affect normal gut motility, but have been shown to delay transit times in the small intestine (Clayton *et al.*, 1999) and colon of humans and rats (Houghton *et al.*, 2000) with abnormally high intestinal propulsion (De Ponti & Tonini, 2001). The mode of action of such antagonists in the peripheral population of 5-HT_3Rs maybe two-fold: i) inhibition of visceral sensitivity to distending stimuli therefore increasing compliance, and ii) inhibiting the ascending and descending 5-HT_3R mediated neuronal pathways involved in peristalsis. The effect of both of these actions results in a slowed transit time. Sadly, alosetron has proved too effective in slowing gut motility, causing severe constipation in some patients, and due to possible links with ischemic colitis (Chang *et al.*, 2006; Gallo-Torres *et al.*, 2006), the drug is only suitable for use in severe IBS-D.

1.11.2.1 The clinical future for 5-HT_3R drugs

5-HT_3R antagonists remain a stalwart of antiemetic treatment, but are losing ground to new drugs that target alternative receptor systems. There is no doubt that 5-HT_3Rs influence an array of CNS processes, but the notion that one 5-HT_3R antagonist alone will offer effective treatment of a CNS disorder must be dispelled if further progress with treatment regimes is to be made. Combination therapy, using drugs that target different neuronal systems, but synergistically affect the same brain region, is the more realistic path to alleviate psychoses, anxiety, memory dysfunction etc.

All clinically used 5-HT_3R drugs are currently antagonists based on a chemical structure that confers nanomolar affinity for the same ligand binding site, with modest improvements in affinity and pharmacokinetics being made in each successive generation. In truth, until 5-HT_3R drugs are designed to target parts of the conformational wave other than the traditional ligand binding pocket, very little additional therapeutic value can be added to those drugs currently available.

Why are there no drugs targeting a 5-HT_3R allosteric binding site? Allosteric sites certainly exist for ethanol (Lovinger, 1999), trichloroethanol (Downie *et al.*, 1995), 5-Hydroxyindole (van Hooft *et al.*, 1997) and general anaesthetics (Parker *et al.*, 1996b). Indeed, it is suspected that PONV is caused by the allosteric potentiation of 5-HT_3Rs by the general anaesthetics used prior to the operation (Barann *et al.*, 2000). Although there are no specific details regarding the allosteric site location, current evidence proposes that the mechanism of this potentiation involves the enhancement of channel gating, rather than ligand binding.

Furthermore, the introduction of 5-HT_{3B} subunits dramatically reduces the extent of potentiation by general anaesthetics (Solt *et al.*, 2005) and ethanol (Hayrapetyan *et al.*, 2005). If drugs can be designed to antagonise allosteric 5-HT_3R sites, this would lead to further advancements in the battle against PONV and alcohol dependence.

Further investigation into the role of corticosteroids and sex hormones on the effectiveness of 5-HT_3R antagonist drug treatment is also required. In spite of established links between gender and numerous emetogenic responses, including the responsiveness to 5-HT_3R antagonists for IBS (Camilleri *et al.*, 1999), risk factors for CINV/PONV (Schnell, 2003), morning sickness and cyclical vomiting syndrome (Lindley & Andrews, 2005), there is still a paucity in the literature regarding the molecular interactions of steroid-base molecules and how they allosterically potentiate 5-HT_3Rs (Wetzel *et al.*, 1998) or affect their expression patterns. Investigation of the allosteric sites in the heteromer will be essential to explain the influence of subunit composition of the level of potentiation. This emphasises the requirement for determining the stoichiometry of the heterologously expressed 5-$HT_{3A/B}$R.

1.12 Aims of the present study

There is currently a gap in the literature regarding the contribution that residues of the h5-HT_{3B} subunit make towards the pharmacology and function of heteromeric 5-HT_3Rs. The present study was designed to explore characteristics of ligand recognition in the 5-$HT_{3A/B}$ receptor binding site.

There were four main aims of the study:

1) Delineate the stoichiometry and arrangement of 5-HT_{3A} and 5-HT_{3B} subunits within the 5-$HT_{3A/B}$R heteromeric receptor, using atomic force microscopy (AFM).

2) Integrate the AFM results with structures of AChBP and nAChR to create a homology model of the heteromeric 5-$HT_{3A/B}$R.

3) Mutate and express (with 5-HT_{3A} subunits) the 5-HT_{3B} subunit as 5-$HT_{3A/B}$Rs. Determine the pharmacology of these receptors using radioligand binding, and further probe functional differences using electrophysiological techniques.

4) Using the homology model and mutagenesis results, determine the contribution of 5-HT_{3B} subunit LBD residues to the pharmacology and function of heterologously expressed 5-$HT_{3A/B}$Rs.

Chapter 2: Materials and Methods

2.1 Materials

2.1.1 Radioligand binding

[^{3}H]GR65630 (3-(5-methyl-1H-imidazol-4-yl)-1-(1-[3H]-methyl-1H-indol-3-yl)-1-propanone) with a typical specific activity of 75.5 Ci/mmol, was purchased from New England Nuclear. [9-methyl-^{3}H]BRL-43694, with a typical activity of 69.5 Ci/mmol, was purchased from PerkinElmer (Beaconsfield, U.K.) Serotonin hydrochloride (5-HT), metoclopramide and HEPES were purchased from Sigma-Aldrich; Granisetron (endo-N-(9-methyl-9-azabicyclo[3,3,1]non-3-yl)-1-methyl-indazole-3-carboxamide) was a generous gift from Glaxo Group Research, and was dissolved in a minimum volume of ethanol and diluted with HEPES buffer (10 mM).

2.1.2 Molecular biology

cDNA clones for the h5-HT_{3A} and h5-HT_{3B} subunits were generous gifts from Dr. E. Kirkness, TIGRA, Maryland, USA. As well as using wildtype untagged 5-HT_3 subunits, both constructs were engineered to express His_6 (six consecutive histidine residues) and Myc, or His_6 and V5 epitope tags at the C-termini, henceforth referred to as 5-$HT_{3A(myc)}$ and 5-$HT_{3B(V5)}$ (see **Figure 10**). This engineering was carried out by Dr. M. Davies, Department of Pharmacology, University of Alberta, Edmonton, Alberta, Canada, who generously provided the constructs for these studies. Both constructs were inserted into pcDNA3.1 (Invitrogen). Boric acid, ethylenediaminetetraacetic acid (EDTA, disodium salt), ampicillin (sodium salt, powder), tris base (2-Amino-2-(hydroxymethyl)-1,3-propanediol), yeast extract (Cat. No. 70161), peptone (from casein pancreatic digest) and agar (Cat. No.:05039) were purchased from Sigma-Aldrich; ethidium bromide solution (Gibco) was mixed with molten agarose before gel casting, at a concentration of ~0.5 $\mu g/ml^{-1}$; calf intestinal alkaline phosphatase and all restriction enzymes were purchased from New England Biolabs (NEB); T4 DNA ligase was purchased from Promega. The DNA polymerase Accuzyme™, dNTPs, agarose (molecular biology grade) and HyperLadder I (molecular weight ladder) were purchased from BioLine; QiaQuick™ PCR Purification and QiaQuick™ Gel Extraction kits (Qiagen) were used for the purification of PCR products and restriction endonuclease digested cDNA; GenElute™ mini-prep kits (Sigma-Aldrich) were used for the amplification and isolation of plasmid DNA from small volumes (2-5 ml) of transformed bacterial suspensions;

Figure 10: Epitope tagging of 5-HT$_{3A}$ and 5-HT$_{3B}$ receptor cDNA. Receptor sequence is underlined, pcDNA3.1 sequence is highlighted in grey. 5-HT$_{3A}$ subunit contains a Myc tag (highlighted in yellow), 5-HT$_{3B}$ subunit contains a V5 tag (highlighted in yellow), and both contain a His$_6$ tag (six consecutive histidine residues, in pink).

Amplification of plasmids for transfection was carried out using the high purity plasmid maxiprep system (Marligen Biosciences, Inc, Ijamsville, MD, USA).

2.1.3 Cell culture

Dulbecco's modified Eagles medium (DMEM) and antibiotic-antimycotic supplement were purchased from Gibco; foetal bovine serum (FBS) was purchase from Hyclone; TSA201 cells were purchased from the European Collection of Cell Cultures (ECACC); HEK293 cells were a gift from Dr. D. Poyner (Aston University, Birmingham); T75 and T175 cell culture flasks (Nunc) were used for cell maintenance and 150mm x 20mm cell culture plates (Corning) were used for transfecting cells.

2.1.4 Cell transfection

BES (N,N-Bis(2-hydroxyethyl)-2-aminoethanesulfonic acid) was purchased from Sigma-Aldrich, sodium chloride from BDH and disodium phosphate from Mallinckrodt Baker (Phillipsburg, NJ, USA); Benzamidine, bacitracin, soybean trypsin inhibitor and PMSF (phenylmethylsulfonyl fluoride), contained within the protease inhibitor cocktail, were purchased from Sigma-Aldrich. Protein concentration determinations used a bicinchoninic acid assay kit (Sigma-Aldrich) containing bicinchoninic acid and $CuSO_4$.; bovine serum albumin (BSA) was used as the protein standard.

2.1.5 SDS-PAGE and Western blotting

Acrylamide/bis-acrylamide (30% Solution), tris-HCl, SDS (sodium dodecyl sulphate), ammonium persulphate, TEMED (N,N,N',N'-tetramethylethylenediamine), glycerol, bromophenol blue were all purchased from Sigma-Aldrich; antibodies towards epitope tags c-Myc (Cat.No.:R950-25) and V5 (Cat. No.:R960-25) were purchased from Invitrogen, and His$_6$ antibody (Cat. No.: 27-4710-01) was purchased from Amersham; goat raised anti-mouse IgG (Fab specific) antibody conjugated to horseradish peroxidase (HRP), phosphate buffered

saline (PBS, Cat. No. P4417), and Tween® 20 were purchased from Sigma-Aldrich; western blot visualisation was madepossible by HRP detection using SuperSignal® West Pico Chemiluminescent Substrate (Pierce) and ECL Western Blotting Substrate (Pierce); developer and fixer chemicals (Jessops, U.K.) were used for the development of exposed Hyperfilm™ (GE Healthcare).

2.2 Methods

2.2.1 Restriction enzyme digests

Restriction site profiles were generated using REBASE™ (Roberts *et al.*, 2007), which was located within the computer program BioEdit v7.0.5.2 (Hall, 1999). Restriction digests of plasmid or PCR amplified cDNA, were performed according to the manufacturers' recommended protocols. Double digests were used if activity of both enzymes was maintained within an appropriate buffer; this was verified using the 'double digest finder' function on the NEB website. Increases in enzyme concentration or incubation times were required for problematic mutants. Complete digestion of the DNA target was verified by running the sample on a 1% agarose gel in TBE buffer (50mM Tris-borate, 0.5mM EDTA, pH 8.0) containing 0.5μg/ml ethidium bromide, and observing the restriction profile for bands of correct size (measured in kilobase pairs, kb). Samples were mixed in a 5:1 (v/v) ratio with DNA loading buffer (0.25% (w/v) bromophenol blue, and 30% (v/v) glycerol) before being loaded onto a 1% agarose gel. Gel electrophoresis of the samples was performed using a Bio-Rad submerged horizontal gel system. For a small gel (7 x 10 cm), the voltage was set to approximately 80mV for 50 minutes. For a large gel (15 x 20 cm), the voltage was 170mV for 90 minutes approximately. DNA fragments were visualised under ultraviolet-light on a transilluminator.

2.2.2 Ligation Reactions

Ligation reactions were not required for mutagenesis using the QuickChange™ kits, but were necessary for mutagenesis using the overlap extension method. Ligation reactions were performed in 0.5ml micro-centrifuge tubes. The total DNA concentration depended upon the application and its difficulty, but was within the range 100-200ng in a total volume of 20 μl. Cut/phosphatase-treated plasmid was gel purified (this could be stored at -80°C) for use in ligations. The DNA concentrations of plasmid and insert were estimated by visualisation on a 1% agarose gel, and subsequently mixed at a ratio of 3:1 according to **Equation 1.**

$$\text{Vector (ng)} \times \frac{\text{Insert (kb)}}{\text{Vector (kb)}} \times \frac{\text{Insert (M)}}{\text{Vector (M)}} = \text{Insert (ng)}$$

Equation 1: Calculation for the quantity of insert required for ligation with a known quantity of vector. The insert (M)/Vector (M) ratio was 1:3 in these experiments.

Overlap extension mutagenesis required ~60 ng of vector to ~50 ng of insert, 2 Units of T4 DNA ligase, 2 µl of 10X ligase buffer (thoroughly mixed by vortexing prior to use), and addition of ddH_20 to a final volume of 20 µl. The reaction was incubated at either 16°C for 16 hours or 22°C for 2-4 hours, although shorter incubation times at this temperature were successful. After incubating, the correct product was confirmed on a 1% agarose gel and the ligation reaction diluted 1:4 with sterile water and promptly stored at -20°C.

2.2.3 Bacterial transformation

Competent bacterial cells were made using standard protocols (Maniatis *et al.*, 1987). Aliquots of 200 µl of these cells were stored in 1.5ml microcentrifuge tubes at -80°C. The diluted ligation reaction was added to 200µl of ice-cold competent cells (thawed on ice), incubated on ice for 30min, heat shocked at 42°C for 90 seconds and then incubated on ice for a further 2 minutes. Competent cells were also transformed with cut and phosphatase treated pcDNA3.1(+), but no ligase treatment, as a negative control to later determine the likelihood of successful recombinant ligations. When using XL10 Gold supercompetent cells from QuickChange™ mutagenesis kits, the heat-shock protocol provided by the manufacturer was followed (Stratagene, La Jolla, California). Transformed bacterial cells were added to 1 ml of pre-warmed (37°C) broth (0.5% (w/v) NaCl, 1% (w/v) peptone, 0.5% yeast extract, 12.5mM $MgCl_2$, 12.5mM $MgSO_4$, 20mM glucose), and subsequently incubated at 37°C for 1hr with shaking at ~300rpm. Cells were centrifuged at 2000 rpm for 5 min, in order to sediment them with minimum structural damage. Supernatant was removed from each tube to allow resuspension (by gentle trituration) in ~100µl of remaining broth. Each transformed bacterial cell suspension was pipetted onto the surface of separate agar-ampicillin plates (0.5% (w/v) NaCl, 1% (w/v) peptone, 0.5% yeast extract, 1.5% agar, 100µg/ml ampicillin), distributed evenly across the surface with a sterile spreader, and incubated (lid face-down) at 37°C overnight. Individual colonies were selected by touching them with a sterile P20 pipette tip and inoculating ~10ml of Luria broth (0.5% (w/v) NaCl, 1% (w/v) peptone, 0.5% yeast extract, 100µg/ml ampicillin). The cultures were grown at 37°C overnight in a shaking

incubator. A GenElute™ kit (Sigma-Aldrich) was used to make a mini-prep of the recombinant plasmids, following the instructions provided with the kit. Plasmid cDNA from the mini-prep was eluted into 50µl of sterile water, which could be stored at -20°C. Three minipreps of three separate colonies for the same cDNA mutant were analysed by automated sequencing (Genomics Lab, University of Birmingham, U.K). This would usually yield at least one positive result for incorporation of a desired mutation. Bioedit sequence alignment editor v7.0.5.2 (Hall, 1999) was used to analyse sequencing data files. Wildtype sequences were aligned to potential mutants and the complementarity function used to quickly detect the presence of any base mutations. Constructs that were determined to contain the chosen mutation and no random mutations, were amplified using a High Purity Plasmid Maxiprep System from Marligen. This kit was used according to the provided instructions. Spectrophotometric analysis at OD_{260} and OD_{280}, in addition to gel electrophoresis on a 1% agarose gel, was used to determine maxi-prep DNA concentration and purity.

2.2.4 DNA precipitation

After agarose gel analysis or failed PCR/cloning steps, DNA was sometimes 'cleaned' if suspected of being contaminated with impurities. The method of choice was ethanol precipitation, which was also employed for concentrating DNA samples that were too dilute. The DNA sample (in 1.5 ml microcentrifuge tube) was mixed with 0.1 volume of 3M sodium acetate and 2 volumes of ethanol; precipitating the DNA. This was placed on ice for ~20 min and then centrifuged in a bench-top microcentrifuge (Sigma 1-13) at maximum speed for 20 min. The supernatant was carefully aspirated and the DNA pellet (not always visible) washed with 1 ml of 70% ethanol. After carefully aspirating the ethanol, the DNA pellet was air dried for approximately 10 minutes and resuspended by gentle agitation in an appropriate volume of sterile H_2O. This process usually gave a yield of ~80%. GeneClean™ spin kits (Stratagene) were also used for the same purpose with similarly efficient results. They were used as directed by the supplied protocol.

2.2.5 Cell culture

For cell maintenance: cells were used from passage 4-10 and grown in T75 or T175 flasks at 37°C under a CO_2/air atmosphere, in 20ml (T75) or 25ml (T175) DMEM supplemented with 10% FCS and 5% antibiotic-antimycotic, until fully confluent. Prior to subculturing, cell culture medium was removed and replaced with a fresh 10ml volume. HEK293 and TSA201 are a semi adherent cell line and were removed from the surface using 2-3 short/sharp collisions of the flask with the cell culture hood surface. Once in suspension, a 1/20 split into

new flasks would yield cells optimally ready for transfection in two days, and further passaging in 3 days.

2.2.6 Transfection

The transfection technique employed, which proved the most reliable, was a calcium phosphate/BES method (Chen & Okayama, 1987). Typically, eighteen 150 x 20mm plates were transfected when ~80% confluent. Prior to making the DNA/transfection mix, the old media was removed from the plates by aspiration and replaced with fresh (being careful not to dislodge growing cells). A total of 540µg of cDNA was added (30µg per plate) to 9 ml of filter sterilised $CaCl_2$ [250mM]. The quantity and purity of all maxi-prep cDNAs was measured by comparison to the bands produced by loading 5µl of HyperLadder I™ (BioLine) on a 1% agarose gel, which represented known quantities of DNA; the details of which are provided in the data sheet supplied with the DNA ladder. This method of quantification was in addition to standard spectrophotometric readings taken at OD_{260} and OD_{280} (Maniatis *et al.*, 1987). Visualisation on a 1% agarose gel was especially necessary when the cDNA was required for heteromeric receptor expression; this was to ensure equivalent amounts of each subunit were being mixed for transfection. The $CaCl_2$/cDNA mixture was allowed to stand for approximately 2 minutes before adding the BES solution (50mM BES, 280mM NaCl, 1.4mM Na_2HPO_4). The pH of this solution is considered to be critical for optimum transfection efficiencies. Only after it was filter sterilised was the solution adjusted to pH 7.03 and aliquots stored at 4°C. The procedure was carried out at room temperature, which required all working solutions to be kept at room temperature before commencing. This cDNA/$CaCl_2$/BES solution was mixed thoroughly and left to stand for at least 5 minutes before adding 1 ml dropwise to each of the 18 plates. The plates were incubated at 37°C until harvesting after 48-72 hours, dependent upon how healthy the cells appeared from microscopic analysis.

2.2.7 Membrane harvesting

After aspiration of media, 3ml of ice-cold harvesting buffer (10 mM HEPES pH 7.5; 100 mM PMSF, 1:1000 (v/v); benzamidine, 0.15 $mgml^{-1}$; bacitracin, 0.08 $mgml^{-1}$; soybean trypsin inhibitor 0.01 $mgml^{-1}$) was added to each plate and cells removed using a cell scraper and pipetted into a centrifuge tube. More harvesting buffer was added to remove residue cells. Cells were homogenised using an Ultra-Turrax homogenizer, model T-25 (Janke und Kunkel K. G., Bremen, Germany) at 24,000rpm for 10 seconds. This homogenate was centrifuged at 27,000g for 20 min at 4°C, the resultant membrane pellet was resuspended in approximately

15ml of ice-cold resuspension buffer (10 mM HEPES, pH 7.5) and homogenised as before. Nuclei, unlysed cells and cell debris were removed by further centrifugation of the supernatant in a bench-top centrifuge (Sigma 1-13) at 1000g for 10 minutes or at maximum speed for 40 seconds. The supernatant was removed and frozen at -80°C until further use.

2.2.8 Protein assay

Protein concentrations were determined using a BCA kit (Sigma-Aldrich). The standard protocol (Smith *et al.*, 1985) was adapted to fit a 96 well plate format. BCA and $CuSO_4$ were mixed 50:1(v/v). BSA was used as a protein standard at a concentration range of 0-70μgml^{-1}, each concentration being pipetted in triplicate into separate wells of the 96-well plate. Membrane samples were diluted to fall within this protein standard range, and 10µl subsequently added to the 96 well plate, also in triplicate. Each of these wells was also filled with 200µl of $CuSO_4$/BCA mix, and the 96-well plate was incubated at 37°C for 30 minutes. The absorbance of each sample was measured at 562 nm using a 96-well plate spectrophotometer (Dynex; MRX). Protein concentrations were determined using linear regression against the BSA standards used in the same experiment. All data were analysed using Microsoft Excel.

2.2.9 Radioligand binding check

To determine the level of expression for separate transfections, 50µl of membrane preparation was tested for binding with 0.8nM [^{3}H] granisetron or 0.5nM [^{3}H] GR65630 in a total volume of 500ul – diluted using HEPES (10mM). Non-specific binding was determined using 300µM metoclopramide. All binding data points were in triplicate. The assay was incubated at room temperature when using [^{3}H]granisetron or 4°C for [^{3}H]GR65630, both were terminated after 1 hour by rapid vacuum filtration through Whatman GF/B filters, soaked for 2 hrs at 4°C in 0.3% polyethyleneimine (Bruns *et al.*, 1983). During filtration, filters were washed three times with 2 ml of HEPES buffer (10mM, pH 7.5, 4°C), and transferred into scintillation vials, to which 4 ml OptiPhase HiSafe™ 2 scintillant (Perkin Elmer) was added and mixed by shaking. The samples were left to stand for approximately 15 minutes before counting DPM using a Packard, Series 1900 scintillation counter.

2.2.10 Saturation binding

For saturation binding experiments; [^{3}H]GR65630 was used over a concentration range of 0.03-1.3 nM. The volume of membrane used, was that which would sequester 5-8% of the total free ligand at the lowest concentration of radioligand used in the assay. This was an approximate calculation, made from data obtained from the binding check. Nonspecific

binding was determined at each radioligand concentration with 300 μM metoclopramide. All data points were in triplicate. All other aspects of the assay were as per the binding check. The assay was terminated after incubation at room temperature for 2.5 hours.

2.2.11 Competition binding

Radioligand concentrations were: 0.6 nM for [^{3}H]GR65630 and 0.8 nM for [^{3}H]granisetron. Membranes were thawed and resuspended immediately prior to assay. The volume of membrane used was that which sequestered 5-8% of the total radioligand DPM counts at the radioligand concentration used. This was determined for each separate batch of transfected cell membranes. Cold ligands were used at a concentration range of 0.2-32.0 nM, for granisetron and 0.1-16 μM for 5-HT. Other aspects of the assay were identical to the binding check. The assay was terminated after incubation at 21°C for 2.5 hours. It should be noted that when [^{3}H]granisetron and granisetron were used in the same assay, it is technically a homologous competitive binding assay, and was used as such to calculate the K_d and B_{max} of granisetron (see data analysis).

2.2.12 SDS-PAGE

Gels of 0.75 mm thickness were cast using a Bio-Rad casting unit from the Mini-PROTEAN 3 System, following the standard SDS-PAGE protocol of Laemmli (Laemmli, 1970). Protein separation was achieved with a 7.5% separating gel [25% acrylamide/bis-acrylamide, 30% Solution, 400mM Tris-HCl (pH 8.8), 0.1% SDS, 0.1% ammonium persulphate, 0.015% TEMED]. A fresh solution of ammonium persulphate was always used for each set of gels. After pouring the vertical resolving gel, a layer of water-saturated butanol was added dropwise to cover the acrylamide surface in order to decrease polymerisation time and flatten the polyacrylamide meniscus, concomitantly reducing the likelihood of wavy gel bands. After the gel was fully polymerised (~20 minutes) and the butanol removed carefully using filter paper, a 4% stacking gel was pipetted on top [13.3% acrylamide/bis-acrylamide, 30% solution, 132mM Tris-HCl (pH 6.8), 0.1% SDS, 0.1% ammonium persulphate, 0.015% TEMED] and a 10-well comb inserted. Cast gels were assembled in electrophoresis apparatus (Mini-PROTEAN 3, Bio-Rad) and the tank filled with 1 litre of running buffer (25mM Tris-base, 192mM glycine, 3.4 mM SDS). Lanes were washed by trituration with buffer to remove partially polymerised acrylamide, using a gel loading pipette tip and pipette.

Samples were aspirated and expelled through a 21G needle 2-3 times to shear long strands of chromosomal DNA and reduce sample viscosity. For samples with a high protein concentration, the high viscosity not only causes a problem with loading the sample into a

well, but also its subsequent entry into the gel matrix. Receptor samples were mixed at a ratio of 1:1 with SDS loading buffer (250mM tris-HCl, 5% SDS, 25% glycerol, 0.06% bromophenol blue), as was the DualVue™ molecular weight marker (GE Healthcare). All samples were heated to 65°C for 30 minutes and 30 µl promptly loaded into gel lanes. The power supply voltage was set to 100V as samples moved through the stacking gel (20 minutes) and 200V through the resolving gel (1 hour). The gel was electrophoresed at 4°C.

2.2.13 Western Blotting

A Mini Trans-Blot® Cell (Bio-Rad) was used for all western blotting applications. PVDF (polyvinylidene difluoride) membrane (GE Healthcare) was cut to the required size (10 x 6 cm) and pre-soaked in methanol for 2 minutes, rinsed twice with ddH_20, and soaked in transfer buffer [25mM tris-base, 192mM glycine, 1.7mM SDS] until required. Following SDS-PAGE, gels were sandwiched in a blotting cassette with PVDF membrane, blotting paper (Sigma-Aldrich) and cassette sponges (soaked in 5% Decon90® prior to use, to eliminate speckling on developed films), and electorphoresed at 55V for 1 hour at 4°C. The membrane was carefully removed with plastic forceps and incubated in blocking buffer [10mM PBS (2.7 mM potassium chloride and 137 mM sodium chloride, pH 7.4), 0.2% Tween® 20, 5% (w/v) dried milk powder] for 1 hour at room temperature with shaking.

Primary antibodies were diluted with PBS-Tween® 20 (10mM PBS, 0.2% (v/v) Tween® 20). V5 antibody was diluted 1:5000, Myc antibody 1:2000 and His antibody 1:10,000. Incubation of the PVDF membrane took place in polythene pouches. The membrane was laid between 2 polythene sheets (Express Polythene, Digbeth, U.K.), which were subsequently heat-sealed around three edges of the PVDF membrane using a heat sealer (Packer Impulse, P400). This polythene pouch made it possible to use very small volumes of diluted antibody (2-3 ml). PVDF membranes were incubated in primary antibody overnight at 4°C or for at least two hours at 22°C. The membrane was not washed between blocking and primary antibody incubation steps; this allowed a small amount of blocking buffer to enter the primary incubation step, which is intended to reduce non-specific binding. Further to primary antibody incubation, the membrane was subjected to the following washes in membrane wash buffer (10mM PBS, 0.2% Tween® 20): 2 x 1 minute, 2 x 5 minute, 2 x 10 minutes. An additional 3 x 10 minute wash steps were required when using the c-Myc primary antibody, to reduce unwanted nonspecific background. All washes took place in small trays containing at least 50 ml of wash buffer; larger volumes improved washing efficiency. The membrane was incubated in secondary antibody for 1-2 hours, followed by the same washing regime

described previously. Secondary antibody was diluted an order of magnitude greater than the primary antibody used for the same blot. Optimisation experiments involved secondary antibody probing of blotted proteins with no primary, in order to determine the threshold at which the secondary antibody lost its specificity and non-specific binding was evident.

ECL (enhanced chemiluminescence) reagents (Pierce) were mixed according to the supplied manufacturer's instructions. Membranes were placed on overhead projection (OHP) sheets and 3 ml of ECL solution added to the correct membrane surface (that to which the SDS-PAGE gel was touching) and incubated for 5 minutes. PVDF membranes were drained of fluid (but not allowed to dry), placed on a fresh OHP sheet and sandwiched with another OHP sheet on top. Air bubbles were removed by gently rubbing over the surface with a tissue. In a darkroom, Hyperfilm™ (GE Healthcare) was placed on top of the PVDF membrane and the autoradiographic cassette closed. Length of exposure to film and development times were altered according to initial results of a 2 minute exposure. Reagents for film development are detailed in the materials section, and were used according to the provided instructions. An Uvitec chemiluminescence imaging system (UVIchem) was used with some western blots for V5-tagged 5-HT_{3B} subunits that were either chimeric or contained point mutations.

Predictions of subunit molecular weights were made using the 'compute pI/MW' tool on the ExPASY server.

2.2.14 Dot blots

Membrane preparations from HEK293 cells transfected with either the tagged homomer or heteromer were applied to a nitrocellulose membrane (GE Healthcare) in 5µl aliquots, at a range of protein concentrations, before and after solubilisation with either SDS or Triton X-100. Protein spots were allowed to dry at 37°C for 1 hour. After this time, the membrane was blocked, washed, probed with antibodies and developed as per the western blotting protocol, but with varying antibody concentrations. Further details of detergent, antibody and protein concentrations are provided in the results section.

2.2.15 Solubilisation of membranes

Throughout the solubilisation procedure, the pH of buffers was maintained at physiological parameters and temperature was maintained at 4°C, in order to reduce protease activity and conformational changes that could cause receptor inactivation. Membrane preparations and ice-cold solubilisation buffer [20mM HEPES, pH 7.5, 4M NaCl, 0.4% Triton X-100] were combined in a 1:1 ratio and mixed using a Ultra-Turrax homogenizer, model T-25 (Janke und Kunkel K. G., Bremen, Germany) at a minimal revolutions per minute (rpm) setting. Care

was taken to avoid generating foam, a sign of oxidation. It was also important to monitor the total protein being solubilised, as the efficiency of solubilisation decreases if the protein concentration of the membrane preparation exceeds ~3.5 $mgml^{-1}$. As the protein concentration increases, so the detergent concentration should be increased to maintain the same ratio of protein to detergent (Hjelmeland & Chrambach, 1984). This was adhered to by maintaining the protein concentration of membrane preparations to 3.0-3.5 $mgml^{-1}$. Aliquots of the membrane-detergent suspension were rotated using a blood tube rotator (Stuart; SB2) angled at 45° from the horizontal, at 4°C for 1 hour in 15ml pyrex® screw-cap test tubes. Samples were spun in Quick-Seal™ pollyallomer centrifuge tubes (Beckman) at 100,000g for 1 hour at 4°C. Piercing the centrifuge tube from the top, the supernatant could be aspirated into a separate vessel using a syringe attached to a G21 needle and triturated 2-3 times to shear DNA, reducing sample viscosity. The remaining pellet was resuspended in membrane buffer for later analysis.

2.2.16 Buffer exchange and desalting

Soluble receptor samples were immediately applied to equilibrated PD10 columns (with a buffer reservoir, Bio-Rad) to replace the high salt and Triton X-100 concentrations with 'soluble receptor buffer' [10mM HEPES, pH 7.5, 0.1% Triton X-100], which does not contain salt and has a lower Triton X-100 concentration, and therefore does not interfere with radioligand binding. The use of PD10 columns was optimised by testing 16 x 0.5 ml elution fractions in a radioligand binding assay (see **2.2.9 Radioligand binding check**) and increasing the volume of sample added to the column in order to maximise the column capacity. The optimised procedure required loading of 3.5 ml of sample, allowing this to drain by gravity flow to the frit, until adding 4.5 ml of desalting buffer [10mM HEPES, pH 7.4, 0.1% Triton X-100] and collecting the last 4 ml of this eluent. Soluble receptor was not conducive to freeze thawing and could only be stored for a limited time at 4°C (4-5 days) before significant loss of binding occurred.

2.2.17 Increasing eluent concentration

Soluble and affinity purified fractions of the receptor were concentrated using VivaSpin™ 20 centrifugal concentrators with a molecular weight cut off of 30,000 Da (Sartorious, Epsom, U.K.), following the provided instructions. Up to 20 ml of sample was concentrated to an extent that was dependant upon the purpose for which it was required. For affinity purification, samples were concentrated to allow a feasible volume to be incubated with affinity resin. For western blotting, samples were concentrated approximately 50-fold. It was

also possible to de-salt soluble samples using VivaSpin™ 20 concentrators by washing the concentrated sample twice with a volume of soluble receptor buffer that was 20-times the final sample volume.

2.2.18 Affinity purification

HEK293 cells transfected with 5-$HT_{3A(myc)}$ or 5-$HT_{3B(V5)}$ tagged DNA, also expressed a His_6 tag on the C-terminus of the receptor. This property facilitated the purification of soluble receptor preparations using HIS-Select™ HC nickel affinity gel (Sigma-Aldrich). Due to the large volume of protein required, a 'batch' method of purification was employed. Affinity gel slurry was resuspended in its 20% ethanol storage buffer, and 2ml was pipetted into a re-used clean PD10 column to give a 1ml bed volume, after draining the column. Rapid and efficient removal of buffer was achieved by connection of the PD10 column tip to a vacuum filtration system. Effluent could be quickly discarded (equilibration and wash steps) or collected (imidazole elutions) for later analysis. The column gel slurry was twice resuspended in 10 ml ddH_2O, which was immediately washed through the column. The same filtration procedure was used to wash the gel slurry twice with ice-cold equilibration/wash buffer [20 mM HEPES, pH 7.6, 250 mM sodium chloride, 0.2% Triton X-100], leaving the dry equilibrated gel in the PD10 column. The soluble protein supernatant was added to the pre-equilibrated gel and rotated using a blood tube rotator (Stuart; SB-2) at a 15° deviation from the horizontal, for gentle mixing at 4°C for at least 1.0 hour. The affinity gel was filtered, washed and filtered three times with wash buffer, then again with an imidazole wash buffer [20 mM HEPES, pH 6.0, 250 mM sodium chloride, 0.2% Triton X-100, 5 mM imidazole]. Protein was eluted off the column with two washes in increasing imidazole concentrations: 2 x 20 mM, 2 x 50 mM and 2 x 150 mM imidazole in elution buffer [20 mM HEPES, pH 6.0, 250 mM sodium chloride, 0.2% Triton X-100].

2.2.19 Atomic Force Microscopy

This work was carried out by our collaborators at the Department of Pharmacology, University of Cambridge (Barrera *et al.*, 2005). Solubilised receptor samples were run through a PD10 column and buffer was exchanged with 1% (wt/vol) CHAPS (3-[3-cholamidopropyl)dimethylammonio]-1-propanesulfonate) before affinity purification. Samples of affinity purified receptor were either left uncomplexed or incubated for 14 hours at 4°C with a 1:2 molar ratio of antibody, with a sample protein concentration of ~0.2 nM. A 45µl aliquot of diluted sample (protein concentration = ~0.04 nM), either uncomplexed or as antibody-receptor complexes, was adsorbed onto a freshly cleaved poly-L-lysine coated mica

coverslip (Goodfellow, Cambridge, UK). The Myc, V5 and His_6 antibodies were incubated separately with both the 5-$HT_{3A(Myc)}$ homomer and 5-$HT_{3A(Myc)/B(V5)}$ heteromer preparations. The V5 and 5-$HT_{3A(Myc)}$ incubation was used as a negative control to ensure the V5 antibody did not cross-react with the 5-HT_{3A} subunit. The coverslip was washed with MiliQ-water after a 10 minute incubation, followed by drying under nitrogen. Samples were imaged in air using a Multimode atomic force microscope (Digital Instruments, Santa Barbara, CA) with silicon cantilevers (MikroMasch, Portland, OR) used in tapping mode at a drive frequency of ~300 kHz and a specified spring constant of 40 N m^{-1}. A minimal imaging force was applied, the target amplitude was ~1.6-1.8 V and amplitude set-point ~ 1.3-1.5 V.

The molecular volume of the protein particles was determined using **Equation 2** and measurements of particle dimensions derived from AFM images. The particles adopt a 'spherical cap' shape after adsorption onto the mica coverslip, from which the heights and half-height radii were measured from multiple cross-sections of the same particle.

$$V_m = (\pi h / 6)(3r^2 + h^2)$$

Equation 2: For the calculation of molecular volumes based on AFM image data, where *h* is the particle height and *r* is the radius (Schneider *et al.*, 1998).

The molecular volume was also calculated based on molecular mass, using **Equation 3**:

$$V_c = (M_0 / N_0)(V_1 + dV_2)$$

Equation 3: For the calculation of molecular volumes based on molecular mass, where N_0 is Avogadro's number, V_1 and V_2 are the partial specific volumes of particle and water, respectively and *d* is the extent of protein hydration (Schneider *et al.*, 1998).

Previously reported values of partial specific volumes of protein and carbohydrate were used to determine the volume contributions of the core protein and attached oligosaccharides, these values were 0.74 cm^3/g and 0.61 cm^3/g respectively.

2.2.20 Mutagenesis

Designed oligonucleotides were synthesised using the 'custom primers' service offered by Invitrogen. Primers were synthesised at the 25 nmol or 50 nmol scale and purified by standard desalting. Two pairs of non-mutagenic primers were designed towards the vector: pcDNA3.1+S [5'-TCA-ACG-GGA-CTT-TCC-AAA-ATG-TCG-3'], pcDNA3.1+AS [5'-

CCA-GCA-TGC-CTG-CTA-TTG-TCT-TC-3'], T7(s) [CGA-CTC-ACT-ATA-GGG-AGA-CCC-AAG-C-3' and BGH [5'- CCA-GGG-TCA-AGG-AAG-GCA-CGG]. These primers could be used in the sequencing reaction or for mutagenesis applications. Lyophilised oligonucleotides were dissolved in sterile water to give final concentration of $1mgml^{-1}$. Aliquots could be stored at -20°C indefinitely.

The polymerase chain reaction (PCR) was used for both site directed mutagenesis and the production of chimeras. The standard protocol used 5ng of template cDNA (5-HT_{3A}-pcDNA3.1(+), 5-$HT_{3A(Myc)}$-pcDNA3.1(+), 5-HT_{3B}-pcDNA3.1(+) or 5-$HT_{3B(V5)}$-pcDNA3.1(+)), 125 ng of each sense and antisense primer, 0.5 mM DNTPs, 1/10 Accuzyme™ Buffer, 2.5U Accuzyme™ polymerase (BioLine), ddH_2O to 50 µl. Mineral oil was layered on top of the reaction to prevent evaporation. PCR temperature cycling and many of the temperature dependant molecular biology reactions were carried out using a TRIO-Thermoblock™ (Biometra, GÎttingen, Germany)

2.2.21 Overlap extension PCR mutagenesis

Mutagenic primer pairs were designed with complete complementarity, 41-49 bases in length, differing only in 3'-5' orientation (**Table 5**). Melting temperature (T_m) was calculated using **Equation 4**, and the guanine and cytosine content (%GC) was calculated using the nucleotide composition function within Bioedit. The design aimed to keep the %GC at ~40% and T_m ~80°C.

$$Tm = 81.5 + 0.41(\%GC) - 675/N - \%mismatch$$

Equation 4: formula for calculating the melting temperature of primers. N is the primer length in bases and %GC and % mismatch are whole numbers.

The nucleotide base mutations were designed to be contained as close to the centre of the primer as possible. All PCR reactions followed the general protocol previously described. Two separate PCR reactions were used to generate products that were subsequently used as two 3' overlapping halves of template in the next PCR reaction. A pictorial explanation of this technique is provided in **Figure 11**. Each of the two reactions contained a sense mutagenic primer with pcDNA3.1 antisense primer, or an antisense mutagenic primer with pcDNA3.1(s) primer. PCR temperature cycling was achieved using a thermoblock: 95°C for

Mutant Name	Primer (5'-3')
W82A (S)	AAAGACAAGTGTAGCGTACCAAGAG
W82A (AS)	CTTGGTACGCTACACTTGTCTTTAAT
Q84R (S)	GACAAGTGTATGGTACCGAGAGGTCTGGAATGATG
Q84R (AS)	CATCATTCCAGACCTCTCGGTACCATACACTTGTC
E85Q (S)	GACAAGTGTATGGTACCAACAGGTCTGGAATGATGAATTTT
E85Q (AS)	AAAATTCATCATTCCAGACCTGTTGGTACCATACACTTGTC
V86Y (S)	GACAAGTGTATGGTACCAAGAGTACTGGAATGATGAATTTTTATCCTGG
V86Y (AS)	CCAGGATAAAAATTCATCATTCCAGTACTCTTGGTACCATACACTTGTC
QEV/RQY (S)	GACAAGTGTATGGTACCGACAGTACTGGAATGATGAATTTT
QEV/RQY (AS)	AAAATTCATCATTCCAGTACTGTCGGTACCATACACTTGTC
S106A (S)	AGAGATCGCCCTACCTCTAAGTG
S106A (AS)	GAGGTAGGGCGATCTCTCTAATC
Y133A (S)	GACCTTCCCGCTGTTTATGT
Y133A (AS)	CATAAACAGCGGGAAGGTC
Y134 (S)	CCTTCCCTATGCTTATGTGAACTC
Y134 (AS)	TTCACATAAGCATAGGGAAGGTC
Y135A (S)	CCCTATGTTGCTGTGAACTCATC
Y135A (AS)	TGAGTTCACAGCAACATAGGGA
E143A (S)	GGGACCATTGCGAACTATAAG
E143A (AS)	TTATAGTTCGCAATGGTCCCAG
E143Q (S)	TGGGACCATTCAGAACTATAAGC
E143Q (AS)	GGCTTATAGTTCTGAATGGTCCC
N144A (S)	ACCATTGAGGCCTATAAGCCC
N144A (AS)	GGGCTTATAGGCCTCAATGG
Y145A (S)	TGAGAACGCTAAGCCCATCC
Y145A (AS)	CTGGATGGGCTTAGCGTTC
I175W (S)	CAAGAGCTGGCTGCATACAGTGGAAGACGTAGACC
I175W (AS)	GTATGCAGCCAGCTCTTGAAGGTCAGGCTGCAATTCTGG

Table 5: A list of primers used for creating 5-HT_{3B}Rs containing point mutations that alter the amino acid residue at the position indicated by the mutant label, and to the amino acid indicated by the letter following the position number. Amino acid mutations are to those residues found in the putative loops A, B, D, E and F.

Figure 11 (overleaf): Schematic representation of the principles of mutagenesis using the overlap extension PCR technique. (*Template cDNA*) A global map of the 5-HT_3R-pcDNA3.1 cDNA template and primers used in both PCR reactions. Parental wildtype template strands are black, double diagonal lines indicate omitted nucleotide sequence. Dashed vertical lines delineate the sections of template covered by two separate PCR reactions: (*PCR1*) section A-B, and (*PCR2*) section C-D. Non-mutagenic pcDNA3.1 sense and antisense (flanking) primers are black, mutagenic primers are green (PCR1) and blue (PCR2), with red letters indicating base mismatches. (*PCR1 and PCR2*) These two PCR reactions span the upstream and downstream sections of template respectively, with mutagenic primers overlapping at their 5' portion. The total distance between primers in each reaction must not exceed the capacity and fidelity limitations of the polymerase enzyme. The annealing stage of cycle one is shown uppermost. Extension stages of the first cycle (cycle 1+) and second cycle (cycle 2+) are shown for each half of the parent template (black) and PCR template (green or blue). Primers annealing to a PCR product template will create a further PCR product that contains desired section of cDNA including the mutant 5-HT_3R gene (in this example). This is shown as the major PCR product after 30 cycles. (*PCR3*) A second round of PCR is carried out, using equal quantities of the gel purified products of PCR1 and PCR2 as template, and both flanking primers in the same reaction. The overlapping 3' portions of PCR1 and PCR2 products create a self-priming template that will extend from these overlapping portions, creating a template for flanking primers in successive PCR cycles. Flanking primers may also anneal and extend the 5' overlapping template from PCR1 and PCR2 products (not shown).

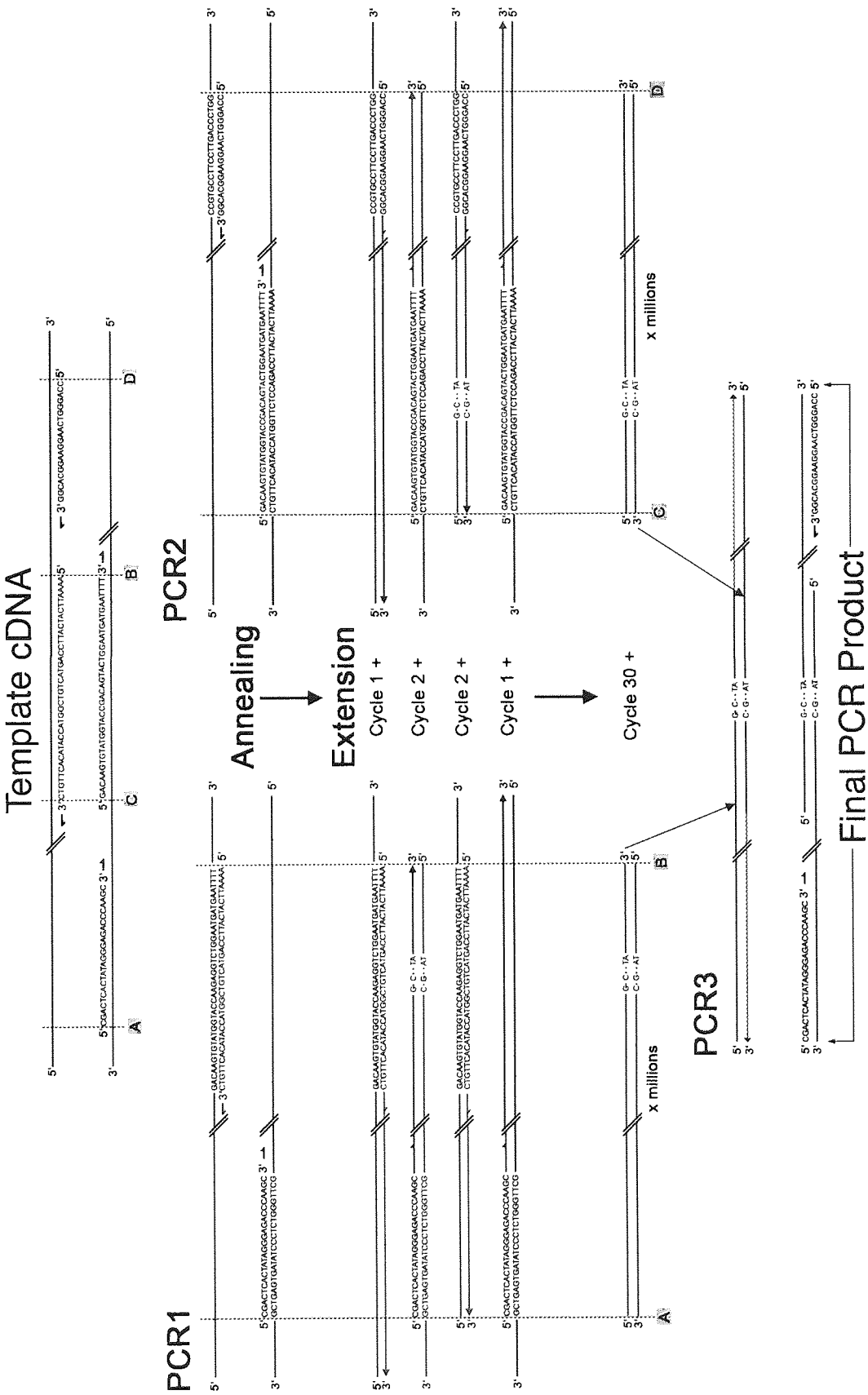
Template cDNA
PCR1
PCR2
PCR3
Annealing
Extension
Cycle 1 +
Cycle 2 +
Cycle 2 +
Cycle 1 +
Cycle 30 +
x millions
x millions
Final PCR Product

2 minutes, 25 x [95°C for 1 minute, 63°C for 1 minute, 72°C for 4 minutes], 72°C for 7 minutes. Both PCR products were gel purified using a QIAquick™ Gel Extraction Kit (Qiagen) and subsequently mixed together in an equal molar ratio. Of this PCR product mixture, 5ng (estimated from 1% agarose gel) was used as template with pcDNA3.1 sense and antisense primers for the next PCR reaction. Cycle conditions were 95°C for 2 minutes, 25 x [95°C for 1 minute, 60°C for 1 minute, 72°C for 4 minutes], 72°C for 7 minutes. All other reagents were as per PCR 1. The PCR product was gel purified and a restriction enzyme double digest set up using HindIII and XbaI, in accordance with the manufacturer's instructions. The products were PCR purified and ligated with pcDNA3.1 previously cut and treated with HindIII/XbaI and CIAP treated.

2.2.22 PCR chimera generation

The base mutations required for creating chimeric 5-HT_{3B}R subunits with binding loop residues identical to those of the 5-HT_{3A}R are mapped in **Figure 12**. These mutations were introduced using the Quickchange™ site directed mutagenesis kit (Stratagene). Although this kit is designed for single point mutations, with appropriate adaptations to the protocol, chimeras could be generated in a stepwise fashion. Primers were designed approximately 40 bases long with a GC% of ~40 and a T_m of ~68°C (**Table 6**). Complementarity between primer pairs was ~50%, which was maintained at the 5' end of the sense mutagenic primer, overlapped with the 5' end of the antisense primer (**Table 6**). Base mutations could not be placed within the first three 5'- bases, more than three sequential mutant bases were avoided and the last two bases of sense and antisense primer were either G or C. Hairpin and primer dimer formations were minimised using web-based software OligoAnalyzer 3.0 (Integrated DNA Technologies, Iowa, USA). Primers did not require purification other than desalting. PCR reactions contained 30 ng of template cDNA [pcDNA3.1-5-$HT_{3B(V5)}$], 125ng of each mutagenic primer, 1 µl of 10mM dNTP mix (2.5 mM each NTP), 2.5U DNA polymerase (*pfu* turbo or *pfu* ultra) and ddH_2O to a final volume of 50 µl overlaid with 40 µl of mineral oil. Negative control reactions contained all of the above but were either deficient in one or both primers, or template, to ensure contamination had been avoided. The QuickChange™ mutagenesis reaction was cycled according to instructions provided by the manufacturer: 95°C for 1 minute, 12 x [95°C for 30 seconds, 55°C for 1 minute, 68° 16 minutes], 7 minutes at 68°C. This was followed by the addition of 10U of Dpn I and an incubation of 2-4 hours. XL10 Gold™/XL1 Blue™ cells (Stratagene) were transformed with 1 µl of Dpn I-treated PCR product (avoiding mineral oil contamination), following the transformation procedure

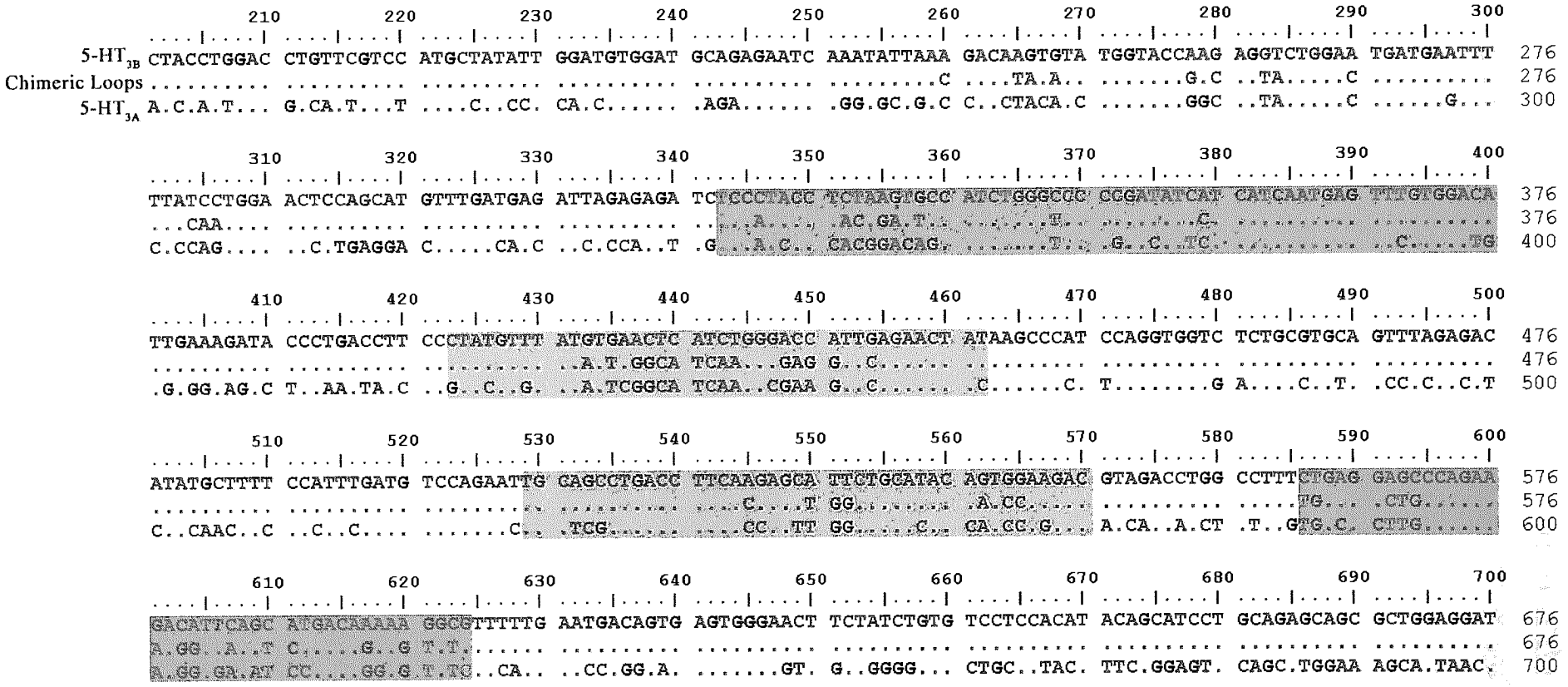

Figure 12: cDNA map of base mutations required to generate chimeric h5-HT$_{3B}$ subunits containing h5-HT$_{3A}$ putative binding loop residues. The N-terminal sequence of 5-HT$_{3B}$ subunit cDNA is shown with all base-letter abbreviations, all other sequences are represented by dots where its sequence is identical to 5-HT$_{3B}$ and the base-letter where it differs. The chimeric loops sequence displays all of the base mutations required to produce every binding loop chimera, thus highlighting the extent of mutagenesis. Putative binding loops are within coloured boxes: , loop-A, loop-E, loop-B, loop-F. Loop C was not mutated.

Chimera	Primer (5'-3')
D1 (S)	CAAATATTAACGACATATATATGGTACCAAGAGGTCTGGAATGATG
D1 (AS)	CCATATATATGTCGTTAATATTTGATTCTCTGCATCCACATCC
D2 (S)	CAAATATTAACGACATATATATGGTACCGACAGTACTGGAATGATG
D2 (AS)	CCATATATATGTCGTTAATATTTGATTCTCTGCATCCACATCC
D3 (S)	GAATTTTTACAATGGAACTCCAGCATGTTTGATGAGATTAGAGAGATC
D3 (AS)	CAAACATGCTGGAGTTCCATTGTAAAAATTCATCAGTCCAG
A1 (S)	GATCTCCATACCTACAGATTCCATCTGGGCCCCCGATATCATCATC
A1 (AS)	CCAGATGGAATCTGTAGGTATGGAGATCTCTCTAATCTCATCA
A2 (S)	CTGGGTCCCCGATATCCTCATCAATGAGTTTGTGGACATTGAAAG
A2 (AS)	GATGAGGATATCGGGGACCCAGATGGAATCTGTAGGTATGG
E1 (S)	GTTTATATTAACCATTCTGGGACCATTGAGAACTATAAGCCC
E1 (AS)	CCCAGAATGGTTAATATAAACATAGGGAAGGTC
E2 (S)	GTTTATATTAGGCATCAAGGGACCATTGAGAACTATAAGC
E2 (AS)	GGTCCCTTGATGCCTAATATAAACATAGGGAAGG
E3 (S)	AAGGGGAGGTTCAGAACTATAAGCCCATCCAGGTGG
E3 (AS)	GTTCTGAACCTCCCCTTGATGCCTAATATAAACATAGGG
B1 (S)	CCTTCACGAGCTGGCTGCATACAGTGGAAGACGTAGACC
B1 (AS)	GCAGCCAGCTCGTGAAGGTCAGGCTGCAATTCTGGACATC
B2 (S)	GCATACAATCCAAGACGTAGACCTGGCCTTTCTGAGGAGC
B2 (AS)	CGTCTTGGATTGTATGCAGCCAGCTCGTGAAGGTCAGG
F1 (S)	CCTTTTGGAGGCTGCCAGAAGACATTCAGCATGACAAAAAGG
F1 (AS)	CTTCTGGCAGCCTCCAAAAGGCCAGGTCTACGTCTTCC
F2 (S)	CCAGAAAAGGTTAAGTCTGACAAAAAGGCGTTTTTGAATGACAGTGAGTG
F2 (AS)	GTCAGACTTAACCTTTTCTGGCAGCCTCCAAAAGGCCAGGTCTACG
F3 (S)	GACAGAAGTGTGTTTTTGAATGACAGTGAGTGGGAACTTC
F3 (AS)	CAAAAACACACTTCTGTCATGCTGAATGTCTTCTGGCAGCC

Table 6: Primers used for creating 5-HT_{3B}R chimeras containing amino acid residues found in the putative loops A-B and D-F of 5-HT_{3A}.

previously described. The amino acid changes for each chimera and partial chimera are illustrated in **Figure 13**, including the name of each chimera, referred to throughout this thesis.

2.2.23 Synthesising capped cRNA transcripts for functional studies

5-HT_3R plasmids (10 µg DNA) containing individual subunit cDNAs were linearised with restriction enzyme XbaI (according to protocol supplied), in a total reaction volume of 20 µl, incubated for 1 hour at 37°C. T7 RNA polymerase (Invitrogen, San Diego, CA) was mixed with the linearised template for in vitro transcription into RNA. The reaction consisted of 11 µl diethylpyrocarbonate-treated (DEPC) water, 10 µl 5X T7 buffer, 1.5 µl RNaseOut™ (33U/µl, Invitrogen), 5 µl 100mM DTT, 5 µl (m7G(5')ppp(5')Gcap) (GibcoBRL), NTP mix

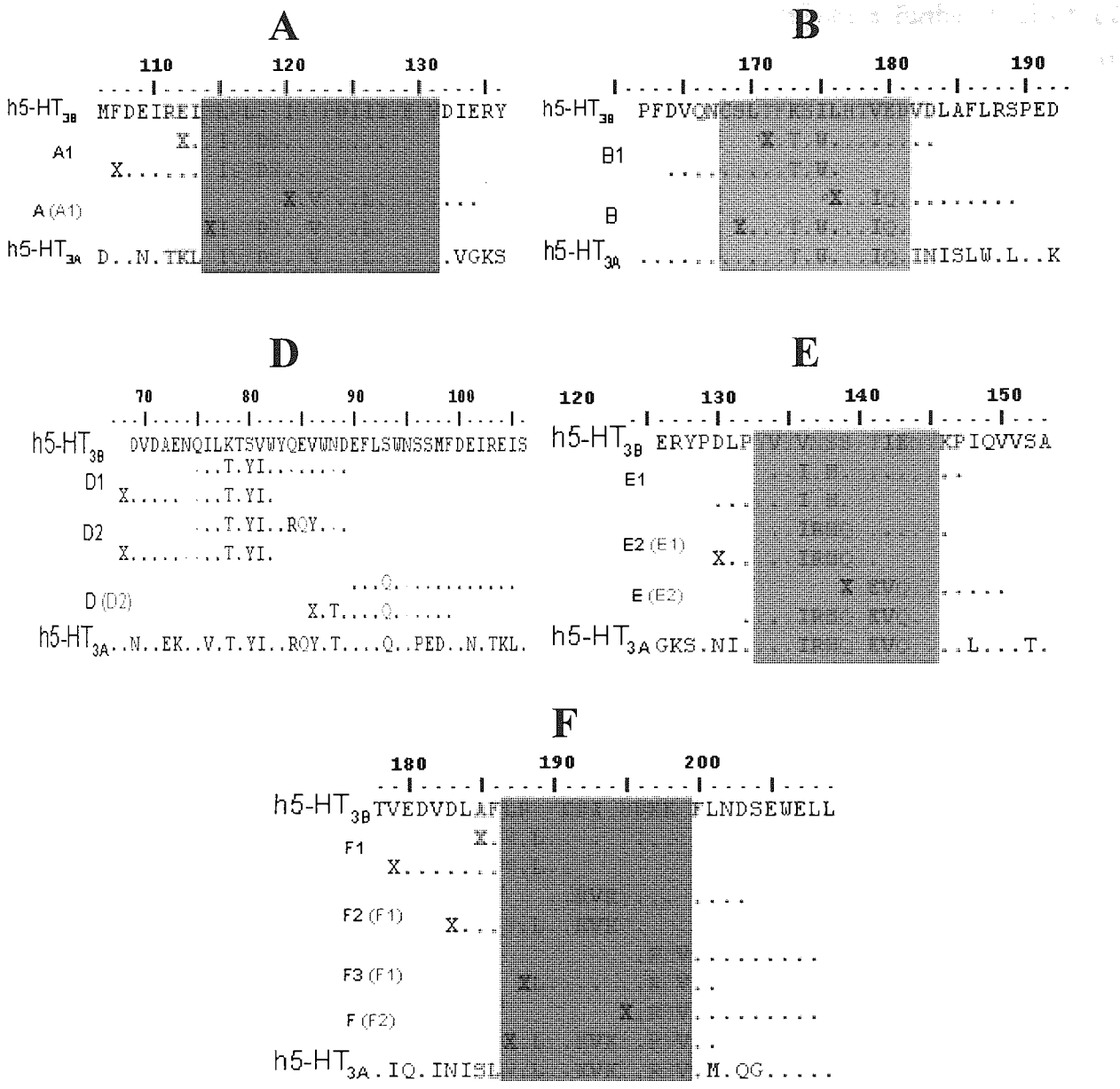

Figure 13: the amino acid sequence of primers required for making 5-HT$_{3B}$ subunit chimeras A, B, D, E and F by PCR. Below each 5-HT$_{3B}$ subunit binding loop sequence are the primers for each reaction, represented by single letter amino acid notation, (X = no amino acid codon). Letters displayed within the primer sequence indicate mutations to the 5-HT$_{3B}$ subunit sequence, dots indicate that the sequence remains unchanged. Alpha numeric legends to the left of the primers refer to the naming nomenclature of each chimera (referred to in thesis main text). The PCR product depends on the template sequence (labelled in grey brackets if 5-HT$_{3B(V5)}$ cDNA was not suitable) and the primer sequence. Final chimera sequence = primer sequence + template sequence.

(10mM, Bioline) 10 µl linear DNA template (5 µg), 1 µl T7 RNA polymerase. The reaction mixture was incubated at 37°C for 1 hour, followed by addition of a further 1 µl of T7 polymerase and incubation for 1 hour at 37°C. DNA was digested by adding 5 µl of RQ1 RNase-Free DNase (Promega) and incubating mixture for 15 minutes at 37°C. The reaction volume was made up to 400 µl with DEPC water and protein was phenol:chloroform extracted from the sample by adding 400 µl UltraPure™ (Invitrogen), vortexing and centrifugation for 5 minutes at top speed in a bench-top microfuge (Sigma 1-13). The aqueous top layer was removed and RNA precipitated by addition of 40 µl of sodium acetate (3M, pH 5.2) and 1 ml of 100% ethanol. After storage of this RNA solution overnight at -20°C, it was centrifuged at 20,000g for 15 minutes at 4°C. After discarding the supernatant, the pellet was washed with 70% ethanol and centrifuged at high speed in a microfuge. The ethanol was removed, the RNA pellet allowed to air dry, and was subsequently resuspended in 10 µl DEPC water. RNA concentration was checked spectrophotometrically and by 1% agarose gel as per DNA maxipreps. The A_{260}/A_{280} ratio for pure RNA should be ~2.0.

Oocytes were maintained at 14 °C in ND96 buffer (96 mM NaCl, 2 mM KCl, 1.8 mM $CaCl_2$, 1 mM $MgCl_2$ and 5 mM HEPES, pH 7.4) supplemented with 100 µg/mL gentamicin (GibcoBRL, Grand Island, NY). For wildtype, chimeric or mutant 5-HT_{3B} subunits, RNA transcripts were mixed in a 1:1 ratio with wild-type 5-HT_{3A} subunit transcripts to generate heteromeric 5-HT_3Rs (final RNA concentration of 1 $\mu g \mu l^{-1}$ in DEPC water); 50 ng of total RNA was microinjected per oocyte. Oocytes were incubated individually in 200 µl ND96 in wells of 96-well plates at 14 °C prior to recording, which took place between 2–7 days following injection.

2.2.24 Two-electrode voltage clamp

Oocytes were placed in a recording chamber (0.5 ml), and while under a standard two electrode voltage clamp, with membrane potentials being held at -60 mV, the oocytes were constantly perfused with frog Ringer's solution (120 mM NaCl, 5 mM HEPES, 2 mM KCl and 1.8 mM $CaCl_2$, pH 7.4). The microelectrodes were filled with 3 M KCl (final resistance of 0.5–2.5 MΩ in ringers solution). Voltage clamp procedures were carried out using a GeneClamp 500 amplifier (Axon Instruments Inc., Foster City, CA, USA). Drug solutions were applied via gravity perfusion of the bath. Oocytes were used for experiments when current responses were stable (±10%) between successive 10 µM 5-HT applications. After agonist challenge, oocytes were perfused with buffer for ≥10 min to permit sufficient time for recovery from desensitization. Agonist-induced currents were recorded using Axoscope 9.0

data acquisition software (Axon Instruments, Inc.). The concentration dependencies of agonist-evoked responses were measured using agonist concentrations that spanned at least three orders of magnitude.

2.3 Data analysis

For saturation binding assays, non-specific was determined at each separate radioligand concentration by the addition of 300 μM metoclopramide. B_{max} and K_d were calculated using a global-fit of specific binding within the iterative curve fitting software of GraphPad Prism, version 4.00 for Windows (GraphPad Software, San Diego, California). The Prism syntax equation is shown in **Equation 5**:

```
Nonspecific=NS*X
Specific=Bmax*X/ (KD + X)
<A> Y = Specific + Nonspecific
<B> Y = Nonspecific
```

Equation 5: Prism 4.0 syntax equation for global fitting of total and nonspecific binding, and determining B_{max} and K_d. Total and nonspecific binding are entered into columns A (<A>) and B (<B>) respectively. KD is the equilibrium dissociation constant (K_d), X is the concentration of free ligand (the value plotted on the x-axis), B_{max} is the maximum binding at equilibrium.

Scatchard analysis (bound vs bound/free ligand) was used as a means to visualise the saturation binding data.

Displacement curves of competitive binding data were plotted using **Equation 6,** contained within the one-site competition model in the Prism™ 4.00 software. Hillslopes were later calculated using **Equation 7**, also within Prism™ 4.00 software.

$$Y = \text{Bottom} + \frac{(\text{Top} - \text{Bottom})}{1 + 10^{\log[D]-\log(IC_{50})}}$$

Equation 6: For the plotting of competition binding data to a one-site competitive binding curve. Top and bottom refer to Y values at the top and bottom of the curve, and log[D] is the logarithm of the concentration of unlabeled drug (plotted on the x axis).

$$Y = Bottom + \frac{(Top - Bottom)}{1 + 10^{(LogIC_{50} - Log[L])nH}}$$

Equation 7: Four parameter logistic equation used for calculation of the Hillslope (nH). Top and bottom refer to Y values at the top and bottom of the curve, and log[L] is the logarithm of the concentration of unlabeled drug (plotted on the x axis).

The Cheng-Prusoff equation (**Equation 8**) was used to calculate the Ki from the IC_{50} previously determined by nonlinear regression of competition binding data.

$$K_i = \frac{IC_{50}}{1 + \frac{[radioligand]}{K_d}}$$

Equation 8: The Cheng-Prusoff equation for calculating the K_i from the IC_{50}.

For homologous binding assays using granisetron, where the K_d and K_i are assumed to be the same, the K_d can be calculated by determining the IC_{50} by nonlinear regression and subtracting the [^{3}H]granisetron concentration in the assay (0.6-0.8 nM). The B_{max} can be calculated using **Equation 9**.

$$B_{max} = \frac{Top - Bottom}{[Radioligand] / (K_d + [Radioligand])}$$

Equation 9: Calculating B_{max} from the top and bottom plateaus of homologous competitive binding assays.

Histograms of AFM subunit-antibody angle measurements were fitted to a Gaussian function by using the nonlinear regression analysis function in GraphPad Prism version 4.00 (GraphPad Software, San Diego, USA).

Statistical analysis was performed with the statistical package included in GraphPad Prism 4.00. All statistical data were analyzed using one-way ANOVA followed by Dunnett's test. Statistical comparison of tagged to equivalent untagged recptors was performed using the Student's t-test (2-tailed), and a paired t-test if binding for both membrane samples was determined in the same assay.

CHAPTER 3: AFM IMAGING

3.1 Introduction

The availability of AChBP crystal structures' conclusively proves the location of Cys-loop LGIC to be at the subunit interfaces of the N-terminal extracellular domain (Brejc *et al.*, 2001). For homomeric 5-HT_{3A}Rs and α7-nAChRs that have no ambiguities in the subunit composition of their interfaces, this information can immediately determine the subunit composition of the binding site, and affirm ligand docking simulations. For heteromeric receptors such as the 5-$HT_{3A/B}$R, this information somewhat complicates the production of accurate homology models, and casts doubt on ligand docking simulations if the number of 5-HT_{3B} subunits and their arrangement is unknown. **Figure 14** highlights the conundrum posed by multiple stoichiometries and their arrangement.

In other Cys-loop receptors, attempts have been made to elucidate the subunit arrangement by the construction of different concatenated subunits, which are heterologously expressed together with single subunits, in an attempt to reconstruct the functional characteristics of the naturally occurring heteromeric receptors (Minier *et al.*, 2004). So far, this has not been carried out with the 5-$HT_{3A/B}$R heteromer.

In the present study, an alternative approach has been adopted. Both the 5-HT_{3A} and 5-HT_{3B} receptor subunit cDNAs were engineered with different epitope tags and subsequently expressed in HEK293 cells, from which membrane preparations were made. To ensure that the epitope tags did not compromise the recognition properties of the receptor, radioligand binding was used to assess receptor expression and affinity of both tagged and untagged receptor preparations.

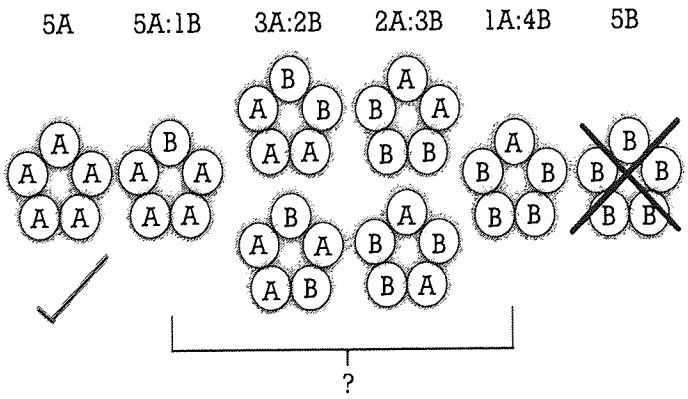

Figure 14: The four possible stoichiometries of the 5-$HT_{3A/B}$R (top) and the six possible subunit arrangements (below). Each arrangement must be ruled out to ensure accurate homology modeling.

The membrane preparations were solubilised and nickel affinity purified, facilitated by the molecular engineering of a C-terminal His_6 tag distal to the epitope tag in the cDNA sequence.

The soluble affinity purified receptor was exposed to subunit specific antibodies, and the receptor-antibody complexes were imaged using atomic force microscopy (AFM), allowing differentiation of both 5-HT_{3A} and 5-HT_{3B} subunits. Performing these studies with the tagged heteromeric receptor would resolve i) the 5-HT_{3A}R subunit when exposed to 5-HT_{3A}R subunit specific antibodies, and ii) the 5-HT_{3B}R subunit when exposed to 5-HT_{3B}R specific antibodies. Integration of both data sets would confirm the distribution of the subunits within the functional heteromeric pentamer.

Tagged cDNA was constructed previously by Dr. Martin Davies, Department of Pharmacology, University of Alberta, Edmonton, Canada. This was also where functional studies of these receptors were carried out, in the laboratory of Dr. Susan M.J. Dunn, and reported here for completeness. The AFM imaging studies were carried out in the laboratory of Dr. J.M. Edwardson, Department of Pharmacology, University of Cambridge as part of this collaborative study.

3.2 Results

3.2.1 Saturation Binding

In saturation binding studies [^{3}H]GR65630 (0.03-1.3 nM) bound with high affinity to a single population of 5-HT_3 receptors in transfected HEK293 cells, evidenced visually by the Scatchard transformations in **Figure 15**. Nonspecific binding in untagged membrane receptor preparations was between 6-10 %, but was much higher for tagged receptors, although both fitted the equation of a straight line (see saturation isotherms in **Figure 15**). Scatchard transformations of the saturation binding data illustrate this increase in nonspecific binding with a shallower slope in tagged membranes compared to untagged membranes (**Figure 15**). This high nonspecific binding was, however, also increased in untagged membrane receptor preparations previously assayed with low nonspecific binding. The problem worsened with prolonged radioligand storage, although the contribution of prolonged membrane storage was not determined. The absence of saturation binding data for 5-$HT_{3A(Myc)/B(V5)}$ membranes is a direct consequence of the high nonspecific binding levels making the plotting of a specific binding curve by nonlinear regression impossible.

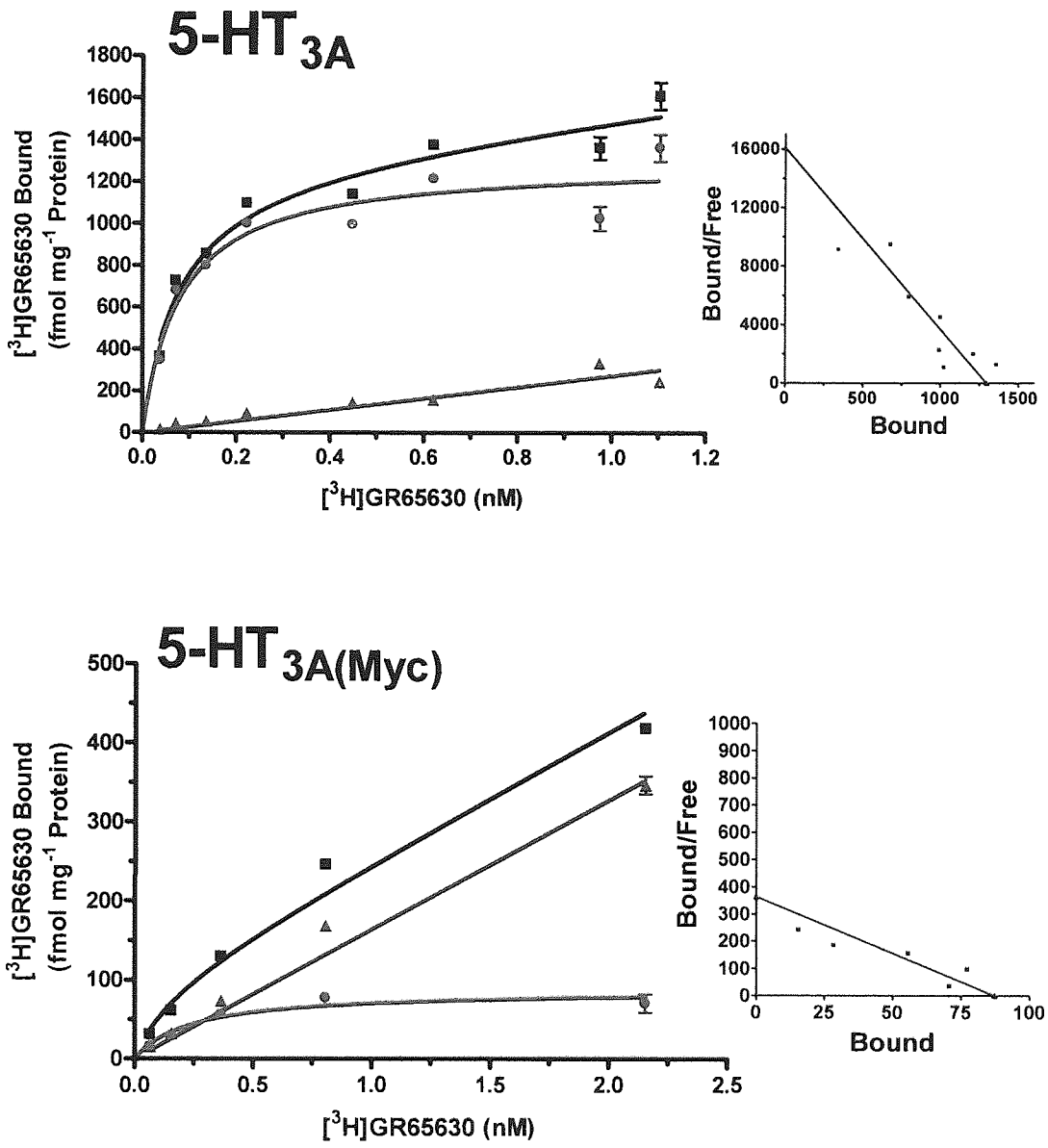

Figure 15: representative saturation data for [^{3}H]GR65630 (0.03 – 10 nM) binding to membranes prepared from transfected HEK293 cells. Scatchard transformations of Bound vs Bound/Free are inset to the right of each nonlinear transformation graph (units are DPM). Headings refer to the subtype of receptor being expressed, where Myc and V5 refer to subunit epitope tags. All [^{3}H]GR65630 concentration points were assayed in triplicate for both total (▪) and nonspecific (▲) in order to calculate specific (●), as described in the methods.

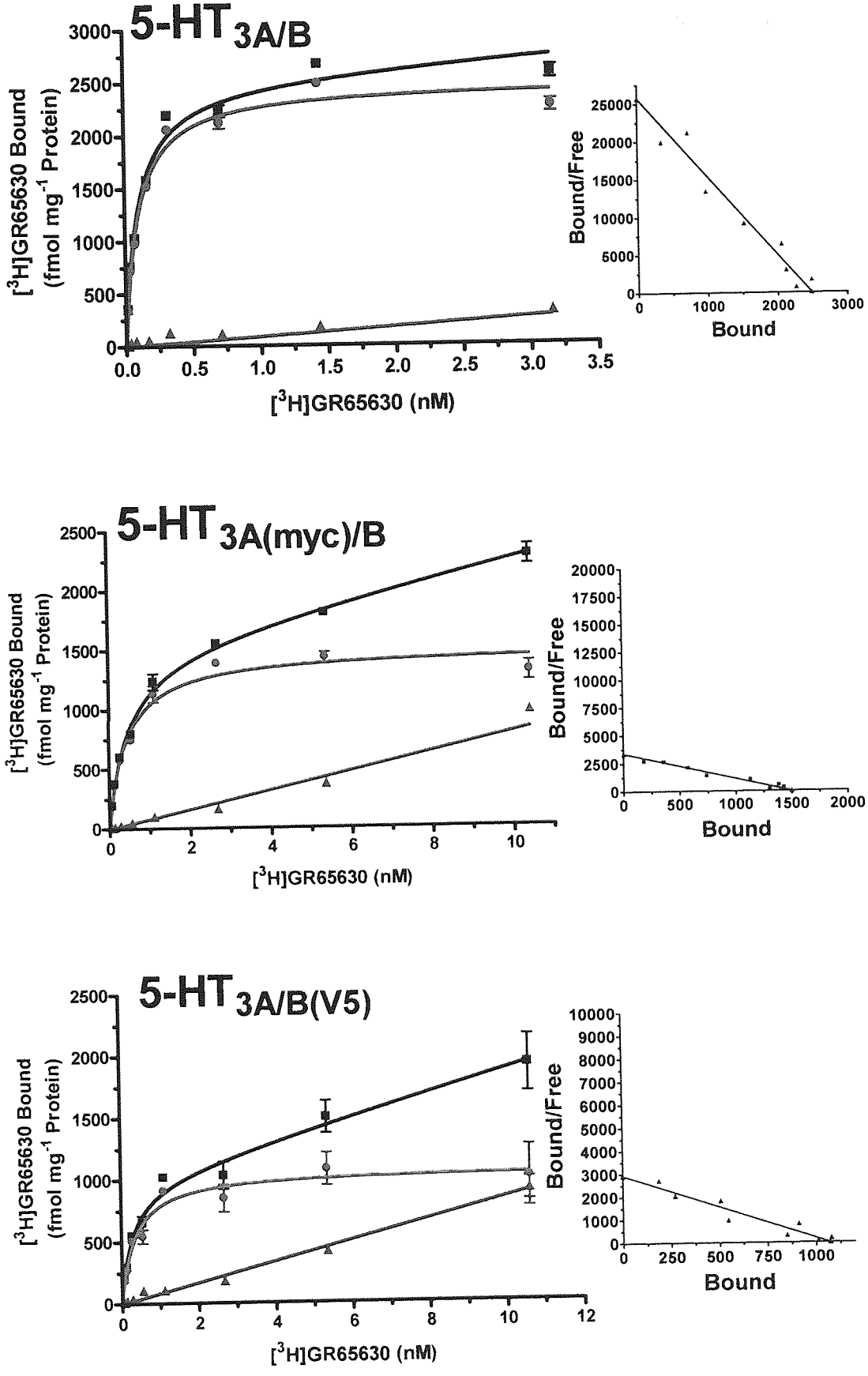

Figure 15: continued from previous page.

Table 7 shows the maximum binding (B_{max}) and equilibrium dissociation constants (K_d) determined by saturation analysis using [^{3}H]GR65630 with 5-HT_3R membrane preparations of wildtype and tagged homomeric and heteromeric receptors. One-way analysis of variance (ANOVA) and Dunnett's post-hoc test show that tagging of 5-HT_{3A}Rs and 5-$HT_{3A/B}$Rs has a small but statistically significant effect on receptor affinity, but has a much larger compromising effect on receptor expression, compared to wildtype receptors (**Table 7**).

The transient expression of wildtype heteromeric receptors is, on average, over 3-fold higher than the levels of homomeric wildtype receptor expression, but expressing 5-$HT_{3A/B}$Rs with either tagged A or B subunits approximately halves this level of expression. Homomeric expression of tagged subunits appears to be much more detrimental, reducing expression by 10-fold, however; the problem of high nonspecific binding was most severe in these receptor membrane preparations.

3.2.2 Competition binding

It has previously been reported that [^{3}H]GR65630 can bind a non-specific site in transiently transfected HEK293 cells, that is not competed for by antagonists typically used in binding experiments (personal communication, Dr. Nicholas Barnes). These high nonspecific binding values will cause inaccuracies in the method of calculating B_{max} from saturation binding experiments, which may itself vary between separate transfections. This concern led to a change in the radioligand used and type of binding experiment: competion binding with [3H]granisetron.

Using [^{3}H]granisetron instead of [^{3}H]GR65630, nonspecific binding in membranes was dramatically reduced to 2–10% of total binding in both tagged and untagged receptor preparations. Separate membrane preparations of cells transfected at different times gave different levels of nonspecific [^{3}H]granisetron binding. As a consequence of this change in radioligand, the effect of tagging has been assessed by competition binding assays using [^{3}H]granisetron, granisetron and 5-HT (**Table 8**), in addition to saturation analysis with [^{3}H]GR65630 (**Table 7**).

Competition studies with granisetron as the radioligand and displacing ligand confirm that 5-$HT_{3A(Myc)}$Rs have a reduced granisetron affinity compared to 5-HT_{3A}Rs, however, the small reduction observed (**Table 8**) was not of comparable magnitude to saturation assay data using [^{3}H]GR65630. A graph of [displacer] vs % binding (**Figure 16**), clearly shows that the respective μM and nM affinities of 5-HT and granisetron are not substantially altered by tagging. The most significant divergence from wildtype affinity is seen in the 5-$HT_{3A(Myc)}$R,

Receptor Expressed	B_{max} (fmol/mg)	pK_d (nM)	Hill Slope	n
5-HT_{3A}	859.0 ± 118.2*#	9.78 ± 0.09*	1.95 ± 0.45	5
5-$HT_{3A(Myc)}$ (*)	80.7 ± 14.9	9.61 ± 0.07	-	3
5-$HT_{3A/B}$ (#)	3284 ± 451.5	9.81 ± 0.02†‡	1.54 ± 0.10	12
5-$HT_{3A(Myc)/B}$ (†)	1425 ± 103.3	9.46 ± 0.06	1.23 ± 0.13	3
5-$HT_{3A/B(V5)}$ (‡)	1400 ± 193.6	9.45 ± 0.02	1.07 ± 0.05	3

Table 7: Determinations of B_{max} and K_d by saturation analysis using [^{3}H]GR65650 saturation binding on 5-HT_{3A} and 5-$HT_{3A/B}$Rs containing tagged and untagged subunit combinations. The bracketed symbol following the name of the expressed receptor is used in subsequent columns to indicate that this subtype of receptor is significantly different to the equivalent untagged receptor value, tested using Dunnett's *post hoc* comparison, after one-way ANOVA. For analysis of B_{max} and K_d values: $P < 0.05$ when 5-HT_{3A} is compared to 5-$HT_{3A(Myc)}$ (*) or 5-$HT_{3A/B}$ (#), $P > 0.0001$ when 5-$HT_{3A/B}$ is compared to 5-$HT_{3A(Myc)/B}$ (†) or 5-$HT_{3A/B(V5)}$ (‡). All receptors tagged with Myc or V5 also bear the His_6 tag.

Table 8:

Receptor Subtype	Granisetron B_{max} (fmol/mg)	Granisetron pK_d (nM)	Granisetron Hillslope	Granisetron n	5-HT pK_i (nM)	5-HT Hillslope	5-HT n
5-HT_{3A}	2542 ± 346	9.35 ± 0.03	1.09 ± 0.1	6	6.82 ± 0.04	0.98 ± 0.05	4
5-$HT_{3A(Myc)}$	268 ±118†	9.30 ± 0.02*	0.99 ± 0.39	8	6.32 ± 0.02$^{\#}$	0.98 ± 0.02	3
5-$HT_{3A/B}$	2078 ± 164.1	9.25 ± 0.03	1.04 ± 0.06	6	6.84 ± 0.05	1.04 ± 0.03	6
5-$HT_{3A/B(V5)}$	1144 ± 87.54*	9.31 ± 0.01	1.19 ± 0.08	3	ND	ND	-
5-$HT_{3A(Myc)/B(V5)}$	1647 ± 202	9.27 ± 0.02	1.07 ± 0.03	11	6.78 ± 0.04	1.15 ± 0.03	8

Table 8: B_{max}, K_d and Hillslope determinations in tagged and untagged 5-HT_{3A}Rs and 5-$HT_{3A/B}$Rs using [^{3}H]granisetron competition binding assays. Granisetron and 5-HT were used as the unlabeled displacing ligands. Student's t-tests were performed on each tagged receptor subtype versus its equivalent untagged subtype, where * is $P < 0.05$, $^{\#}$ is $P < 0.005$ and † is $P < 0.0005$. Student's paired t-tests between untagged 5-HT_{3A} and 5-$HT_{3A/B}$Rs were performed, statistical significance is indicated in grey, where * is $P < 0.05$. ND = not determined due to insufficient data collection.

Figure 16:

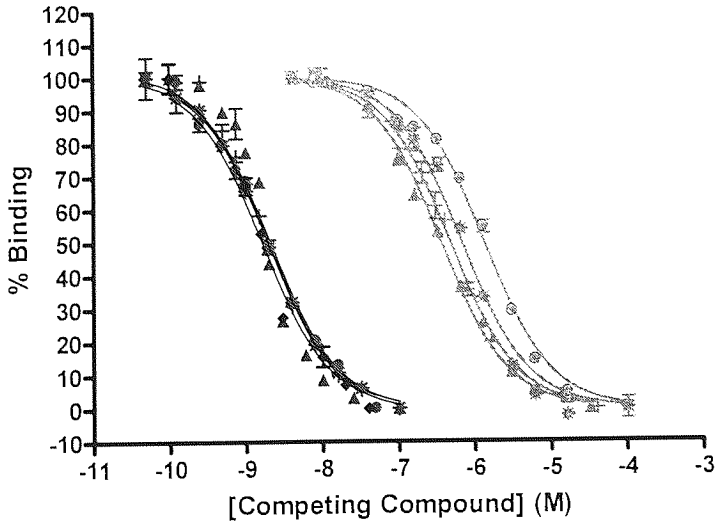

Figure 16: Representative examples of competition binding from the table above. For 5-HT competition experiments; 5-HT_{3A} (▲), 5-$HT_{3A(Myc)}$ (●), 5-$HT_{3A/B}$ (+), 5-$HT_{3A(Myc)/B(V5)}$ (×), and granisetron competition experiments; 5-HT_{3A}(▲), 5-$HT_{3A(Myc)}$ (●), 5-$HT_{3A/B}$ (+), 5-$HT_{3A/B(V5)}$ (♦), 5-$HT_{3A(Myc)/B(V5)}$ (*). Data points represent the mean ± SEM.

which has a 3-fold lower affinity for 5-HT than the 5-HT_{3A}R. The 5-$HT_{3A/B}$R heteromer demonstrates no significant changes in granisetron or 5-HT affinity due to tagging of either 5-HT_{3A} or 5-HT_{3B} subunits. Conversely, granisetron affinity for 5-$HT_{3A/B}$Rs was significant less than that of 5-HT_{3A}Rs, although this was not a substantial difference. It was noted that the Myc-tagged homomer did not express as robustly and consistently, compared to the expression of the untagged homomer or indeed the tagged heteromer.

3.2.3 Cell surface expression

HEK293 and TSA201 cells transfected with tagged 5-HT_3R subunits were tested for positive cell surface expression by confocal laser scanning microscopy and immunofluorescence. The images in **Figure 17** demonstrate the successful translocation of tagged homomeric and heteromeric receptors from the Golgi apparatus to the plasma membrane surface. Transfected cells expressing tagged 5-HT_{3A}Rs or 5-$HT_{3A/B}$Rs gave positive fluorescence signals when incubated with either anti-His_6 or anti-Myc antibodies. The anti-V5 antibody displayed fluorescence with heteromeric receptor only. Untransfected cells and cells transfected with untagged subunits displayed no fluorescence (not shown).

3.2.4 Solubilisation

A range of detergent and salt concentrations were tested for 5-HT_3R solubilisation efficiency from transfected cells. Dot blots were performed to examine the compatibility of the western blot detection system with the solubilisation procedure (not shown). A Triton X-100 concentration of 0.2% and a salt concentration of 2 M (final concentrations) produced a solubilisation efficiency of 60-75%, which was in agreement with, and occasionally surpassed the solubilisation efficiencies reported for other 5-HT_3Rs and LGIC receptors. Solubilised 5-$HT_{3A(Myc)/B(V5)}$ receptor preparations were tested by competition assay to determine the effect of solubilisation on receptor affinity. A small (16 %), but statistically significant reduction in receptor affinity was observed (**Table 10**).

3.2.5 Affinity purification

The nickel affinity resin was calibrated for use with 5-HT_3Rs by analysing elution fractions from different strength imidazole washes using radioligand binding and protein assays (**Figure 18**). The majority of protein in the samples was eluted in the first wash fraction (5 mM imidazole elution contained 19.23 ± 0.24 mg from a total 20.0 mg loaded; ± SEM, n = 4), but the majority of 5-HT_3R was detected over imidazole concentrations of 80-140 mM. Western blotting was also able to demonstrate the efficiency of protein removal (**Figure 19**). When excess protein was added to SDS-PAGE wells and resultant blots probed with high

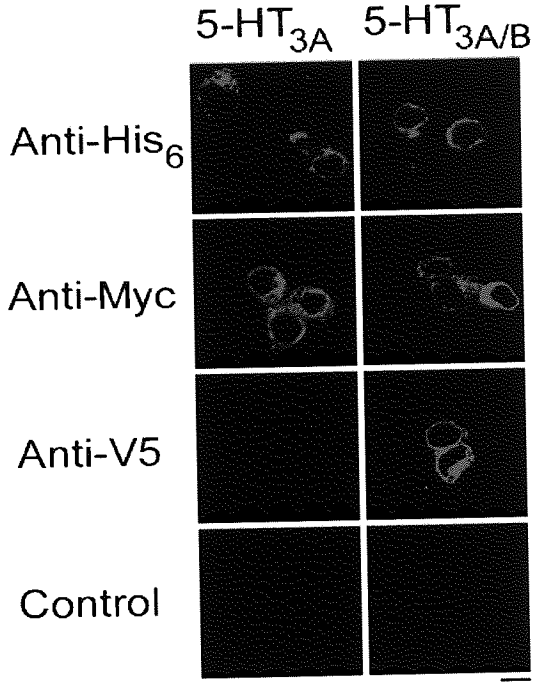

Figure 17: Immunofluorescence of TSA201 cells transfected with 5-$HT_{3A(Myc)}$ and 5-$HT_{3B(V5)}$ subunit cDNAs. Cells were fixed, permeabilised, and incubated with a single primary monoclonal antibody, indicated by labels. Incubation in cy3-conjugated goat anti-mouse secondary antibody followed. Control experiments involved incubation of secondary antibody with fixed cells, having no prior exposure to primary. Cells were imaged by confocal laser scanning microscopy. Bottom right is the 10 µm scale bar.

Receptor Subtype	Receptor State	K_d (nM)	Hill Slope	n
5-$HT_{3A(Myc)/B(V5)}$	Native Membranes	0.55 ± 0.02	1.07 ± 0.03	11
5-$HT_{3A(Myc)/B(V5)}$	Solubilised	0.64 ± 0.07†	1.09 ± 0.1	7

Table 10: The effect of solubilisation on 5-$HT_{3A(Myc)/B(V5)}$ receptor affinity, determined using homologous binding assays with [^{3}H]granisetron (~0.6 nM) and granisetron (0.03 -1.3 nM). Statistical comparison was by Student's t-test, where † = P<0.0001. Receptor membranes were solubilised with 0.2 % Triton X-100 and 2M NaCl (final concentration), followed by desalting.

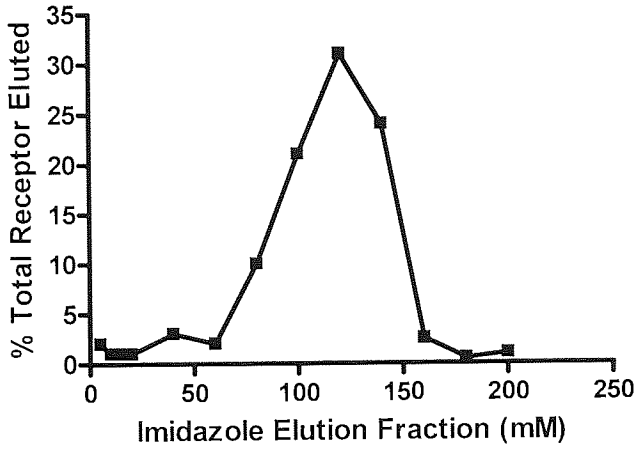

Figure 18: Profile of 5-$HT_{3A(Myc)/B(V5)}$ receptor binding in elution fractions from nickel affinity column, tested by radioligand binding with [^{3}H[granisetron. n = 2.

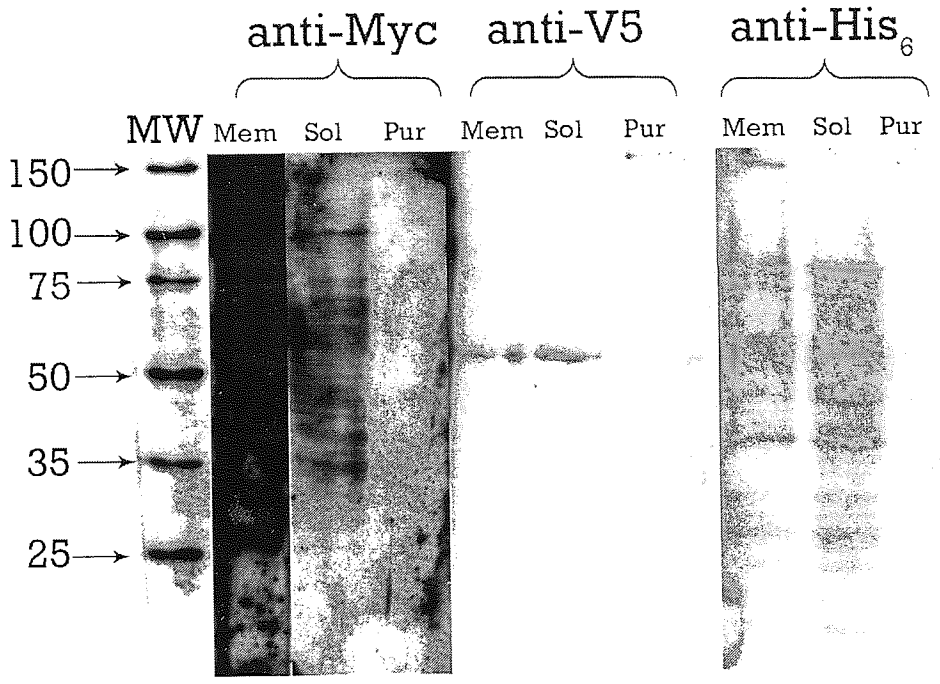

Figure 19: Western blot of membrane (Mem), solubilised (Sol) and affinity purified (Pur) samples of HEK293 cells transiently expressing 5-$HT_{3A(Myc)/B(V5)}$ receptors. Each triplicate of identical samples was probed with a different antibody: Myc (1:1000), V5 (1:2000) and His_6 (1:2000) monoclonal antibodies, as captioned. Secondary antibody was added 10-fold more dilute than the respective primary antibody for each blot. A total of 50 µg protein was loaded into SDS-PAGE wells (7.5 % gel) for membrane and soluble samples, but because protein quantification of affinity purified samples was not possible, a maximum volume (35 µl) of sample was loaded. Molecular weights are indicated on the far left, determined by DualVue™ Markers (Amersham).

concentrations of antibody, nonspecific protein bands could be detected in membrane and soluble fractions after ECL™ development. These bands disappeared after affinity purification **(Figure 19)**.

Unfortunately, the use of an affinity resin and multiple de-salting steps diluted the final receptor concentration beyond the threshold of the Western blotting detection limits. Concentration of the affinity purified sample was required to enable enough tagged receptor to be loaded onto a 7.5 % SDS-PAGE gel and subsequently visualised. Samples typically required concentrating by 10-fold, after which, positive immunological detection of distinct bands in the range of 50-55 kDa was possible, with no other bands outside of this range **(Figure 20)**. Affinity purified 5-$HT_{3A(Myc)}$ samples probed with anti-Myc antibody gave an intense positive band of ~55 kDa, but produced no immunologically reactive bands to anti-V5 antibody. Affinity purified 5-$HT_{3A(Myc)/B(V5)}$ samples probed with anti-Myc antibody gave two positive bands at ~50 kDa and ~55 kDa, and one intense ~50 kDa band when probed with anti-V5. The predicted subunit molecular weights were 56.3 kDa for 5-$HT_{3A(Myc)}$ and 53.8 kDa for 5-$HT_{3B(V5)}$, determined using the 'compute pI/MW' tool on the ExPASY server. This calculation does not take account of any protein glycosylation state.

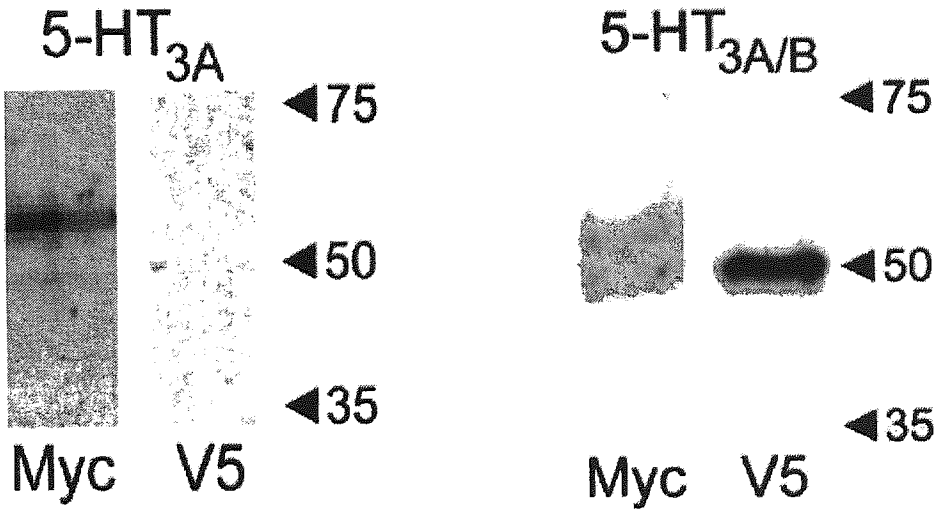

Figure 20: Western blot detection of concentrated affinity purified samples of 5-$HT3_{A(Myc)}$ and 5-$HT_{3A(Myc)/B(V5)}$ receptor, probed with both Myc (1:2000) and V5 (1:5000) monoclonal antibodies. Secondary antibody was added at a dilution 10-Fold greater than that of the primary antibody being detected. Molecular weights are indicated on the right of each receptor blot. Sample proteins were separated on a 7.5 % SDS-PAGE gel.

Anti-His_6 antibody probed 5-$HT_{3A(Myc)/B(V5)}$R sample blots also detected an intense band in the 50-55 kDa range, which was not present in control samples (**Figure 21**). Reducing the signal intensity and running the sample on a 12 % gel allowed two closely spaced but separate bands to be detected (highlighted in **21**, far right image), the lower band being more intense. These upper and lower bands should represent h5-HT_{3A} and h5-HT_{3B} subunits respectively.

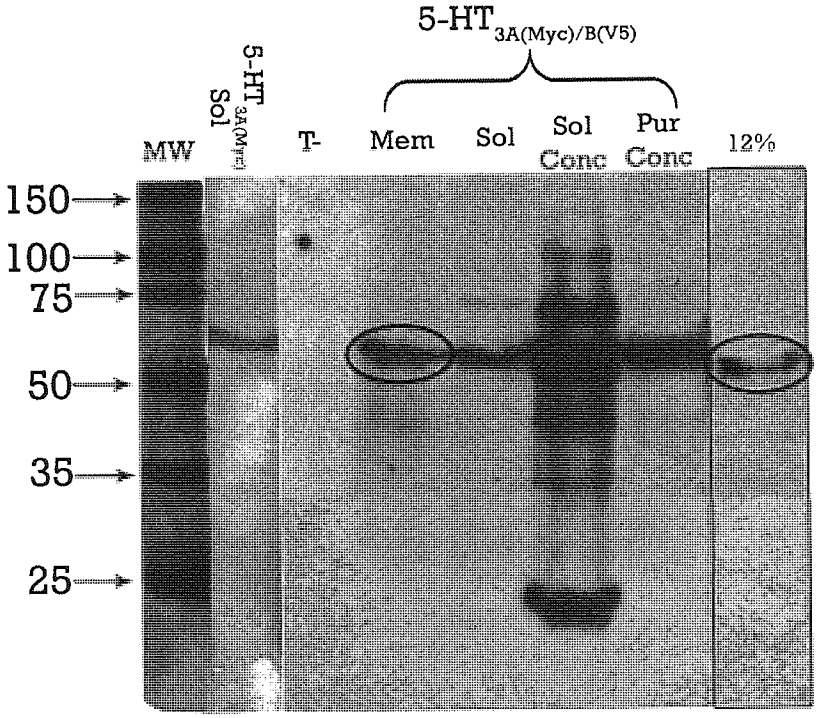

Figure 21: Western blot detection of 5-$HT_{3A(Myc)}$ and 5-$HT_{3B(V5)}$ subunits using anti-His_6 primary antibody (1:5000). Each 7.5 % SDS-PAGE gel lane was loaded with 20 µg of total protein, either from solubilised (Sol) 5-$HT_{3A(Myc)}$ receptors or 5-$HT_{3A(Myc)/B(V5)}$ from different stages of the purification process: crude membrane preparations (Mem), solubilised (Sol), solubilised and 20-fold concentrated (Sol Conc), affinity purified and concentrated (Pur Conc). The encircled 5-$HT_{3A(Myc)/B(V5)}$ membrane sample was also probed with anti-His_6 antibody on a 12 % SDS-PAGE gel, where it is possible to see two separate immunologically positive bands at ~50-55 kDa. The molecular weight markers shown on the far left are pertinent to the 7.5 % gels only.

3.2.6 Western blotting troubleshooting

Problems with high background signal levels were experienced with two anti-Myc antibodies, manufactured by Cell Signalling and Calbiochem, and used initially for probing membrane and soluble receptor samples (**Figure 22**). By contrast, low background signal was demonstrated on identical blots of the same receptor samples using anti-V5 and anti-Myc antibodies manufactured by Invitrogen (**Figure 22**). The change to an Invitrogen anti-Myc antibody improved the signal to noise ratio for 5-$HT_{3(Myc)}$ subunit detection, although immunoreactivity was still less sensitive than the anti-V5 antibody. This lack of sensitivity complicated the detection of 5-$HT_{3A(Myc)}$ subunits. Only the anti-His_6 antibody was able to satisfactorily determine the presence of 5-HT_{3A} subunits in the soluble 5-$HT_{3A(Myc)}$ homomeric receptor (**Figure 21**).

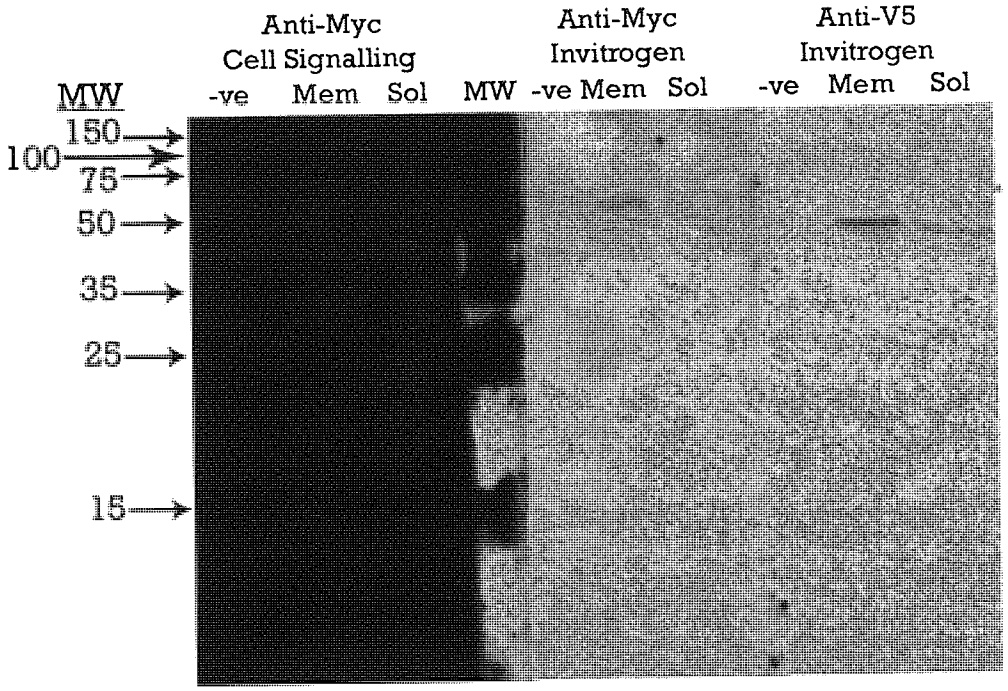

Figure 22: Western blot detection of membrane (Mem), Soluble (Sol) and affinity purified (Pur) samples of 5-$HT_{3A(Myc)/B(V5)}$ receptor expressed in HEK293 cells. Typical results using different antibodies are depicted, highlighting the problem of nonspecific background noise (anti-Myc, Cell Signalling). Similar results were obtained with anti-Myc antibody from Calbiochem (not shown). Results using two anti-Myc antibodies are shown, manufactured by Cell Signalling (1:2000) and Invitrogen (1:2000). Anti-V5 antibody (1:5000) is shown for comparison of differences in signal to noise ratio. Molecular weights are indicated on the far left.

Control samples were loaded onto each blot, and included samples of HEK293 cells that were either untransfected, or transfected with untagged 5-HT_3Rs. No bands corresponding to those positively identified as 5-HT_3 subunits were detected in lanes containing these controls. The western blots published by Boyd *et al.* (2002) showed a nonspecific band at ~50 kDa, when HEK293 control cells were probed with anti-Myc antibody. Knowing that this could possibly interfere with the detection of our subunits, SDS-PAGE gels were overloaded with 5-$HT_{3A/B}$R (untagged) samples and probed with higher than usual primary antibody concentration and exposure time. Only under these extreme conditions could an obvious nonspecific band be detected at ~50 kDa in anti-Myc probed control samples. This was extremely faint in comparison to the intense band at 51 kDa, and was accompanied by other nonspecific bands of different molecular weights.

3.3 Atomic force microscopy

3.3.1 Particle measurments

Purified 5-HT_3R preparations were adsorbed onto separate mica coverslips and dried. Both receptor subtypes, 5-HT_{3A}R and 5-$HT_{3A/B}$R, were observed as homogenous spreads of particles (**Figure 23$_{B-E}$**). Samples of mock transfected cells contained no particles (**Figure 23$_A$**), suggesting that the particles seen attached to the mica coverslip in **Figure 23$_{B-E}$** were the purified 5-HT_3 receptor.

AFM measurements were made of the particles adhered to mica coverslips, to determine the correlation between their dimensions (height and radius) and that predicted for 5-HT_3R. The radius was measured with the AFM tip positioned at half the particle height to account for the overestimation often made by the AFM scanning tip, due to its size being comparable to the particles measured. Due to the biological nature of the sample being measured and inherent variation in its topography, determination of these specific coordinates (radius at half height) were an approximation. Errors in the calculation of these measurements showed a Gaussian distribution, allowing a mean height to be calculated that best represents the true particle dimensions. This method has been used previously with success in calculating volume for particles with disparate molecular masses (Schneider *et al.*, 1998). These dimensions were used to calculate molecular volumes by using **Equation 2 (Chapter 2)**. The frequency distributions of the calculated molecular volumes are shown in **Figure 23$_{J-K}$**. Neither 5-HT_{3A}R nor 5-$HT_{3A/B}$R samples showed significant differences between peak and mean values

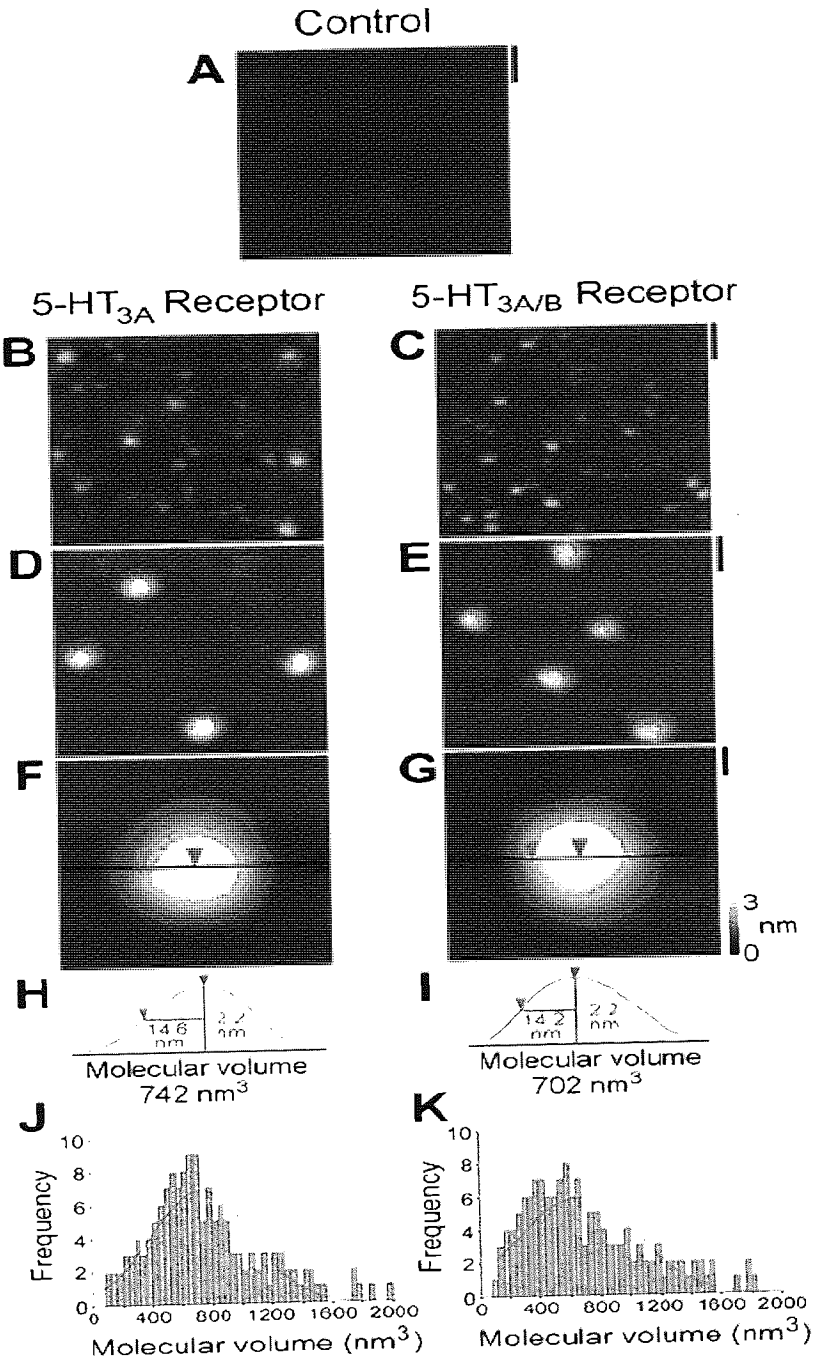

Figure 23: AFM imaging of 5-HT_{3A}Rs and 5-$HT_{3A/B}$Rs. (*A*) Low-magnification image of a sample prepared from mock-transfected cells (Scale bar, 100 nm). Low-magnification images of affinity purified samples of cells expressing (*B*) 5-HT_{3A}R and (*C*) 5-$HT_{3A/B}$R (Scale bar, 100 nm). Images *(D)* and *(E)* are medium-magnification (scale bar, 50 nm), *(F) and (G)* are high-magnification images (Scale bar, 10 nm) of single receptors. A colour-height scale is shown at the right. (*H and I*) Sections through the receptors shown in F and G at the positions indicated by the lines. The height of the receptors and their radii at half height are shown. (*J) and (K*) are frequency distributions of molecular volumes of 5-HT_{3A} (*J*) and 5-$HT_{3A/B}$ (*K*) receptors.

($P > 0.05$). The mean values of the molecular volumes (± SE) were 757 ± 31 nm^3 (n = 149) for the 5-HT_{3A} receptor and 704 ± 33 nm^3 (n = 144) for the 5-$HT_{3A/B}$ receptor. The molecular volume was also calculated on the basis of molecular mass of each receptor: 275 kDa (5 x 55 kDa) for 5-HT_{3A}Rs, ~50 kDa of which was accounted for by attached oligosaccharides (Monk *et al.*, 2004). By integrating these values into **Equation 2 (Chapter 2)**, a molecular volume of 511 nm^3 is proposed for 5-HT_{3A}R subunits, 32% smaller than that calculated for the particles from the measured AFM dimensions. The molecular volumes of 5-HT_{3A}Rs and 5-$HT_{3A/B}$Rs were not significantly different ($P > 0.05$).

3.3.2 Visualisation of receptor-antibody complexes

Prior to the study of receptor-antibody complexes, the appearance of uncomplexed antibodies and receptors was determined by imaging both entities separately, illustrated in **Figure 24_{A-B}** (left and centre images) using 5-HT_{3A}R samples as an example. The receptor particles and antibodies each took the form of homogenous populations, distinguishable by size. Suspensions of purified receptor particles not incubated with antibody but imaged as a negative control, produced a background of 2-2.6% false positive receptor-antibody complexes (**Table 10**; receptor alone). All false positives had no more than one antibodyapparently complexed with receptor. Similarly, when anti-V5 antibody and 5-$HT_{3A(Myc)}$ receptor particles were imaged, 2.5% of receptor particles appeared to have one antibody bound. This was expected to reflect the same false positive phenomenon observed in the negative control.

5-HT_{3A}R and 5-$HT_{3A/B}$R affinity purified samples imaged after incubation with anti-His_6 or anti-Myc monoclonal antibodies, revealed that the majority of antibody and receptor particles were free in suspension uncomplexed (**Figure 24_{A-B}**, right-hand images), with just 28-41.2% of receptor particles forming apparent receptor-antibody complexes when supplied with appropriate antibody in suspension (**Table 10**).

Strangely, the probability of finding a receptor with one, two, three, four or five antibodies attached does not follow a binomial distribution; the frequency of multiple subunit-antibody binding events is over represented (see **Table 10**). Although antibody-receptor binding events should follow a binomial distribution in suspension, the probability of attachment to the poly-(L-lysine) coated coverslip may be biased towards receptor complexes with the greater electrostatic attraction to poly-(L-lysine), i.e. those multiply complexed receptors.

Images of the different receptor-antibody complexes described in **Table 10** are captured in **Figure 24_{C-E}**. The visualisation of five anti-His_6 antibodies complexed with one receptor

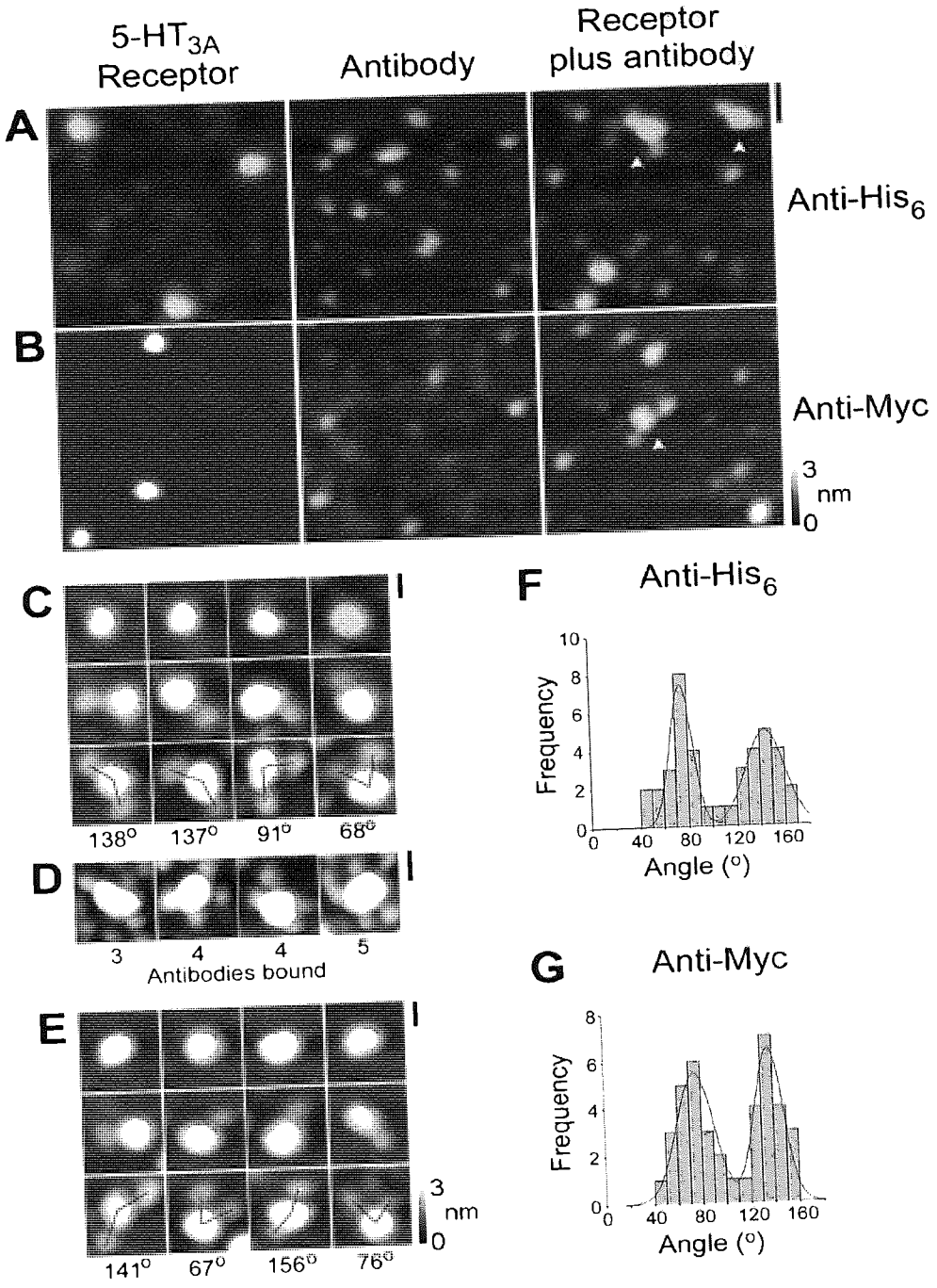

Figure 24: AFM imaging of complexes between homomeric 5-HT_{3A}Rs and anti-His_6 and anti-Myc antibodies. (*A and B*) Images of receptors alone (*Left*), antibodies alone (*Centre*), and receptor-antibody complexes (*Right*). (Scale bar = 50 nm). (*C and E*) Zoomed images of receptors that are uncomplexed (*Top*) or bound by one (*Middle*) or two (*Bottom*) antibodies; the corresponding frequency distribution of the angles for each specific antibody is to the right (F and G). (*D*) Zoomed images of receptors bound by three to five anti-His_6 antibodies (number of antibodies is indicated below the image). (Scale bars: *C-E* = 20 nm.) (*F and G*) Frequency distributions of angles between anti-His_6 (*F*) or anti-Myc (*G*).

5-HT_{3A} Receptor:

No. of Receptor Bound Antibodies	Receptor Alone		Receptor + anti-His_6 Antibody		Receptor + anti-Myc Antibody		Receptor + anti-V5 Antibody	
	n	%	n	%	n	%	n	%
0	149	97.4	331	69.7	238	63.0	156	97.5
1	4	2.6	98	20.6	95	25.1	4	2.5
2	0	0.0	40	8.4	40	10.6	0	0
3	0	0	1	0.2	4	1.0	0	0.0
4	0	0.0	4	0.9	1	0.3	0	0.0
5	0	0.0	1	0.2	0	0.0	0	0.0
5-$HT_{3A/B}$ Receptor:								
0	144	98.0	372	72.0	230	62.5	187	58.8
1	3	2.0	101	19.5	92	26.1	87	27.3
2	0	0.0	40	7.7	40	11.4	40	12.6
3	0	0.0	3	0.6	0	0.0	4	1.3
4	0	0.0	1	0.2	0	0.0	0	0.0
5	0	0.0	0	0.0	0	0.0	0	0.0

Table 11: Antibody tagging profiles for 5-HT_{3A}Rs and 5-$HT_{3A/B}$Rs samples visualised by AFM. Receptor alone category is a negative control determining the average number of artefactual receptor-antibody complexes.

particle is evidence that steric hindrances do not make these multiple binding events impossible.

3.3.3 Antibody angle measurments in 5-$HT_{3A(Myc)}$R samples

For 5-HT_{3A}R particles with two antibody attachments (**Figure 24$_{C-E}$**), peak antibody height and peak receptor height coordinates were connected by a line, to form two lines from which an angle could be measured. For both anti-His_6 and anti-Myc antibodies, the plotted frequency distributions had two clear peaks: 72 ± 3° (n = 21) and 144 ± 3° (n = 19) for the anti-His_6 antibody and 73 ± 3° (n = 20) and 136 ± 3° (n = 20) for the anti-Myc antibody (**Figure 24$_{F-G}$**). This data indicates that the antibody-bound subunits were either adjacent (expected angle 72°) or separated by another subunit (expected angle 144°). The frequency of angles measured at ~72° and ~144° are very similar, indicating that it is just as likely to find two antibodies together as it is to find them separated by another subunit. This also confirms that any steric hindrance does not prevent antibodies being in close proximity.

3.3.4 Antibody angle measurements in 5-$HT_{3A(Myc)/B(V5)}$R samples

Frequency of 5-$HT_{3A/B}$R particles forming complexes with different numbers of His_6, Myc or V5 antibody were recorded (**Table 10**). These frequency distributions show that no more than two anti-Myc antibodies, and no more than three anti-V5 antibodies were observed to bind the 5-$HT_{3A/B}$R particles. **Figure $25_{A\text{-}C}$** shows galleries of images of receptors with zero, one, and two bound antibodies for all three types of antibody. Corresponding frequency distributions of the angles between pairs of bound antibodies are shown in **Figure $25_{D\text{-}F}$**. The frequency distribution of the anti-His_6 and the anti-V5 receptor antibodies had two peaks, with means of 73 ± 3° (n = 15) and 145 ± 2° (n = 25) for the anti-His_6 antibody and 74 ± 3° (n = 18) and 140 ± 3° (n = 22) for the anti-V5 antibody. The distribution for the anti-Myc antibody, however, was a single peak, with a mean distribution of 140 ± 3° (n = 40).

To summarise, these results indicate: (i) the B subunit can either be adjacent (**Figure $25_{G(i)}$**) or separated by another subunit (**Figure $25_{G(ii)}$**); (ii) the A subunit is always separated by another subunit (**Figure $25_{G(iii)}$**); (iii) both the A and B subunits are present in the 5-$HT_{3A/B}$R in multiple copies. The only possible subunit stoichiometry that fits these data is 2A:3B and the only possible arrangement of subunits around the receptor rosette is B-B-A-B-A (**Figure 25_{H}**).

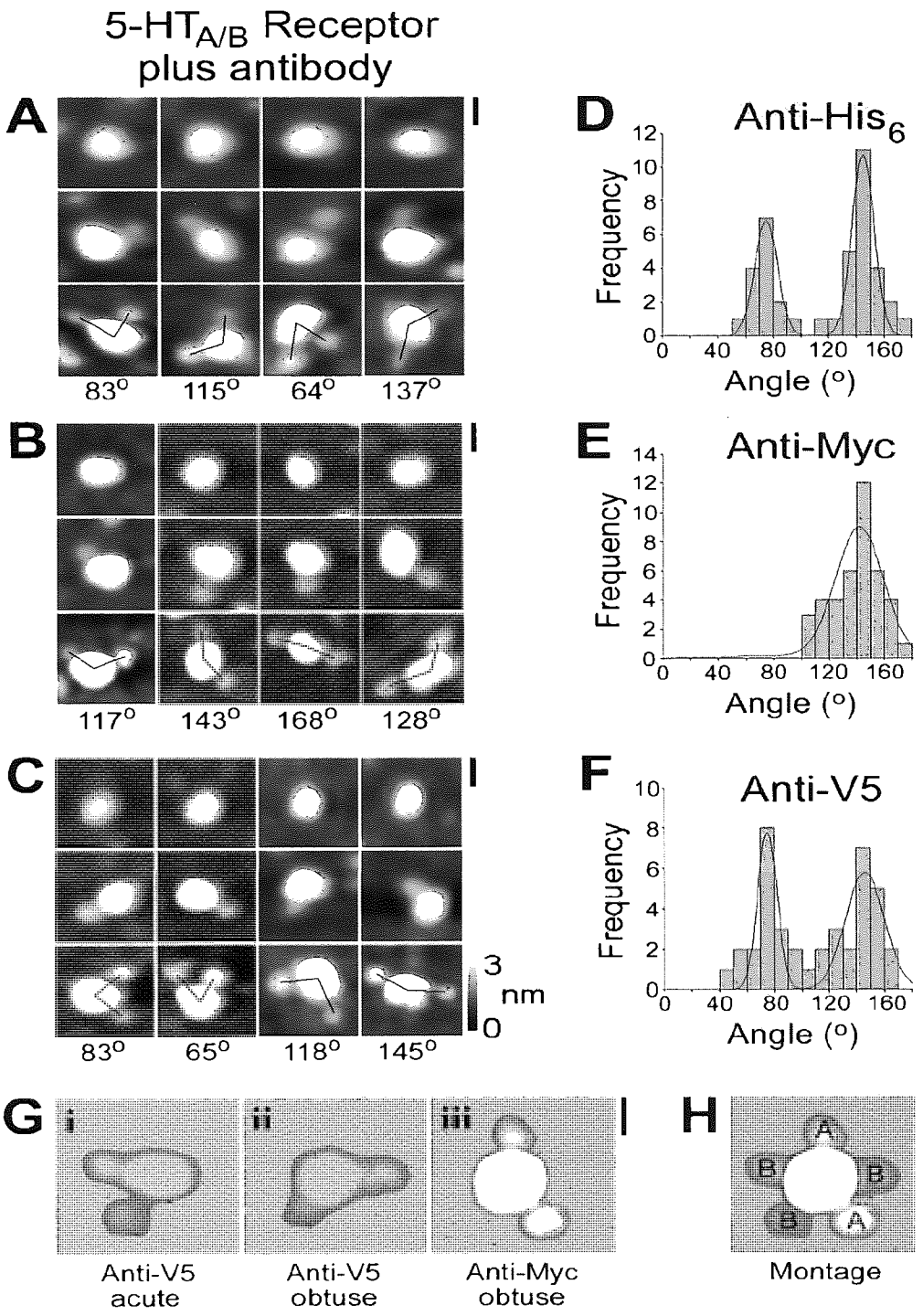

Figure 25: AFM images of complexes between 5-HT3$_{A/B}$Rs and *(A)* anti-His$_6$, *(B)* anti-Myc and *(C)* anti-V5 antibodies. Receptor images are either of uncomplexed (top), or bound by one (middle) or two (bottom) antibodies. *(D-F)* The corresponding frequency distribution of the angles for each specific antibody. (*G*) Zoomed images of receptors that are doubly bound by either (Gi and Gii) anti-V5 or (Gii) anti-Myc antibodies. (*H*) Superimposition of images Gi-Giii to illustrate the obligatory B-B-A-B-A arrangement of subunits around the receptor rosette. All scale bars = 20 nm.

3.4 Discussion

Prior to receptor imaging, wildtype 5-HT_3Rs were tagged, solubilised and affinity purified. These processes caused relatively small changes in the expression and pharmacology of 5-$HT_{3A/B}$Rs. The subsequent AFM data define the stoichiometry and pentameric arrangement of the 5-HT_{3A} and 5-HT_{3B} subunits within the heteromeric 5-HT_3R, and suggests that transfecting HEK293 cells with equal quantities of 5-HT_{3A} and 5-HT_{3B} cDNA results in the formation of only one heteromeric 5-HT_3R with the same stoichiomertry and arrangement, that is B-B-A-B-A.

3.4.1 Tagging

In order to validate the AFM studies, it was important to show that tagging did not change the expression of subunits and alter the receptor pharmacology. Similar tags have previously been used with the 5-HT_3R with no detrimental effect on their pharmacology in HEK293 and TSA201 cells (Davies, P. A. *et al.*, 1999; Boyd *et. al.*, 2003; Kelley *et al.*, 2003; Monk *et al.*, 2004). However, limited data exists for C-terminal tagging. The presence of a modified C-terminus could potentially interfere with tyrosine and alanine residues of 5-HT_{3A}Rs, which have been shown to affect expression (Pons *et al.*, 2004). The largest effect on expression, was seen with 5-$HT_{3A(Myc)}$Rs, demonstrated here by a 10-fold decrease in B_{max}. It is unclear to what extent this reduction was due to tagging, the inadequacies of a temperamental transfection procedure, or both. Indeed, immunofluorescence measurements (**Figure 17**) do not show a 10-fold reduction in 5-$HT_{3A(Myc)}$ expression compared to 5-$HT_{3A(Myc)/B(V5)}$, as is suggested by both [^{3}H]GR65630 saturation binding data in **Table 7** and competition binding in **Table 8**. However, the immunofluorescence pictures are of hand-picked cells rather than representing a whole population of cells. So, although cells transfected with 5-$HT_{3A(Myc)}$ subunit cDNA are quite capable of expression levels comparable to untagged cDNA, there may be a lower proportion of transfected to untransfected cells. Indeed, transient transfections are notoriously inconsistent and inefficient (Schlaeger, E.J. *et al.*, 2007), but offer a cost efficient alternative to electroporation and lipid-micelle based techniques.

It is clear, from saturation and competition binding data, that reductions in B_{max} do not similarly affect the K_d of any of the tagged receptors, which further suggests that tagging has a very minor effect on the affinity of the 5-HT_3R, compared to other such studies. The affinities of 5-$HT_{3A(Myc)/B(V5)}$Rs showed no significant difference from WT, suggesting that the neither of the tags affect binding. At the time of performing the experiments, the priority

was to establish the ability of the chosen antibodies to specifically identify the respective tagged subunits. The fact that the affinity of heteromeric receptors for 5-HT or granisetron was not detrimentally affected by tagging, and the homomer had demonstrated a very small decrease in affinity for GR65650, was enough evidence that tagging was not detrimental to the receptor binding sites present in our membrane preparations. This conclusion is substantiated by microscope images of receptor immunofluorescence (**Figure 17**), which shows significant levels of surface expression of 5-$HT_{3A(Myc)}$ subunit homomers, comparable to 5-$HT_{3A(Myc)/B(V5)}$R expression.

Surprisingly there was a significant difference in [^{3}H]granisetron affinity between untagged heteromeric and untagged homomeric receptors. This may reflect subtle differences in binding between the two different 5-HT_3R subtypes. This reduction in binding affinity was greater than that observed due to tagging, which further confirms the relatively minor effect of tagging upon the function of the receptor; both wildtype 5-HT_{3A} and 5-$HT_{3A/B}$ receptors being fully functional.

3.4.2 Solubilisation

Although solubilisation and purification of the 5-HT_3R is a well-established technique, performed in various cell lines (N1E-115, Lummis *et al.*, 1990; NCB-20, McKernan *et al.*, 1990; NG108-15, Boess *et al.*, 1992b), it was still necessary to test the optimum efficiency of solubilisation and whether receptors were adversely affected by the solubilisation conditions. Triton X-100 was chosen for its compatibility with radioligand studies (Fletcher *et al.*, 1997), and NaCl for its reported enhancement to receptor recovery (Boess *et al.*, 1992a). The presence of salt in receptor samples was found to be detrimental to the binding assay (data not shown), but its removal through desalting columns restored ligand binding, with a small decrease in receptor affinity that concurs with previous work (Boess *et al.*, 1992a). This decrease probably reflects the removal of membrane lipids around the receptor, and is unlikely to represent a change in the whole receptor architecture, which was our primary concern.

3.4.3 Western blotting

Western blotting ensured that membrane, soluble, and affinity purified preparations of tagged 5-HT_{3A}Rs and 5-$HT_{3A/B}$Rs were able to specifically bind the monoclonal antibodies used in later AFM imaging studies. Both 5-HT_{3A} and 5-HT_{3B} subunits exist as glycosylated and unglycosylated forms (see **Chapter 1**). The anti-V5 antibody detects 5-HT_{3B} primarily in the unglycosylated state. Glycosylation state is important for the assembly, stability and cell

surface expression of 5-HT_{3A}R (Monk *et al.*, 2004; Quirk *et al.*, 2004). Indeed, prevention of N-linked glycosylation with tunicamycin prevents cell surface expression and increases the intracellular pool of receptors. The protein isolated as a 50 kDa band is probably intracellular unglycosylated 5-HT_{3A}, and not that expressed on the cell surface. The possibility that these two forms of 5-HT_{3A} subunit might affect the outcome of our experiments should be considered. By cross-linking all subunits with dimethyl pimelimidate (primary amine crosslinker) before western blotting, it has previously been shown that tunicamycin treated cells, unlike untreated cells, lack high molecular weight bands. They only produced bands at molecular weights indicative of monomers; concluding that unglycosylated receptors are unable to form oligomers (Boyd *et al.*, 2002). Further, by separating native protein complexes using blue native PAGE (a form of gel electrophoresis that can does not require denaturing of proteins, capable of separating proteins up to 10,000 kDa) on purified 5-HT_{3A}Rs from xenopus oocytes, demonstrated an absence of intermediate assembly states compared to nAChR α7-subunits, concluding that assembly of the 5-HT_3 receptor subunits occurs rapidly after synthesis within the ER. Similar conclusions have been drawn from experiments with other Cys-loop receptors (Smith, M. M. *et al.*, 1986 (nAChR); Connolly *et al.*, 1996 ($GABA_A$)). It is therefore likely that even receptors that have not arrived at the plasma membrane are nonetheless correctly assembled. The immunofluorescence images also indicate that a considerable number of 5-HT_3 receptors are expressed at the plasma membrane, by virtue of their ring-like appearance. It should be emphasised that there is no evidence from the data presented, for the existence of more than one population of receptors.

3.4.4 Atomic force microscopy

To confirm that the particles identified as receptors were indeed 5-HT_3Rs, their dimensions were measured and the derived volume compared to that derived from molecular weight predictions. The disagreement between the two values can be explained by a number of limitations to the estimations. When proteins are adsorbed onto mica for AFM studies, they spread themselves over the polar mica surface, making the protein appear flattened from protein dimension measurements (Schneider *et al.*, 1998). Detergent that binds the receptor can also cause incongruities between AFM measurements and predicted values, as demonstrated by AFM of the $GABA_A$ receptor (Neish *et al.*, 2003), and gel filtration of solubilised 5-HT_3Rs (42% greater than estimation, Boess *et al.*, 1992). No significant differences were recorded between dimension measurements of homomeric and heteromeric receptors, in spite of heteromeric receptors containing three of the smaller 5-HT_{3B} subunits. It

would be interesting to use AFM to measure the dimensions of 5-HT_3R heteromers containing the truncated 5-HT_{3A} or 5-HT_{3D} subunit, to determine whether AFM is sensitive enough to detect these differences or if the receptor compensates for the size differences by making structural rearrangements.

The binding pocket for 5-HT_3R agonists and antagonists comprises six binding loops (A-F), three from each adjacent 5-HT_3R subunit (see **Chapter 1**). A stoichiometry of B-B-A-B-A creates three possible binding sites: 2 x A-B, 2 x B-A and 1 x B-B. The homomer has five identical (A-A) binding sites composed of the same amino acid residues, but this disparity in binding sites is not reflected by differences in ligand affinity. The competition binding data showed that the homomer has comparatively higher affinity for both 5-HT and granisetron compared to the heteromer, as has previously been demonstrated (Brady *et al.*, 2001); however, the difference is surprisingly small when compared to point mutation effects such as F107N, which causes a 10-fold loss in affinity (Steward *et al.*, 2000). The most parsimonious explanation relates this lack of effect to the 67% sequence similarity (48% sequence identity, determined using the alignment in **Chapter 1**) between the putative binding loops of 5-HT_{3A} and 5-HT_{3B} subunits. The fact that the Hill coefficient for agonist activation in the heteromer is approximately half that of the homomer when assessed by electrophysiology (Davies, P. A. *et al.*, 1999; Boyd *et al.*, 2002), still suggests that the different interfaces provide non-equivalent agonist binding sites.

3.5 Implications of a B-B-A-B-A arrangement

Channel conductance of 5-HT_3 receptors is largely controlled by amino acid residues surrounding portals in the HA stretch (see **Chapter 1**, Kelley *et al.*, 2003; Peters *et al.*, 2004). These residues differ between 5-HT_{3A} and 5-HT_{3B} subunits, and this accounts for differences in conductance. **Figure 26** shows the critical conductance-controlling amino acids of the HA stretch in a 5-$HT_{3A/B}$R with a subunit arrangement of B-B-A-B-A. This stoichiometry agrees with the data published by Kelley *et al.* (2003), which suggests that a pentameric 5-HT_{3B} receptor would have a conductance of 22 pS, with each subunit contributing 4.4 pS to the conductance, by proportion. Therefore, a stoichiometry of B-B-A-B-A should have a predicted single channel conductance of 13.2 pS, comparable to that recorded (Davies, P. A. *et al.*, 1999; Kelley *et al.*, 2003). The single channel conductance (γ) measurements by Kelley *et al.* (2003) demonstrated very little variance, even though multiple receptors in transfected

HEK293 cell membranes were tested. This substantiates the existence of a single population of receptors with the same conductance, and thus, stoichiometry.

The crystal structure of the acetylcholine binding protein (Brejc *et al.*, 2001) has been used as a template to refine the structural models of the nicotinic actetylcholine receptor, where the subunit stoichiometry (Reynolds *et al.*, 1978) and arrangement (Karlin *et al.*, 1983) are known. It should now be possible to extend this analysis to the heteromeric 5-HT_3 receptor, to characterise the potential agonist binding sites.

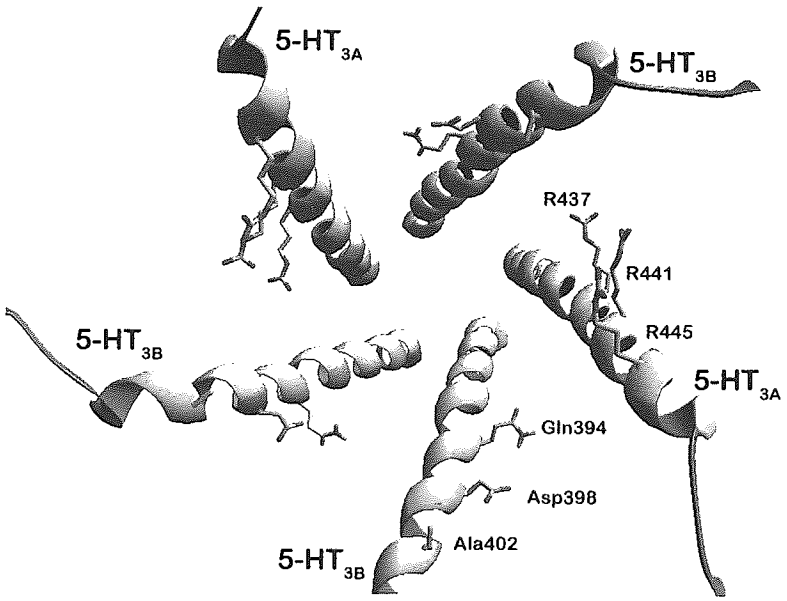

Figure 26: The B-B-A-B-A pentameric arrangement of five HA stretch (TM3-TM4 linker) helices lining the cation exit paths in the 5-$HT_{3A/B}$R, as viewed from the extracellular synaptic cleft (extracellular and TM domains are removed for clarity). Visible amino acids are stick representations of those residues responsible for differences in conductance between 5-HT_{3A}R and 5-$HT_{3A/B}$R subtypes (Kelley *et al.*, 2003; Peters *et al.*, 2004). It is now clear from this model that three of the ion portal exits are much more accessible when the amphipathic helix is provided by a 5-HT_{3B} subunit.

CHAPTER 4: HOMOLOGY MODELING

4.1 Introduction

Structural models provide valuable tools that can facilitate the interpretation of protein structure-function studies carried out by mutagenic analyses. Structurally resolved proteins, with significant homology to the protein of interest, can be used as templates for the construction of a homology model. In 2001 a soluble protein was isolated from the freshwater snail *Lymnaea stagnalis* (Smit et al, 2001), and was shown to exhibit ligand recognition characteristics very similar to nAChRs. Its structure was determined to a resolution of 2.7Å by X-ray crystallography (PDB entry: 1I9B, Brejc *et al.* 2001) and proved to be a close structural homologue of the extracellular domain of the nAChR previously determined by electron microscopic analysis (Unwin, 2005). There is relatively low amino acid sequence homology (24%) between the AChBP and extracellular domain of its closest Cys-loop family relative, the human α7-nAChR. However, the secondary structure of AChBP and all Cys-loop LGICs have the same scaffold which allows accurate predictions for the placement of amino acid residues (Sine *et al.* 2002; Sine *et al.* 2004), particularly within the highly conserved structure of the binding pocket. Such models have now been published in abundance for the Cys-loop family of receptors, the 5-HT_3R being no exception (see **General Introduction**).

4.1.1 Current homology models

A number of homology models from different research groups have now been published for the mouse homomeric 5-HT_3 receptor (m5-HT_{3A}R), using the AChBP as a template (Maksay *et al.* 2003; Reeves *et al.* 2003; Schreiter *et al.* 2003; Suryanarayanan *et al.* 2005; Yan and White 2005), some of which have subsequently been docked with antagonists. However, the AChBP structure best represents the open-channel state of the receptor (see **General Introduction**), which makes it a questionable choice of template for antagonist docking. The co-crystalised buffer molecule simulates the effects of an agonist, causing subunit rotations and the contraction of the loops, particularly the C-loop, towards the 'lid closed' conformation discussed in the **General Introduction** (and also Karlin 2002; Henchman *et al.* 2005). The result is a much smaller binding pocket volume, seemingly too small to accommodate large antagonists such as granisetron.

This problem has recently been addressed by Joshi *et al.* (2006) by docking granisetron into a m5-HT_{3A}R homology model based on the recently published closed-channel (apo) template of

nAChR obtained from *Torpedo marmorata* (2BG9, Unwin 2005). Currently, only one homology model of the human 5-$HT_{3A/B}$R (h5-$HT_{3A/B}$R) has been published (Maksay *et al.* 2004), based on the *Ls*-AChBP x-ray crystallography structure (PDB entry: 1I9B, Brejc *et al.* 2001). This homology model was not concerned with stoichiometry or arrangement of subunits within the 5-$HT_{3A/B}$R, but rather the interface between 5-HT_{3A} and 5-HT_{3B} subunits and how manually rotating these subunits alters the simulated binding characteristics of the receptor.

4.1.2 Aims of the new models

Now that the stoichiometry and architecture of the heteromeric h5-$HT_{3A/B}$R has been delineated (**Chapter 3**), we have been able to construct 5-$HT_{3A/B}$R and 5-HT_{3A}R homology models based on the 2BG9 atomic structure. This is the first 5-$HT_{3A/B}$R homology model with the correct subunit arrangement, and the first published 5-$HT_{3A/B}$R model based on the apo structure of nAChR.

It was highly desirable to make detailed comparisons of our 5-HT_3R binding pocket in the apo conformation to that of the agonist bound state using the same template nAChR. However, the agonist occupied state of the complete nAChR structure is only available at low resolution (9 Å, Unwin 1995); this work is currently being refined (personal communication, Unwin). In its absence, the 5-$HT_{3A/B}$R has been modelled using the more traditional AChBP template 1UV6 (Celie *et al.* 2004), bearing in mind that the structure of AChBP differs from the nAChR in several important respects: AChBP is i) homomeric, ii) is structurally symmetrical, and iii) most closely resembles the ligand-bound desensitised conformation. It is this last feature that makes 1UV6 a valuable additional template for comparing the relative positions of binding pocket residues before and after 5-HT binding. The natural agonist 5-HT was docked at the three distinct interfaces present in the heteromeric receptor, identified by the AFM results: A-B, B-A, and B-B.

4.2 Methods

The h5-HT_{3A} and h5-HT_{3B} subunits were aligned with the nAChR sequences from *Torpedo marmorata* using the software Clustal W (Thompson *et al.* 1994). Part of the TM3-TM4 intracellular loop of the 2BG9 structure is not resolved, leaving no template upon which modeling can be based. Consequently, amino acid sections P343-C421 and Q334-K378 (see **Figure 2** for sequence numbering) of h5-HT_{3A} and h5-HT_{3B} subunits respectively, were removed from the alignment by concatenation. The resulting alignments were used to

construct homology models of both homomeric h5-HT_{3A}Rs and heteromeric h5-$HT_{3A/B}$Rs using 2GB9 (Unwin 2005) as a structural template. In the case of the heteromeric receptor, the h5-HT_{3A} subunits were associated structurally with α subunits of the nAChR, and the h5-HT_{3B} subunits with the β, γ and δ subunits of the nAChR. MODELLER version 8.2 (Sali and Blundell 1993) was used to construct separate homology models for the homomeric and heteromeric receptor. These models represent the un-liganded, or ground state of the receptor. Using the same approach, a homology model was also constructed for heteromeric h5-$HT_{3A/B}$R using as the template, 1UV6 (Celie *et al.* 2004), an AChBP structure determined in the presence of carbamoylcholine.

The agonist, 5-HT was docked into the models using the docking program GOLD (Jones *et al.* 1995; Nissink *et al.* 2002). In the studies carried out using the AChBP as template, a docking envelope for the agonist was constructed representing the most probable docking area for the ligand, from an analysis of the highest scoring docked poses. In the studies using the nAChR as the template, the single lowest energy docked pose was selected from 400 poses generated. The antagonist granisetron was docked only to the nAChR-based homology model, as we have not yet developed an appropriate template for modelling 5-HT_3Rs occupied by an antagonist.

4.3 Results

4.3.1 5-HT_3R apo models

The atomic resolution images of homology modeled h5-HT_{3A}Rs and h5-$HT_{3A/B}$Rs are pictured in **Figure 27** in their pentameric subunit arrangement, and with only two subunits comprising the binding site interface being shown. In the 2BG9 structure, two ACh binding sites lie at the α–γ and α–δ subunit interfaces, viewed in an anticlockwise direction around the pentamer from the extracellular face (Unwin 2005). The interfaces of our h5-HT_{3A}R and h5-$HT_{3A/B}$R homology models are equivalent to the α-δ interface of the 2BG9 template, with the 5-HT_{3A} subunit being equivalent to the α-subunit, and the 5-HT_{3B} subunit assumes the non-α subunit role in the 5-$HT_{3A/B}$R. The 5-HT_{3B} subunit is unlikely to be homologous to the α-subunit because it is deficient in a cation-π binding residue equivalent to W183 (Beene *et al.* 2002, and subsequent discussion).

4.3.1.1 Intersubunit interactions

Intersubunit interactions have been predicted for residues that span the subunit interface (**Figure 28**) and are orientated within 4 Å from each other. D132 does not fall within this 4 Å

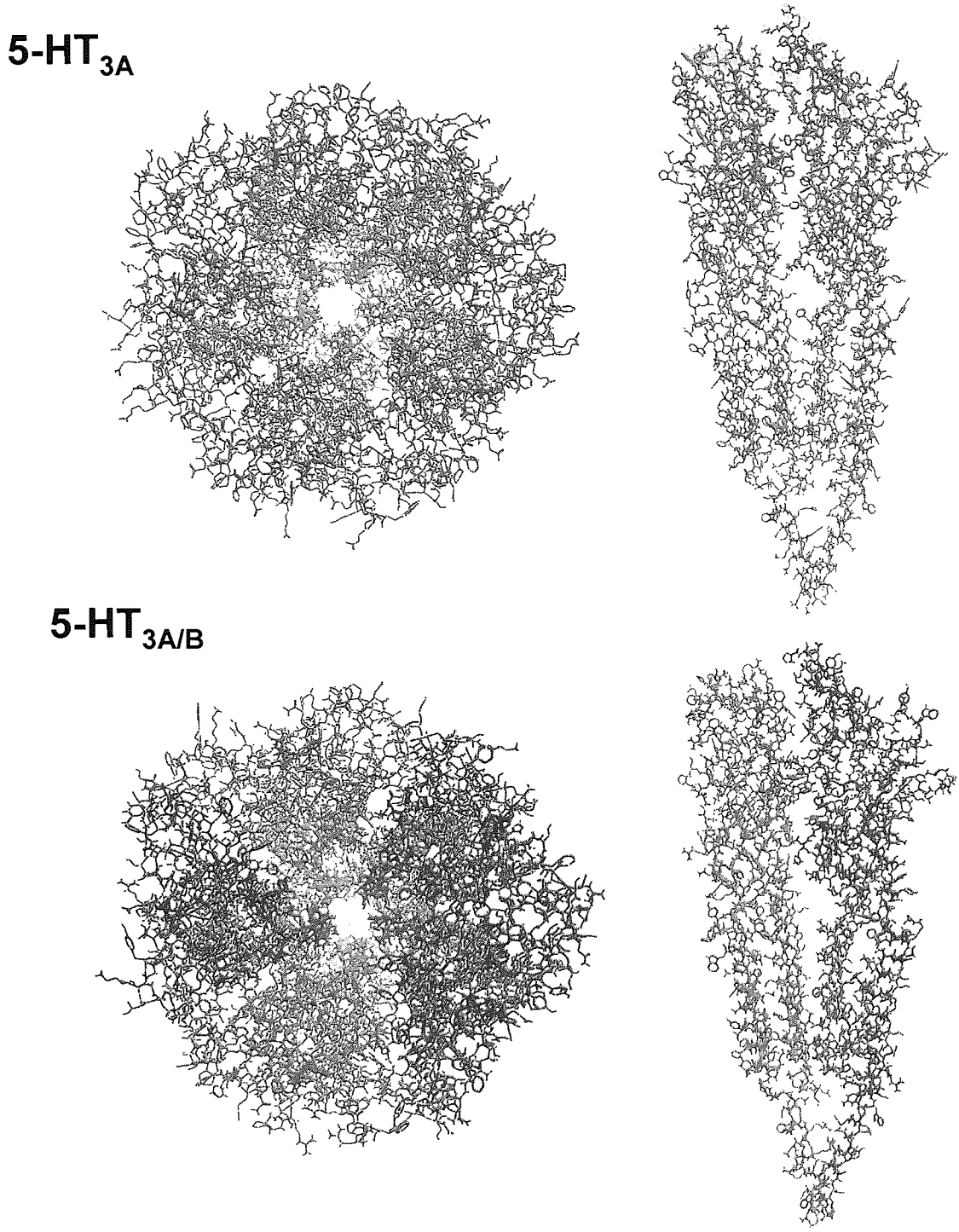

Figure 27: Full homology models of the h5-HT_{3A}R and 5-$HT_{3A/B}$R structures in the apo conformation. Both models are based on the 2BG9 template. (*Left*) Five pentamerically arranged subunits of the 5-HT_3R viewed from the extracellular face, looking down the long axis of symmetry. (*Right*) two binding interface subunits viewed perpendicular to the long axis, 5-HT_{3A} subunit amino acids are red, 5-HT_{3B} subunit amino acids are blue.

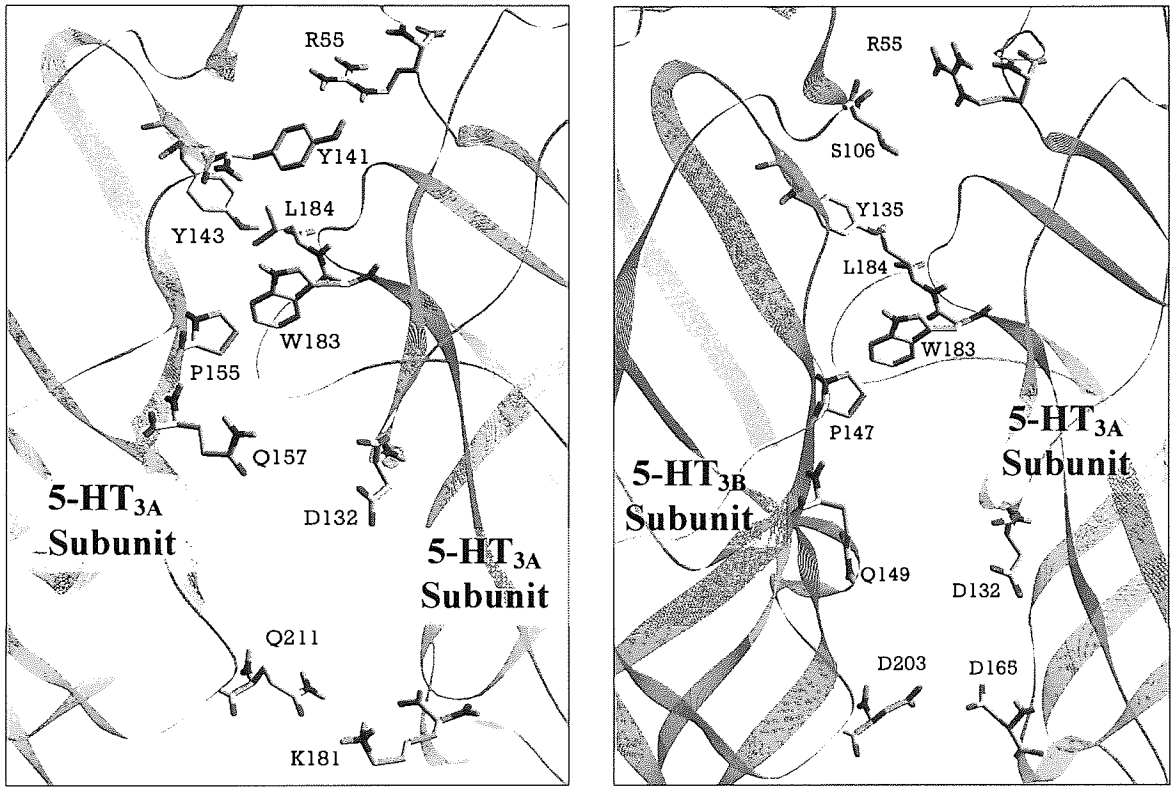

Figure 28: Intersubunit interactions between amino acid residues of the A-A (left) and A-B subunits (right) interfaces, viewed from the channel and looking towards the C-loop. These 5-HT$_3$R models are based on 2BG9 (Unwin, 2005). Only those amino acids that are predicted to make intersubunit interactions have been displayed as stick representations. Putative binding loops are coloured as per Figure 2. This depiction of the binding site is also a useful means of appreciating the distances between subunits in this apo conformation, compared to the agonist-bound state models used later, where the distances between these residues is measurably altered.

cut-off in our models, but due to potential limitations in the alignment and subsequent testing of alternative rotamers (see Discussion), has been included. From subunits of the A-A interface, predicted residue interactions include (principal face-complementary face): R55-S106, H185-Y141, L184-Y143, W183-P155, D132-Q187/W65 and K181-Q211. At the A-B interface (5-HT_{3B} residues will be highlighted in bold from this point on): R55-**S106**, L184-**Y135**, W183-**P147**, D132-**Q149** and D165-**D203**.

4.4 Closed channel docking

Zoomed images of the 5-HT_{3A}R and 5-$HT_{3A/B}$R binding pocket interfaces are shown in **Figure 29** with the natural agonist, 5-HT, and granisetron in docked positions chosen from their single best docked pose, representative of the highest populated cluster for each ligand. Those amino acid residues within 7Å of the docked ligand are visible, coloured according to the loop to which they belong, with grey residues representing those outside of the putative binding loop region. **Table 11** gives the measured distances between atoms of residues in close proximity to docked 5-HT and granisetron in the homomer and heteromer, and includes residues previously implicated as being proximal to a bound ligand by other research groups. **Table 12** is a quick-reference to highlight those residues that have a predicted location within 5 Å of either 5-HT or granisetron. This is a threshold distance used by most researchers to assess whether a residue is likely to interact. In our closed channel model, the significance of this threshold is even greater.

Figure 29 (overleaf): Amino acid residues comprising the 5-HT and granisetron binding pockets in homomeric h5-HT3A and heteromeric 5-HT3A/BRs. Docked ligands are coloured orange, and amino acid residues are coloured according to the loop to which they belong. Images are of the receptor viewed perpendicular to the long axis, from the (*left*) extracellular and (*right*) luminal side. The exact orientation chosen is that which gives the clearest view of all the displayed residues, i.e. not all orientations are exactly the same. (*a and b*) The interface between two 5-HT3A subunits in the 5-HT3AR or (*c and d*) one 5-HT3A subunit and one 5-HT3B subunit in a 5-HT3A/BR is depicted with (*a and c*) the natural agonist, 5-HT, or (*b and d*) granisetron docked. Amino acids shown are those within 7 Å of the docked ligand, colour coded according to the binding loop to which they belong: loop-A, loop-B, loop-C, loop-D, loop-E, loop-F. Those residues coloured grey are those not associated with any of the canonical binding loops.

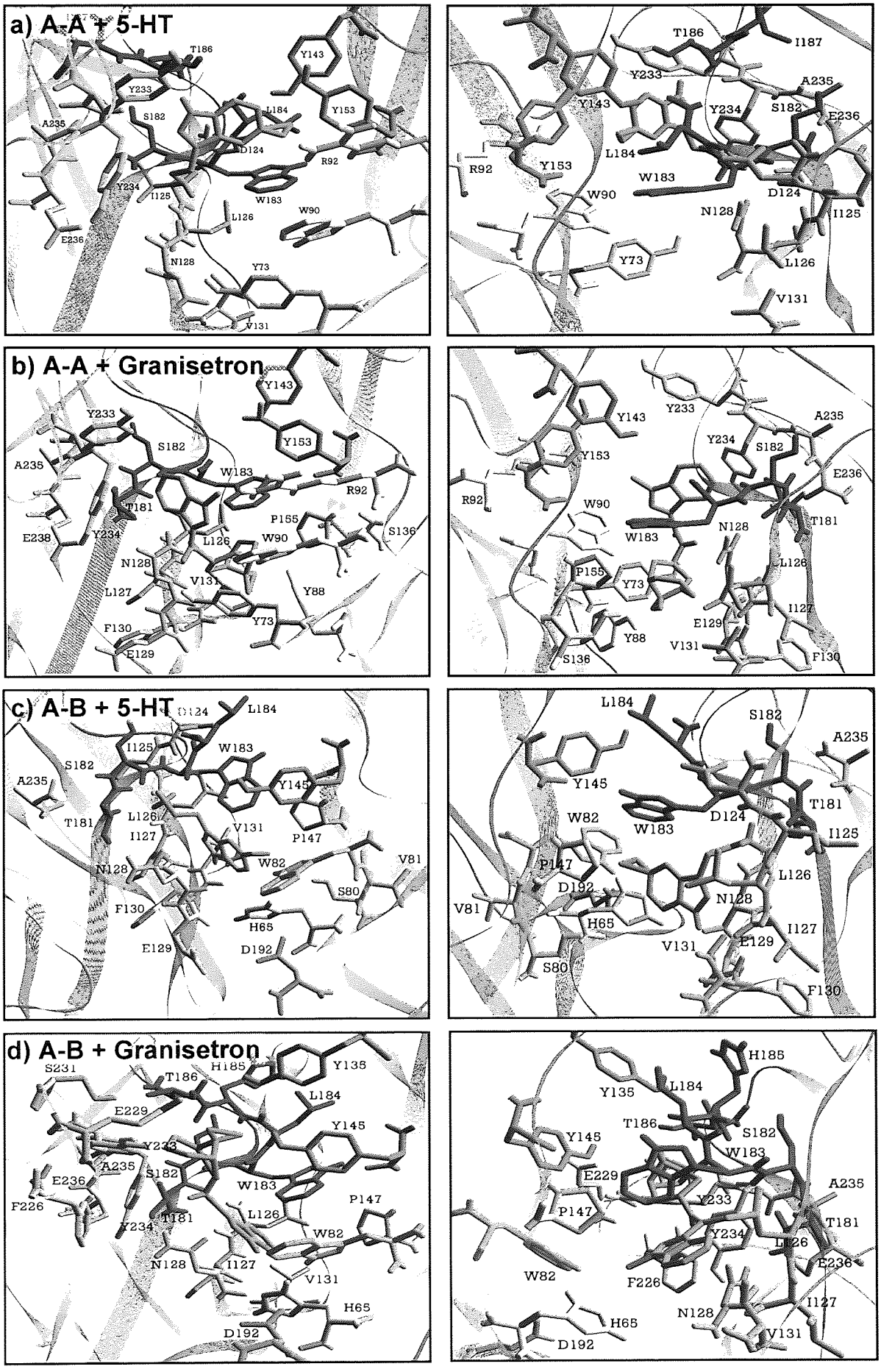
a) A-A + 5-HT
T186
Y143
Y233
S182
L184
Y153
A235
D124
R92
Y234
I125
W183
W90
L126
E236
N128
Y73
V131
T186
I187
Y233
A235
Y143
Y234
S182
E236
L184
R92
Y153
W183
W90
D124
N128
I125
Y73
L126
V131
b) A-A + Granisetron
Y143
Y233
S182
Y153
A235
W183
R92
T181
P155
S136
E238
Y234
L126
W90
N128
V131
Y88
L127
Y73
F130
E129
Y143
Y233
A235
Y234
S182
Y153
E236
R92
W90
T181
N128
W183
P155
L126
Y73
I127
E129
Y88
V131
F130
S136
c) A-B + 5-HT
D124
L184
I125
W183
S182
A235
Y145
T181
L126
V131
I127
P147
N128
W82
V81
S80
F130
H65
E129
D192
L184
S182
A235
Y145
T181
W82
W183
D124
I125
P147
L126
D192
N128
V81
H65
I127
V131
E129
S80
F130
d) A-B + Granisetron
S231
T186
H185
Y135
L184
E229
Y145
Y233
A235
S182
E236
W183
F226
P147
T181
L126
Y234
W82
N128
I127
V131
H65
D192
H185
Y135
L184
T186
Y145
S182
W183
E229
A235
P147
Y233
T181
Y234
L126
E236
W82
F226
N128
I127
H65
V131
D192

Loop	5-HT_{3A}/5-HT_{3B} Residue	A-A 5-HT	A-A Granisetron	A-B 5-HT	A-B Granisetron
β1	Y73/**H65**	OH-N/S-1° (7.1)	OH-O/S-CO (2.4) π-C/S-TR (3.4)	NH-O/S-OH (3.9)	OH-N/S-AR (5.1)
D	Y88/**S80**	O-OH/S-IR (9.8)	OH-N/S-TR (3.4)	O-OH/S-OH (5.7)	OH-N/S-AR (7.9)
D	I89/**V81**	O-OH/M-IR (9.7)	-	O-OH/M-OH (6.2)	-
D	W90/**W82**	π-π/S-IR (7.2)	π-π/S-AR (4.8) π-C/S-TR (5.1)	NH-O/S-OH (2.2) π-π/S-IR (4.4)	π-π/S-AR (4.9) OH-N/S-AR (4.2)
D	Y91/**Y83**	-	-	NH-O/M-OH (7.6)	NH-N/M-AR (10.0)
D	R92/**Q84**	NH-O/S-OH (6.6)	NH-N/S-AR (5.5)	S-OH (8.6)	NH-N/S-TR (8.1)
D	Q93/**E85**	NH-O/M-OH (8.6)	-	M-OH (11.5)	NH-N/M-TR (12.5)
D	Y94/**V86**	π-π /S-IR (13.8)	-	M-OH (15.6)	NH-N/M-TR (15.0)
A	D124	O-NH/S-1° (6.2)	O-NH/S-N1 (7.7)	O-NH/M-1° (3.1)	NH-O/S-N1 (8.7)
A	I125	N-NH/M-1° (7.3)	-	O-NH/M-1° (4.0)	NH-O/M-N1 (8.9)
A	L126	OH-N/M-1° (4.9)	S-TR (3.5)	O-NH/M-1° (2.9)	M-AR (4.2)
A	I127	O-NH/M-1° (7.4)	M-TR (3.9)	O-NH/M-IR (2.2)	M-AR (4.3)
A	N128	NH-N/S-1° (2.8)	N-NH/S-N1 (2.0)	O-NH/M-IR (2.3)	NH-O/S-N1 (5.3)
A	E129	NH-N/M-1° (8.5)	M-TR (4.5)	N-NH/M-IR (4.0)	NH-N/M-AR (7.1)
A	F130	π-π/S-IR (15.6)	M-TR (5.3)	O-NH/M-IR (3.2)	-
A	V131	S-IR (12.0)	S-TR (3.4)	S-IR/ (3.1)	S-AR (4.6)
β5	S136/ **Y128**	OH-O/S-IR (10.2)	OH-N/S-TR 5.6)	π-π (9.2)	-
E	Y143/**Y135**	OH-O/S-OH (2.4)	O-NH/S-AR (6.4)	S-IR (11.4)	OH-N/S-TR (4.9)
E	Q151/**E143**	NH-O/S-OH (7.0)	O-NH/S-AR (10.0)	S-IR (12.7)	S-TR (7.7)
E	Y153/**Y145**	π-π/S-IR (3.8) O-OH/S-OH (4.4)	O-NH/S-AR (5.8)	S-IR (6.6)	OH-N/S-TR (4.1)
E	P155/**P147**	N-OH/S-OH (7.0)	C-π/S-TR (3.4)	S-OH (4.2)	S-AR (6.1)

Table 11 (continued on next page): angstrom distances measured between computationally docked 5-HT/granisetron and proximal amino acid residues of the putative binding pocket at A-A and A-B interfaces. Angstrom measurements are in brackets with preceding text indicating interacting atoms (before /) the functional group in which they are located in the amino acid and ligand respectively, thus (atoms of amino acid)-(atoms of ligand)/(Main chain (M) or Side chain (S) of amino acid)-(Functional group of ligand). Where, for 5-HT IR = indole ring, 1° = primary amine, OH = hydroxyl group. For granisetron AR = aromatic ring, TR = tropane ring, N1 = nitrogen of peptide bond, CO is the carbonyl group within the peptide bond. For both π-π = two interacting delocalized electron clouds from two aromatic ring structures (measured as closest carbon atoms). The absence of side chain, main chain, or functional group notation, indicates no specific interaction can be determined in the orientation predicted, but distances between proximal atoms have still been measured.

Loop	5-HT$_{3A}$/5-HT$_{3B}$ Residue	A-A 5-HT	A-A Granisetron	A-B 5-HT	A-B Granisetron
B	T179/**T171**	O-NH/S-1° (6.7)	O-NH/M-1° (6.4)	O-NH/M-1° (5.4)	O-NH/S-N1 (6.5)
B	T181	OH-N/S-1° (3.9) O-NH/M-1° (3.6) NH-N/M-1° (5.8)	S-AR (4.1)	O-NH/ S-1° (4.5) O-NH/M-1° (2.1) NH-N/ M-1° (3.5)	OH-N1/S-N1 (3.9)
B	S182	O-NH/M-1° (2.0)	M-AR (3.6)	OH-N/S-1° (5.0) O-NH/M-1° (2.7) N-NH/M-1° (4.8)	O-NH/S-N1 (4.8) M-TR (3.6)
B	W183	O-NH/M-1° (2.0) **π-N/S-1° (3.1)** π-π/S-IR (3.6)	π-π/S-AR (3.6) O-NH/M-1°(5.3)	O-NH/ M-1° (2.2) **π-N/S-1° (4.8)** π-π /S-1° (3.1)	π-π/S-AR (3.1) S-TR (4.4) O-NH/S-N1 (4.3)
B	L184	O-OH/ M-IR (3.9) N-NH/M-1° (3.9)	-	NH-N/M-1° (5.4)	S-TR (2.3)
B	T186	O-NH/ S-IR (2.1)	-	-	OH-N/S-TR (3.8)
F	W195/**L187**	π-π/S-IR (15.8)	NH-N/S-AR (14.2)	-	S-TR (15.4)
F	R196/**R188**		NH-N/S-AR (13.5)	-	-
F	K200/**D192**	NH-O/M-OH (17.6)		O-OH/S-IR (6.7)	O-NH/S-AR (6.2)
F	K202/**Q194**				NH-N/S-AR (12.2)
F	S206/**K198**		OH-N/S-AR (11.6)	-	NH-N/S-AR (13.3)
F	V207/**A199**		S-TR (9.7)	O-OH/M-OH (10.9)	NH-N/S-AR (13.9)
β9	R224	O-NH/M-IR (8.3)	-	NH-O/S-OH (13.0)	NH-N/M-N1 (8.2)
C	F226	C-C/S-IR (9.0)	π-π/S-AR (8.4)	π-π/S-IR (12.4)	π-C/S-TR (6.2)
C	S227	O-NH/M-IR (14)	O-NH/M-AR (15.1)	NH-O/M-OH (15.9)	S-TR (10.9)
C	M228	S-NH/S-IR (11.9)	S-NH/S-AR (10.5)	S-OH (11.5)	S-C/S-TR (7.6)
C	E229	N-NH/S-IR (9.3) N-NH/M-IR (10.9)	N-NH/S-AR (10.2) N-NH/M-AR (11.8)	O-OH/S-OH (14.4)	S-TR (6.4) O-NH/S-N1 (10.6)
C	S231	OH-N/S-IR (8.00)	OH-N/S-TR (11.9)	OH-O/S-OH (14.6)	OH-N/S-TR (7.0)
C	Y233	π-π/S-IR (4.2) O-NH/S-IR (6.4)	π-π/S-AR (4.6) OH-N/S-PR (8.0) OH-O/S-N1 (6.4)	π-π/S-IR (12.2) OH-O/S-OH (12.6)	S-TR (2.9) OH-N/S-TR (7.6)
C	Y234	π-N/S-1° (7.3) π-π/S-IR (3.4) NH-N/M-IR (3.8)	π-π/S-AR (3.8) O-NH/S-AR (8.9)	π-π/S-IR (9.1) OH-N/S-1° (9.2) π-N/S- 1° (7.2)	OH-N/S-N1 (4.3) π-π/S-AR (7.2) S-TR (3.0)
C	A235	NH-N/M-IR (7.1)	M-AR (6.2)	O-NH/S-1° (6.7)	O-NH/M-N1 (6.9)
C	E236	O-NH/ S-1° (6.3) O-NH/S-IR (9.9)	O-π/S-AR (6.2) O-NH/S-N1 (7.3)	O-NH/S-1° (8.5)	O-NH/S-N1 (6.5)
C	M237	-	S-AR (9.0)	NH-N/M-1° (7.7)	O-NH/M-N1 (11.0)

Table 11: continued from previous page.

$5\text{-}HT_{3A}/5\text{-}HT_{3B}$ Loop and Residue		2BG9 Model				1UV6 Model (5-HT Binding)		
		A-A 5-HT	A-A Granisetron	A-B 5-HT	A-B Granisetron	A-B	B-A	B-B
β1	Y73/H65	-	+	+	-			
D	Y88/S80	-	+	-	-			
D	W90/W82	-	+	+	+	+	+	+
D	R92./Q84					+	+	
β3	S114/S106					+		
A	D124/D116	-	-	+	-			
A	I125/I117	-		+	-			
A	L126/I118	+	+	+	+			
A	I127/I119	-	+	+	+			
A	N128/N120	+	+	+	+			
A	E129/E121	-	+	+	-			
A	F130/F122	-	-	+	-			
E	Y141/Y133					+	+	+
E	Y143/Y135	+	-	-	+	+	+	+
E	R145/N137							+
E	Q151/E143						+	+
E	N152/N144						+	+
E	Y153/Y145	+	-	-	+		+	+
E	P155/P147	-	+	+	-			
B	T179/T171							+
B	T181/K173	+	+	+	+	+	+	+
B	S182/S174	+	+	+	+	+	+	+
B	W183/I175	+	+	+	+	+	+	+
B	L184/L176	+	-	-	+	+	+	
B	H185/H177					+	+	+
B	T186/T178	+	-	-	+			
F	V207/A199						+	
C	F226/I217					+	+	
C	S227/L218					+	+	
C	M228/Q219						+	+
C	E229/S220						+	+
C	S230/S221						+	+
C	S231/A222					+	+	+
C	N232/G223						+	+
C	Y233/G224	+	+	-	+	+		
C	Y234/F225	+	+	-	+		+	+
C	K238/Q229					+		

Table 12: Residues of the $5\text{-}HT_3R$ binding site that are within 5 Å (+) of ligands docked into both the apo and ligand bound receptor conformation.

4.4.1 5-HT at the A-A interface

Our 5-HT docked model is similar to the predicted 5-HT docking model by Suryanarayanan *et al.* (2005). The closed channel A-A interface model shows that the 5-HT docks in close proximity to a number of aromatic residues: the primary amine is docked just 3.1 Å from the aromatic ring of W183 and 2.0 Å from its main chain carbonyl group; its hydroxyl group is within 5 Å of the E-loop residues Y143 and Y153; and its indole ring is just 3.4 Å from making π-π interactions with Y234 from the C-loop. The primary amine is also close to a number of other residues of the A-and B-loop of the principal subunit, whilst the indole ring is positioned to the centre of the putative binding pocket and towards the C-loop. It is possible for residues of the B-loop to primarily interact with the primary amine via hydrogen bonds, though T186 may make such interactions via the indole amine group. Of the C-loop residues, only Y233, Y234 and E236 are within 6.3 Å of any part of the 5-HT molecule. The majority of residues from the complementary subunit are relatively distant, with F-loop residues an average of 17 Å from any part of the 5-HT molecule. Only the aromatic E-loop residues Y143 and Y153 are within 4 Å of the hydroxyl or indole ring of the 5-HT molecule, with Y143 capable of making hydrogen bonding interactions.

4.4.2 Granisetron at the A-A interface

The tropane ring of granisetron is docked pointing towards the channel lumen, whereas the indazole ring is closer to the C-loop. **Figure 30** shows models of the A-A and A-B binding pockets and superimposes the docked 5-HT and granisetron molecules within them. This clearly shows that the aromatic ring of granisetron assumes a near identical position to that predicted for the primary amine group of 5-HT at this interface, between Y234 (C-loop) and W183 (B-loop), whilst the amine group of granisetron's aromatic ring structure potentially interacts with residues from the E-loop (see **Table 11**). The main chain of W183 does not interact as intimately with granisetron compared to the primary amine of 5-HT, however, it is feasible for π-π interactions to occur between respective aromatic rings, which are separated by 3.6 Å. The proximity of granisetron to W183 also means that the side chain of the B-loop residue T181 and main chain carbonyl group of S182 are in close proximity (~4.0 Å from the aromatic ring). The side chain of N128 (A-loop) is the closest residue to the docked granisetron molecule, located just 2.0 Å from the nitrogen that links the tropane and indazole ring. Many C-loop residues are distant in comparison to the docked position of 5-HT, which

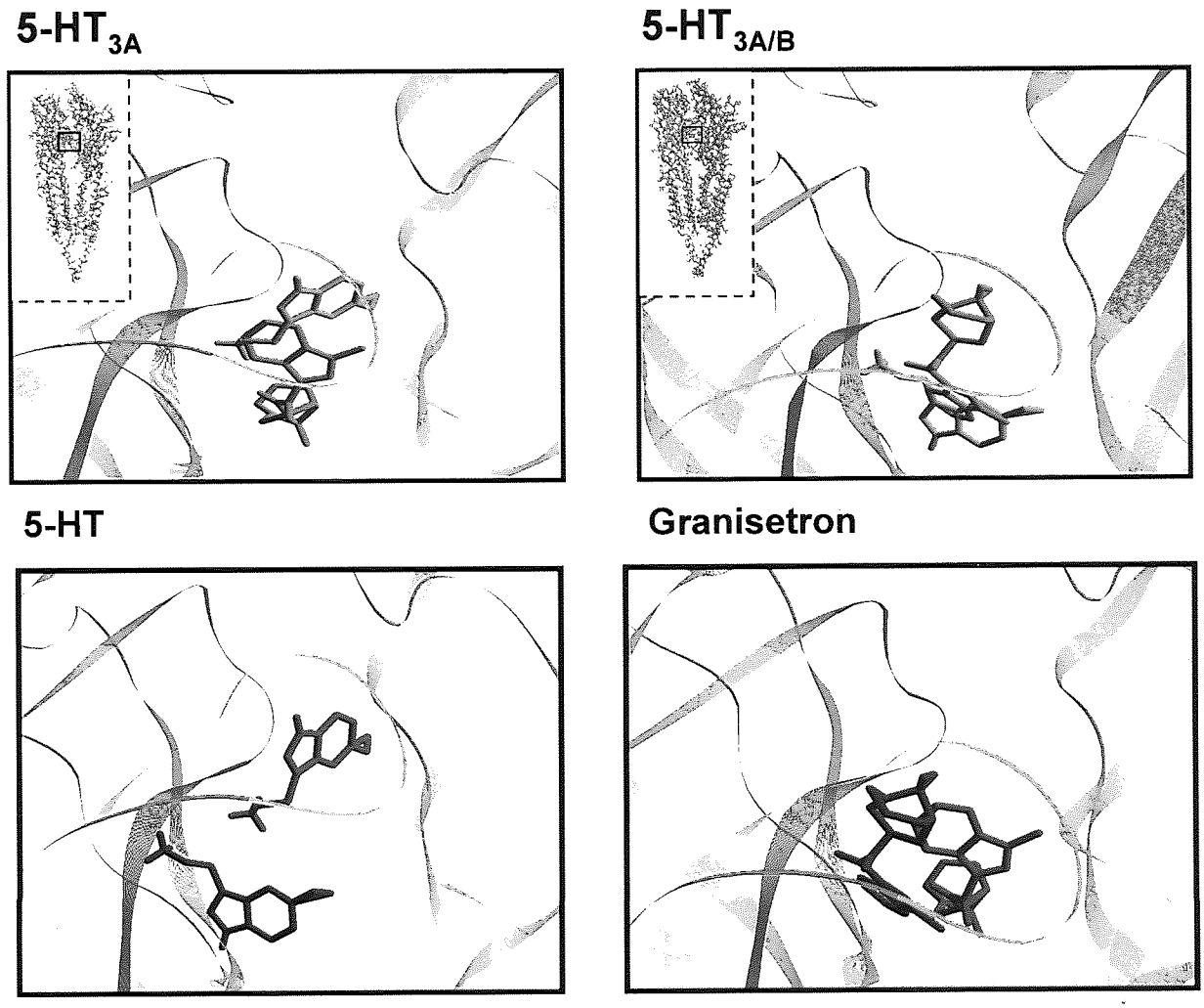

Figure 30: A comparison of the single best docked poses for 5-HT and granisetron at the 5-HT$_{3A}$R A-A and 5-HT$_{3A/B}$R A-B interfaces in the 5-HT$_3$R homology models based on 2BG9 (Unwin, 2005). (*Top: 5-HT$_{3A}$ and 5-HT$_{3A/B}$*) Inset is the global atomic structure of two subunits that compose the two binding interfaces A-A (h5-HT$_{3A}$) and A-B (h5-HT$_{3A/B}$). The ligand docking arena is within the solid black square. The main pictures are an enlargement of the ligand docking area with 5-HT (light orange) and granisetron (dark orange) located in their lowest energy docking positions at the interfaces indicated. (*Bottom: 5-HT and granisetron*) To compare docking positions of the same ligand at A-A (red ligand structure) and A-B (blue ligand structure) interfaces, docking position coordinates have been superimposed within a generic binding site for both 5-HT and granisetron, as indicated. The recognition loops are colour coded as before.

reflects the slightly more 'buried' docking position of granisetron towards the hydrophobic residues of the A-loop, closer to the channel lumen at the back of the binding pocket. The Y73 residue does not belong to a binding loop, but is just 2.4 Å from the carbonyl group of granisetron. Y88 is the only residue of the D-loop within 3.5 Å of any part of the granisetron molecule. All E- and F-loop residues are over 5 Å from granisetron, with the exception of P155, which has its side chain 3.4 Å from the tropane ring.

4.4.3 5-HT at the A-B interface

To compare how the binding interface affects the relative docking position of each ligand, **Figure 30** has superimposed the A-A and A-B interface docking co-ordinates of the same ligand onto one general atomic structure of the 5-HT_3R binding interface. This shows that 5-HT assumes a docking position notably closer to the principal subunit binding loops relative to its docking position in the homomeric receptor. Specifically, the discrepancy between the 5-HT primary amine position is 3.4 Å, where this group is buried between the A- and B-loop residues (**Table 11**) at the A-B interface. The rest of the molecule is much lower in the binding pocket (closer to the plasma membrane), and it is less likely that it would interact with W183 from such a position. Due to the upside-down orientation of the indole ring (pyrrole amine points down towards plasma membrane), 5-HT is docked considerably lower in the binding pocket in the heteromer (**Figure 30**). As a consequence, the C-loop residues are relatively distant, because the arm of the C-loop is significantly higher than the docked 5-HT molecule.

4.4.4 Granisetron at the A-B interface

Once again granisetron occupies the same general docking arena at the A-B binding interface as that predicted for previous docking simulations, but, as was the case for 5-HT A-B interface docking, it is located slightly closer to the A- and B-loop residues. The orientation of the granisetron molecule is opposite to that found in the homomer; the tropane ring is closest to the top of the receptor, above the aromatic ring, which is oriented towards the plasma membrane (towards TMD). Granisetron docking orientations depicted in **Figure 30** show that granisetron docked at the A-B interface requires just a 180° rotation around its long axis to alter the indole nitrogen position to fit that of the A-A interface, unlike the two 5-HT docking orientations; 5-HT would need to flip 180° around both axis of rotation to move its hydroxyl group and indole amine to matching orientations.

Potential π-π interactions between the benzene rings of granisetron and W183 are within 3.1 Å, as per 5-HT docking. The closest C-loop residues are Y233 and Y234, which are ~3.0 Å

away. The complementary subunit residues of all the loops are further from the granisetron molecule than found when the antagonist is docked into the A-A interfacial binding site, with notable exceptions: W90 could make potential π-π interactions being a similar distance from the aromatic ring of granisetron (4.9 Å), and Y143 and Y153 hydroxyl groups were much closer to the tropane ring at the A-B interfacial binding site.

4.5 Open/desensitized channel docking

The binding pocket of the open/desensitized receptor is much smaller in volume than the closed apo state receptor. By docking the simplest ligand, 5-HT, into this much more restrictive environment, it is it is feasible to explore the presence of potential binding sites at all three interfaces present in the heteromeric receptor with a B-B-A-B-A subunit arrangement: A–B, B-A and B-B **(Figure 31)**. The interfaces between subunits are established as sites of drug interaction in all LGICs, making each one a potential site of agonist/antagonist binding or allosteric modulation. Comparison of the properties at each of these interfaces, and the amino acids from which they are composed, provides useful information that can be correlated to how this environment affects ligand binding.

Figure 31 is a schematic representation of predicted docking envelopes, showing residues within 5 Å of the docked envelope that are colour coded with respect to the canonical recognition loops upon which they are found, the complete loops being shown in full in the schematic. A different colour scheme has been used to represent the binding loops for these models due to computational limitations.

Compared to the previous models based on the apo receptor conformation, it is clear that in all binding interfaces, the C-loop has moved to a capped conformation, restricting access to the binding site from the extracellular side. The F-loop has also moved closer to the binding pocket, though poor atomic resolution in this region means that such interpretations must be treated with caution.

The clusters of 5-HT docking events are in the same region of the ligand binding pocket for all three interfaces. The A-B interface supports a larger number of docking positions, stretching much further from the E-loop to the back bone of the B-loop (L178-T179), compared to B-A and B-B interfacial binding. The B-A interface supports binding between the B- and E-loops, but rather focuses around the B-loop residues **K173** and **S174** in the absence of a tryptophan at position 175. The B-B interface supports binding at principal face

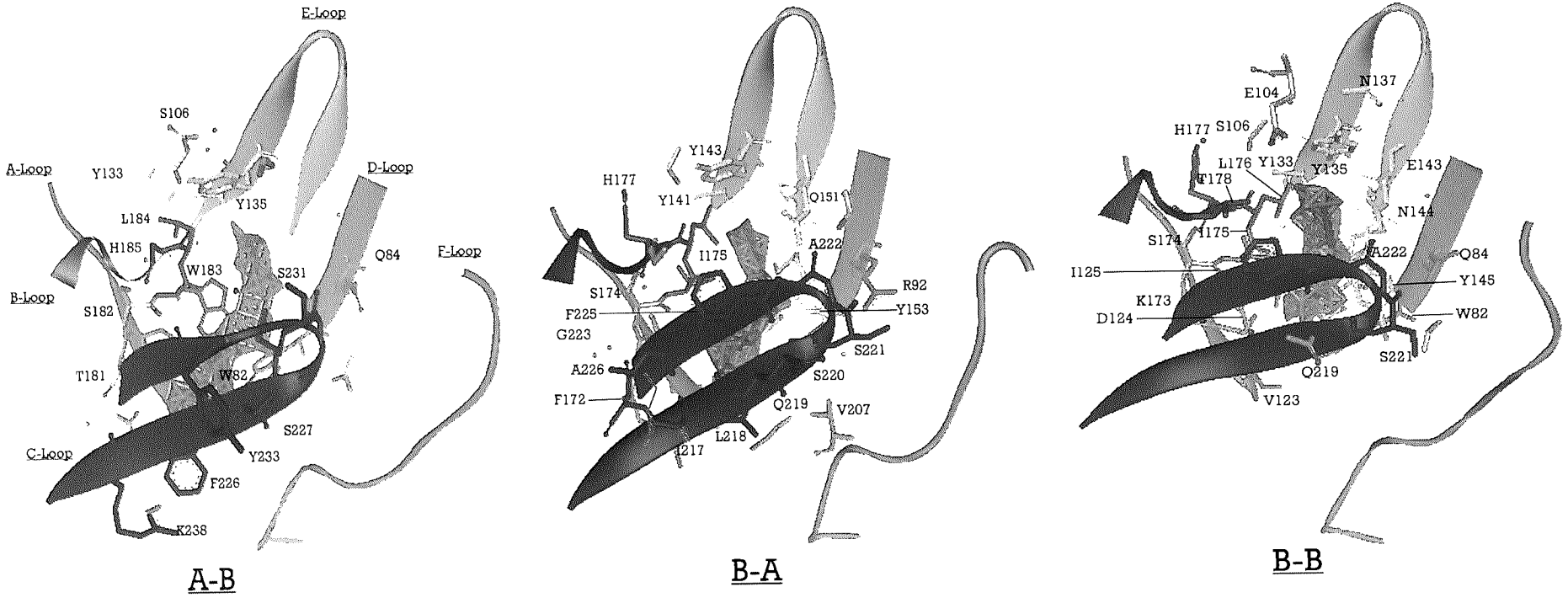

Figure 31: Recognition envelopes for the natural agonist 5-HT at the homology model of the heteromeric $5HT_{3A/B}R$, generated from the agonist (carbamylcholine) occupied AChBP template (1UV6, Celie *et al.*, 2004). All three distinct interfaces of the model are shown and are colour coded in the same manner to those shown above. However, the lowest energy cluster of the docked poses of the agonist are shown in khaki, rather than the single representative docked pose, as used in the previous figures. The recognition loops colour coded, together with their amino acids that are within 5 Å of the docked ligand: A = red, B = green, C = blue, D = purple, E = yellow, F = cyan, those residues coloured grey are not associated with any of the canonical binding loops.

residues in a similar envelope of docking events as the B-A interface, but much less emphasis is placed on E-loop residues.

4.6 Discussion

The atomic coordinates from nAChR electron micrograph images and the crystal structure of *Ls*-AChBP have been used to create homology models that best resemble the respective closed- and open-channel conformations of h5-HT_{3A}Rs and h5-$HT_{3A/B}$Rs. Using these homology models and the docking program GOLD, granisetron and 5-HT have been docked, and their most likely (energy minimised) positions within the binding pocket of 5-HT_{3A}Rs and 5-$HT_{3A/B}$Rs selected. These models have been used to identify potentially important binding site interactions and to investigate the influence of the 5-HT_{3B} subunit, not only at the A-B interface, but also at the B-B and B-A interface, which formed part of our model. Comparing the nAChR-based model to the AChBP-based model, changes to the secondary structure conformation and residues that influence binding differentially between the open and closed channel conformations have been identified.

4.7 Closed-channel Docking

The accuracy of any 5-HT_3 ligand docking model can generally be assessed by the proximity of functional groups to the integral W183 residue and other aromatic residues known to form the conventional aromatic box (Brejc *et al.* 2001). Indeed, all ligands docked at each interface are in close proximity to the majority of these aromatic residues, although they differ in orientation when compared to other docking models (Maksay *et al.* 2003; Reeves *et al.* 2003; Maksay *et al.* 2004; Thompson *et al.* 2005).

There are noticeably more residues from the principal subunit contributing potential binding interactions with 5-HT in both A-A and A-B models, another well recognised feature of agonist binding (Celie *et al.* 2004), and possibly indicative of a division of labour between the principal and complementary subunit residues: principal subunits maintain binding site integrity, whereas complementary subunits have a greater functional role which is maintained with fewer interactions, although still significant.

Binding of 5-HT and granisetron therefore involves a majority of interactions from principal face residues of the 5-HT_{3A} subunit.

4.7.1 5-HT docking interactions

4.7.1.1 B-loop

In concurrence with Reeves *et al.* (2003), the carbonyl group of W183 is tantalisingly close to the primary amine of 5-HT at the A-A and A-B interface, suggesting that hydrogen bonding is possible. The W183 main chain carbonyl is a hydrogen bond acceptor of positively charged ligand functional groups (Celie *et al.* 2004). If the primary amine is situated as proposed, between the A- and B-loop mainchains (see **Figure 29**; 5-HT A-A), it places the indole ring close to the W183 residue, so that π-π interactions would be preferable, contrary to the strong evidence for a cation-π interaction by Beene *et al.* (2002). However, the saturated carbon chain of 5-HT that connects the primary amine is relatively flexible, and it is conceivable that this cationic group could move into a more favourable cation-π binding position with W183, with minimal disruption to the indole ring. This is less likely at the A-B interface docking position due to the primary amine being so close to the A and B loops. However, it is unlikely for such an important interaction to differ between interfaces that have demonstrated virtually indistinguishable affinities for agonist, but rather, this 5-HT docking position represents an early orientation that alters upon conformational change within the binding pocket.

At the B-A and B-B interfaces, there is no centrally located tryptophan within the binding pocket equivalent to the W183 residue found at interfaces where 5-HT_{3A} forms the principal binding face. It is highly likely that the presence of an isoleucine residue at the equivalent position to W183 in 5-HT_{3B} (I175) contributes to the loss of binding at these interfaces. This hypothesis was tested further by mutating the I175 residue to tryptophan using the modeling program DeepView, and selecting the lowest energy rotamer (rotational isomer). The results of this process in **Figure 32** show that this mutation places a tryptophan in an equally prominent location within the centre of the binding pockets of both B-A and B-B, as compared to the A-A interface. Furthermore, these mutant B-A and B-B interfaces bear an overall resemblance to the putative binding pockets of A-B and A-A interfaces in terms of structure and residue positioning, although the C-loop looks incapable of fulfilling the role played in 5-HTA subunits, due to poor sequence identity. Results such as this can be tested with mutagenesis (see **Chapter 5**).

4.7.1.2 A-loop

Previous mutagenic and single channel conductance data in nAChRs has suggested that the A-loop (part of 'loop 5' according to some published nomenclature) is the first loop to move in response to agonist binding (Chakrapani *et al.* 2003), and residues at the apex of this loop

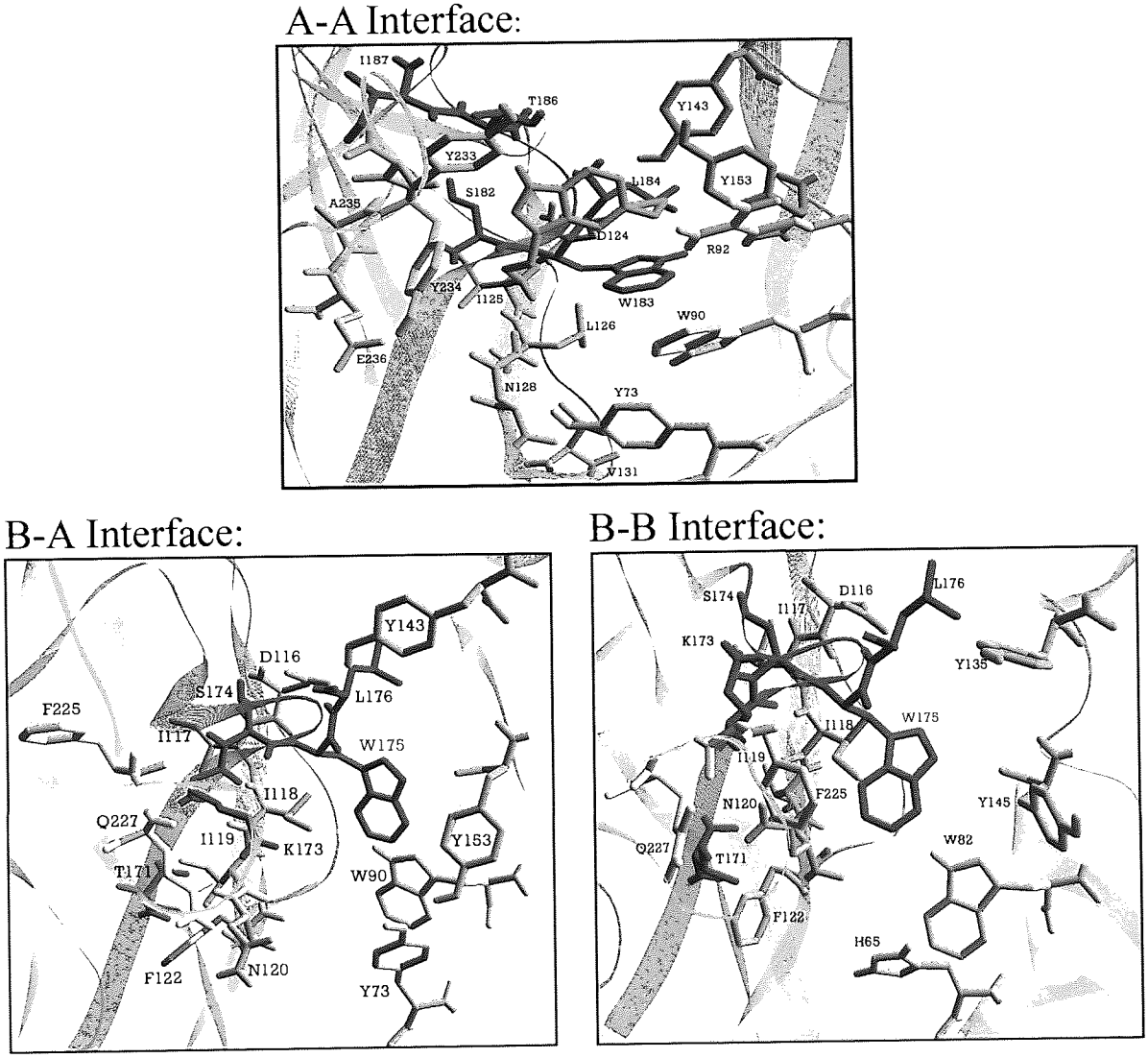

Figure 32: *In silico* introduction of an I175W mutation (in red font) in the 5-HT$_{3B}$ subunit and comparison of the binding pockets at all three types of 5-HT$_3$R interface. Both 5-HT$_{3A}$R and 5-HT$_{3A/B}$R homology models are based on the 2BG9 apo structure (Unwin, 2005). 5-HT is shown docked at the A-A interface to indicate the important general docking arena, and how residues around this area are affected by the mutation. Putative binding loops are highlighted in different colours: loop-A, loop-B, , , loop-F.

act as a latch that maintains the gating equilibrium of the receptor in favour of the closed-channel conformation. This functionality is reflected by the large number of residues conserved within this loop in the Cys-loop family (WxPDIxIxExxD), which probably serves to maintain the correct 5-HT_3R gating equilibrium. Furthermore, it seems likely that the effect of mutating certain A-loop residues at one binding interface may not be isolated to that interface alone (Akk 2001), adding a further selective pressure to conserve the amino acids in this loop.

As a result of this high amino acid sequence identity between A-loop regions of 5-HT_{3A} and 5-HT_{3B} subunits, there is little discernable difference between its secondary structure and the position of amino acids at the B-A and B-B interfaces (not shown), compared to the A-B or A-A interface. Only E129 is an exception, as it faces the binding pocket at the A-B interface, but faces the inner β-sheet at the A-A interface. This discrepancy possibly indicates that E129 favours the environment of the binding pocket in this region. This high sequence identity is a puzzling feature of the 5-HT_{3B} subunit because if neither the A-, B- or C-loop contribute to ligand binding, there is no selective pressure to conserve these residues. This paradox could mean i) they do play a role in ligand binding, ii) they play a role in intersubunit interactions, iii) they have an integral structural/functional role. The A-loop can indeed make potential interactions with residues of apposing anti-clockwise subunits, which makes intersubunit interactions highly likely (**Figure 28**). Our homology models also show that the A-loop descends towards the TM2-TM3 linker, but is almost 15 Å from directly contacting it at both the A-A and A-B interfaces, making it unlikely that this loop impinges upon TM2-TM3, as has previously been suggested (Chakripani 2003). The mobility of this loop is linked to gating in the α-subunit of nAChR (Chakrapani *et al.* 2003), but may also be a function required of 5-HT_{3B} subunits. The functional role of 5-HT_{3B} is a recurring theme. A-loop residues in ligand binding will be discussed further in the 1UV6 modeling section.

The A-A interface docking model (**Figure 29**; 5-HT + A-A) shows that only N128 is significantly close to the primary amine of 5-HT, whereas E129 and F130 residues are over 12 Å from the docked 5-HT molecule. This is a surprising result considering the pharmacophore data that suggests both of these A-loop residues affect receptor binding and function (Boess *et al.* 1997; Steward *et al.* 2000). At the A-B interface, the orientation of 5-HT means that both the primary amine and the amine of the indole ring interact with A- and B-loop residues, particularly the back bone of the A-loop, including E129 and F130, which supports previous mutagenic data (Boess *et al.* 1997; Steward *et al.* 2000). The docking of 5-HT at the A-B interface may, with its closer proximity to E129 and F130 and better

orientation of these residues, represent a more accurate depiction of the initial position adopted by this agonist.

In the α_1-nAChR subunit A-loop, residue Y93 (Y89 in Ls-AChBP) is believed to play a critical role in controlling the gating equilibrium (Auerbach *et al.* 1996; Akk and Steinbach 2000; Akk 2001), and probably interacts with agonist via its hydroxyl group (Sine *et al.* 1994; Celie *et al.* 2004). In the β_2-GABA$_A$R subunit A-loop, residue Y97 (aligns to Y93 of α1-nAChR) is responsible for the major cation-π interaction (Padgett *et al.* 2007), an indication of ability of A-loop residues at this vicinity to make direct binding interactions. It is surely a simple matter to find the equivalent residues within the 5-HT$_3$R subunits and extrapolate this information? Unfortunately, a major caveat regarding the A-loop is that the sequence alignment between α1-nAChR and 5-HT$_{3A}$ subunits is ambiguous between the fully conserved WxPD motif and D132 residue (conserved in 5-HT$_3$ and nAChR); a factor previously noted to cause similar discrepancies in homology modeling (Reeves *et al.* 2003). In previous models, I125 has been deleted before the alignment, and a gap introduced after V142, with a subsequent improvement in the docking results (Maksay *et al.* 2003), though this method is far from optimal because I125 belongs to a triple hydrophobic-residue motif, which is a common feature of 5-HT$_3$ and nAChRs. An alternative solution has been the insertion of a gap after D111 of α1-nAChR and after V131 of the 5-HT$_{3A}$ subunit (see sequence numbering in **Figure 2**), as performed recently by Sullivan *et al.* (2006). Adopting this method for our homology model aligns E129 (5-HT$_{3A}$ subunit) with Y93 in α1-nAChR, and F130 into closer proximity to the ligand binding arena, in accordance with current binding data (Boess *et al.* 1997; Steward *et al.* 2000).

The difficulties finding an appropriate alignment may actually reflect a significant difference in the function or mechanism within the apex of this loop. Supporting this argument comes from the discussed m5-HT$_{3A}$ mutagenic data of this loop (Boess *et al.*, 1997; Steward *et al.*, 2000; Sullivan *et al.*, 2006). Effects on gating, binding and expression are attributed to a triplet of residues ($N^{128}E^{129}F^{130}$) in the 5-HT$_3$R, whearas only Y93 has such effects in the nAChR. The alignment of E129 (5-HT$_{3A}$ subunit) with Y93 (α1-nAChR) is also a more satisfactory solution, considering the current data regarding the apex of the A-loop: i) only E129 remains fully conserved between all 5-HT$_3$ subunits (A-E), and ii). E129 will be capable of hydrogen bonding with ligands, as predicted for Y89 in Ls-AChBP (Celie *et al.* 2004).

At both the A-A and A-B interfaces the highly conserved D124 side chain is positioned such that it can form hydrogen bonds with the main chain of W183 (NH···O = 2.4 Å) and that of other B-loop residues: L184 (2.4 Å), and H185 (3.8 Å), which strongly supports the notion

that this acidic residue D124 stabilises this section of the B-loop, and thus the position of W183.

Overall, the A-loop exhibited some interesting and unexpected influences upon binding and potentially demonstrates multiple intra-subunit interactions. The modeling suggests that the A-loop influences function to a greater extent than agonist binding, but this function is identical at the A-A and A-B interfaces. The impact of A-loop residues on the B-loop is most likely to affect ligand affinity.

4.7.1.3 D-loop

Due to 5-HT adopting a relatively high docking position (Figure 26) within the putative binding pocket at the A-A interface (region II according to Joshi *et al.*, 2006), aromatic box residues F226 and W90 in the lower part of the binding pocket are more than 7 Å from any part of the docked agonist, in spite of previous studies showing that aromatic residues at position 90 are essential for agonist binding in the m5-HT_{3A}R (Yan *et al.* 1999; Spier and Lummis 2000). Although W90 is distant in our model, it is still close enough to contribute to the aromatic/hydrophobic and hydrophilic nature of the binding pocket, and possibly make binding interactions prior to the conformational rearrangement of the binding pocket. The docking position of 5-HT is slightly lower in the putative binding pocket at the A-B interface, so that W82 (W90 in 5-HT_{3A}; residues in bold typeface refer to the 5-HT_{3B} subunit) is within hydrogen bonding distance (2.2 Å) of the 5-HT hydroxyl group, and 4.4 Å separate both indole rings so that a π-π interaction is probable, and highly likely after contraction of the binding pocket. However, removal of the delocalized electron cloud causes very little change from wild type binding (Beene *et al.* 2002), suggesting that it is the bulk of the aromatic residue, and not the π-electron cloud, that contributes to the binding affinity. Furthermore, although the W90-aligned residue in nAChR, γW55 (Xie and Cohen 2001), has been shown to be critical for binding and located within the binding pocket (by covalent attachment to affinity labels) it has not yet shown evidence of direct agonist interaction (Chiara *et al.* 1998). There is no evidence therefore, of molecular interactions between agonist and this D-loop residue that requires them to be in close proximity, thus validating the A-B interface model.

R92 has previously been implicated by Yan *et al.* (1999) as an important residue for 5-HT and granisetron binding. However, our model and that of Reeves *et al.* (2003) shows that R92 is unlikely to be involved with direct 5-HT interactions, but is more likely to be involved in an intersubunit interaction with the C-loop. The binding effects of R92 mutations may be attributable to the disturbance of these interactions, which form part of the conformational

wave (Grosman *et al.* 2000). At the A-A interface of the closed channel, R92 (D-loop) and E229 (C-loop) are 6.8 Å apart, but the position and orientation of these residues is such that anticlockwise subunit rotations could bring the E229 residue into close proximity of R92, enabling a salt bridge interaction, which may facilitate activation in the 5-HT_{3A} subunit (Yan *et al.* 1999; Beene *et al.* 2004). This mechanism is also possible for the equivalent residues at the A-B interface, E229 and **Q84**, which are 7.8 Å apart in the closed channel conformation. Residue **Q84** has been shown not to draw the C-loop residue E229 into such close contact even after 15° subunit rotations (Maksay *et al.* 2004), which could have implications for binding and/or downstream rotations leading to the opening of the channel. Such salt bridge interactions can be investigated by site directed mutagenesis.

In the apo conformation, it is difficult to attribute any major agonist binding interactions to the D-loop residues using the predicted docking position in our model. Intersubunit interactions are also unlikely in this conformation.

4.7.1.4 E-Loop

A universal feature of the Cys-loop receptor family is that amino acids aligned to Y143 and Y153 of the 5-HT_{3A} subunit significantly affect agonist binding (Westh-Hansen *et al.* 1997; Chiara *et al.* 1999), though the specific importance of tyrosine in these locations appears to be a unique feature of the 5-HT_3R. Y143 is conserved in all but one of the 5-HT_3R subunits (5-HT_{3D}; **Y135** in 5-HT_{3B}), whereas Y153 is only conserved in 5-HT_{3A} and 5-HT_{3B} (**Y145**); however, a tyrosine is present one base before the Y153-aligned position in 5-HT_{3C} and 5-HT_{3E}, which indicates a requirement for a tyrosine in this locality.

The two β-strands that comprise the E-loop form an antiparallel β-strand loop, which brings Y143/**Y135** and Y153/**Y145** residues into close proximity of each other, and pointing towards the W183 residue of the B-loop. Both models (A-A and A-B interface) show that the Y143/**Y135** residue likely makes hydrogen bonding interactions with B-loop residues, stabilising this loop and forming part of the 'back wall' of the binding pocket (Brejc *et al.* 2001). The interaction of agonists with W183 (B-loop) could trigger the displacement of E-loop residues, as well as the β5 and β6 strands to which they belong, to propagate a conformational change that enhances the affinity of 5-HT. It is noteworthy that the movement of β5 would probably alter the conformation of the A-loop apex, which is known to influence the channel gating equilibrium (Chakrapani *et al.* 2003), and indeed changes to channel gating have been observed in the AChR as a result of E-loop mutations (Ohno *et al.* 1996).

Mutation of Y143 and Y153 has previously demonstrated deleterious effects on 5-HT binding affinity in m5-HT_{3A}R membranes (Venkataraman *et al.* 2002; Beene *et al.* 2004), and modeling using density functional theory (Melis *et al.* 2006). Melis *et al.* (2006) showed that delocalising the π-electron clouds of Y143 and Y153 with fluorine causes the bond energy to increase over wildtype, suggesting that hydrogen bonding interactions rather than π-π interactions occur with 5-HT. This is further substantiated by our 5-HT docking model at the A-A interface, where just 2.4 and 4.4 Å separate the hydroxyl groups of 5-HT and tyrosine residues 143 and 153 respectively (**Figure 29;** 5-HT A-A). This A-A interface model also concurs with the current mutagenesis evidence provided by Venkataraman *et al.* (2003), who also predicted the involvement of both Y143 and Y153, due to the deleterious effect of Y143A and Y153A mutations on binding and function. Furthermore, in *Ls*-AChBP x-ray crystallographic data, the equivalent E-loop residues (R104 and M114 respectively) contact carbamoylcholine in the active conformation (Celie *et al.* 2005). This evidence suggests that Y143 and Y153 are directly involved in agonist binding.

At the A-B interface the 5-HT indole hydroxyl group is sandwiched between **Y145** and **W82** of the E- and D-loop respectively, making interactions with **Y135** unlikely in this closed state conformation. If this is correct, and we assume that 5-$HT_{3A/B}$R binding data will be the same as the 5-HT_{3A}R (currently h5-$HT_{3A/B}$R is untested), a conformational change must occur after initial agonist binding, which either alters the position of the β5-strand, or causes slight adjustment to the pitch of the 5-HT hydroxyl group itself. Both events would bring the 5-HT hydroxyl and **Y135** into closer proximity. Indeed this is predicted for modeling in the active open-channel conformation in **Figure 31** (A-B), which shows 5-HT docking closer to **Y135** than Y145 as a result of relative subunit rotations and the reduction in binding pocket volume. It should also be considered that previous 5-HT_{3A}R models are based on the homomeric template of AChBP, which could influence the docking results differently to a heteromer based model. If our A-A and A-B interface models of the apo conformation of 5-HT_3R are correctly representing differential 5-HT binding interactions, these should be discerned by appropriate point mutations with radioligand binding and electrophysiological testing.

If any of the complementary binding residues of 5-HT_3Rs take part in agonist binding within the apo conformation, tyrosine residues within the E-loop are by far the most promising candidates. At the A-A interface it is predicted that these tyrosines systematically coordinate the orientation of the 5-HT molecule throughout the E-loop movement, each with varying strengths of hydrogen bonding interaction as the inner β-sheet of the LBD rotates. The predicted binding site of 5-HT at the A-B interface may be different, but the homology model

of this binding site still contains these tyrosines in very similar positions. Until more pharmacological data become available for the 5-$HT_{3A/B}$R, it is difficult to envisage these E-loop residues not playing an important role in binding.

4.7.1.5 C-loop

In our closed channel models of both the A-A and A-B interface, few C-loop residues are predicted to be close enough to 5-HT to make binding interactions, which means that the C-loop structure is further away from the binding site than predicted in the AChBP-based models (Brejc *et al.*, 2001; Celie *et al.*, 2004). The well established movement of the C-loop (Hansen *et al.*, 2005) has been taken into account when assessing the docking predictions for 5-HT at the apo state interfaces. Amino acid residues more than 3.5 Å were still declared important for binding if the ligand was situated in the projected path of C-loop movement (Hansen *et al.*, 2005), which would feasibly bring the amino acid within binding distance of the ligand molecule. These predictions were substantiated by our 1UV6-based models.

There is incontrovertible evidence that both aromatic and acidic residues within the E225-E236 region of the C-loop influence the binding and gating characteristics of agonists (Schreiter *et al.* 2003; Suryanarayanan *et al.* 2005). The gating mechanism (see **General Introduction**) is most likely transmitted through the movement of the β10-strand (part of the C-loop), which concomitantly affects the movement of R245, further linked to the movement of TM2 via the TM2-TM3 proline in the 5-HT_3 (Lummis *et al.* 2005) and nAChR receptors (Cheng *et al.* 2006; Sine and Engel 2006). It is predicted that this movement opens the channel.

Variations in the C-loop sequence are responsible for dramatic changes in binding affinity of different drugs (Hope *et al.* 1999). This property makes Cys–loop receptor alignments challenging and necessitates manual manipulations of Clustal X results, reducing the consistency of alignments between research groups due to varying interpretations of the available data for this region (for comparison see Schreiter *et al.* 2003; Suryanarayanan *et al.* 2005). It is generally agreed that the C-loop of the 5-HT_{3A} subunit is one or two residues shorter than the C-loop of α-, γ-, and δ-nAChR subunits, and that of the 5-HT_{3B} subunit is shorter still by a further residue. However, due to poor sequence conservation, sequence alignments in this region cannot yet be considered definitive. Assuming that the tip of the 5-HT_{3A}R C-loop makes close contact with agonist, as occurs in the nAChR (Damle and Karlin 1980), it should be possible to resolve alignment issues of the C-loop in the 5-HT_{3A}R by cysteine scanning mutagenesis, or a similar delineating method. Until such a method is

employed for the 5-HT_3R, caution will have to be applied to interpretations based on current alignments.

At the A-A interface, residues Y233 and Y234 are closest C-loop residues to the docked 5-HT molecule, at just 4.2 Å from the indole ring. Due to the relative orientations of Y234 and the aromatic ring of 5-HT, π-π interactions are possible, assuming that the C-loop moves towards W183 (Hansen *et al.* 2005). Hydrogen bonds are less likely because the hydroxyl group of the Y234 residue has been shown superfluous for agonist binding (Beene *et al.* 2004). In the absence of these described interactions, the presence of two tyrosines at such an influential position on this highly mobile loop could indicate a steric role, as the bulk of tyrosine has been shown important in agonist binding (Beene *et al.* 2004). At the A-B interface, the deeper docking position of 5-HT means that the closest C-loop residue to 5-HT is Y234 (7.2 Å from the primary amine group). However, the orientation of Y234 may still interact with either the aromatic ring or primary amine after the C-loop has changed conformation. Surprisingly, Y233 is orientated differently in our A-B interface model, making it difficult to foresee any feasible binding role, contradictory to current binding evidence in m5-$HT3_A$R (Suryanarayanan *et al.* 2005).

The F226 sidechain projects into the binding pocket and towards the B-loop residues, strongly suggesting a binding role when the C-loop moves inwards, in addition to coordinated B-loop interactions. However, phenylalanine lacks the hydroxyl group required for hydrogen bonding interactions with the hydroxyl-rich region of the B-loop (residue numbers 179-182); an interaction previously identified in the crystal structures (Celie *et al.* 2004). The hydroxyl-rich B-loop region not only projects purposefully towards the C-loop, but is a feature of all the Cys-loop family of receptors, making its absence in 5-HT_3Rs inconceivable. It is therefore predicted that this interaction occurs via an alternative residue, either due to misalignment of Cys-loop sequences, or differences in the length and structure of this loop. The most suitable hydrogen bonding candidate residues predicted by our model are R224 and E225.

4.7.1.5.1 C-loop Intrasubunit interactions

Residue E225 has previously been shown to affect both 5-HT binding and response, but the charge on this residue is not as important as its length (Schreiter *et al.* 2003). Furthermore, it is positioned at the centre-back portion of loop, pointing away from the binding pocket, which makes it difficult to foresee residue interactions in either the closed channel state or subsequent to the conformational change. If E225 were to adopt a more inwardly facing orientation, this would make hydrogen-bonding interactions between itself and T179 more

likely. Although the C-loop residue R224 has not previously been tested biochemically, its predicted position relative to the docked 5-HT molecule makes hydrogen-bonding interactions with T179 a distinct possibility; after small inward movements of C-loop arm. The situation of both R224 and E225, proximal to the C-loop tip, means that the formation of hydrogen bonds between this region of the C-loop and the B-loop (T179) may allow the long arm of the C-loop to bend towards the binding pocket as the B-loop moves in response to agonist binding. A similar mechanism has also been proposed for the nAchR (Grutter *et al.* 2003).

Further stabilisation of the C-loop structure is possible via E236 and T179 interactions at both A-A and A-B interfaces. Thus T179 of the B-loop, E236 and R224/E225 form a triad of interactions, also predicted by molecular dynamics simulations of the α7-nAChR (Cheng *et al.* 2006). Like E225, the E236 residue dramatically alters binding and gating when it is mutated to a residue of different length, rather than removing the electrostatic charge (Schreiter *et al.* 2003).

The backbone of Y233-Y234 may also be able to interact with T186-I187 (B-loop), homologous to interactions responsible for slow-channel myasthenic syndrome, which alters the channel kinetics properties of binding, speeding up association and slowing dissociation rates of ACh.

The highly conserved residues E80 (preceding the D-loop) and R245 (C-loop) are within salt bridging distance in the 5-HT_{3A} subunit of the 5-HT_{3A}R and 5-$HT_{3A/B}$R, meaning that any alteration to the β10-strand, such as the upward and outward motions described by Cheng *et al.* (2006), would disrupt and release E80, which could then interact with the TM2-TM3 loop. This mechanism is not supported within the 5-HT_{3B} subunit of our ground-state 5-$HT_{3A/B}$R model because it is only capable of hydrogen bonding interactions between the equivalent residues **A72-R236,** but alanine does not have the length to interact with the TM1-TM2 linker. As a result, the 5-HT_{3A}R and 5-$HT_{3A/B}$R would be expected to differ in the number of TM2 domains actively coupled to binding, due to the differing number of 5-HT_{3A} subunits from which they are composed: the 5-HT_{3A}R can potentially activate five TM2 domains, whereas 5-$HT_{3A/B}$R can only activate two. The absence of such an interaction in the 5-HT_{3B} subunit is probably inconsequential if B-A interfaces do not partake in ligand binding, as the 5-HT_{3B} subunit C-loop β10 strand will not be induced to move inward by agonist.

Comparing both interfacial models **Figure 29** and **Figure 31** shows that C-loop closure causes a reduction in the binding site volume and solvent accessibility. Such changes are predicted to affect ligand binding affinity as well as the binding kinetics (Hansen *et al.* 2005). The influential role of C-loop residues on ligand affinity is also evidenced by the disparate

binding affinities of identical ligands at 5-HT_3R orthologs (Hope *et al.* 1999). The two properties (affinity and function) may not be mutually exclusive i.e. ligands derive a lot of binding energy from the C-loop, which must then move inwards to make contact, concomitantly moving the R245 residue on the β10 strand.

Overall the C-loop at both A-A and A-B interfaces influences the shape of the binding pocket and access to the binding site. Residues close to the hinge region (Y234 identified as the hinge region: Bourne *et al.* 2005; Hansen *et al.* 2005; Cheng *et al.* 2006) interact with the B-loop in the resting state, to maintain its closed-state conformation. 5-HT almost certainly interferes with these interactions by intercalating between W183 and Y234, to begin the closure of the C-loop. Residues towards the tip of the C-loop, previously too distant from the docked 5-HT molecule, can now make ligand-binding interactions, as well as interact with D-loop and B-loop residues (see relevant section) to stabilise its changing conformation.

4.7.1.6 F-loop

Poor resolution of the F-loop remains a bugbear for all homology modeling predictions, whether based on AChBP or the nAChR. The majority of current ligand binding data for 5-HT_{3A} subunit F-loop point mutants concerns the antagonists granisetron (Thompson *et al.* 2006) and curare (Zhang *et al.* 2007), with limited and unremarkable data available for 5-HT pharmacology that do not show dramatic deviations from wildtype. D192 is the only residue predicted to project into the binding site, within 7 Å of the 5-HT molecule at the A-B binding site, but not the A-A binding site.

The F-loop is similar to the C-loop with regards to its postion at the front entrance of the binding site. Significant differences between 5-HT_{3A} subunit and 5-HT_{3B} subunit F-loop sequences could impact upon C- and F-loop interactions, opening and closing of the binding site and antagonist affinity. Sadly, until more complete crystal structure and 5-HT binding data become available, speculation about the role of individual residues on 5-HT affinity will be too hypothetical to be useful.

4.7.2 Granisetron docking interactions

The binding sites of granisetron and 5-HT were always expected to overlap because of the competitive nature to granisetron's antagonism. Indeed, our models show that granisetron and 5-HT dock into the same interfacial arena (**Figure 30**), docking in close proximity to the same B- (W183, T181, and S182), A-loop (N128) residues. Granisetron can therefore compete with 5-HT for electrostatic interactions with residue W183 as well as other B- and A-loop residues, concomitantly preventing entry of 5-HT into the binding site from above and below the C-

loop. Granisetron may prevent channel opening by restricting the relative apposing subunit rotations via D-loop interactions, but not necessarily by complete prevention of C-loop movement, as only the A-B interface model places granisetron within binding distance of Y234.

5-HT, being a small molecule, cannot simultaneously interact with binding loops (possibly the same ones as granisetron) by traversing large distances, but rather relies on movements of the binding pocket structure around it, making sequential interactions. The much larger molecular structure of granisetron increases the number of binding loop residues this molecule can interact with at any one time, potentially preventing sequential movements of the conformational change (Chakrapani *et al.*, 2004). This large structure obviously reduces the number of positions that the ligand binding pocket can accommodate, and possibly explains why granisetron has been docked into the A-A and A-B interfaces in very similar positions in our models, differing only by the opposite orientation of the tropane and aromatic rings. The docked orientation at the A-A interface, with the aromatic ring between W183 and Y234, is similar to other homology docking predictions using the 1I9B AChBP structure (Maksay *et al.* 2003; Yan and White 2005), although the absolute position of all three, relative to each atom, do not entirely agree.

Comparison of the predicted docking positions of granisetron at the A-A and A-B interfaces shows that altering the subunit comprising the complementary face of the binding site alters the orientation of the ligand considerably (**Figure 2**). This is difficult to rationalise because granisetron has very similar affinity at h5-HT_{3A}Rs and h5-$HT_{3A/B}$Rs (**Chapter 3**), yet proposed π-π interactions involving the intercalation of the indazole ring between aromatic groups involves W183-Y234 and W183-**W82** at the A-A and A-B interfaces respectively. Disparity in such an influential interaction would surely translate into measurable discrepancies in receptor function and/or affinity. Interestingly, Yan *et al.* (2005) similarly docked granisetron with the tropane ring sandwiched between W183 and Y234, but discounted this prediction using double mutant-cycle analysis, which proffered that the tropane ring was interacting with W90, in spite of the less energetically favourable nature of such a docking conformation, and not being representative of the most frequent docking cluster. It will be interesting to perform such double mutant cycle analysis on the 5-$HT_{3A/B}$R to determine if granisetron does bind in an alternative conformation at the A-B interface.

Granisetron makes potential interactions with multiple residues from nearly all of the binding loops of the principal and complementary subunits. This is another consequence of being a large moleule, and also having the functional requirement of preventing multiple loop

movements, rather than the permissive role of agonists. Each of these loops will be discussed individually.

4.7.2.1 C-loop

Physically prohibiting C-loop movements is an obvious mechanism of antagonism by such a large molecule as granisetron within the binding pocket, assuming that movement of this loop is a prerequisite of channel opening. In our granisetron docked model and those previously published, the length of the granisetron molecule (from the tropane to aromatic ring) has not been docked traversing from the B-loop to the C-loop, as would be expected of steric hindrance mechanism involving the prevention of inward C-loop movement. Rather, granisetron has been docked in a more parallel orientation with respect to the subunit long axis, which is an orientation that features in snake venom toxins and antagonists docked at the nAChR (Bourne *et al.* 2005; Celie *et al.* 2005; Hansen *et al.* 2005).

The inward C-loop movement is probably restricted via a π-π interaction of granisetron's indazole ring with Y234, just 3.8 Å away in our A-A interface model. This method of antagonism is similar to that described by x-ray crystallographic data for AChBP (Bourne *et al.* 2005; Celie *et al.* 2005; Hansen *et al.* 2005), where the residue thought to form the C-loop hinge is involved with strong aromatic interactions. This residue aligns to Y234 in the 5-HT_{3A} subunit. It is likely that the interaction of granisetron with Y234 restricts the movement of the C-loop, opposite to the effects of 5-HT docking previously described.

4.7.2.2 A-Loop

The location of E129 in the A-loop relative to the granisetron docking position is most important in determining the validity of the model because this residue is responsible for significant granisetron binding interactions (Boess *et al.* 1997; Thompson *et al.* 2005; Sullivan *et al.* 2006). Unfortunately E129 is located in the very apex of the A-loop, which combined with the residue's orientation (away from the binding pocket) is too far removed from the binding pocket to make contact with granisetron in either the A-A or A-B interfaces. It is still possible that, rather than directly binding granisetron, E129 affects the shape of the binding site, part of the conformational change or expression of the subunit. The conclusions of Sullivan *et al.* (2006) certainly reinforce this latter possibility.

The granisetron docking position at both interfaces makes interactions possible with multiple residues just before the apex of the A-loop, possibly to stabilise the loop in the closed channel conformation. Previously, granisetron has not been dramatically affected by an N128 mutation (Thompson *et al.* 2005), and although N128A affects *d*-tubocurarine binding by

nearly an order of magnitude, this is thought to be due to a steric affect on this strikingly large, rigid molecule (Yan *et al.* 2006).

4.7.2.3 B-loop

The A-A interface docking of granisetron concurs with previous models that predict the intercalation of the indazole ring between W183 (B-loop) and Y234 (Thompson *et al.* 2005). The orientation at the A-B interface will be considered when interpreting further 5-$HT_{3A/B}$R binding data, but using current binding data, it is difficult to rationalise this mode (see beginning of granisetron section).

T179 has been shown to reduce granisetron affinity 10-fold when mutated to alanine (Thompson *et al.* 2005). However, the orientation and marginally higher docking position than that predicted by Thompson *et al.* (2005) indicates that T179 plays a less significant role for granisetron binding in this model. It should be noted that the B-loop is relatively static, maintaining the crucial W183 residue centrally within the space of the binding pocket (Celie *et al.*, 2004; Celie *et al.*, 2005a; Celie *et al.*, 2005b). Any perturbations to the structure of the B-loop would be expected to affect the binding of ligands in some way, as indicated by another B-loop mutation S181A, which caused a significant increase in affinity (Reeves *et al.* 2005). These mutations do not necessarily indicate direct binding.

4.7.2.4 D-loop

The priority of antagonist binding appears to be the formation of a rigid bridge between principal (A- and B-loop) and complementary (D-loop) residues, thus preventing the relative rotations of apposing subunits, the mechanical operation predicted to lead to channel opening (Unwin 2005). Unlike the docking of 5-HT at the A-A interface, which does not come close to D-loop residues, both granisetron docked models (A-A and A-B interface) show a definite tendency for either of the granisetron's ring structures to gravitate towards W90/**W82** (D-loop) and Y73/**H65** (adjacent to the D-loop region in tertiary structure) residues.

It is clear from our model that Y94 is not part of the granisetron binding site, although Yan *et al.* (1999) have reported that its mutation to alanine causes a 3 fold loss of granisetron affinity. The aromatic nature of this residue must make contributions to the aromatic properties of the binding site, particularly important in this complementary-face location. However, it is also noted that previous Y94A and Y94S m5-HT_{3A} mutants have displayed WT properties (Price and Lummis 2004).

With regards to the hydrophobicity in this area of complementary face residues, Y73, Y88 and W90 all contribute to this hydrophobicity at the A-A interface and virtually abut the

granisetron tropane ring. Although Y73 and Y88 are not recognized as being part of any binding loop, and a previous Y73A mutant in the m5-HT_{3A} homomer receptor has previously shown no significant difference in affinity to WT (Thompson *et al.* 2005), their cumulative properties may have some function.

4.7.2.5 E-loop

According to both A-A and A-B interface models presented here, it is unlikely that the granisetron molecule is able to interact with any residues from the E-loop in the channel closed state. This is in agreement with the conclusions of binding data at the 5-HT_{3A} homomer receptor, which showed only modest (<10 fold) changes in granisetron affinity (Venkataraman *et al.* 2002). **Y133** and not **Y135** potentially interacts with W183 in A-B in our closed channel model.

Granisetron affinity is not as greatly affected by E-loop mutations, but this is not a universal feature of 5-HT_3R antagonists, as curare and lerisetron both lose affinity due to Y143A and Y153A mutations. However, these antagonists contain more functional groups and are generally much larger than granisetron; this being a feature that probably contributes to addition bridging interactions between subunits that prevents both interfacial subunits rotating.

4.7.2.6 F-loop residue interactions

Only one residue of the F-loop, **D192**, can be identified as being within 7 Å of 5-HT and granisetron molecules, and this is specific to the 5-HT_{3B} subunit at the A-B interface. From this docking information it can be inferred that for ligands to bind F-loop residues in the apo conformation, they must be larger than granisetron to be able to bridge the gap from A- and B-loop regions to residues of the F-loop (see Zhang *et al.*, 2006).

Two distinct regions within the F-loop are affected by amino acid mutations (Thompson *et al.*, 2006), each region associated with particular movements of the loop. Our apo docking model has evidently captured the ligand docking conformation of the 5-HT_3R before these transitions take place. This is corroborated by our active state model, **Figure 31**. Until these movements are better understood and for the same reasons discussed for 5-HT docking, further hypothoses regarding the F-loop would be too speculative.

4.8 Open-channel docking

Our modeling of the 5-$HT_{3A/B}$R in the active state confirmed the previously published data regarding conformational changes (Maksay *et al.*, 2003; Reeves *et al.*, 2003; Maksay *et al.*,

2004; Thompson *et al.*, 2005; Thompson *et al.*, 2006), as well as translating this information in the context of how 5-HT_{3B} subunit residues may affect ligand binding at its A-B, B-A and B-B binding interfaces.

4.8.1 5-HT docking at the A-B interface

The A-B interface of the 5-$HT_{3A/B}$R model based on 1UV6 (Celie *et al.* 2004) has been used in combination with the apo state models as a way of deciphering the changing role of residues as they move between both conformational states, exemplified by the C-loop. The anticlockwise rotation of the C-loop that occurs at all interfaces, brings its tip (M228 and E229 in the 5-HT_{3A} subunit, and **S221** and **A222** in the 5-HT_{3B} subunit) into close contact with 5-HT, as well as reducing the distance between all C-loop residues and the agonist. As a consequence, it is clear that 5-HT derives a significant proportion of binding energy from these residues (Hope *et al.*, 1999; Schreiter *et al.*, 2003; Beene *et al.*, 2004; Price & Lummis, 2004; Suryanarayanan *et al.*, 2005; Thompson *et al.*, 2005). However, in the apo conformation observed in our homology models, only one residue (Y234) at the A-A interface is within range of influencing the binding of 5-HT. The means that 5-HT must derive much of its initial binding energy from residues discussed for the apo structures, most significantly W183.

4.8.2 5-HT docking at the B-A and B-B interfaces

In the ligand bound conformation it is much clearer that W183 defines the back-wall of the binding cavity at the A-B interface. It is expected that its absence at interfaces where 5-HT_{3B} subunits provide principal face residues (replaced by **I175**), binding will be precluded. Certainly, mutations to W183 in 5-HT_{3A}Rs causes either a loss of binding or substantial loss of affinity (Spier & Lummis, 2000; Thompson *et al.*, 2005). It is surprising then that the recognition envelopes still show docking to a very similar binding arena as A-A and A-B interfaces. It is appreciated that ligand docking is by no means proof that binding occurs *in vivo*; however it does indicate that the shape of the binding pocket is conducive to 5-HT interacting with the same subset of binding pocket residues. It is therefore possible that 5-HT has some affinity for the open state conformation of the B-A and B-B interfaces. Certainly, the two tyrosine residues are still present in the E-loops of both 5-HT_{3A} and 5-HT_{3B} subunits, and are shown to be close enough to provide hydrogen bonding interactions.

A predictable limitation to B-A and B-B interfaces acting as *bona fides* binding sites is the shortness of the 5-HT_{3B} subunit C-loop, and the lack of homology to that of the 5-HT_{3A} subunit, particularly in those residues previously identified as influencing ligand binding.

Even though at the B-A and B-B interfaces the 5-HT_{3B} C-loop is modeled on an alpha-type subunit (one that forms a binding site), there is one major difference in its structure and interactions of its residues. The 5-HT_{3A} subunit C-loop wraps around the ligand significantly, whereas the 5-HT_{3B} subunit C-loop tip points more towards the F-loop than it does the ligand binding site. The residues at the tip of the C-loop at B-A and B-B interfaces are extremely close (**S221**-K200 is 2.8 Å and **S221-K198** is 3.3 Å). Whether these interactions between the C-loop and F-loop contribute significantly the pharmacology of the 5-$HT_{3A/B}$R as a whole remains to be tested.

Chapter 5: 5-HT$_{3B}$ Subunit Mutagenesis

5.1 Introduction

A significant amount of mutagenic and computational modeling data currently exist to describe the m5-HT$_{3A}$R ligand binding pocket and the residues therein that make ligand binding interactions and affect function (for illustration see **Appendix**: m5-HT$_{3A}$ mutations). Such detailed mutagenesis data do not exist for the h5-HT$_{3A/B}$R, in spite of recognition that 5-HT$_{3B}$ subunits impart functionally distinct properties on the 5-HT$_{3A/B}$R (Peters *et al.*, 2005) expressed in distinct CNS areas (Monk *et al.*, 2001; Reeves & Lummis, 2006) and the PNS (Davies *et al.*, 1999; Dubin *et al.*, 1999; Tzvetkov *et al.*, 2007). The reasons for this current lack of mutagenic data for the 5-HT$_{3A/B}$R could be three fold: i) relative to the 5-HT$_{3A}$, the 5-HT$_{3B}$ subunit has only recently been discovered and established protocols are for 5-HT$_{3A}$Rs, ii) it is simpler to interpret mutagenic data for 5-HT$_{3A}$Rs using a homology model with the correct stoichiometry and arrangement of subunits, and iii) 5-HT$_{3A/B}$Rs are not unequivocally discernable from 5-HT$_{3A}$Rs in radioligand binding assays.

It is currently speculated that the 5-HT$_{3B}$ subunit contributes complementary face residues to two ligand binding sites in 5-HT$_{3A/B}$Rs. This is surmised from the knowledge that 5-HT$_{3A}$ subunits provide viable principal face residues in 5-HT$_{3A}$Rs with a Hill coefficient of ~4.0, but the introduction of 5-HT$_{3B}$ subunits in 5-HT$_{3A/B}$Rs reduces the Hill coefficient to ~2.0, thus reducing the number of binding sites. Therefore, 5-HT$_{3B}$ subunits must be deficient in principal face residues integral for binding. Comparing the amino acid sequences in putative binding loops A and B (**Figure 2**) between 5-HT$_{3A}$ and 5-HT$_{3A/B}$ subunits reveals 68 % identity. The availability of more powerfully predictive 5-HT$_3$R homology models (including our own), makes the demarcations of putative binding loops somewhat dated, proving that many of the residues are far removed from the binding site. In essence, only a handful of residues could be responsible for the absence of binding capabilities at the A- and B-loop. The C-loop shares less than 20 % sequence homology between 5-HT$_{3A}$ and 5-HT$_{3B}$ subunits, but homology modeling of the 5-HT$_{3A/B}$R suggests that this loop has limited contact with 5-HT and granisetron in the apo state, rather, it is the A- and B- loops primarily responsible for these ligands being able to dock.

The contrasting functional and pharmacological properties of 5-HT$_{3A}$Rs and 5-HT$_{3A/B}$Rs (see **General Introduction**) have been attributed to the 5-HT$_{3B}$ subunit (Davies *et al.*, 1999; Dubin *et al.*, 1999) (Stewart *et al.*, 2003), specifically the TM (Das & Dillon, 2005) and

intracellular domains (Kelley *et al.*, 2003; Peters *et al.*, 2004; Peters *et al.*, 2005), but not the ECD. The reduced number of binding sites of a heteromer allows mutagenesis to be targeted to amino acids of binding loops within subunit interfaces not predicted to form a binding site. Studying the putative binding loop residues (A, B, D, E and F) within h5-HT$_{3B}$ subunits could attribute more specific functional and possibly pharmacological roles to the h5-HT$_{3B}$ subunit. If residues of the A- and B-loops are not part of the binding site in h5-HT$_{3B}$ subunits, their mutation could potentially reveal more about the structural role of particular residues, without the ambiguities caused by binding and the conformational wave being interlinked (Colquhoun, 1998).

The B-A interface of apo conformation 5-HT$_{3A/B}$R homology models in **Chapter 4** have been compared to the A-B interface to identify possible candidate residues for mutagenesis, to reinstate the ligand binding capabilities of the B-A and/or B-B interfaces. The most significant difference at the B-A and B-B interfaces is the replacement of the cation-π binding tryptophan with an isoleucine at position W183/**I175.** The effects of re-introducing a tryptophan in this position have been shown, by *in silico* mutagenesis (**Figure 32**), to be beneficial for ligand binding at B-B and B-A interfaces.

In the present study, chimeras of the h5-HT$_{3B}$ subunit have been engineered to contain each of the binding loop sequences of the h5-HT$_{3A}$ subunit in separate chimers (A, B, D, E and F). Point mutations have also been performed in the h5-HT$_{3B}$ subunit based on the homology modeling and previous mutagenic data from the m5-HT$_{3A}$R, to determine its concurrence with 5-HT$_{3A/B}$R radioligand binding and functional properties.

5.2 Results

5.2.1 Technical considerations

The choice of point mutations has been based on our homology models from **Chapter 4**. Due to unpredictability in time demands made by computational docking simulations, all of the point mutations were made before the docking data in this chapter were available.

Two mutagenesis techniques were employed to generate point mutations. The overlap extension technique (see **Chapter 2**) was successfully used to make both point mutations (Q84E, E85Q and V86Y) and multiple mutations (QEV^{84}RQY^{86}). Its use in further rounds of mutagenesis was precluded by an alteration to the polymerase enzyme by the manufacturers, which detrimentally affected the efficiency of the technique. Subsequent mutagenesis experiments used the QuickChange™ Mutagenesis kit (Stratagene). Although the supplied instructions were followed for the generation of point mutations, modifications were required

for the efficient production of chimeras containing multiple single point mutations (detailed in **Chapter 2**). Both methods used very high fidelity polymerase enzymes, capable of producing PCR products with no extraneous mutations.

HEK293 cells were co-transfected with mutant h5-HT$_{3B(V5)}$ and wild type h5-HT$_{3A}$ subunit cDNAs. Preliminary [^{3}H]granisetron binding checks were made to verify the expression of h5-HT$_3$R (data not shown). Further analysis of the membrane fraction by western blotting was used to determine the successful transfection of the mutant 5-HT$_{3B(V5)}$ subunit (**Figure 33**). The effect of mutating h5-HT$_{3B}$ subunits on the pharmacology of 5-HT$_{3A/B(V5mutant)}$Rs was measured by comparing granisetron and 5-HT binding affinities to those of wildtype tagged 5-HT$_{3B}$ subunits in 5-HT$_{3A/B(V5)}$Rs. All receptor subtypes were transiently expressed in HEK293 mammalian cells.

It was the intention of this present study to perform functional electrophysiology experiments on all mutant 5-HT$_{3B}$ subunits. This thesis only presents such data for the D-loop chimera and 5-HT$_{3B(I175W)}$ mutant (the V5 tag is present in all mutant subunits but will not be included in the title of the mutant) due to to the limited availability of viable xenopus oocytes and time constraints. Only 5-HT$_{3A/BChimD(V5)}$ was assessed by myself for its functional properties, other voltage-clamp experiments were carried out by our collaborators at the University of Alberta, Canada.

The amino acid changes contained within chimeras A, B, D, E and F and their intermediate chimeric subunits are illustrated in **Figure 34.** Sequencing of the F1 chimera revealed the incorporation of an extraneous alanine mutation (**Figure 34**), incorporated via a faulty sense primer. Fortunately the robustness of downstream PCR steps reversed this mutation, so that the F2 chimera and final F-loop chimera were error-free. Problems were experienced with the expression of this F1 mutant, which neither produced a positive western blot nor demonstrated [^{3}H]granisetron binding. The chimera D2 also expressed very poorly from both sets of transfections. Only one experiment with satisfactory radioactive counts was achieved, this was using [^{3}H]granisetron as the competing ligand.

HEK293 cells transfected with h5-HT$_{3A}$ and h5-HT$_{3B(mutant)}$ cDNA subunits containing **N144A** or **Y145A** mutations did not produce positive 50 kDa bands in western blots, indicating that expression of these h5-HT$_{3B(V5)}$ subunits was compromised. Neither did these mutant receptors demonstrate specific binding with [^{3}H]granisetron, also indicating that 5-HT$_{3A}$ subunits were absent from the cell membrane preparations. It is possible that these

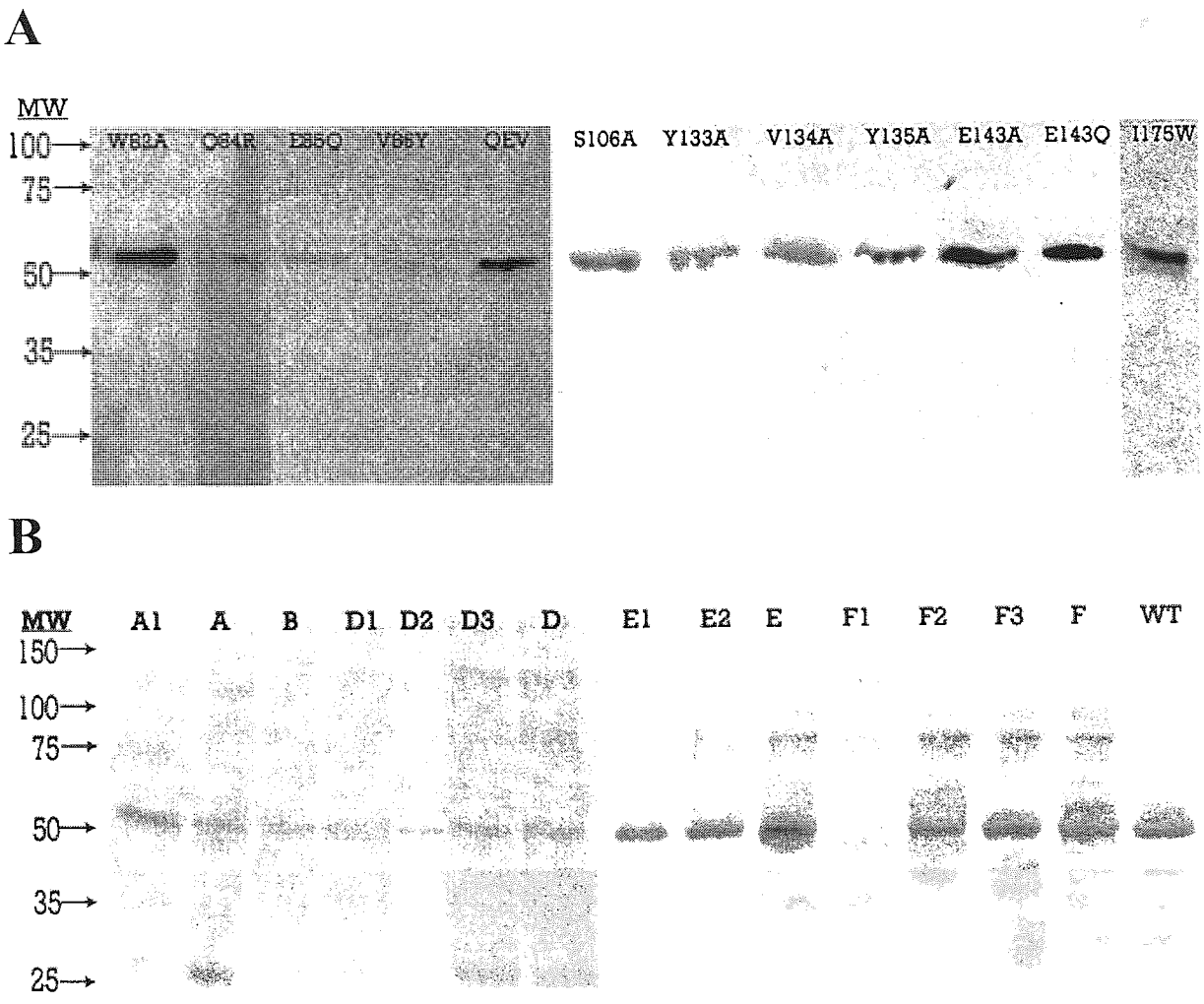

Figure 33: Western blot detection of mutant 5-HT$_{3B}$ subunits expressed as 5-HT$_{3A/B(Mut)}$Rs in transiently transfected HEK293 cells. Membrane preparations of 5-HT$_{3A/B(Mut)}$Rs were run on SDS-PAGE gels, blotted onto PVDF and subsequently probed with anti-V5 antibody (1:5000 dilution) and HRP-conjugated secondary (1:50,000). Mutant 5-HT$_{3B}$ subunits contained either (Top: *A*) point mutations or (Bottom: *B*) chimeric binding loops. In (*A*) 50 µg of total protein (loaded onto SDS-PAGE gel) was imaged using photographic film and chemical developing agents, whereas those blots in (*B*) were detecting 10 µg total protein (A, B and D chimeras) and 20 µg (E and F chimeras) total protein imaged using a chemiluminescence imaging system (UVIchem). WT = wild type 5-HT$_{3A/B(V5)}$. Membrane preparations of untransfected HEK293 cells and untagged 5-HT$_{3A/B}$Rs were similarly probed but did not produce any positive bands (not shown). For chimera nomenclature, see *Figure 34*.

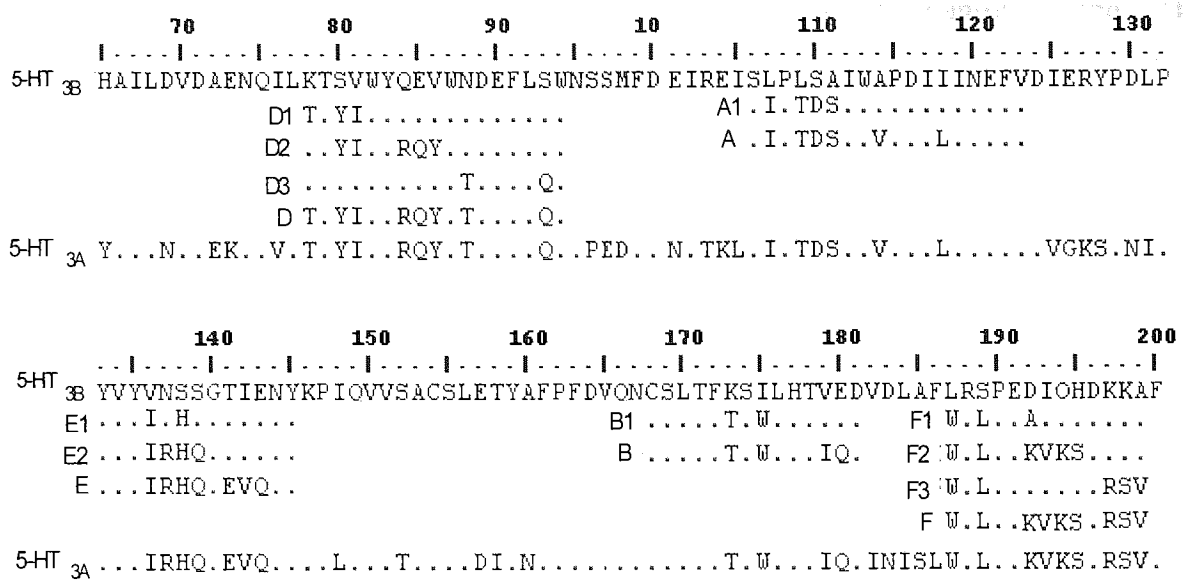

Figure 34: An overview of the amino acid changes to each 5-HT$_{3B}$ subunit binding loop for 5-HT$_{3B}$/5-HT$_{3A}$ chimeric subunits. Dots indicate sequence identity to 5-HT$_{3B}$. Amino acid numbering refers to the 5-HT$_{3B}$ sequence; equivalent 5-HT$_{3A}$ numbering is +8.

particular mutations are responsible for the loss of receptor expression, though it must also be considered that a low success rate of cell transfections was occurring at the same time as these experiments.

5.2.2 Point mutations

Point mutations W82A, S106A, Y133A, V134A, Y135A and E143Q, all caused significant increases in receptor affinity for granisetron, although all increases were less than 2-fold compared to 5-HT$_{3A/B(V5)}$, its equivalent wildtype (**Figure 35**). The same mutant receptors, with the exception of W82A, also showed increased affinities for 5-HT, but none were greater than 3-fold. W82A showed no significant difference from wildtype 5-HT affinity. E85Q, V86Y and $Q^{84}E^{85}V^{86}\rightarrow R^{84}Q^{85}Y^{86}$ (subsequently referred to as **QEV**/RQY) demonstrated higher affinity for 5-HT compared to wild type (<3 fold), despite showing no significant difference in granisetron binding. Interestingly, receptors containing the point mutation E143A displayed a significant decrease in affinity for granisetron but a significant increase in affinity for 5-HT (**Figure 32**).

5.2.3 Chimeras

The A1 and full A-Loop chimera showed a higher affinity for both granisetron and 5-HT, compared to wild type 5-HT$_{3A/B(V5)}$ (**Figure 36**). The full A-loop chimera in fact showed the greatest increase in affinity for 5-HT (4-fold). Chimera D3 showed just a 1.5 fold increased affinity for granisetron and a 2-fold increase for 5-HT. The full D-loop chimera showed even greater increases in affinity for both granisetron and 5-HT over the D3 chimera. Although the granisetron affinity exhibited by the E1 and full E-loop chimeras were not significantly different from wild type, surprisingly E2 did demonstrate a small increase in affinity that was statistically significant. All partial chimeras of the E-loop, as well as the full chimera, showed a ~3.5-fold increase in affinity for 5-HT, with the full chimera showing the marginally higher affinity of the three. Partial F-loop chimeras F2 and F3 and the full F-loop chimeras showed increases in affinity for both granisetron and 5-HT, this increase was more marked for 5-HT (**Figure 33**).

5.2.4 Two-electrode voltage clamping

The majority of the electrophysiological work was performed in Canada by the research group of Dr. Susan Dunn, Department of Pharmacology, University of Alberta (see **Acknowledgements**). I performed the same experiments on the 5-HT$_{3A/B\underline{ChimD}}$R, but due to time constraints and problems with oocyte viability, the remaining data-set (**Table 14**) were performed as part of this collaboration.

Table 13 contains dose-response data, focusing on the D-loop 5-HT$_{3B}$ subunit mutants, but also includes the I175W mutant. It was hoped that electrophysiology data for all these mutants could be plotted as a normalised dose-response curve, as exemplified by **Figure 37** using my 5-HT$_{3BChimD}$ mutant. However the individual data points were not available at the time this thesis was submitted, although the calculated EC$_{50}$ and Hillslope data is included in **Table 13**.

The wildtype 5-HT$_{3A}$Rs and 5-HT$_{3A/B}$Rs have now been well characterised using the voltage clamping technique, comparatively more so than any of the mutant 5-HT$_{3B}$ subunits expressed in xenopus oocytes. It appears that expressing 5-HT$_{3B(V5)}$ causes an increase in potency of 5-HT at the 5-HT$_{3A/B(V5)}$R by 7.6-fold (**Table 13**). The difference in 5-HT potency at the two subtypes of receptor is ~23-fold, 5-HT being more potent at the 5-HT$_{3A}$R, as has previously been published (Dubin *et al.*, 1999).

Loop	Point Mutation	*pK$_d$ (nM) Mean ± SEM*	Fold change	*n*
	WT	9.25 ± 0.03	-	6
D	W82A	9.51 ± 0.11	↓ 1.7	3
D	Q84R	9.24 ± 0.10	↑ 1.1	5
D	E85Q	9.31 ± 0.03	↓ 1.1	7
D	V86Y	9.19 ± 0.01	↑ 1.2	2
D	**QEV/RQY**	9.30 ± 0.02	↓ 1.1	5
A	S106A	9.50 ± 0.03	↓ 1.8	5
E	Y133A	9.35 ± 0.04	↓ 1.2	4
E	V134A	9.43 ± 0.03	↓ 1.5	5
E	Y135A	9.35 ± 0.02	↓ 1.2	5
E	E143A	9.13 ± 0.004	↑ 1.3	4
E	E143Q	9.39 ± 0.02	↓ 1.4	4
B	I175W	9.33 ± 0.04	↓ 1.2	5

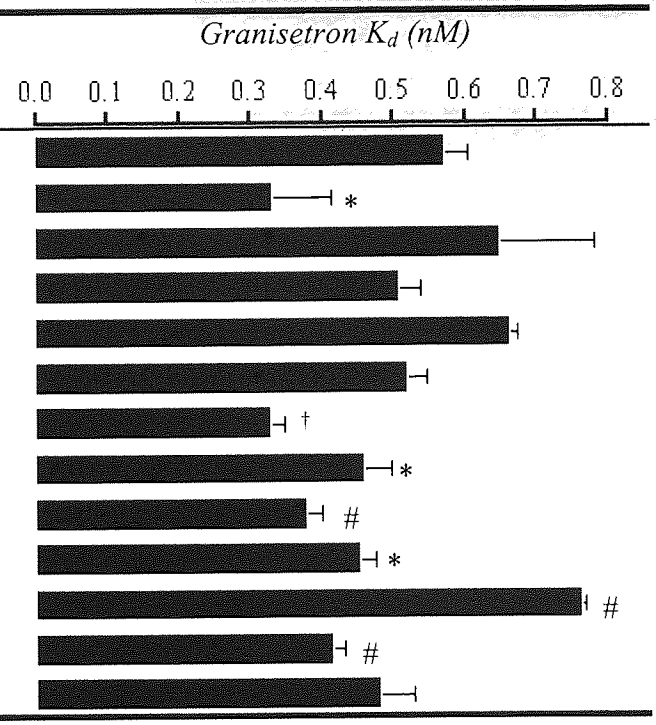

Loop	*Point Mutation*	*pK$_i$ (nM) Mean ± SEM*	Fold Change	*n*
	WT	3.84 ± 0.05	-	6
D	W82A	3.88 ± 0.02	↓ 1.1	3
D	Q84R	4.13 ± 0.06	↓ 2	5
D	E85Q	4.31 ± 0.02	↓ 3	7
D	V86Y	4.31 ± 0.03	↓ 3	2
D	**QEV/RQY**	4.24 ± 0.06	↓ 2	5
A	S106A	4.25 ± 0.03	↓ 2.6	5
E	Y133A	4.19 ± 0.02	↓ 2.3	4
E	V134A	4.25 ± 0.05	↓ 2.6	5
E	Y135A	4.10 ± 0.03	↓ 1.8	5
E	E143A	4.50 ± 0.01	↓ 4.7	4
E	E143Q	4.13 ± 0.03	↓ 2	4
B	I175W	3.96 ± 0.07	↓ 1.3	5

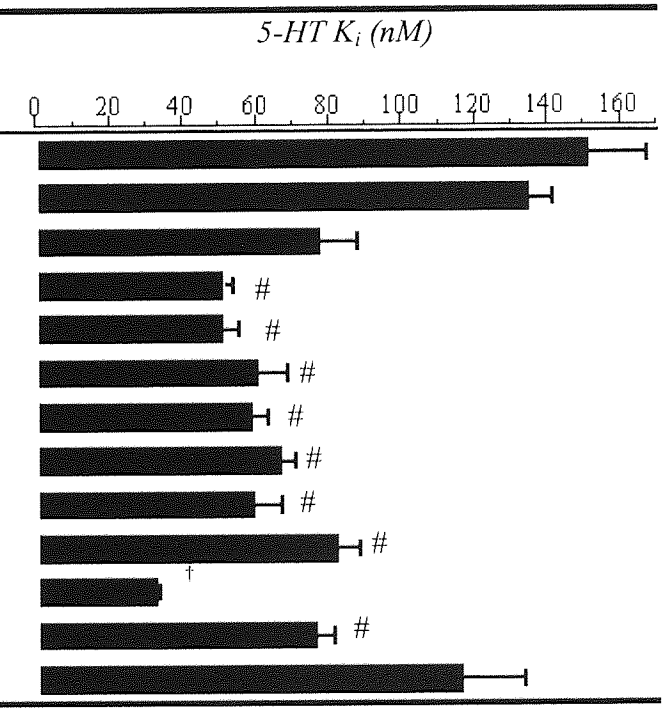

Figure 35: Effects of 5-HT$_{3B}$ mutagenesis on granisetron and 5-HT affinity (K_d and K_i respectively), measured by competition with [^{3}H]granisetron. Mutations were within the putative binding loops of the 5-HT$_{3B}$ subunit as indicated, and were either alanine mutations or 5-HT$_{3B}$ → 5-HT$_{3A}$ mutations. One-way ANOVA followed by Dunnett's *post-hoc* test was performed for each tagged receptor subtype versus the wild type 5-HT$_{3A/B(V5)}$, where * is $P < 0.05$, $^{\#}$ is $P < 0.005$ and † is $P < 0.0001$.

Chimera	*pK$_d$ (nM) Mean ± SEM*	Fold Change	*n*
WT	9.25 ± 0.03	-	6
A1	9.44 ± 0.04	↓ 1.5	4
A	9.47 ± 0.03	↓ 1.6	4
B	9.36 ± 0.05	↓ 1.3	4
D1	9.3 ± 0.05	↓ 1.1	4
D2	9.46	↓ 1.6	1
D3	9.45 ± 0.05	↓ 1.6	2
D	9.53 ± 0.07	↓ 1.8	5
E1	9.30 ± 0.01	↓ 1.1	3
E2	9.37 ± 0.03	↓ 1.3	4
E	9.32 ± 0.02	↓ 1.2	4
F2	9.46 ± 0.02	↓ 1.4	4
F3	9.38 ± 0.02	↓ 1.3	3
F	9.50 ± 0.04	↓ 1.8	4

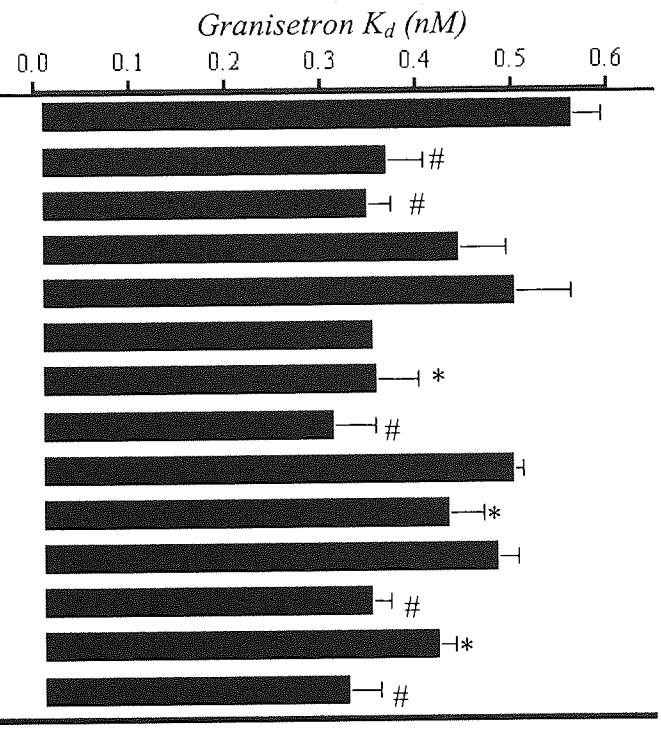

Chimera	*pK$_i$ (nM) Mean ± SEM*	Fold Change	*n*
WT	3.84 ± 0.05	-	6
A1	4.05 ± 0.04	↓ 1.6	4
A	4.44 ± 0.09	↓ 4.0	4
B	4.20 ± 0.04	↓ 2.3	4
D1	4.25 ± 0.04	↓ 2.6	4
D3	4.14 ± 0.03	↓ 2.0	3
D	4.30 ± 0.02	↓ 2.9	5
E1	4.39 ± 0.06	↓ 3.6	3
E2	4.36 ± 0.02	↓ 3.4	4
E	4.42 ± 0.06	↓ 3.7	4
F2	4.40 ± 0.08	↓ 3.6	3
F3	4.36 ± 0.03	↓ 3.4	3
F	4.28 ± 0.06	↓ 2.7	4

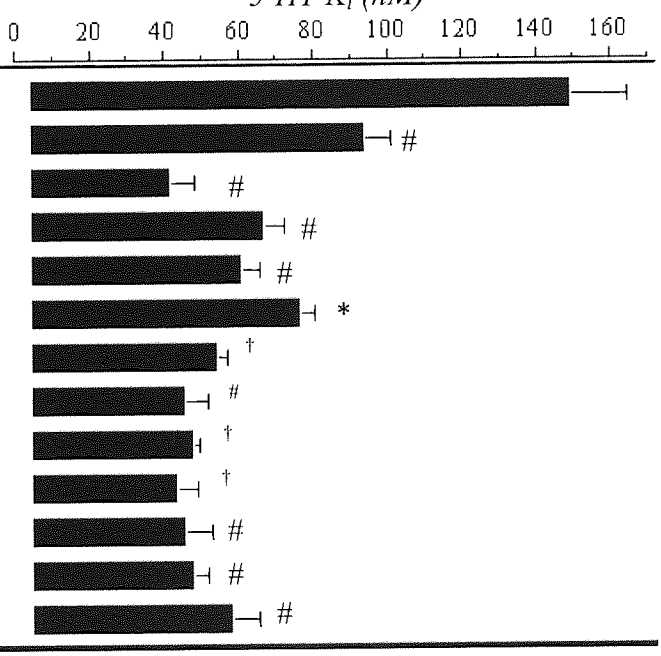

Figure 36: Effects of expressing 5-HT$_{3B}$→5-HT$_{3A}$ putative binding loop chimeras on granisetron and 5-HT affinity, measured by competition with [^{3}H]granisetron. One-way ANOVA followed by Dunnett's post-hoc test was performed for each tagged receptor subtype versus the wild type 5-HT$_{3A/B(V5)}$, where * is P < 0.05, $^{\#}$ is P < 0.005 and † is P < 0.0001.

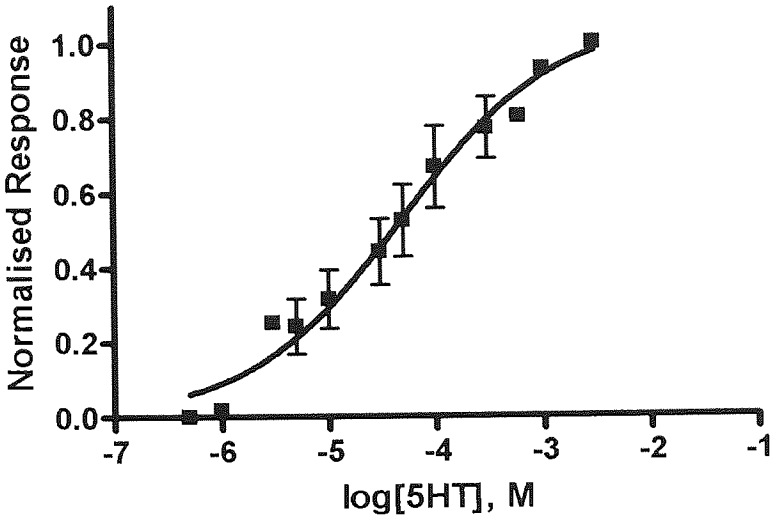

Figure 37: Representative dose-response curve for 5-HT and receptor subtype 5-HT$_{3A/BChimD}$, measured electrophysiologically in xenopus oocytes by the voltage-clamp technique (n = 3). Error bars represent standard error of the mean (± SEM). Current responses were normalised to the maximal current (I_{max}).

Receptor Subtype	5-HT			Curare			Picrotoxin		
	EC_{50} (μM)	nH	n	K_i (μM)	nH	n	K_i	nH	n
5-HT$_{3A}$	1.01 ± 0.02	3.52	4	4.1 ± 1.1	1.74 ± 0.1	3	14.8	0.92 ± 0.2	3
5-HT$_{3A/B}$	23.6 ± 0.11	0.72	4	54.9 ± 20.8	1.13 ± 0.1	3	144.0	1.4 ± 0.6	3
5-HT$_{3A/B(V5)}$	3.1 ± 0.62	1.3 ± 0.1	3						
5-HT$_{3A/B(Q84R)}$	9.8 ± 4.8	1.2 ± 0.07	3						
5-HT$_{3A/B(E85Q)}$	3.4 ± 1.2	1.4 ± 0.2	3						
5-HT$_{3A/B(V86Y)}$	4.4 ± 1.4	1.2 ± 0.2	3						
5-HT$_{3A/B(QEV/RQY)}$	6.7 ± 2.3	1.7 ± 0.4	4						
5-HT$_{3A/BChimD}$	45.4 ± 2.4	0.7 ± 0.01	3						
5-HT$_{3A/BI175W(V5)}$	1.2 ± 0.12	2.6 ± 0.54	3	0.56 ± 0.34	1.03 ± 0.06	4	6.38 ± 1.1	0.79 ± 0.04	3

Table 13: Two-electrode voltage-clamp recordings of EC_{50} (5-HT), K_i (curare and picrotoxin) and Hillslope values (nH) of wildtype and mutant 5-HT$_3$Rs in transfected xenopus oocytes. For determining the K_i of curare and picrotoxin in the 5-HT$_{3A}$ homomer and 5-HT$_{3I175W}$ mutant [5-HT] = 1 μM, heteromer [5-HT] = 20 μM. K_i values from competition experiments were calculated from the IC_{50} values using the Cheng-Prussof correction (*Equation 8*). All of these mutant 5-HT$_{3B}$ subunits contain the V5 tag.

Due to the preliminary nature of the data in Table 13, no statistical analysis has been possible; but, it is clear that the most substantial result is that 5-HT has a 15-fold greater potency at the 5-HT$_{3B\underline{ChimD}}$R, but the Hillslope remains within the range determined for h5-HT$_{3A/B}$R and h5-HT$_{3A/B(V5)}$Rs. Other mutations detailed in **Table 13** do not have a similarly dramatic effect on 5-HT potency.

The antagonists curare and picrotoxin have also been tested for their ability to antagonise the response of both h5-HT$_{3A}$Rs and h5-HT$_{3A/B}$Rs to 5-HT, but with differential affinities. Indeed, the results in **Table 13** show that curare and picrotoxin are 13- and 10-fold more potent at homomeric receptors, but this differential is not as marked as published for m5-HT$_3$Rs (Das *et al.*, 2003; Hope *et al.*, 1999). These results are specifically for comparing with the same experiments performed on 5-HT$_{3A/BI175W(V5)}$Rs. This mutant demonstrates a higher affinity for curare and picrotoxin than both 5-HT$_{3A}$Rs and 5-HT$_{3A/B}$Rs. The Hillslopes are not as dramatically affected, but neither of the Hillslopes for picrotoxin or curare differ wildly between homomeric and heteromeric receptors, unlike that for 5-HT.

5.3 Discussion

Receptor mutagenesis and homology modeling are used synergistically to improve the molecular model: results of point mutations can be rationalised by the ligand docking, as well as showing inaccuracies in the docking position, which can be later improved. Mutagenesis in the m5-HT$_3$ receptor homomer has previously resulted in some dramatic changes in binding and function that have allowed for the selection of appropriate docked poses (Price & Lummis, 2004; Yan & White, 2005). Surprisingly, the mutagenesis presented in this thesis does not affect the binding of the heteromeric h5-HT$_3$R to the same extent that has been observed for the homomer, i.e. changes are not greater than 10-fold. Preliminary electrophysiological studies with the mutant 5-HT$_{3A/B(I175W)}$R do however show functional differences of greater magnitude.

5.3.1 Technical considerations

This study has focused on 5-HT$_{3B}$ subunit residue mutations on the putative binding loops, as these regions have already received much attention in mutagenesis and binding studies of the homomeric m5-HT$_{3A}$R (see **Appendix**: m5-HT$_{3A}$ mutations), and provide a valuable set of data with which our results can be compared and contrasted. Our mutagenesis experiments used 5-HT$_{3B(V5)}$ subunit cDNA as a template in order to create mutant 5-HT$_{3B}$ subunits that could be detected using commercially available anti-V5 antibody, already shown to exhibit

high specificity in **Chapter 3**. The presence of V5-positive bands on western blots demonstrates that the HEK293 cells have successfully expressed 5-HT$_{3B}$ protein subunits, but does not verify whether this expression is on the cell surface or only intracellular. The results of radioligand binding studies presented here can therefore be interpreted in two ways. Firstly, that the mutant 5-HT$_{3B}$ subunits are expressed intracellularly but not at the surface. Secondly, the 5-HT$_{3B}$ subunits are expressed at the cell surface, and although these residues contribute to the structure of the binding pocket, the nature of the binding mechanism in 5-HT$_{3A/B}$Rs means that the mutated residues do not have critical influences on ligand binding. This is the conclusion supported by our homology model (**Chapter 4**).

The first interpretation is considered unlikely because the chosen mutations are not only residues that have previously demonstrated robust expression (**Appendix**: m5-HT$_{3A}$ mutations), but many are also reversions to residues already found in the 5-HT$_{3A}$ subunit (**S106A** is a notable exception that has never been tested before). Our homology model also confirms that the 5-HT$_{3B}$ subunit residues adopt a structural arrangement almost identical to that of 5-HT$_{3A}$. Together this means that the mutant residues are in the same protein environment as they would be in the 5-HT$_{3A}$R, causing minimum unfavourable interactions that are normally responsible for misfolding, such as steric hindrances and electrostatic clashes.

The expression of 5-HT$_{3A}$Rs rather than 5-HT$_{3A/B}$Rs in the presence of both 5-HT$_{3A}$ and 5-HT$_{3B}$ subunit cDNAs is also unlikely, considering previous reports of how 'promiscuous' this subunit is whilst assembling in the presence of other LGIC subunits (van Hooft *et al.*, 1998).

The effect of mutating multiple amino acids is not comparable to previous studies in m5-HT$_{3A}$Rs, which means that each chimera has an undetermined effect on cell surface expression. However, it is usually the case that residues highly conserved in the LGIC family are those responsible for dramatic effects on expression (Spier & Lummis, 2000; Price & Lummis, 2004). Conserved residues between 5-HT$_{3A}$ and 5-HT$_{3B}$ subunits have obviously not been altered in the chimera studies or 5-HT$_{3B}$ → 5-HT$_{3A}$ (exchange of 5-HT$_{3B}$ mutations for the sequence aligned residues of 5-HT$_{3A}$) point mutations.

A further concern of this study is the possibility that the 5-HT$_{3B(V5)}$ subunit is not expressed on the surface of oocytes. This concern is evidenced by **Table 14**, where introducing both 5-HT$_{3A}$ and 5-HT$_{3B(V5)}$ subunit mRNA into the oocytes causes expression of receptors with a similar EC_{50} as 5-HT$_{3A}$R homomers. This possibility is, however, considered unlikely. Our AFM results show conclusively that 5-HT$_{3B(V5)}$ is expressed on the surface of TSA201 cells (**Figure 17**), and it is more often the case that proteins which do not express well in

mammalian cells, are expressed with no problems in xenopus oocytes. This phenomenon is thought to be related to the low temperature (16 °C) at which the oocytes are stored whilst the injected mRNA is being translated into protein subunits. Lower temperatures are more conducive to correct folding. Preliminary experiments using curare and picrotoxin also suggest that 5-HT$_{3A/B(V5)}$Rs have the recognition properties of a heteromer (personal communication, Dr. Susan Dunn). It is accepted that the V5 tag has affected receptor function in some way, which is interesting in itself, but the position of the tag at the C-terminus is unlikely to affect recognition properties.

5.3.2 Mutagenesis of the 5-HT$_{3A/B}$R binding pocket

Our homology models suggest that the presence of the 5-HT$_{3B}$ subunit in 5-HT$_{3A/B}$Rs does not drastically alter the binding site structure. It maintains the aromatic binding pocket and the position of key complementary face residues. It is reasonable to expect, therefore, that 5-HT$_{3B}$ → 5-HT$_{3A}$ mutations in this region should have similar effects in mutant 5-HT$_{3A}$Rs and 5-HT$_{3A/B}$Rs. However none of the mutations in this study produced the dramatic changes in ligand binding affinity seen in similar studies on m5-HT$_{3A}$Rs: why? In homomeric 5-HT$_3$Rs, mutating 5-HT$_{3A}$ subunits affects all five potential binding interfaces, rather than the two A-B interfaces identified for the heteromer by our AFM and modelling studies. It is therefore reasonable to predict that the effects of mutating 5-HT$_{3A}$ subunits will have more pronounced consequences in homomeric receptors, compared to heteromeric receptors. Also, species variation between principal face residues of h5-HT$_{3A}$ and m5-HT$_{3A}$ subunits may play a part in reducing the extent of observed effects. Certainly, the m5-HT$_{3A}$R homomer demonstrates significant differences in its affinity for a number of ligands when compared to the human transcript (Hope *et al.*, 1999), suggesting that key residues, particularly those of the C-loop, make binding of certain ligands non-equivalent between species. The use of m5-HT$_{3A}$Rs as a model system indicative of pharmacologically relevant residues is invaluable. However, the extent to which these effects will be replicated in h5-HT$_{3A}$Rs and h5-HT$_{3A/B}$Rs is obviously questionable.

The 5-HT$_{3A/B}$R subunit arrangement of B-B-A-B-A, determined by our AFM studies (**Chapter 3**), identifies that 5-HT$_{3B}$ subunits must form the complementary face. This follows logically if 5-HT$_{3A}$ subunits are accepted as providing the principal face residues (Brejc *et al.*, 2001) and the principal faces at 5-HT$_{3A}$ subunits are only adjacent to the complementary faces at 5-HT$_{3B}$ subunits in an anticlockwise direction. With this in mind, it is more likely that

changes to the amino acid residues within the D-, E-, and F-loops of the 5-HT$_{3B}$ subunit will directly affect ligand binding.

5.3.2.1 D-Loop

The m5-HT$_{3A}$R D-loop residues have previously been scrutinised by a series of point mutation experiments, each demonstrating significant cell-surface expression (**Appendix**: m5-HT$_{3A}$ mutations). W90 (**W82** in the 5-HT$_{3B}$ subunit), R92 (**Q84**), Y94 (**V86**) have all been implicated in granisetron binding in the homomer, whereas only R92 (**Q84**) has been implicated in 5-HT binding (Yan *et al.*, 1999).

The 5-HT and [^{3}H]granisetron binding affinity of the **5-HT$_{3A/B\underline{W82A}}$** receptor was not detrimentally affected. This is surprising in light of our homology modelling and docking results placing **W82** within hydrogen bonding distance of 5-HT and within 5 Å of granisetron in the apo conformation. It is possible that the environment of the A-B binding interface causes ligands to gain more binding energy from principal face residues, thus reducing the influence of complementary residues, as indicated by our homology models (**Figure 29** and **Figure 30**). Previously, AChBP crystal structures, and biochemical studies such as photolabeling and SCAM, have all implicated this tryptophan as featuring within the binding pocket of *Torpedo californica* nAChR (Chiara & Cohen, 1997; Chiara *et al.*, 1998; Chiara *et al.*, 1999) and GABA$_A$Rs (Smith & Olsen, 1994; Boileau *et al.*, 1999). Such tryptophan residues are most commonly associated with π-π or cation-π interactions, thought to provide the major attractive forces within the ligand binding pocket of the 5-HT$_3$R (Beene *et al.*, 2002) and other LGICs (Zhong *et al.*, 1998; Lester *et al.*, 2004). Molecular dynamics simulations in the AChBP describe an agonist mediated interaction between two tryptophan residues that align to W183 and W90/**W82.** Other research groups have determined that a W90A mutation causes the total ablation of 5-HT and granisetron binding in the homomeric receptor (Yan *et al.*, 1999; Thompson *et al.*, 2005), in spite of being expressed robustly (Thompson *et al.*, 2005). However, most published data agrees that a tryptophan at position 90 in the m5-HT$_{3A}$ subunit is in fact not essential for binding or expression, but rather its hydrophobicity and bulk are important for maintaining a functional binding site: W90F 5-HT$_{3A}$ subunit mutants affect neither 5-HT affinity nor EC$_{50}$ (Yan *et al.*, 1999), and removing the π-electron cloud of tryptophan has no effect on binding (Beene *et al.*, 2002). This is also true for other LGIC receptors: phenylalanine substitutions to the *Torpedo californica* nAChR aligned residues, γW55 and δW57, largely affected channel opening (Akk, 2002), though binding data is not yet available for W55A (for information on a W55A mutant tested with

other drugs see Gay *et al.*, 2007). Leucine mutations to both the **W82** aligned residues in nAChR (γW55 and δW57) and GABA$_A$R (α$_1$F64) show substantial reductions in affinity for both antagonist (curare) and agonist (GABA) respectively (Xie & Cohen, 2001; Akk, 2002). Again, the cause of this is expected to be the loss of bulk from this amino acid position.

Substituting the tryptophan for alanine at position **82** (as is the case for our W82A mutant) will remove the bulk required to maintain high affinity binding. The most parsimonious explanation for **W82A** showing wildtype binding is that the expression of mutant 5-HT$_{3B}$ subunits is impaired and the predominant receptor subtype is homomeric. This could easily be refuted by further analysis of 5-HT$_{3B}$ subunit surface expression, but until such experiments are performed, it remains a possibility. An alternative explanation is that the intersubunit interactions that W90/**W82** are involved in are different between A-A and A-B interfaces. In the heteromeric *Torpedo californica* nAChR, mutations to W55 in the α-subunit, although associated with providing principal face residues, was still determined to alter the function of the receptor (Kapur *et al.*, 2006). Expression of 5-HT$_{3A(W90A)/B}$Rs would be a way of determining the location of residue which causes the loss of affinity. If this receptor still has low/no affinity for ligands it should be possible to allocate the effect to a 5-HT$_{3A}$ subunit specific site, provided that expression of 5-HT$_{3A}$R homomers can be ruled out.

It is well established that amino acid residues R92/**Q84**, Q93/**E85**, and Y94/**V86** comprise the same β-strand structure (β2) determined to form part of the binding pocket and/or signal transduction mechanism (Boileau *et al.*, 1999; Yan *et al.*, 1999). This sequence is not conserved in the 5-HT$_{3B}$ subunit and may confer a subtle nuance in the binding or gating properties. By mutating these 5-HT$_{3B}$ subunit residues to those found in 5-HT$_{3A}$, the contribution of these residues to binding and gating can be established. Neither the 5-HT$_{3B}$ subunit individual point mutations nor the triple **QEV**/RQY mutation caused substantial shifts in affinity for either 5-HT or granisetron.

In m5-HT$_{3A}$Rs, it has previously been shown that Y94 does not affect the agonist binding pocket (Price & Lummis, 2004) despite affecting granisetron binding (Yan *et al.*, 1999). According to our homology modeling, Q93/**E85** does not contribute to ligand binding because its position on the β-strand of the D-loop causes it to be orientated projecting away from the binding pocket. It was hoped that by testing three consecutive residues in such a prominent position on a predicted β-strand, binding effects would be seen in an 'every other residue' pattern, i.e. **Q84**R and **V86**Y. Although effects were seen with 5-HT binding with these D-loop mutants, no such patterns emerged.

In the homomeric receptor R92A has previously shown modest (6-fold) decreases in granisetron affinity but substantial (15-fold) decreases in 5-HT affinity, although a R92K mutation had a less dramatic effect (Thompson *et al.*, 2005).

The absence of distinct ligand binding interaction for all D-loop residues does not preclude these residues from making discrete interactions at some stage of the ligand binding process, and could still facilitate the conformational changes that lead to the opening of the channel.

The response of 5-HT$_{3A/B\underline{ChimD}}$Rs to 5-HT is obviously reduced compared to its wildtype counterpart (**Table 13**), though these data require additional statistical analysis. This effect is probably opposite to what one would expected, because 5-HT$_{3A}$Rs have a lower EC_{50} than 5-HT$_{3A/B}$Rs, therefore placing these D-loop residues in the same location of 5-HT$_{3B}$ subunits should enhance the response. This mutant serves to highlight the complexity of heterogeneity in receptors.

5.3.2.2 E-loop

The 5-HT$_3$R E-loop residues are predominantly aromatic/hydrophobic in nature, with hydrogen bonding capabilities. Three tyrosine residues; Y141/**Y133**, Y143/**Y135** and Y153/**Y145** have been identified as major influences to ligand binding (Venkataraman *et al.*, 2002; Beene *et al.*, 2004; Thompson *et al.*, 2005). According to crystal structure data, this loop contributes a number of residues to the ligand binding pocket of *Ls*-AChBP (R104, V106, L112, M114, Brejc *et al.*, 2001; L102, R104, L112, M114, Celie *et al.*, 2004). It is perhaps expected that the removal of aromatic residues from the E-loop, as occurs with alanine scanning, would cause disruption to the binding pocket, as has previously been demonstrated in the m5-HT$_{3A}$ homomeric receptor (**Appendix**: m5-HT$_{3A}$ mutations). However, within the cohort of E-loop mutations presented here, only **E143A** produced a significant loss of affinity for granisetron and the most significant gain in affinity for 5-HT, although these changes from WT were still relatively small (< 4 fold). Residue **E143** aligns with L112 of *Ls*-AChBP, but is not conserved within the 5-HT$_{3A-E}$ receptor subunits, and is somewhat removed from our docked ligand models. At the aligned E143 position, 5-HT$_3$ subunits A-E contain residues with long aliphatic side chains that the 5-HT$_{3A}$R and $_{5\text{-HT3A/B}}$ subunit modeling predicts will project towards, and possibly contact E229 of the C-loop, possibly influencing its movements. Minor alterations in the binding affinity of 5-HT may be due to minor alterations to the C-loop movement. The less pronounced changes in binding affinity for **E143Q** suggest that this substitution provides the required environment to maintain normal C-loop movements. The importance of these assertions are moderated by the

magnitude to which this alanine mutant affects binding (< 5 fold), and the consideration that other research groups have found that the equivalent residue in the m5-HT$_{3A}$R has a greater effect on granisetron binding (Venkataraman *et al.*, 2002).

The moderate change in 5-HT affinity of the **Y135A** mutant was somewhat surprising, considering that it has previously been shown to cause a >100-fold reduction in affinity in the m5-HT$_3$R homomer (Venkataraman *et al.*, 2002). The radioligand binding results do, however, support our docked ligand homology model, which places this residue high in the binding pocket relative to 5-HT, making direct interaction unlikely in the closed and open state. Two separate research groups have reported that Y143A causes a total loss of functional response to 5-HT in the m5-HT$_{3A}$R homomer (Venkataraman *et al.*, 2002; Price & Lummis, 2004), and one other group has reported severe reductions to the response (Beene *et al.*, 2004), implying that this residue is essential for function in the m5-HT$_{3A}$R homomer. Functional testing of our **Y135A** mutant is required to determine its role in responding to 5-HT.

The aromatic nature of the **Y145** residue is conserved within the LGIC family, and it would be expected that removal of an aromatic residue would cause some reduction in binding affinity. Transfections of the **Y145A** mutant were unsuccessful, frustrating attempts to determine whether this residue binds any ligands in 5-HT$_{3A/B}$R, as is predicted by our docking models.

Interaction of the E-loop residues with agonist has consistently been determined as important for the correct functioning of all LGICs. The exact residues involved do vary. None of the E-loop chimeras caused dramatic changes in the binding affinity of 5-HT or granisetron. The small increase in 5-HT affinity that did occur is present in chimera E1, suggested that either **V136I** or **S138H** is responsible. These residues lie closer to the tip of the E-loop and are unlikely to interact with ligand, and more likely to interact with residues of the β5 strand, such as **F99**, **E104** and **I105**.

5.3.2.3 F-loop

The F-loop chimeras modestly increased the affinity of 5-HT binding whilst leaving the binding affinity of granisetron relatively unaffected. An increase in affinity by the introduction of alanine and conservative mutations was also demonstrated by Thompson *et al.* (2006). Movement of the F-loop to cause the enhancement of agonist but not antagonist affinity is a phenomenon previously identified in the nAChR (Martin *et al.*, 1996).

The F-loop is predicted to be the furthest loop away from the W183-centred A-B binding site (**Figure 28**; A-B). However, it is noted that this conformation has shifted modestly closer to the binding site at the B-A interface (**Figure 28**; B-A). This could mean that the amino acid composition of the F-loop in 5-HT$_{3A}$ subunit causes a change in conformation that enhances agonist binding, all be it to a modest degree. An exhaustive mutagenic study of the F-loop (Thompson *et al.*, 2006) has identified two regions at opposing ends of the putative loop that alter antagonist affinity, purportedly through changes in F-loop movement around W195 (**L187**) and D204 (**D196**). All of the F-loop chimeras contained an **L187**W mutation and chimeras F, F2 and F3 had mutations around the **D196** residue, perhaps affecting the structure of this loop. Any F-loop chimeras containing a **L187**W mutation would be expected to cause an increase in affinity, as shown in the present study. An **L187**W mutant in the canine 5-HT$_{3A}$R orthologue concurs with our result, but also establishes a potency and efficacy role for this residue with other ligands (Jensen *et al.*, 2006). Considering the subtleness of the changes in affinity between the F-loop chimeric receptors and WT receptors, it is unwise to suggest any major role for these 5-HT$_{3B}$ regions until further more convincing evidence is available.

The poor transfection efficiency of our F1 chimera makes it difficult to attribute binding effects, caused by the other F-loop chimeras, to one particular subset of residue. Thus if residue **L187**W does increase the affinity, it is possible that either **DIQH**/KVKS or **KKA**/RSV amino acid exchanges found in chimera F2 and F3 respectively, could also be responsible for altering the affinity of 5-HT. Of these residues S203/**H195**, R205/**K197**, and S206/**A198** have been shown to have substantial effects on granisetron affinity when mutated to alanine or conservative mutations are made (Thompson *et al.*, 2005; Thompson *et al.*, 2006). An identical mutation to that performed in these studies, R205K, caused a 4.1 fold reduction in the EC$_{50}$ of 5-HT (Zhang *et al.*, 2007), although the binding characteristics remain undetermined.

A small number of F-loop amino acid residues have been implicated in affecting curare affinity (Zhang *et al.*, 2007). It would be interesting to test the effect of our F-loop chimera on the relative affinities of curare for wildtype and chimeric 5-HT$_{3A/B}$R.

5.3.2.4 A-loop

The **S106** mutation causes an increase in binding affinity for both 5-HT and granisetron that is unlikely to be due to direct enhancement of ligand binding interactions. Our homology model (**Chapter 4**), suggests that, despite the **S106** residue being located in a loop that is not part of the canonical binding site, it is still closer to this site than that of the B-B or B-A interface. It

may also make intersubunit interactions that link the 5-HT$_{3A}$ and 5-HT$_{3B}$ subunits at the A-B interface and could influence the structure of the binding pocket (see **Figure 28**).

The docking data for 5-HT and granisetron predicts a much lower binding arena, relative to the S106 residue (**Figure 28**), which makes it unlikely for direct interactions with a bound ligand. **S106** of the 5-HT$_{3B}$ subunit could potentially make hydrogen bonding interactions with **Y135** within the same subunit or H185 or R55 from the adjacent 5-HT$_{3A}$ subunit at the A-B interface (**Figure 28**). The **Y135** residue has also been mutated to alanine, but did not produce as marked increases in affinity. Further mutagenesis will be required to investigate the role of R55. If the changes in ligand affinity for this residue are similarly modest, it is unlikely that these residues represent a significant contribution to binding.

Very few residues of the A-loop were mutated for the creation of A-loop chimeras. This is because, unlike the D-, E-, F-, and C- loops, the amino acid composition of the A-loop is relatively conserved between the 5-HT$_{3A}$ and 5-HT$_{3B}$ subunits. As previously stated, few of these residues are likely to impact upon the binding pocket, due to their predicted location at the B-A and B-B interfaces. However, our radioligand binding results show that the full A-loop chimera caused the largest increase in 5-HT affinity, with mutations **A114**V and **I118**L contribute substantially (2.4-fold) compared to the four mutations of the A1 chimera (1.7-fold). These residues are located in an innocuous position on the A-loop, just above the apex, in the non functional binding site region. This does not prevent mutations in this location affecting binding at adjacent sites (see Kapur *et al.* 2006), especially in a loop with so much influence on function (Chakrapani *et al.* 2003). This loop is a direct link from B-A and B-B interfaces to the A-B binding site, its own movement possibly influencing that of the E-loop.

5.3.2.5 B-loop

Using our closed state homology model and *in silico* mutation of the I175 residue to a tryptophan, it was demonstrated that the B-A binding site was not unlike the amino acid environment of the A-B interface (**Figure 32**). It was therefore our hypothesis that the introduction of a **I175W** mutation into the 5-HT$_{3B}$ subunit would create up to three additional binding sites and mimic some of the properties of a homomeric 5-HT$_{3A}$R, especially an increased Hillslope. However, the **I175W** mutant showed no significant differences in binding affinities for either granisetron or 5-HT compared to wild type, when tested by competition binding. Neither did the Hillslope for 5-HT approach that of the homomer when assessed by electrophysiology. It is now evident that although this mutation did demonstrate

some interesting functional characteristics, it is unlikely that our hypothesis was correct, and no extra 5-HT binding sites were generated.

Electrophysiological analysis of the 5-HT$_{3A/B\underline{I175W(V5)}}$ mutant receptor showed that the K_i values of both curare and picrotoxin decreased beyond the K_i values of the homomer, implying that the binding characteristics of this mutant neither resembled a 5-HT$_{3A}$R nor a 5-HT$_{3A/B}$R. The only data that could assist in explaining this result is from studies concerning the differences in curare affinity between human and mouse orthologues of 5-HT$_{3A}$Rs (Hope *et al.*, 1999; Zhang *et al.*, 2007). No data exists that determines any reason for differences observed in this study, regarding curare affinity for 5-HT$_{3A}$Rs and 5-HT$_{3A/B}$Rs. The studies of orthologs have determined that C-loop (Hope *et al.*, 1999) and F-loop (Zhang *et al.*, 2007) residues are largely responsible for differences in curare binding affinity and potency, in addition to predictions that the planar ring of curare intercalates between W183 (B-loop) and Y234/**F225** (Maksay *et al.*, 2003). It is possible that the placement of an additional tryptophan residue (**W175**) at the B-loop position of both the B-A and B-B interfaces creates two further binding sites for curare. However, the creation of a curare binding site at the B-A and B-B interfaces lacks credibility, principally because of the important role the C-loop plays in curare binding (Hope *et al.*, 1999) in the 5-HT$_{3A}$R and the lack of sequence conservation between this loop in the 5-HT$_{3A}$ and 5-HT$_{3B}$ subunit. No amino acid identities are found between the aligned h5-HT$_{3B}$ and m5-HT$_{3A}$ subunit residues suspected to contribute the 160-fold loss of affinity between mouse and human residue replacements, and only two residues (Y222/**Y215** and V242/**V233**) are identical between 5-HT$_{3A}$ and 5-HT$_{3B}$ subunits. The length and movement of the C-loop are obviously critical features that define the binding site. Until these parameters are quantified for the 5-HT$_{3B}$ subunit, it is difficult to know the effects of the poor sequence conservation and its effects on the binding affinities of not only curare, but all ligands. From the protein alignment alone (**Figure 2**), it seems unlikely that the C-loop of the 5-HT$_{3B}$ subunit could make interactions with the curare molecule that could maintain sufficiently high affinity binding, mimicking that provided by 5-HT$_{3A}$ subunits.

A more rational explanation is that the mutation of a residue located in a B-A or B-B non-binding interface causes perturbation of the A-B interfacial binding site, which causes the change in affinity of curare. The W183 residue is certainly integral to the binding and gating mechanism, and potentially involved with an allosteric mechanism that enhances subsequent binding at other A-A interfaces within the same homomeric receptor: the homomeric receptor demonstrates a Hillslope of ~4, which indicates that the binding mechanism has a degree of cooperativity. The B-loop is between β7 (outer β sheet) and β8 (inner β-sheet), thus

potentially influencing the movements of the inner β-sheet relative to the outer. It is known that, in the *Torpedo* AChR, the inner β-sheet of the α subunit is rotated 10° anticlockwise in the closed conformation, relative to non-α subunits (Unwin, 2005). If W183/**I175** has a part to play in the relative positions of the β-sheets, the introduction of an **I175W** mutation may, to some extent, mimic the rotational difference of α-subunits, causing the more open conformation of the binding pocket, concomitantly increasing the affinity of curare.

Picrotoxin has been shown to be a non-competitive, use-dependant inhibitor of the 5-HT$_3$R, thought to bind within the channel itself (Das *et al.*, 2003). So, how can a point mutation in the ECD affect the TMD? The receptor gating mechanism relies on the transmission of a conformational wave from the ECD to the TMD via a closely linked series of structural rearrangements (Grosman *et al.*, 2000). At the A-B interface, W183 is very close to aromatic residues of the E-loop, making intersubunit interaction possible in the resting state. Both the B- and E-loops are connected directly to the Cys-loops of apposing subunits, such that any movement could be transduced to the Cys-loop, and further to the TM2.

This interaction between the B- and E-loops would be unlikely at the wild type B-A and B-B interfaces, because the tryptophan has been replaced with an isoleucine, concomitantly affecting the position of the TM2 residues responsible for binding picrotoxin. A disturbance to residues that influence this conformational wave will therefore have potential repercussions on the structural conformation of any other residues also linked to this mechanism of channel opening, including the ligand binding site and channel itself (Colquhoun, 1998). This theory is not without a precedent that is particularly relevant to the functional experiments presented in **Table 13**: experiments on the glycine receptor have demonstrated that picrotoxin binding alters the conformation of the M2-M3 loop (Hawthorne & Lynch, 2005), which is also part of the gating machinery and a pivotal component of the conformational wave. Further, mutation to the GABA$_C$ receptor TM2 results in the loss of the competitive binding component of picrotoxin (Wang *et al.*, 1995).

The mouse TM6' (6th amino acid from the start of the lipid bylayer) residue asparagine, when mutated to threonine, has previously been shown to increase the affinity of the heteromer for picrotoxin 5-fold, and the mutation to serine at the same position causes further increases in affinity, but remains 4-fold lower than homomeric receptors (Das & Dillon, 2005). The presence of serine at the 6' position in h5-HT$_{3B}$ subunits of h5-HT$_{3A/B}$Rs is probably responsible for the smaller differential in picrotoxin affinity seen in our functional studies (<10-fold), compared to that of the mouse (28-fold). Amino acid residues in the TM2 of m5-HT$_3$R have undergone extensive mutagenic analysis, but even after accounting for the further

contributions of residues at the 2' and 7' positions, the curare binding affinity of the heteromer does not reach that of the homomer, indicating that further accountable residues must lie outside the TM2 domain, comprising a different part of the conformational wave.

The Hillslope for 5-HT binding is usually found to be close to 2 for the heteromer but closer to 4 for the homomer; a reflection of the larger number of 5-HT binding sites contained within the homopentameric arrangement of 5-HT$_{3A}$ subunits. The structural rearrangements induced by agonist binding may facilitate the binding of further agonist molecules, thus raising the Hillslope, especially in the 5-HT$_{3A}$R which must contain five equivalent binding sites. The Hillslope for curare and picrotoxin binding to 5-HT$_{3A/B\underline{I175W(V5)}}$ **(Table 13)** does not indicate a change from heteromeric to homomeric receptor characteristics with regards to the number of binding sites. The comparative Hillslopes for picrotoxin binding are not as divergent because picrotoxin causes inhibition by interacting with channel residues, probably from each subunit TM2, and is therefore unlikely to have an allosteric mechanism, as is indicated by the Hillslopes of 0.92 and 1.4 at the homomeric and heteromeric receptors respectively. The Hillslope data for curare binding may indicate some allosteric mechanism in the homomer, but it is only indicative of a maximum of two binding sites, compared to the one site of the heteromer. Quite why curare would have one binding site at the heteromer, but two binding sites at the homomer is difficult to explain without further experimental data.

In addition to a cation-π interaction, it is believed that the agonist RNH_3^+ group is also able to interact with Y234 in the homomer, via π-π interactions. The 5-HT$_{3B}$ residue which aligns to Y234 in 5-HT$_{3A}$ is **F225**. According to the model of the heteromer, this residue positions itself in a similar spatial orientation as the Y234 residue of the homomer. **Figure 32** shows the 5-HT$_{3B}$ subunit as the principle face, containing the I175W mutation. The position of **F225** at the B-B interface is such that it is feasible for a RNH_3^+ group to become sandwiched between W175 and F225, as is expected for high affinity binding of any ligand. At the B-A interface, it is energetically unfavourable to place F225 within the binding pocket and in this orientation would be unable to influence the binding of ligands.

Biochemical data and, more recently, crystal structure data has concluded that ligand binding occurs at the subunit interface, where a principal (+) subunit provides loops A-C and a complementary (-) subunit provides loops D-F for ligand interactions. The assumption has been that both sets of loops, A-C and D-F provide mutually exclusive binding interactions, where loops D-F of the principal subunit and A-C of the complementary subunit are expected to be redundant. In receptors such as the α7-nAChR and the 5-HT$_{3A}$R homomer, the validity of this hypothesis is inconsequential, and furthermore not testable, because both sets of

binding loops of each subunit are inevitably involved in binding. In fact, the role of complementary binding loop residues from principal face subunits has only recently been explored in the muscle-type nicotinic acetylcholine receptor (Kapur *et al.*, 2006). In this instance, residue mutations of the A- and D-loop from the respective complementary and principal subunits (γ-α interface), were unexpectedly shown to affect the potency of acetylcholine, despite homology modelling predicting that this interface had no involvement in binding. Our homology model and docking demonstrates that it is not impossible for 5-HT to bind at the B-A and B-B interfaces, and that the putative binding pocket residues that would potentially contribute to binding interaction from the 5-HT$_{3B}$ subunits are not dissimilar in nature to those provided by loops A-C from the 5-HT$_{3A}$ subunit. The demonstrable importance of the 5-HT$_{3A}$ residue W183 for 5-HT binding, by virtue of its ability to facilitate cation-π and π-π interactions, is well established in the homomer (Beene *et al.*, 2002), and therefore expected to make an identical contribution at the A-B interface in the heteromer. The equivalent residue in the 5-HT$_{3B}$ subunit is **I175**, which is able to maintain the hydrophobicity of the binding pocket, but is deficient in a delocalised π-electron cloud and thus prevents binding at the B-A and B-B interfaces. Indeed, a W183I mutant in the homomeric m5-HT$_{3A}$R homomer ablates both [^{3}H]granisetron binding and the functional response to 5-HT (Lochner & Lummis, 2005).

CHAPTER 6: General Discussion

The aim of this study was to determine the stoichiometry of the 5-$HT_{3A/B}$ heteromeric receptor. This was successfully achieved using atomic force microscopy (**Chapter 3**), the results of which indicated that the subunits are arranged in a rosette formation with a B-B-A-B-A stoichiometry when viewed anti-clockwise from the extracellular synapse. These studies cannot account for all possible nuances of natively expressed 5-HT_3Rs (Hussy *et al.*, 1994) or different heterologous expression systems; but, the correlation of functional data from our heterologous HEK293 expression system to that found *in vivo*, compels us to believe that the B-B-A-B-A stoichiometry is responsible for the predominant functional characteristics previously measured by other research groups. In the absence of electrophysiological data that correlates the incorporation of 5-HT_{3C-E} subunits to the modulation of 5-HT_3R function, the B-B-A-B-A stoichiometry is the most plausible explanation for functional variance. More importantly, the B-B-A-B-A stoichiometry is the preferred subunit arrangement in the HEK293 expression system, used here, and which remains the predominant method for testing the effect of mutagenesis to 5-HT_{3A} subunits (see **Appendix:** mutations to the mouse 5-HT_{3A}R).

It was hoped that during the course of this work that concatemers could be generated which would reinforce the AFM stoichiometric determination. By creating an A-B-A trimeric concatemer and transfecting HEK293 cells with 5-HT_{3B} monomeric subunits, it would be possible to show that this constrained arrangement is quite capable of forming functional receptors. It is predicted that concatenation of other subunit combinations will lead to non-functional receptors. Concatenation would further lead to the ability to target receptor mutations to specific single subunits. This would greatly enhance our understanding of the contribution each subunit makes towards binding and function. The construction and expression of such concatemers remains a technically demanding challenge, that has so far alluded all 5-HT_3R research groups.

The efficiency and consistency of cDNA transfection greatly hindered the analysis of receptor mutagenesis experiments. The problem regarding transient transfections using chemical procedures such as calcium phosphate and PEI can be circumvented by instead using an electroporation method such as nucleofector™ II, supplied by AMAXA (Cologne, Germany). This technique has been used with highly efficient and consistent results by other research groups (personal communication with Dr. Sarah Lummis, Cambridge University), where

more traditional chemical methods have proved problematic. Switching to such a system would require initial calibration, to assess the effect of changing transfection procedure on the receptor pharmacology and function.

This new evidence for a B-B-A-B-A stoichiometry was used in combination with the nAChR closed-channel structure (Unwin, 2005) to generate a homology model. The model was used in combination with 5-HT and granisetron docking simulations, which predicted the same putative binding arenas for 5-HT and granisetron docking at both the A-A and A-B interfaces. The primary amine group of the 5-HT molecule is obligated to make intimate interactions with the A-loop backbone and W183 (B-loop) at both the A-A and A-B interface, while the indole group adopts different orientations due to the large binding pocket volume of the closed-channel receptor. These different orientations are expected to confer different binding affinities, which conflicts with the binding data from **Chapter 3**. It is therefore proposed that the first step for 5-HT binding involves interactions between the primary amine group and principal face residues within the A- and B-loop, with a large contribution being made via cation-π interactions. From this initial binding event, the specific movements of both the A-loop and C-loop can be coordinated. It is predicted that both of these loops can make intersubunit interactions with directly apposed complementary loop residues (**Figure 28**), causing the concomitant rotation of the adjacent complementary subunit. This narrows the binding pocket (**Figure 31**) and constricts the 5-HT molecule to an orientation where molecular interactions involving R92 (Yan *et al.*, 1999), Y143 and Y153 (Venkataraman *et al.*, 2002) correlate with current ligand binding data, and account for a small but significant proportion of the observed binding affinity.

The antagonist granisetron appears to preferentially dock towards the principal face residues. This is demonstrated clearly in our closed-state model A-B interface (**Figure 29**). It is assumed that the antagonist must 'cover all the bases' by deriving a significant proportion of its binding energy from a π-π interaction with W183; directly competing with agonist binding, as well as restricting movement of the A-loop and C-loop. The proximity of the tropane ring to C-loop hinge residue (Y234) at the A-B interface, alludes to a physical hindrance mechanism that could be generic to all LGIC. Surprisingly our models show that complementary residues, normally associated with granisetron binding, are not in appropriate proximity for significant interactions to occur. However, it is likely that the reduction in binding pocket volume, as occurs after agonist binding (**Figure 31**), would rectify this apparent anomaly, and highlights the need for further molecular modeling in combination with molecular dynamics, to examine the effect of 5-HT_3R conformational changes on

antagonist binding. A further technical consideration is that the ground- and bound-state crystal structures of the AChR and AChBP may be in alternative conformations to those adopted by 5-HT_3Rs. This is likely to affect predictions regarding the much larger antagonists, such as granisetron, which rely on a larger number of intersubunit contacts, in addition to those core interactions with principal face residues.

Further modeling and mutagenesis of 5-HT_{3A} and 5-HT_{3B} subunits will require focusing on the problem of ambiguous alignments in the region of the A-loop and C-loop, which remains a source of potential error in current interpretations of docking data. However, our model has provided an invaluable visualisation of possible binding interactions and how 5-HT_{3B} subunits may contribute to binding and function. These theories have been tested by mutagenesis, the effects of which were subsequently tested by ligand binding and electrophysiological recordings, with the later proving more successful at discerning deviations from wildtype properties; unlike the pharmacology of binding, which demonstrated very subtle difference.

The models presented here will represent the foundation of further mutagenesis experiments, involving both h5-HT_{3A} and 5-HT_{3B} subunits, and will be instrumental for rationalising results obtained from such experimentation.

List of References

Abi-Dargham A, Laruelle M, Wong DT, Robertson DW, Weinberger DR & Kleinman JE. (1993). Pharmacological and regional characterization of [3H]LY278584 binding sites in human brain. *J Neurochem* **60,** 730-737.

Adrien J, Tissier MH, Lanfumey L, Haj-Dahmane S, Jolas T, Franc B & Hamon M. (1992). Central action of 5-HT3 receptor ligands in the regulation of sleep-wakefulness and raphe neuronal activity in the rat. *Neuropharmacology* **31,** 519-529.

Akk G. (2001). Aromatics at the murine nicotinic receptor agonist binding site: mutational analysis of the alphaY93 and alphaW149 residues. *J Physiol* **535,** 729-740.

Akk G. (2002). Contributions of the non-alpha subunit residues (loop D) to agonist binding and channel gating in the muscle nicotinic acetylcholine receptor. *J Physiol* **544,** 695-705.

Akk G & Steinbach JH. (2000). Structural elements near the C-terminus are responsible for changes in nicotinic receptor gating kinetics following patch excision. *J Physiol* **527 Pt 3,** 405-417.

Alexander SP, Mathie A & Peters JA. (2006). Guide to receptors and channels, 2nd edition. *Br J Pharmacol* **147 Suppl 3,** S1-168.

Auerbach A, Sigurdson W, Chen J & Akk G. (1996). Voltage dependence of mouse acetylcholine receptor gating: different charge movements in di-, mono- and unliganded receptors. *J Physiol* **494,** 155-170.

Balfour JA & Goa KL. (1997). Dolasetron. A review of its pharmacology and therapeutic potential in the management of nausea and vomiting induced by chemotherapy, radiotherapy or surgery. *Drugs* **54,** 273-298.

Barann M, Meder W, Dorner Z, Bruss M, Bonisch H, Gothert M & Urban BW. (2000). Recombinant human 5-HT3A receptors in outside-out patches of HEK 293 cells: basic properties and barbiturate effects. *Naunyn Schmiedebergs Arch Pharmacol* **362,** 255-265.

Barnes JM, Barnes NM, Costall B, Deakin JF, Ironside JW, Kilpatrick GJ, Naylor RJ, Rudd JA, Simpson MD, Slater P & et al. (1990). Identification and distribution of 5-HT3 recognition sites within the human brainstem. *Neurosci Lett* **111,** 80-86.

Barnes JM, Barnes NM, Costall B, Naylor IL, Naylor RJ & Rudd JA. (1990). Topographical distribution of 5-HT3 receptor recognition sites in the ferret brain stem. *Naunyn Schmiedebergs Arch Pharmacol* **342,** 17-21.

Barnes NM & Sharp T. (1999). A review of central 5-HT receptors and their function. *Neuropharmacology* **38,** 1083-1152.

Barrera NP, Herbert P, Henderson RM, Martin IL & Edwardson JM. (2005). Atomic force

microscopy reveals the stoichiometry and subunit arrangement of 5-HT3 receptors. *Proc Natl Acad Sci U S A* **102,** 12595-12600.

Beene DL, Brandt GS, Zhong W, Zacharias NM, Lester HA & Dougherty DA. (2002). Cation-pi interactions in ligand recognition by serotonergic (5-HT3A) and nicotinic acetylcholine receptors: the anomalous binding properties of nicotine. *Biochemistry* **41,** 10262-10269.

Beene DL, Price KL, Lester HA, Dougherty DA & Lummis SC. (2004). Tyrosine residues that control binding and gating in the 5-hydroxytryptamine3 receptor revealed by unnatural amino acid mutagenesis. *J Neurosci* **24,** 9097-9104.

Belelli D, Balcarek JM, Hope AG, Peters JA, Lambert JJ & Blackburn TP. (1995). Cloning and functional expression of a human 5-hydroxytryptamine type 3AS receptor subunit. *Mol Pharmacol* **48,** 1054-1062.

Bera AK, Chatav M & Akabas MH. (2002). GABA(A) receptor M2-M3 loop secondary structure and changes in accessibility during channel gating. *J Biol Chem* **277,** 43002-43010.

Bertaccini EJ, Shapiro J, Brutlag DL & Trudell JR. (2005). Homology modeling of a human glycine alpha 1 receptor reveals a plausible anesthetic binding site. *J Chem Inf Model* **45,** 128-135.

Blandina P, Goldfarb J, Craddock-Royal B & Green JP. (1989). Release of endogenous dopamine by stimulation of 5-hydroxytryptamine3 receptors in rat striatum. *J Pharmacol Exp Ther* **251,** 803-809.

Blanton MP, McCardy EA, Fryer JD, Liu M & Lukas RJ. (2000). 5-hydroxytryptamine interaction with the nicotinic acetylcholine receptor. *Eur J Pharmacol* **389,** 155-163.

Blier P & Bouchard C. (1993). Functional characterization of a 5-HT3 receptor which modulates the release of 5-HT in the guinea-pig brain. *Br J Pharmacol* **108,** 13-22.

Blower P. (1995). A pharmacologic profile of oral granisetron (Kytril tablets). *Semin Oncol* **22,** 3-5.

Blundell JE. (1984). Serotonin and appetite. *Neuropharmacology* **23,** 1537-1551.

Boess FG, Beroukhim R & Martin IL. (1995). Ultrastructure of the 5-hydroxytryptamine3 receptor. *J Neurochem* **64,** 1401-1405.

Boess FG, Lummis SC & Martin IL. (1992). Molecular properties of 5-hydroxytryptamine3 receptor-type binding sites purified from NG108-15 cells. *J Neurochem* **59,** 1692-1701.

Boess FG & Martin IL. (1992). Purification and characterization of 5-HT3 receptors from NG108-15 neuroblastoma x glioma cells. *Biochem Soc Trans* **20,** 217S.

Boess FG, Steward LJ, Steele JA, Liu D, Reid J, Glencorse TA & Martin IL. (1997). Analysis

of the ligand binding site of the 5-HT3 receptor using site directed mutagenesis: importance of glutamate 106. *Neuropharmacology* **36,** 637-647.

Boileau AJ, Evers AR, Davis AF & Czajkowski C. (1999). Mapping the Agonist Binding Site of the GABAA Receptor: Evidence for a beta -Strand. *J Neurosci* **19,** 4847-4854.

Bork P, Holm L & Sander C. (1994). The immunoglobulin fold. Structural classification, sequence patterns and common core. *J Mol Biol* **242,** 309-320.

Bountra C, Gale JD, Gardner CJ, Jordan CC, Kilpatrick GJ, Twissell DJ & Ward P. (1996). Towards understanding the aetiology and pathophysiology of the emetic reflex: novel approaches to antiemetic drugs. *Oncology* **53 Suppl 1,** 102-109.

Bourne Y, Talley TT, Hansen SB, Taylor P & Marchot P. (2005). Crystal structure of a Cbtx-AChBP complex reveals essential interactions between snake alpha-neurotoxins and nicotinic receptors. *Embo J* **24,** 1512-1522.

Bouzat C, Gumilar F, Spitzmaul G, Wang HL, Rayes D, Hansen SB, Taylor P & Sine SM. (2004). Coupling of agonist binding to channel gating in an ACh-binding protein linked to an ion channel. *Nature* **430,** 896-900.

Boyd GW, Doward AI, Kirkness EF, Millar NS & Connolly CN. (2003). Cell surface expression of 5-hydroxytryptamine type 3 receptors is controlled by an endoplasmic reticulum retention signal. *J Biol Chem* **278,** 27681-27687.

Boyd GW, Low P, Dunlop JI, Robertson LA, Vardy A, Lambert JJ, Peters JA & Connolly CN. (2002). Assembly and cell surface expression of homomeric and heteromeric 5-HT3 receptors: the role of oligomerization and chaperone proteins. *Mol Cell Neurosci* **21,** 38-50.

Brady CA, Dover TJ, Massoura AN, Princivalle AP, Hope AG & Barnes NM. (2007). Identification of 5-HT3A and 5-HT3B receptor subunits in human hippocampus. *Neuropharmacology* **52,** 1284-1290.

Brady CA, Stanford IM, Ali I, Lin L, Williams JM, Dubin AE, Hope AG & Barnes NM. (2001). Pharmacological comparison of human homomeric 5-HT3A receptors versus heteromeric 5-HT3A/3B receptors. *Neuropharmacology* **41,** 282-284.

Brejc K, van Dijk WJ, Klaassen RV, Schuurmans M, van Der Oost J, Smit AB & Sixma TK. (2001). Crystal structure of an ACh-binding protein reveals the ligand-binding domain of nicotinic receptors. *Nature* **411,** 269-276.

Brisson A & Unwin PN. (1985). Quaternary structure of the acetylcholine receptor. *Nature* **315,** 474-477.

Brown AM, Hope AG, Lambert JJ & Peters JA. (1998). Ion permeation and conduction in a human recombinant 5-HT3 receptor subunit (h5-HT3A). *J Physiol* **507 (Pt 3),** 653-665.

Bruns RF, Lawson-Wendling K & Pugsley TA. (1983). A rapid filtration assay for soluble

receptors using polyethylenimine-treated filters. *Anal Biochem* **132,** 74-81.

Bruss M, Barann M, Hayer-Zillgen M, Eucker T, Gothert M & Bonisch H. (2000). Modified 5-HT3A receptor function by co-expression of alternatively spliced human 5-HT3A receptor isoforms. *Naunyn Schmiedebergs Arch Pharmacol* **362,** 392-401.

Bruss M, Gothert M, Hayer M & Bonisch H. (1998). Molecular cloning of alternatively spliced human 5-HT3 receptor cDNAs. *Ann N Y Acad Sci* **861,** 234-235.

Bufton KE, Steward LJ, Barber PC & Barnes NM. (1993). Distribution and characterization of the [3H]granisetron-labelled 5-HT3 receptor in the human forebrain. *Neuropharmacology* **32,** 1325-1331.

Butler A, Elswood CJ, Burridge J, Ireland SJ, Bunce KT, Kilpatrick GJ & Tyers MB. (1990). The pharmacological characterization of 5-HT3 receptors in three isolated preparations derived from guinea-pig tissues. *Br J Pharmacol* **101,** 591-598.

Camilleri, Mayer, Drossman, Heath, Dukes, Mcsorley, Kong, Mangel & Northcutt. (1999). Improvement in pain and bowel function in female irritable bowel patients with alosetron, a 5-HT3 receptor antagonist
doi:10.1046/j.1365-2036.1999.00610.x. *Alimentary Pharmacology & Therapeutics* **13,** 1149-1159.

Campobasso F. (1972). The irritable bowel syndrome. *J Am Osteopath Assoc* **71,** 1002-1005.

Campos-Caro A, Sala S, Ballesta JJ, Vicente-Agullo F, Criado M & Sala F. (1996). A single residue in the M2-M3 loop is a major determinant of coupling between binding and gating in neuronal nicotinic receptors. *Proc Natl Acad Sci U S A* **93,** 6118-6123.

Carboni E, Acquas E, Frau R & Di Chiara G. (1989). Differential inhibitory effects of a 5-HT3 antagonist on drug-induced stimulation of dopamine release. *Eur J Pharmacol* **164,** 515-519.

Celie PH, Kasheverov IE, Mordvintsev DY, Hogg RC, van Nierop P, van Elk R, van Rossum-Fikkert SE, Zhmak MN, Bertrand D, Tsetlin V, Sixma TK & Smit AB. (2005). Crystal structure of nicotinic acetylcholine receptor homolog AChBP in complex with an alpha-conotoxin PnIA variant. *Nat Struct Mol Biol* **12,** 582-588.

Celie PH, Klaassen RV, van Rossum-Fikkert SE, van Elk R, van Nierop P, Smit AB & Sixma TK. (2005). Crystal structure of acetylcholine-binding protein from Bulinus truncatus reveals the conserved structural scaffold and sites of variation in nicotinic acetylcholine receptors. *J Biol Chem* **280,** 26457-26466.

Celie PH, van Rossum-Fikkert SE, van Dijk WJ, Brejc K, Smit AB & Sixma TK. (2004). Nicotine and carbamylcholine binding to nicotinic acetylcholine receptors as studied in AChBP crystal structures. *Neuron* **41,** 907-914.

Chakrapani S, Bailey TD & Auerbach A. (2003). The role of loop 5 in acetylcholine receptor channel gating. *J Gen Physiol* **122,** 521-539.

Chakrapani S, Bailey TD & Auerbach A. (2004). Gating dynamics of the acetylcholine receptor extracellular domain. *J Gen Physiol* **123,** 341-356.

Champaneria S, Costall B, Naylor RJ & Robertson DW. (1992). Identification and distribution of 5-HT3 recognition sites in the rat gastrointestinal tract. *Br J Pharmacol* **106,** 693-696.

Chang L, Chey WD, Harris L, Olden K, Surawicz C & Schoenfeld P. (2006). Incidence of ischemic colitis and serious complications of constipation among patients using alosetron: systematic review of clinical trials and post-marketing surveillance data. *Am J Gastroenterol* **101,** 1069-1079.

Changeux JP, Galzi JL, Devillers-Thiery A & Bertrand D. (1992). The functional architecture of the acetylcholine nicotinic receptor explored by affinity labelling and site-directed mutagenesis. *Q Rev Biophys* **25,** 395-432.

Chen C & Okayama H. (1987). High-efficiency transformation of mammalian cells by plasmid DNA. *Mol Cell Biol* **7,** 2745-2752.

Chen JP, van Praag HM & Gardner EL. (1991). Activation of 5-HT3 receptor by 1-phenylbiguanide increases dopamine release in the rat nucleus accumbens. *Brain Res* **543,** 354-357.

Cheng A, McDonald NA & Connolly CN. (2005). Cell surface expression of 5-hydroxytryptamine type 3 receptors is promoted by RIC-3. *J Biol Chem* **280,** 22502-22507.

Cheng MH, Cascio M & Coalson RD. (2007). Homology modeling and molecular dynamics simulations of the alpha1 glycine receptor reveals different states of the channel. *Proteins* **68,** 581-593.

Cheng X, Lu B, Grant B, Law RJ & McCammon JA. (2006). Channel opening motion of alpha7 nicotinic acetylcholine receptor as suggested by normal mode analysis. *J Mol Biol* **355,** 310-324.

Cheng X, Wang H, Grant B, Sine SM & McCammon JA. (2006). Targeted molecular dynamics study of C-loop closure and channel gating in nicotinic receptors. *PLoS Comput Biol* **2,** e134.

Chiara DC & Cohen JB. (1997). Identification of amino acids contributing to high and low affinity d-tubocurarine sites in the Torpedo nicotinic acetylcholine receptor. *J Biol Chem* **272,** 32940-32950.

Chiara DC, Middleton RE & Cohen JB. (1998). Identification of tryptophan 55 as the primary site of [3H]nicotine photoincorporation in the [gamma]-subunit of the Torpedo nicotinic acetylcholine receptor. *FEBS Letters* **423,** 223-226.

Chiara DC, Xie Y & Cohen JB. (1999). Structure of the agonist-binding sites of the Torpedo nicotinic acetylcholine receptor: affinity-labeling and mutational analyses identify gamma Tyr-111/delta Arg-113 as antagonist affinity determinants. *Biochemistry* **38,**

6689-6698.

Clayton NM, Sargent R, Butler A, Gale J, Maxwell MP, Hunt AA, Barrett VJ, Cambridge D, Bountra C & Humphrey PP. (1999). The pharmacological properties of the novel selective 5-HT3 receptor antagonist, alosetron, and its effects on normal and perturbed small intestinal transit in the fasted rat. *Neurogastroenterol Motil* **11,** 207-217.

Colquhoun D. (1998). Binding, gating, affinity and efficacy: the interpretation of structure-activity relationships for agonists and of the effects of mutating receptors. *Br J Pharmacol* **125,** 924-947.

Connolly CN, Krishek BJ, McDonald BJ, Smart TG & Moss SJ. (1996). Assembly and cell surface expression of heteromeric and homomeric gamma-aminobutyric acid type A receptors. *J Biol Chem* **271,** 89-96.

Consolo S, Bertorelli R, Russi G, Zambelli M & Ladinsky H. (1994). Serotonergic facilitation of acetylcholine release in vivo from rat dorsal hippocampus via serotonin 5-HT3 receptors. *J Neurochem* **62,** 2254-2261.

Corringer PJ, Le Novere N & Changeux JP. (2000). Nicotinic receptors at the amino acid level. *Annu Rev Pharmacol Toxicol* **40,** 431-458.

Costall B, Domeney AM, Kelly ME, Tomkins DM, Naylor RJ, Wong EH, Smith WL, Whiting RL & Eglen RM. (1993). The effect of the 5-HT3 receptor antagonist, RS-42358-197, in animal models of anxiety. *Eur J Pharmacol* **234,** 91-99.

Costall B & Naylor RJ. (2004). 5-HT3 receptors. *Curr Drug Targets CNS Neurol Disord* **3,** 27-37.

Cromer BA, Morton CJ & Parker MW. (2002). Anxiety over GABA(A) receptor structure relieved by AChBP. *Trends Biochem Sci* **27,** 280-287.

Damle VN & Karlin A. (1980). Effects of agonists and antagonists on the reactivity of the binding site disulfide in acetylcholine receptor from Torpedo californica. *Biochemistry* **19,** 3924-3932.

Dando TM & Perry CM. (2004). Aprepitant: a review of its use in the prevention of chemotherapy-induced nausea and vomiting. *Drugs* **64,** 777-794.

Das P, Bell-Horner CL, Machu TK & Dillon GH. (2003). The GABA(A) receptor antagonist picrotoxin inhibits 5-hydroxytryptamine type 3A receptors. *Neuropharmacology* **44,** 431-438.

Das P & Dillon GH. (2003). The 5-HT3B subunit confers reduced sensitivity to picrotoxin when co-expressed with the 5-HT3A receptor. *Brain Res Mol Brain Res* **119,** 207-212.

Das P & Dillon GH. (2005). Molecular determinants of picrotoxin inhibition of 5-hydroxytryptamine type 3 receptors. *J Pharmacol Exp Ther* **314,** 320-328.

Davies M, Newell JG & Dunn SM. (2001). Mutagenesis of the GABA(A) receptor alpha1

subunit reveals a domain that affects sensitivity to GABA and benzodiazepine-site ligands. *J Neurochem* **79,** 55-62.

Davies PA, Pistis M, Hanna MC, Peters JA, Lambert JJ, Hales TG & Kirkness EF. (1999). The 5-HT3B subunit is a major determinant of serotonin-receptor function. *Nature* **397,** 359-363.

De Deurwaerdere P, Stinus L & Spampinato U. (1998). Opposite change of in vivo dopamine release in the rat nucleus accumbens and striatum that follows electrical stimulation of dorsal raphe nucleus: role of 5-HT3 receptors. *J Neurosci* **18,** 6528-6538.

De Ponti F & Tonini M. (2001). Irritable bowel syndrome: new agents targeting serotonin receptor subtypes. *Drugs* **61,** 317-332.

Deane CM & Lummis SC. (2001). The role and predicted propensity of conserved proline residues in the 5-HT3 receptor. *J Biol Chem* **276,** 37962-37966.

Derkach V, Surprenant A & North RA. (1989). 5-HT3 receptors are membrane ion channels. *Nature* **339,** 706-709.

Domeney AM, Costall B, Gerrard PA, Jones DN, Naylor RJ & Tyers MB. (1991). The effect of ondansetron on cognitive performance in the marmoset. *Pharmacol Biochem Behav* **38,** 169-175.

Dorostkar MM & Boehm S. (2007). Opposite effects of presynaptic 5-HT3 receptor activation on spontaneous and action potential-evoked GABA release at hippocampal synapses. *J Neurochem* **100,** 395-405.

Dougherty DA. (1996). Cation-pi interactions in chemistry and biology: a new view of benzene, Phe, Tyr, and Trp. *Science* **271,** 163-168.

Downie DL, Hope AG, Belelli D, Lambert JJ, Peters JA, Bentley KR, Steward LJ, Chen CY & Barnes NM. (1995). The interaction of trichloroethanol with murine recombinant 5-HT3 receptors. *Br J Pharmacol* **114,** 1641-1651.

Dubin AE, Huvar R, D'Andrea MR, Pyati J, Zhu JY, Joy KC, Wilson SJ, Galindo JE, Glass CA, Luo L, Jackson MR, Lovenberg TW & Erlander MG. (1999). The pharmacological and functional characteristics of the serotonin 5-HT(3A) receptor are specifically modified by a 5-HT(3B) receptor subunit. *J Biol Chem* **274,** 30799-30810.

Edmonds CJ. (1970). Electrical potentials of the sigmoid colon and rectum in irritable bowel syndrome and ulcerative colitis. *Gut* **11,** 867-874.

Eisele JL, Bertrand S, Galzi JL, Devillers-Thiery A, Changeux JP & Bertrand D. (1993). Chimaeric nicotinic-serotonergic receptor combines distinct ligand binding and channel specificities. *Nature* **366,** 479-483.

Eisenberg P, Figueroa-Vadillo J, Zamora R, Charu V, Hajdenberg J, Cartmell A, Macciocchi A & Grunberg S. (2003). Improved prevention of moderately emetogenic chemotherapy-induced nausea and vomiting with palonosetron, a pharmacologically

novel 5-HT3 receptor antagonist: results of a phase III, single-dose trial versus dolasetron. *Cancer* **98,** 2473-2482.

Emerit MB, Martres MP, Miquel MC, el Mestikawy S & Hamon M. (1995). Differentiation alters the expression of the two splice variants of the serotonin 5-HT3 receptor-A mRNA in NG108-15 cells. *J Neurochem* **65,** 1917-1925.

Ferezou I, Cauli B, Hill EL, Rossier J, Hamel E & Lambolez B. (2002). 5-HT3 receptors mediate serotonergic fast synaptic excitation of neocortical vasoactive intestinal peptide/cholecystokinin interneurons. *J Neurosci* **22,** 7389-7397.

Fletcher S & Barnes NM. (1997). Purification of 5-hydroxytryptamine3 receptors from porcine brain. *Br J Pharmacol* **122,** 655-662.

Fuller RW & Clemens JA. (1981). Role of serotonin in the hypothalamic regulation of pituitary function. *Adv Exp Med Biol* **133,** 431-444.

Gallo-Torres H, Brinker A & Avigan M. (2006). Alosetron: ischemic colitis and serious complications of constipation. *Am J Gastroenterol* **101,** 1080-1083.

Gan TJ, Meyer T, Apfel CC, Chung F, Davis PJ, Eubanks S, Kovac A, Philip BK, Sessler DI, Temo J, Tramer MR & Watcha M. (2003). Consensus guidelines for managing postoperative nausea and vomiting. *Anesth Analg* **97,** 62-71, table of contents.

Gao F, Bren N, Burghardt TP, Hansen S, Henchman RH, Taylor P, McCammon JA & Sine SM. (2005). Agonist-mediated conformational changes in acetylcholine-binding protein revealed by simulation and intrinsic tryptophan fluorescence. *J Biol Chem* **280,** 8443-8451.

Gay EA, Bienstock RJ, Lamb PW & Yakel JL. (2007). Structural determinates for apolipoprotein E-derived peptide interaction with the alpha7 nicotinic acetylcholine receptor. *Mol Pharmacol* **72,** 838-849.

Gebauer A, Merger M & Kilbinger H. (1993). Modulation by 5-HT3 and 5-HT4 receptors of the release of 5-hydroxytryptamine from the guinea-pig small intestine. *Naunyn Schmiedebergs Arch Pharmacol* **347,** 137-140.

Gershon MD. (1999). Review article: roles played by 5-hydroxytryptamine in the physiology of the bowel. *Aliment Pharmacol Ther* **13 Suppl 2,** 15-30.

Glaum SR, Brooks PA, Spyer KM & Miller RJ. (1992). 5-Hydroxytryptamine-3 receptors modulate synaptic activity in the rat nucleus tractus solitarius in vitro. *Brain Res* **589,** 62-68.

Goldsby RA, Kindt TJ, Osborne BA & Kuby J. (2003). *Immunology*. W.H. Freeman, New York.

Gordon JC, Sarbin NS, Barefoot DS & Pinkus LM. (1990). Solubilization of a 5-HT3 binding site from rabbit small bowel muscularis membranes. *Eur J Pharmacol* **188,** 313-319.

Gralla R, Lichinitser M, Van Der Vegt S, Sleeboom H, Mezger J, Peschel C, Tonini G, Labianca R, Macciocchi A & Aapro M. (2003). Palonosetron improves prevention of chemotherapy-induced nausea and vomiting following moderately emetogenic chemotherapy: results of a double-blind randomized phase III trial comparing single doses of palonosetron with ondansetron. *Ann Oncol* **14,** 1570-1577.

Grosman C, Zhou M & Auerbach A. (2000). Mapping the conformational wave of acetylcholine receptor channel gating. *Nature* **403,** 773-776.

Grutter T, Prado de Carvalho L, Le Novere N, Corringer PJ, Edelstein S & Changeux JP. (2003). An H-bond between two residues from different loops of the acetylcholine binding site contributes to the activation mechanism of nicotinic receptors. *Embo J* **22,** 1990-2003.

Gurley DA & Lanthorn TH. (1998). Nicotinic agonists competitively antagonize serotonin at mouse 5-HT3 receptors expressed in Xenopus oocytes. *Neurosci Lett* **247,** 107-110.

Habib AS & Gan TJ. (2003). Pharmacotherapy of postoperative nausea and vomiting. *Expert Opin Pharmacother* **4,** 457-473.

Hall TA. (1999). BioEdit: a user-friendly biological sequence alignment editor and analysis program for Windows 95/98/NT. In *Nucleic Acids Symposium Series*, pp. 95-98.

Hanna MC, Davies PA, Hales TG & Kirkness EF. (2000). Evidence for expression of heteromeric serotonin 5-HT(3) receptors in rodents. *J Neurochem* **75,** 240-247.

Hansen MB. (2003). Neurohumoral control of gastrointestinal motility. *Physiol Res* **52,** 1-30.

Hansen MB & Jaffe BM. (1994). 5-HT receptor subtypes involved in luminal serotonin-induced secretion in rat intestine in vivo. *J Surg Res* **56,** 277-287.

Hansen SB, Radic Z, Talley TT, Molles BE, Deerinck T, Tsigelny I & Taylor P. (2002). Tryptophan fluorescence reveals conformational changes in the acetylcholine binding protein. *J Biol Chem* **277,** 41299-41302.

Hansen SB, Sulzenbacher G, Huxford T, Marchot P, Taylor P & Bourne Y. (2005). Structures of Aplysia AChBP complexes with nicotinic agonists and antagonists reveal distinctive binding interfaces and conformations. *Embo J* **24,** 3635-3646.

Hapfelmeier G, Tredt C, Haseneder R, Zieglgansberger W, Eisensamer B, Rupprecht R & Rammes G. (2003). Co-expression of the 5-HT3B serotonin receptor subunit alters the biophysics of the 5-HT3 receptor. *Biophys J* **84,** 1720-1733.

Hargreaves AC, Lummis SC & Taylor CW. (1994). Ca2+ permeability of cloned and native 5-hydroxytryptamine type 3 receptors. *Mol Pharmacol* **46,** 1120-1128.

Hawthorne R & Lynch JW. (2005). A picrotoxin-specific conformational change in the glycine receptor M2-M3 loop. *J Biol Chem* **280,** 35836-35843.

Hayrapetyan V, Jenschke M, Dillon GH & Machu TK. (2005). Co-expression of the 5-

HT(3B) subunit with the 5-HT(3A) receptor reduces alcohol sensitivity. *Brain Res Mol Brain Res* **142,** 146-150.

Henchman RH, Wang HL, Sine SM, Taylor P & McCammon JA. (2005). Ligand-induced conformational change in the alpha7 nicotinic receptor ligand binding domain. *Biophys J* **88,** 2564-2576.

Herrstedt J. (2004). Risk-benefit of antiemetics in prevention and treatment of chemotherapy-induced nausea and vomiting. *Expert Opin Drug Saf* **3,** 231-248.

Hesketh PJ. (2004). New treatment options for chemotherapy-induced nausea and vomiting. *Support Care Cancer* **12,** 550-554.

Hickok JT, Roscoe JA, Morrow GR, Bole CW, Zhao H, Hoelzer KL, Dakhil SR, Moore T & Fitch TR. (2005). 5-Hydroxytryptamine-receptor antagonists versus prochlorperazine for control of delayed nausea caused by doxorubicin: a URCC CCOP randomised controlled trial. *Lancet Oncol* **6,** 765-772.

Hjelmeland LM & Chrambach A. (1984). Solubilization of functional membrane proteins. *Methods Enzymol* **104,** 305-318.

Hope AG, Belelli D, Mair ID, Lambert JJ & Peters JA. (1999). Molecular determinants of (+)-tubocurarine binding at recombinant 5-hydroxytryptamine3A receptor subunits. *Mol Pharmacol* **55,** 1037-1043.

Hope AG, Downie DL, Sutherland L, Lambert JJ, Peters JA & Burchell B. (1993). Cloning and functional expression of an apparent splice variant of the murine 5-HT3 receptor A subunit. *Eur J Pharmacol* **245,** 187-192.

Houghton LA, Foster JM & Whorwell PJ. (2000). Alosetron, a 5-HT3 receptor antagonist, delays colonic transit in patients with irritable bowel syndrome and healthy volunteers. *Aliment Pharmacol Ther* **14,** 775-782.

Hoyer D, Hannon JP & Martin GR. (2002). Molecular, pharmacological and functional diversity of 5-HT receptors. *Pharmacol Biochem Behav* **71,** 533-554.

Hoyer D & Martin G. (1997). 5-HT receptor classification and nomenclature: towards a harmonization with the human genome. *Neuropharmacology* **36,** 419-428.

Humphrey PP, Bountra C, Clayton N & Kozlowski K. (1999). Review article: the therapeutic potential of 5-HT3 receptor antagonists in the treatment of irritable bowel syndrome. *Aliment Pharmacol Ther* **13 Suppl 2,** 31-38.

Hussy N, Lukas W & Jones KA. (1994). Functional properties of a cloned 5-hydroxytryptamine ionotropic receptor subunit: comparison with native mouse receptors. *J Physiol* **481 (Pt 2),** 311-323.

Isenberg KE, Ukhun IA, Holstad SG, Jafri S, Uchida U, Zorumski CF & Yang J. (1993). Partial cDNA cloning and NGF regulation of a rat 5-HT3 receptor subunit. *Neuroreport* **5,** 121-124.

Jensen TN, Nielsen J, Frederiksen K & Ebert B. (2006). Molecular cloning and pharmacological characterization of serotonin 5-HT(3A) receptor subtype in dog. *Eur J Pharmacol* **538,** 23-31.

Johnson DS & Heinemann SF. (1995). Detection of 5-HT3R-A, a 5-HT3 receptor subunit, in submucosal and myenteric ganglia of rat small intestine using in situ hybridization. *Neurosci Lett* **184,** 67-70.

Johnson PJ, Bornstein JC, Furness JB, Woollard DJ & Orrman-Rossiter SL. (1994). Characterization of 5-hydroxytryptamine receptors mediating mucosal secretion in guinea-pig ileum. *Br J Pharmacol* **111,** 1240-1244.

Jones BJ & Blackburn TP. (2002). The medical benefit of 5-HT research. *Pharmacol Biochem Behav* **71,** 555-568.

Jones DN, Barnes NM, Costall B, Domeney AM, Kilpatrick GJ, Naylor RJ & Tyers MB. (1992). The distribution of 5-HT3 recognition sites in the marmoset brain. *Eur J Pharmacol* **215,** 63-67.

Jones G, Willett P & Glen RC. (1995). Molecular recognition of receptor sites using a genetic algorithm with a description of desolvation. *J Mol Biol* **245,** 43-53.

Joshi PR, Suryanarayanan A, Hazai E, Schulte MK, Maksay G & Bikadi Z. (2006). Interactions of granisetron with an agonist-free 5-HT3A receptor model. *Biochemistry* **45,** 1099-1105.

Kadowaki M, Wade PR & Gershon MD. (1996). Participation of 5-HT3, 5-HT4, and nicotinic receptors in the peristaltic reflex of guinea pig distal colon. *Am J Physiol* **271,** G849-857.

Kapur A, Davies M, Dryden WF & Dunn SM. (2006). Activation of the Torpedo nicotinic acetylcholine receptor. The contribution of residues alphaArg55 and gammaGlu93. *Febs J* **273,** 960-970.

Karlin A. (2002). Emerging structure of the nicotinic acetylcholine receptors. *Nat Rev Neurosci* **3,** 102-114.

Karlin A & Akabas MH. (1995). Toward a structural basis for the function of nicotinic acetylcholine receptors and their cousins. *Neuron* **15,** 1231-1244.

Karlin A, Holtzman E, Yodh N, Lobel P, Wall J & Hainfeld J. (1983). The arrangement of the subunits of the acetylcholine receptor of Torpedo californica. *J Biol Chem* **258,** 6678-6681.

Karnovsky AM, Gotow LF, McKinley DD, Piechan JL, Ruble CL, Mills CJ, Schellin KA, Slightom JL, Fitzgerald LR, Benjamin CW & Roberds SL. (2003). A cluster of novel serotonin receptor 3-like genes on human chromosome 3. *Gene* **319,** 137-148.

Kash TL, Jenkins A, Kelley JC, Trudell JR & Harrison NL. (2003). Coupling of agonist

binding to channel gating in the GABA(A) receptor. *Nature* **421,** 272-275.

Katsurabayashi S, Kubota H, Tokutomi N & Akaike N. (2003). A distinct distribution of functional presynaptic 5-HT receptor subtypes on GABAergic nerve terminals projecting to single hippocampal CA1 pyramidal neurons. *Neuropharmacology* **44,** 1022-1030.

Kawa K. (1994). Distribution and functional properties of 5-HT3 receptors in the rat hippocampal dentate gyrus: a patch-clamp study. *J Neurophysiol* **71,** 1935-1947.

Kelley SP, Dunlop JI, Kirkness EF, Lambert JJ & Peters JA. (2003). A cytoplasmic region determines single-channel conductance in 5-HT3 receptors. *Nature* **424,** 321-324.

Kilpatrick GJ, Jones BJ & Tyers MB. (1987). Identification and distribution of 5-HT3 receptors in rat brain using radioligand binding. *Nature* **330,** 746-748.

Kilpatrick GJ, Jones BJ & Tyers MB. (1988). The distribution of specific binding of the 5-HT3 receptor ligand [3H]GR65630 in rat brain using quantitative autoradiography. *Neurosci Lett* **94,** 156-160.

Kilpatrick GJ, Jones BJ & Tyers MB. (1989). Binding of the 5-HT3 ligand, [3H]GR65630, to rat area postrema, vagus nerve and the brains of several species. *Eur J Pharmacol* **159,** 157-164.

Laemmli UK. (1970). Cleavage of structural proteins during the assembly of the head of bacteriophage T4. *Nature* **227,** 680-685.

Lambert JJ, Peters JA, Hales TG & Dempster J. (1989). The properties of 5-HT3 receptors in clonal cell lines studied by patch-clamp techniques. *Br J Pharmacol* **97,** 27-40.

Lankiewicz S, Lobitz N, Wetzel CH, Rupprecht R, Gisselmann G & Hatt H. (1998). Molecular cloning, functional expression, and pharmacological characterization of 5-hydroxytryptamine3 receptor cDNA and its splice variants from guinea pig. *Mol Pharmacol* **53,** 202-212.

Laporte AM, Koscielniak T, Ponchant M, Verge D, Hamon M & Gozlan H. (1992). Quantitative autoradiographic mapping of 5-HT3 receptors in the rat CNS using [125I]iodo-zacopride and [3H]zacopride as radioligands. *Synapse* **10,** 271-281.

Laube B, Maksay G, Schemm R & Betz H. (2002). Modulation of glycine receptor function: a novel approach for therapeutic intervention at inhibitory synapses? *Trends Pharmacol Sci* **23,** 519-527.

Law RJ, Henchman RH & McCammon JA. (2005). A gating mechanism proposed from a simulation of a human alpha7 nicotinic acetylcholine receptor. *Proc Natl Acad Sci U S A* **102,** 6813-6818.

Le Novere N, Corringer PJ & Changeux JP. (1999). Improved secondary structure predictions for a nicotinic receptor subunit: incorporation of solvent accessibility and experimental data into a two-dimensional representation. *Biophys J* **76,** 2329-2345.

Le Novere N, Grutter T & Changeux JP. (2002). Models of the extracellular domain of the nicotinic receptors and of agonist- and Ca2+-binding sites. *Proc Natl Acad Sci U S A* **99,** 3210-3215.

Leslie RA, Reynolds DJ, Andrews PL, Grahame-Smith DG, Davis CJ & Harvey JM. (1990). Evidence for presynaptic 5-hydroxytryptamine3 recognition sites on vagal afferent terminals in the brainstem of the ferret. *Neuroscience* **38,** 667-673.

Lester HA, Dibas MI, Dahan DS, Leite JF & Dougherty DA. (2004). Cys-loop receptors: new twists and turns. *Trends Neurosci* **27,** 329-336.

Lindley KJ & Andrews PL. (2005). Pathogenesis and treatment of cyclical vomiting. *J Pediatr Gastroenterol Nutr* **41 Suppl 1,** S38-40.

Lloyd EJ & Andrews PR. (1986). A common structural model for central nervous system drugs and their receptors. *J Med Chem* **29,** 453-462.

Lochner M & Lummis SCR. (2005). Structural and Functional Study of the Serotonin 5-$HT_{3A/B}$ Receptor Binding Site. *Proceedings of the British Pharmacological Society at http://wwwpA2onlineorg/abstracts/Vol3Issue2abst123Ppdf* **31**.

Lovinger DM. (1999). 5-HT3 receptors and the neural actions of alcohols: an increasingly exciting topic. *Neurochem Int* **35,** 125-130.

Lummis SC, Beene DL, Lee LW, Lester HA, Broadhurst RW & Dougherty DA. (2005). Cis-trans isomerization at a proline opens the pore of a neurotransmitter-gated ion channel. *Nature* **438,** 248-252.

Lummis SC, Kilpatrick GJ & Martin IL. (1990). Characterization of 5-HT3 receptors in intact N1E-115 neuroblastoma cells. *Eur J Pharmacol* **189,** 223-227.

Lynch JW, Rajendra S, Pierce KD, Handford CA, Barry PH & Schofield PR. (1997). Identification of intracellular and extracellular domains mediating signal transduction in the inhibitory glycine receptor chloride channel. *Embo J* **16,** 110-120.

Maksay G, Bikadi Z & Simonyi M. (2003). Binding interactions of antagonists with 5-hydroxytryptamine3A receptor models. *J Recept Signal Transduct Res* **23,** 255-270.

Maksay G, Simonyi M & Bikadi Z. (2004). Subunit rotation models activation of serotonin 5-HT3AB receptors by agonists. *J Comput Aided Mol Des* **18,** 651-664.

Malone HM, Peters JA & Lambert JJ. (1991). Physiological and pharmacological properties of 5-HT3 receptors--a patch clamp-study. *Neuropeptides* **19 Suppl,** 25-30.

Maniatis T, Fritsch E & Sambrook J. (1987). *Molecular Cloning A Laboratory Manual.*

Maricq AV, Peterson AS, Brake AJ, Myers RM & Julius D. (1991). Primary structure and functional expression of the 5HT3 receptor, a serotonin-gated ion channel. *Science* **254,** 432-437.

Martin M, Czajkowski C & Karlin A. (1996). The contributions of aspartyl residues in the acetylcholine receptor gamma and delta subunits to the binding of agonists and competitive antagonists. *J Biol Chem* **271,** 13497-13503.

Maura G, Andrioli GC, Cavazzani P & Raiteri M. (1992). 5-Hydroxytryptamine3 receptors sited on cholinergic axon terminals of human cerebral cortex mediate inhibition of acetylcholine release. *J Neurochem* **58,** 2334-2337.

McHardy G. (1971). Management of chronic constipation and "irritable bowel syndrome": a clinical test. *J La State Med Soc* **123,** 405-408.

McIntosh TK & Barfield RJ. (1984). Brain monoaminergic control of male reproductive behavior. I. Serotonin and the post-ejaculatory refractory period. *Behav Brain Res* **12,** 255-265.

McKernan RM, Gillard NP, Quirk K, Kneen CO, Stevenson GI, Swain CJ & Ragan CI. (1990). Purification of the 5-hydroxytryptamine 5-HT3 receptor from NCB20 cells. *J Biol Chem* **265,** 13572-13577.

McMahon LL & Kauer JA. (1997). Hippocampal interneurons are excited via serotonin-gated ion channels. *J Neurophysiol* **78,** 2493-2502.

Melis C, Chau PL, Price KL, Lummis SC & Molteni C. (2006). Exploring the binding of serotonin to the 5-HT3 receptor by density functional theory. *J Phys Chem B* **110,** 26313-26319.

Merahi N, Orer HS, Laporte AM, Gozlan H, Hamon M & Laguzzi R. (1992). Baroreceptor reflex inhibition induced by the stimulation of serotonin3 receptors in the nucleus tractus solitarius of the rat. *Neuroscience* **46,** 91-100.

Mihic SJ, Whiting PJ, Klein RL, Wafford KA & Harris RA. (1994). A single amino acid of the human gamma-aminobutyric acid type A receptor gamma 2 subunit determines benzodiazepine efficacy. *J Biol Chem* **269,** 32768-32773.

Minier F & Sigel E. (2004). Techniques: Use of concatenated subunits for the study of ligand-gated ion channels. *Trends Pharmacol Sci* **25,** 499-503.

Miquel MC, Emerit MB, Gingrich JA, Nosjean A, Hamon M & el Mestikawy S. (1995). Developmental changes in the differential expression of two serotonin 5-HT3 receptor splice variants in the rat. *J Neurochem* **65,** 475-483.

Miyake A, Mochizuki S, Takemoto Y & Akuzawa S. (1995). Molecular cloning of human 5-hydroxytryptamine3 receptor: heterogeneity in distribution and function among species. *Mol Pharmacol* **48,** 407-416.

Miyazawa A, Fujiyoshi Y, Stowell M & Unwin N. (1999). Nicotinic acetylcholine receptor at 4.6 A resolution: transverse tunnels in the channel wall. *J Mol Biol* **288,** 765-786.

Miyazawa A, Fujiyoshi Y & Unwin N. (2003). Structure and gating mechanism of the

acetylcholine receptor pore. *Nature* **423,** 949-955.

Monk SA, Desai K, Brady CA, Williams JM, Lin L, Princivalle A, Hope AG & Barnes NM. (2001). Generation of a selective 5-HT3B subunit-recognising polyclonal antibody; identification of immunoreactive cells in rat hippocampus. *Neuropharmacology* **41,** 1013-1016.

Monk SA, Williams JM, Hope AG & Barnes NM. (2004). Identification and importance of N-glycosylation of the human 5-hydroxytryptamine3A receptor subunit. *Biochem Pharmacol* **68,** 1787-1796.

Morales M, Battenberg E, de Lecea L & Bloom FE. (1996). The type 3 serotonin receptor is expressed in a subpopulation of GABAergic neurons in the rat neocortex and hippocampus. *Brain Res* **731,** 199-202.

Morales M, Battenberg E, de Lecea L, Sanna PP & Bloom FE. (1996). Cellular and subcellular immunolocalization of the type 3 serotonin receptor in the rat central nervous system. *Brain Res Mol Brain Res* **36,** 251-260.

Morales M, McCollum N & Kirkness EF. (2001). 5-HT(3)-receptor subunits A and B are co-expressed in neurons of the dorsal root ganglion. *J Comp Neurol* **438,** 163-172.

Morales M & Wang SD. (2002). Differential composition of 5-hydroxytryptamine3 receptors synthesized in the rat CNS and peripheral nervous system. *J Neurosci* **22,** 6732-6741.

Morrow GR, Hickok JT, Burish TG & Rosenthal SN. (1996). Frequency and clinical implications of delayed nausea and delayed emesis. *Am J Clin Oncol* **19,** 199-203.

Mu TW, Lester HA & Dougherty DA. (2003). Different binding orientations for the same agonist at homologous receptors: a lock and key or a simple wedge? *J Am Chem Soc* **125,** 6850-6851.

Navari RM. (2003). Pathogenesis-based treatment of chemotherapy-induced nausea and vomiting--two new agents. *J Support Oncol* **1,** 89-103.

Navari RM. (2004). Aprepitant: a neurokinin-1 receptor antagonist for the treatment of chemotherapy-induced nausea and vomiting. *Expert Rev Anticancer Ther* **4,** 715-724.

Neish CS, Martin IL, Davies M, Henderson RM & Edwardson JM. (2003). Atomic force microscopy of ionotropic receptors bearing subunit-specific tags provides a method for determining receptor architecture. *Nanotechnology* **14,** 864-872.

Neya T, Mizutani M & Yamasato T. (1993). Role of 5-HT3 receptors in peristaltic reflex elicited by stroking the mucosa in the canine jejunum. *J Physiol* **471,** 159-173.

Niesler B, Frank B, Kapeller J & Rappold GA. (2003). Cloning, physical mapping and expression analysis of the human 5-HT3 serotonin receptor-like genes HTR3C, HTR3D and HTR3E. *Gene* **310,** 101-111.

Niesler B, Walstab J, Combrink S, Moller D, Kapeller J, Rietdorf J, Bonisch H, Gothert M,

Rappold G & Bruss M. (2007). Characterization of the novel human serotonin receptor subunits 5-HT3C,5-HT3D, and 5-HT3E. *Mol Pharmacol* **72,** 8-17.

Nissink JW, Murray C, Hartshorn M, Verdonk ML, Cole JC & Taylor R. (2002). A new test set for validating predictions of protein-ligand interaction. *Proteins* **49,** 457-471.

Ohno K, Wang HL, Milone M, Bren N, Brengman JM, Nakano S, Quiram P, Pruitt JN, Sine SM & Engel AG. (1996). Congenital myasthenic syndrome caused by decreased agonist binding affinity due to a mutation in the acetylcholine receptor epsilon subunit. *Neuron* **17,** 157-170.

Padgett CL, Hanek AP, Lester HA, Dougherty DA & Lummis SC. (2007). Unnatural amino acid mutagenesis of the GABA(A) receptor binding site residues reveals a novel cation-pi interaction between GABA and beta 2Tyr97. *J Neurosci* **27,** 886-892.

Parker RM, Barnes JM, Ge J, Barber PC & Barnes NM. (1996). Autoradiographic distribution of [3H]-(S)-zacopride-labelled 5-HT3 receptors in human brain. *J Neurol Sci* **144,** 119-127.

Parker RM, Bentley KR & Barnes NM. (1996). Allosteric modulation of 5-HT3 receptors: focus on alcohols and anaesthetic agents. *Trends Pharmacol Sci* **17,** 95-99.

Paudice P & Raiteri M. (1991). Cholecystokinin release mediated by 5-HT3 receptors in rat cerebral cortex and nucleus accumbens. *Br J Pharmacol* **103,** 1790-1794.

Peters JA, Hales TG & Lambert JJ. (2005). Molecular determinants of single-channel conductance and ion selectivity in the Cys-loop family: insights from the 5-HT3 receptor. *Trends Pharmacol Sci* **26,** 587-594.

Peters JA, Kelley SP, Dunlop JI, Kirkness EF, Hales TG & Lambert JJ. (2004). The 5-hydroxytryptamine type 3 (5-HT3) receptor reveals a novel determinant of single-channel conductance. *Biochem Soc Trans* **32,** 547-552.

Peters JA, Malone HM & Lambert JJ. (1993). An electrophysiological investigation of the properties of 5-HT3 receptors of rabbit nodose ganglion neurones in culture. *Br J Pharmacol* **110,** 665-676.

Pinkus LM, Sarbin NS, Barefoot DS & Gordon JC. (1989). Association of [3H]zacopride with 5-HT3 binding sites. *Eur J Pharmacol* **168,** 355-362.

Pons S, Sallette J, Bourgeois JP, Taly A, Changeux JP & Devillers-Thiery A. (2004). Critical role of the C-terminal segment in the maturation and export to the cell surface of the homopentameric alpha 7-5HT3A receptor. *Eur J Neurosci* **20,** 2022-2030.

Portas CM, Bjorvatn B, Fagerland S, Gronli J, Mundal V, Sorensen E & Ursin R. (1998). On-line detection of extracellular levels of serotonin in dorsal raphe nucleus and frontal cortex over the sleep/wake cycle in the freely moving rat. *Neuroscience* **83,** 807-814.

Pratt GD, Bowery NG, Kilpatrick GJ, Leslie RA, Barnes NM, Naylor RJ, Jones BJ, Nelson DR, Palacids JM, Slater P & et al. (1990). Consensus meeting agrees distribution of 5-

HT3 receptors in mammalian hindbrain. *Trends Pharmacol Sci* **11,** 135-137.

Price KL & Lummis SC. (2004). The role of tyrosine residues in the extracellular domain of the 5-hydroxytryptamine3 receptor. *J Biol Chem* **279,** 23294-23301.

Purohit P & Auerbach A. (2007). Acetylcholine Receptor Gating: Movement in the {alpha}-Subunit Extracellular Domain. *J Gen Physiol* **130,** 569-579.

Quirk PL, Rao S, Roth BL & Siegel RE. (2004). Three putative N-glycosylation sites within the murine 5-HT3A receptor sequence affect plasma membrane targeting, ligand binding, and calcium influx in heterologous mammalian cells. *J Neurosci Res* **77,** 498-506.

Rapport MM, Green AA & Page IH. (1948). Serum Vasoconstrictor (Serotonin) .4. Isolation and Characterization. *Journal of Biological Chemistry* **176,** 1243-1251.

Reeves DC, Jansen M, Bali M, Lemster T & Akabas MH. (2005). A role for the beta 1-beta 2 loop in the gating of 5-HT3 receptors. *J Neurosci* **25,** 9358-9366.

Reeves DC & Lummis SC. (2006). Detection of human and rodent 5-HT3B receptor subunits by anti-peptide polyclonal antibodies. *BMC Neurosci* **7,** 27.

Reeves DC, Sayed MF, Chau PL, Price KL & Lummis SC. (2003). Prediction of 5-HT3 receptor agonist-binding residues using homology modeling. *Biophys J* **84,** 2338-2344.

Reynolds JA & Karlin A. (1978). Molecular weight in detergent solution of acetylcholine receptor from Torpedo californica. *Biochemistry* **17,** 2035-2038.

Rickert KW & Imperiali B. (1995). Analysis of the conserved glycosylation site in the nicotinic acetylcholine receptor: potential roles in complex assembly. *Chem Biol* **2,** 751-759.

Roberts MH. (1984). 5-Hydroxytryptamine and antinociception. *Neuropharmacology* **23,** 1529-1536.

Roberts RJ, Vincze T, Posfai J & Macelis D. (2007). REBASE--enzymes and genes for DNA restriction and modification. *Nucleic Acids Res* **35,** D269-270.

Ronde P & Nichols RA. (1997). 5-HT3 receptors induce rises in cytosolic and nuclear calcium in NG108-15 cells via calcium-induced calcium release. *Cell Calcium* **22,** 357-365.

Ronde P & Nichols RA. (1998). High calcium permeability of serotonin 5-HT3 receptors on presynaptic nerve terminals from rat striatum. *J Neurochem* **70,** 1094-1103.

Rovira JC, Ballesta JJ, Vicente-Agullo F, Campos-Caro A, Criado M, Sala F & Sala S. (1998). A residue in the middle of the M2-M3 loop of the beta4 subunit specifically affects gating of neuronal nicotinic receptors. *FEBS Lett* **433,** 89-92.

Rovira JC, Vicente-Agullo F, Campos-Caro A, Criado M, Sala F, Sala S & Ballesta JJ. (1999). Gating of alpha3beta4 neuronal nicotinic receptor can be controlled by the loop M2-M3 of both alpha3 and beta4 subunits. *Pflugers Arch* **439,** 86-92.

Rubenstein EB. (2004). Palonosetron: a unique 5-HT3 receptor antagonist indicated for the prevention of acute and delayed chemotherapy-induced nausea and vomiting. *Clin Adv Hematol Oncol* **2,** 284-289.

Sali A & Blundell TL. (1993). Comparative protein modelling by satisfaction of spatial restraints. *J Mol Biol* **234,** 779-815.

Saqi MA, Russell RB & Sternberg MJ. (1998). Misleading local sequence alignments: implications for comparative protein modelling. *Protein Eng* **11,** 627-630.

Sawynok J & Reid A. (1991). Noradrenergic and purinergic involvement in spinal antinociception by 5-hydroxytryptamine and 2-methyl-5-hydroxytryptamine. *Eur J Pharmacol* **204,** 301-309.

Schapira M, Abagyan R & Totrov M. (2002). Structural model of nicotinic acetylcholine receptor isotypes bound to acetylcholine and nicotine. *BMC Structural Biology* **2,** 1.

Schmidt AW & Peroutka SJ. (1989). Three-dimensional steric molecular modeling of the 5-hydroxytryptamine3 receptor pharmacophore. *Mol Pharmacol* **36,** 505-511.

Schneider SW, Larmer J, Henderson RM & Oberleithner H. (1998). Molecular weights of individual proteins correlate with molecular volumes measured by atomic force microscopy. *Pflugers Arch* **435,** 362-367.

Schnell FM. (2003). Chemotherapy-Induced Nausea and Vomiting: The Importance of Acute Antiemetic Control
10.1634/theoncologist.8-2-187. *Oncologist* **8,** 187-198.

Schreiter C, Hovius R, Costioli M, Pick H, Kellenberger S, Schild L & Vogel H. (2003). Characterization of the ligand-binding site of the serotonin 5-HT3 receptor: the role of glutamate residues 97, 224, AND 235. *J Biol Chem* **278,** 22709-22716.

Schworer H, Racke K & Kilbinger H. (1991). Cisplatin increases the release of 5-hydroxytryptamine (5-HT) from the isolated vascularly perfused small intestine of the guinea-pig: involvement of 5-HT3 receptors. *Naunyn Schmiedebergs Arch Pharmacol* **344,** 143-149.

Scott DB, Blanpied TA, Swanson GT, Zhang C & Ehlers MD. (2001). An NMDA receptor ER retention signal regulated by phosphorylation and alternative splicing. *J Neurosci* **21,** 3063-3072.

Seidel MF, Weinreich GF, Stratz T & Muller W. (2007). 5-HT3 receptor antagonists regulate autonomic cardiac dysfunction in primary fibromyalgia syndrome. *Rheumatol Int* **27,** 1025-1030.

Sellers EM, Higgins GA & Sobell MB. (1992). 5-HT and alcohol abuse. *Trends Pharmacol*

Sci **13,** 69-75.

Silman I & Karlin A. (1969). Acetylcholine receptor: covalent attachment of depolarizing groups at the active site. *Science* **164,** 1420-1421.

Sine S, Quiram P, Papanikolaou F, Kreienkamp H & Taylor P. (1994). Conserved tyrosines in the alpha subunit of the nicotinic acetylcholine receptor stabilize quaternary ammonium groups of agonists and curariform antagonists. *J Biol Chem* **269,** 8808-8816.

Sine SM & Engel AG. (2006). Recent advances in Cys-loop receptor structure and function. *Nature* **440,** 448-455.

Sine SM, Wang HL & Bren N. (2002). Lysine scanning mutagenesis delineates structural model of the nicotinic receptor ligand binding domain. *J Biol Chem* **277,** 29210-29223.

Sine SM, Wang HL & Gao F. (2004). Toward atomic-scale understanding of ligand recognition in the muscle nicotinic receptor. *Curr Med Chem* **11,** 559-567.

Smit AB, Syed NI, Schaap D, van Minnen J, Klumperman J, Kits KS, Lodder H, van der Schors RC, van Elk R, Sorgedrager B, Brejc K, Sixma TK & Geraerts WP. (2001). A glia-derived acetylcholine-binding protein that modulates synaptic transmission. *Nature* **411,** 261-268.

Smith G & Olsen R. (1994). Identification of a [3H]muscimol photoaffinity substrate in the bovine gamma-aminobutyric acidA receptor alpha subunit. *J Biol Chem* **269,** 20380-20387.

Smith MM, Schlesinger S, Lindstrom J & Merlie JP. (1986). The effects of inhibiting oligosaccharide trimming by 1-deoxynojirimycin on the nicotinic acetylcholine receptor. *J Biol Chem* **261,** 14825-14832.

Smith PK, Krohn RI, Hermanson GT, Mallia AK, Gartner FH, Provenzano MD, Fujimoto EK, Goeke NM, Olson BJ & Klenk DC. (1985). Measurement of protein using bicinchoninic acid. *Anal Biochem* **150,** 76-85.

Solt K, Stevens RJ, Davies PA & Raines DE. (2005). General anesthetic-induced channel gating enhancement of 5-hydroxytryptamine type 3 receptors depends on receptor subunit composition. *J Pharmacol Exp Ther* **315,** 771-776.

Soubrie P. (1986). [Serotonergic neurons and behavior]. *J Pharmacol* **17,** 107-112.

Spath M. (2002). Current experience with 5-HT3 receptor antagonists in fibromyalgia. *Rheum Dis Clin North Am* **28,** 319-328.

Speranskiy K, Cascio M & Kurnikova M. (2007). Homology modeling and molecular dynamics simulations of the glycine receptor ligand binding domain. *Proteins* **67,** 950-960.

Spier AD & Lummis SC. (2000). The role of tryptophan residues in the 5-Hydroxytryptamine(3) receptor ligand binding domain. *J Biol Chem* **275,** 5620-5625.

Spier AD, Wotherspoon G, Nayak SV, Nichols RA, Priestley JV & Lummis SC. (1999). Antibodies against the extracellular domain of the 5-HT3 receptor label both native and recombinant receptors. *Brain Res Mol Brain Res* **67,** 221-230.

Standley S, Roche KW, McCallum J, Sans N & Wenthold RJ. (2000). PDZ domain suppression of an ER retention signal in NMDA receptor NR1 splice variants. *Neuron* **28,** 887-898.

Staubli U & Xu FB. (1995). Effects of 5-HT3 receptor antagonism on hippocampal theta rhythm, memory, and LTP induction in the freely moving rat. *J Neurosci* **15,** 2445-2452.

Steward LJ, Boess FG, Steele JA, Liu D, Wong N & Martin IL. (2000). Importance of phenylalanine 107 in agonist recognition by the 5-hydroxytryptamine(3A) receptor. *Mol Pharmacol* **57,** 1249-1255.

Steward LJ, West KE, Kilpatrick GJ & Barnes NM. (1993). Labelling of 5-HT3 receptor recognition sites in the rat brain using the agonist radioligand [3H]meta-chlorophenylbiguanide. *Eur J Pharmacol* **243,** 13-18.

Stewart A, Davies PA, Kirkness EF, Safa P & Hales TG. (2003). Introduction of the 5-HT3B subunit alters the functional properties of 5-HT3 receptors native to neuroblastoma cells. *Neuropharmacology* **44,** 214-223.

Sudweeks SN, Hooft JA & Yakel JL. (2002). Serotonin 5-HT(3) receptors in rat CA1 hippocampal interneurons: functional and molecular characterization. *J Physiol* **544,** 715-726.

Sugita S, Shen KZ & North RA. (1992). 5-hydroxytryptamine is a fast excitatory transmitter at 5-HT3 receptors in rat amygdala. *Neuron* **8,** 199-203.

Sullivan NL, Thompson AJ, Price KL & Lummis SC. (2006). Defining the roles of Asn-128, Glu-129 and Phe-130 in loop A of the 5-HT3 receptor. *Mol Membr Biol* **23,** 442-451.

Suryanarayanan A, Joshi PR, Bikadi Z, Mani M, Kulkarni TR, Gaines C & Schulte MK. (2005). The loop C region of the murine 5-HT3A receptor contributes to the differential actions of 5-hydroxytryptamine and m-chlorophenylbiguanide. *Biochemistry* **44,** 9140-9149.

Sussman JL, Harel M, Frolow F, Oefner C, Goldman A, Toker L & Silman I. (1991). Atomic structure of acetylcholinesterase from Torpedo californica: a prototypic acetylcholine-binding protein. *Science* **253,** 872-879.

Sussman JL, Harel M & Silman I. (1993). Three-dimensional structure of acetylcholinesterase and of its complexes with anticholinesterase drugs. *Chem Biol Interact* **87,** 187-197.

Tavorath R & Hesketh PJ. (1996). Drug treatment of chemotherapy-induced delayed emesis.

Drugs **52,** 639-648.

Tecott LH, Maricq AV & Julius D. (1993). Nervous system distribution of the serotonin 5-HT3 receptor mRNA. *Proc Natl Acad Sci U S A* **90,** 1430-1434.

Thompson AJ, Padgett CL & Lummis SC. (2006). Mutagenesis and molecular modeling reveal the importance of the 5-HT3 receptor F-loop. *J Biol Chem* **281,** 16576-16582.

Thompson AJ, Price KL, Reeves DC, Chan SL, Chau PL & Lummis SC. (2005). Locating an antagonist in the 5-HT3 receptor binding site using modeling and radioligand binding. *J Biol Chem* **280,** 20476-20482.

Thompson JD, Higgins DG & Gibson TJ. (1994). CLUSTAL W: improving the sensitivity of progressive multiple sequence alignment through sequence weighting, position-specific gap penalties and weight matrix choice. *Nucleic Acids Res* **22,** 4673-4680.

TIGfAR. (2000). *Dexamethasone alone or in combination with ondansetron for the prevention of delayed nausea and vomiting induced by chemotherapy. The Italian Group for Antiemetic Research*, vol. 342.

Tricklebank MD, Forler C, Middlemiss DN & Fozard JR. (1985). Subtypes of the 5-HT receptor mediating the behavioural responses to 5-methoxy-N,N-dimethyltryptamine in the rat. *Eur J Pharmacol* **117,** 15-24.

Turner TJ, Mokler DJ & Luebke JI. (2004). Calcium influx through presynaptic 5-HT3 receptors facilitates GABA release in the hippocampus: in vitro slice and synaptosome studies. *Neuroscience* **129,** 703-718.

Tzvetkov MV, Meineke C, Oetjen E, Hirsch-Ernst K & Brockmoller J. (2007). Tissue-specific alternative promoters of the serotonin receptor gene HTR3B in human brain and intestine. *Gene* **386,** 52-62.

Uetz P, Abdelatty F, Villarroel A, Rappold G, Weiss B & Koenen M. (1994). Organisation of the murine 5-HT3 receptor gene and assignment to human chromosome 11. *FEBS Lett* **339,** 302-306.

Unwin N. (1993). Nicotinic acetylcholine receptor at 9 A resolution. *J Mol Biol* **229,** 1101-1124.

Unwin N. (1995). Acetylcholine receptor channel imaged in the open state. *Nature* **373,** 37-43.

Unwin N. (2005). Refined structure of the nicotinic acetylcholine receptor at 4A resolution. *J Mol Biol* **346,** 967-989.

Unwin N, Miyazawa A, Li J & Fujiyoshi Y. (2002). Activation of the nicotinic acetylcholine receptor involves a switch in conformation of the alpha subunits. *J Mol Biol* **319,** 1165-1176.

van Hooft JA, Spier AD, Yakel JL, Lummis SC & Vijverberg HP. (1998). Promiscuous

coassembly of serotonin 5-HT3 and nicotinic alpha4 receptor subunits into Ca(2+)-permeable ion channels. *Proc Natl Acad Sci U S A* **95,** 11456-11461.

van Hooft JA, van der Haar E & Vijverberg HP. (1997). Allosteric potentiation of the 5-HT3 receptor-mediated ion current in N1E-115 neuroblastoma cells by 5-hydroxyindole and analogues. *Neuropharmacology* **36,** 649-653.

van Hooft JA & Yakel JL. (2003). 5-HT3 receptors in the CNS: 3B or not 3B? *Trends Pharmacol Sci* **24,** 157-160.

Vanner SJ, Depew WT, Paterson WG, DaCosta LR, Groll AG, Simon JB & Djurfeldt M. (1999). Predictive value of the Rome criteria for diagnosing the irritable bowel syndrome. *Am J Gastroenterol* **94,** 2912-2917.

Venkataraman P, Venkatachalan SP, Joshi PR, Muthalagi M & Schulte MK. (2002). Identification of critical residues in loop E in the 5-HT3ASR binding site. *BMC Biochem* **3,** 15.

Wang JM, Zhang L, Yao Y, Viroonchatapan N, Rothe E & Wang ZZ. (2002). A transmembrane motif governs the surface trafficking of nicotinic acetylcholine receptors. *Nat Neurosci* **5,** 963-970.

Wang TL, Hackam AS, Guggino WB & Cutting GR. (1995). A single amino acid in gamma-aminobutyric acid rho 1 receptors affects competitive and noncompetitive components of picrotoxin inhibition. *Proc Natl Acad Sci U S A* **92,** 11751-11755.

Weiss B, Mertz A, Schrock E, Koenen M & Rappold G. (1995). Assignment of a human homolog of the mouse Htr3 receptor gene to chromosome 11q23.1-q23.2. *Genomics* **29,** 304-305.

Werner P, Kawashima E, Reid J, Hussy N, Lundstrom K, Buell G, Humbert Y & Jones KA. (1994). Organization of the mouse 5-HT3 receptor gene and functional expression of two splice variants. *Brain Res Mol Brain Res* **26,** 233-241.

Westh-Hansen SE, Rasmussen PB, Hastrup S, Nabekura J, Noguchi K, Akaike N, Witt M-R & Nielsen M. (1997). Decreased agonist sensitivity of human GABAA receptors by an amino acid variant, isoleucine to valine, in the [alpha]1 subunit. *European Journal of Pharmacology* **329,** 253-257.

Wetzel CH, Hermann B, Behl C, Pestel E, Rammes G, Zieglgansberger W, Holsboer F & Rupprecht R. (1998). Functional antagonism of gonadal steroids at the 5-hydroxytryptamine type 3 receptor. *Mol Endocrinol* **12,** 1441-1451.

Xie Y & Cohen JB. (2001). Contributions of Torpedo nicotinic acetylcholine receptor gamma Trp-55 and delta Trp-57 to agonist and competitive antagonist function. *J Biol Chem* **276,** 2417-2426.

Yakel JL & Jackson MB. (1988). 5-HT3 receptors mediate rapid responses in cultured hippocampus and a clonal cell line. *Neuron* **1,** 615-621.

Yakel JL, Shao XM & Jackson MB. (1990). The selectivity of the channel coupled to the 5-HT3 receptor. *Brain Res* **533,** 46-52.

Yakel JL, Shao XM & Jackson MB. (1991). Activation and desensitization of the 5-HT3 receptor in a rat glioma x mouse neuroblastoma hybrid cell. *J Physiol* **436,** 293-308.

Yan D, Meyer JK & White MM. (2006). Mapping residues in the ligand-binding domain of the 5-HT(3) receptor onto d-tubocurarine structure. *Mol Pharmacol* **70,** 571-578.

Yan D, Schulte MK, Bloom KE & White MM. (1999). Structural features of the ligand-binding domain of the serotonin 5HT3 receptor. *J Biol Chem* **274,** 5537-5541.

Yan D & White MM. (2005). Spatial orientation of the antagonist granisetron in the ligand-binding site of the 5-HT3 receptor. *Mol Pharmacol* **68,** 365-371.

Yang J. (1990). Ion permeation through 5-hydroxytryptamine-gated channels in neuroblastoma N18 cells. *J Gen Physiol* **96,** 1177-1198.

Yang J, Mathie A & Hille B. (1992). 5-HT3 receptor channels in dissociated rat superior cervical ganglion neurons. *J Physiol* **448,** 237-256.

Yuan SY, Bornstein JC & Furness JB. (1994). Investigation of the role of 5-HT3 and 5-HT4 receptors in ascending and descending reflexes to the circular muscle of guinea-pig small intestine. *Br J Pharmacol* **112,** 1095-1100.

Zazpe A, Artaiz I & Del Rio J. (1994). Role of 5-HT3 receptors in basal and K(+)-evoked dopamine release from rat olfactory tubercle and striatal slices. *Br J Pharmacol* **113,** 968-972.

Zerangue N, Schwappach B, Jan YN & Jan LY. (1999). A new ER trafficking signal regulates the subunit stoichiometry of plasma membrane K(ATP) channels. *Neuron* **22,** 537-548.

Zhang R, Wen X, Militante J, Hester B, Rhubottom H, Sun H, Leidenheimer N, Yan D, White M & Machu T. (2007). The Role of Loop F Residues in Determining Differential d-Tubocurarine Potencies in Mouse and Human 5-Hydroxytryptamine 3A Receptors. *Biochemistry* **46,** 1194-1204.

Zhong W, Gallivan JP, Zhang Y, Li L, Lester HA & Dougherty DA. (1998). From ab initio quantum mechanics to molecular neurobiology: a cation-pi binding site in the nicotinic receptor. *Proc Natl Acad Sci U S A* **95,** 12088-12093.

Zoldan J, Friedberg G, Livneh M & Melamed E. (1995). Psychosis in advanced Parkinson's disease: treatment with ondansetron, a 5-HT3 receptor antagonist. *Neurology* **45,** 1305-1308.

Appendix: Mutations to the mouse 5-HT$_{3A}$R

Loop	Mutant	Granisetron Kd/Ki Fold change	5-HT Ki Fold Change	EC_{50} Fold Change	Reference
α1	Y50F	NB		NB	(Price & Lummis, 2004)
α1	Y50A	NB		NB	(Price & Lummis, 2004)
α1	Y50S	NB		NB	(Price & Lummis, 2004)
β1	W60S	↑ 1.2		↑ 1.1	(Spier & Lummis, 2000)
β1	I71A	↑ 1.2			(Thompson *et al.*, 2005)
β1	I71L	↑ 1.0			(Thompson *et al.*, 2005)
β1	Y73A	↑ 1.1			(Price & Lummis, 2004)
β1	Y73A	↑ 1.1			(Thompson *et al.*, 2005)
β1	Y73S	↑ 1.8			(Thompson *et al.*, 2005)
β1	Y73S	↑ 1.8			(Price & Lummis, 2004)
D	T86A	↓ 2	↑ 2		(Yan *et al.*, 1999)
D	T87A	↓ 1.25	0		(Yan *et al.*, 1999)
D	Y88A	↓ 1.25			(Price & Lummis, 2004)
D	Y88S	↓ 1.4			(Price & Lummis, 2004)
D	Y88A	↑ 1.5	↑ 2		(Yan *et al.*, 1999)
D	I89A	0	0		(Yan *et al.*, 1999)
D	W90A	NB			(Thompson *et al.*, 2005)
D	W90A	↑ 10	↑ 2		(Yan *et al.*, 1999)
D	W90Y	↑ 5.4		↑ 3.8	(Spier & Lummis, 2000)
D	W90Y	↑ 2.9			(Thompson *et al.*, 2005)
D	W90S	NB		NR	(Spier & Lummis, 2000)
D	W90F	↑ 19			(Yan & White, 2005)
D	Y91F	↑ 2.5		↑ 1.4	(Price & Lummis, 2004)
D	Y91A	NB		NR	(Price & Lummis, 2004)
D	Y91S	NB		NR	(Price & Lummis, 2004)
D	Y91A	0	↑ 2		(Yan *et al.*, 1999)
D	R92A	↑ 5.8			(Thompson *et al.*, 2005)
D	R92A	↑ 6	↑ 15		(Yan *et al.*, 1999)
D	R92K	↑ 3.2			(Thompson *et al.*, 2005)
D	R92Y	↑ 5.9			(Yan & White, 2005)
D	Q93A	0	0		(Yan *et al.*, 1999)
D	Y94A	↑ 1.3			(Price & Lummis, 2004)
D	Y94A	↑ 3	↑ 2		(Yan *et al.*, 1999)
D	Y94S	↑ 1.2			(Price & Lummis, 2004)
D	W95A	0	0		(Yan *et al.*, 1999)
D	E98Q	↓ 1.6		0	(Schreiter *et al.*, 2003)*
D	E98D	↑ 1.3		0	(Schreiter *et al.*, 2003)

The effect of 5-HT$_{3A}$R single point mutations on the affinity of granisetron and 5-HT, and the functional response to 5-HT. Affinity constants (K_i) measured by competition binding using [^{3}H]granisetron, except where * denotes K_i values measured by competition with [^{3}H]GR65630. ↓ = affinity constant reduction (affinity increase), ↑ = affinity constant increase (reduction in affinity). NB = no binding, NR = no response.
(Continued on next pages.)

APPENDIX: Mutations to the m5-HT$_{3A}$R

Loop	Mutant	Kd/Ki Granisetron Fold change	Ki 5-HT Fold Change	EC_{50} Fold Change	Reference
A	N128A	↑ 1.3			(Thompson *et al.*, 2005)
A	N128A	↓1.3			Sullivan *et al.* (2006)
A	N128D	↑ 1.6			(Thompson *et al.*, 2005)
A	N128D	↓ 1.5			Sullivan *et al.* (2006)
A	N128E	↓ 2.6			Sullivan *et al.* (2006)
A	N128L	↓ 2.4			Sullivan *et al.* (2006)
A	N128Q	↑ 1.9			Sullivan *et al.* (2006)
A	N128R	↓ 1.2			Sullivan *et al.* (2006)
A	N128V	↓ 1.3			Sullivan *et al.* (2006)
A	E129A	NB			(Thompson *et al.*, 2005)/ Sullivan *et al.* (2006)
A	E129D	↑ 828.6	↑ 132.1	0	(Boess *et al.*, 1997)*
A	E129D	NB			Sullivan *et al.* (2006)
A	E129N	↑ 550.0	↑ 30.1	↑ 7.3	(Boess *et al.*, 1997)*
A	E129G	NB			Sullivan *et al.* (2006)
A	E129H	NB			Sullivan *et al.* (2006)
A	E129K	NB			Sullivan *et al.* (2006)
A	E129N	NB			Sullivan *et al.* (2006)
A	E129Q	NB			Sullivan *et al.* (2006)
A	F130A	↑ 3.7			Sullivan *et al.* (2006)
A	F130Y	↑ 1.3	↑ 13.0	↑ 8.8	(Steward *et al.*, 2000)*
A	F130Y	0			Sullivan *et al.* (2006)
A	F130W	↑ 3.5			Sullivan *et al.* (2006)
A	F130N	↑ 8.7	↓ 10	↓ 5	(Steward *et al.*, 2000)*
E	Y141A	↑ 28.0		NR	(Price & Lummis, 2004)
E	Y141A	↑ 2.8	↑ 1.3	NR	(Venkataraman *et al.*, 2002)
E	Y141A	↑ 28.0		↑ 2.4	(Beene *et al.*, 2004)
E	Y141F	↑ 3.1			(Price & Lummis, 2004)
E	Y141F	↑ 3.1		↓ 1.25	(Beene *et al.*, 2004)
E	Y141S	NB		NR	(Price & Lummis, 2004)
E	Y141S	NB		↑ 4.1	(Beene *et al.*, 2004)
E	V142A	↑ 2.6	↑ 1.1		(Venkataraman *et al.*, 2002)
E	Y143A	↑ 3.9			(Thompson *et al.*, 2005)
E	Y143A	↑ 3.8		NR	(Price & Lummis, 2004)
E	Y143A	↑ 4.6	↑ 108.1	NR	(Venkataraman *et al.*, 2002)
E	Y143A	↑ 3.8		↑ 307.8	(Beene *et al.*, 2004)
E	Y143A	↑ 4.1			(Joshi *et al.*, 2006)
E	Y143S	↑ 3.5		↑ 340.1	(Price & Lummis, 2004)
E	Y143S	↑ 3.5		↑ 410.4	(Beene *et al.*, 2004)
E	Y143F	↑ 1.7			(Thompson *et al.*, 2005)
E	Y143F	↑ 1.7			(Price & Lummis, 2004)
E	Y143F	↑ 1.7		↑ 68.3	(Beene *et al.*, 2004)
E	Y143F	↑ 3.5			(Joshi *et al.*, 2006)
E	V144A	↑ 1.9	↓ 3.3		(Venkataraman *et al.*, 2002)
E	H146A	↑ 1.3	↓ 2.5		(Venkataraman *et al.*, 2002)
E	R147A	↑ 2.4	↓1.25		(Venkataraman *et al.*, 2002)
E	G148A	NB			(Venkataraman *et al.*, 2002)
E	E149A	↑ 5.3	↑ 1.0		(Venkataraman *et al.*, 2002)
E	V150A	NB			(Venkataraman *et al.*, 2002)
E	Q151A	↑ 6.4	↑ 2.3		(Venkataraman *et al.*, 2002)
E	N152A	↑ 7.0	↑ 1.9		(Venkataraman *et al.*, 2002)

m5-HT$_{3A}$Rs mutants: continued from previous page.

APPENDIX: Mutations to the m5-$HT_{3A}R$

Loop	Mutant	Kd/Ki Granisetron Fold change	Ki 5-HT Fold Change	EC_{50} Fold Change	Reference
A	N128A	↑ 1.3			(Thompson *et al.*, 2005)
A	N128A	↓1.3			Sullivan *et al.* (2006)
A	N128D	↑ 1.6			(Thompson *et al.*, 2005)
A	N128D	↓ 1.5			Sullivan *et al.* (2006)
A	N128E	↓ 2.6			Sullivan *et al.* (2006)
A	N128L	↓ 2.4			Sullivan *et al.* (2006)
A	N128Q	↑ 1.9			Sullivan *et al.* (2006)
A	N128R	↓ 1.2			Sullivan *et al.* (2006)
A	N128V	↓ 1.3			Sullivan *et al.* (2006)
A	E129A	NB			(Thompson *et al.*, 2005)/ Sullivan *et al.* (2006)
A	E129D	↑ 828.6	↑ 132.1	0	(Boess *et al.*, 1997)*
A	E129D	NB			Sullivan *et al.* (2006)
A	E129N	↑ 550.0	↑ 30.1	↑ 7.3	(Boess *et al.*, 1997)*
A	E129G	NB			Sullivan *et al.* (2006)
A	E129H	NB			Sullivan *et al.* (2006)
A	E129K	NB			Sullivan *et al.* (2006)
A	E129N	NB			Sullivan *et al.* (2006)
A	E129Q	NB			Sullivan *et al.* (2006)
A	F130A	↑ 3.7			Sullivan *et al.* (2006)
A	F130Y	↑ 1.3	↑ 13.0	↑ 8.8	(Steward *et al.*, 2000)*
A	F130Y	0			Sullivan *et al.* (2006)
A	F130W	↑ 3.5			Sullivan *et al.* (2006)
A	F130N	↑ 8.7	↓ 10	↓ 5	(Steward *et al.*, 2000)*
E	Y141A	↑ 28.0		NR	(Price & Lummis, 2004)
E	Y141A	↑ 2.8	↑ 1.3	NR	(Venkataraman *et al.*, 2002)
E	Y141A	↑ 28.0		↑ 2.4	(Beene *et al.*, 2004)
E	Y141F	↑ 3.1			(Price & Lummis, 2004)
E	Y141F	↑ 3.1		↓ 1.25	(Beene *et al.*, 2004)
E	Y141S	NB		NR	(Price & Lummis, 2004)
E	Y141S	NB		↑ 4.1	(Beene *et al.*, 2004)
E	V142A	↑ 2.6	↑ 1.1		(Venkataraman *et al.*, 2002)
E	Y143A	↑ 3.9			(Thompson *et al.*, 2005)
E	Y143A	↑ 3.8		NR	(Price & Lummis, 2004)
E	Y143A	↑ 4.6	↑ 108.1	NR	(Venkataraman *et al.*, 2002)
E	Y143A	↑ 3.8		↑ 307.8	(Beene *et al.*, 2004)
E	Y143A	↑ 4.1			(Joshi *et al.*, 2006)
E	Y143S	↑ 3.5		↑ 340.1	(Price & Lummis, 2004)
E	Y143S	↑ 3.5		↑ 410.4	(Beene *et al.*, 2004)
E	Y143F	↑ 1.7			(Thompson *et al.*, 2005)
E	Y143F	↑ 1.7			(Price & Lummis, 2004)
E	Y143F	↑ 1.7		↑ 68.3	(Beene *et al.*, 2004)
E	Y143F	↑ 3.5			(Joshi *et al.*, 2006)
E	V144A	↑ 1.9	↓ 3.3		(Venkataraman *et al.*, 2002)
E	H146A	↑ 1.3	↓ 2.5		(Venkataraman *et al.*, 2002)
E	R147A	↑ 2.4	↓1.25		(Venkataraman *et al.*, 2002)
E	G148A	NB			(Venkataraman *et al.*, 2002)
E	E149A	↑ 5.3	↑ 1.0		(Venkataraman *et al.*, 2002)
E	V150A	NB			(Venkataraman *et al.*, 2002)
E	Q151A	↑ 6.4	↑ 2.3		(Venkataraman *et al.*, 2002)
E	N152A	↑ 7.0	↑ 1.9		(Venkataraman *et al.*, 2002)

m5-HT_{3A}Rs mutants: continued from previous page.

Loop	Mutant	Kd/Ki Granisetron Fold change	Ki 5-HT Fold Change	EC_{50} Fold Change	Reference
E	Y153A	↑ 7.6			(Thompson *et al.*, 2005)
E	Y153A	↑ 11.3		↑ 50.5	(Price & Lummis, 2004)
E	Y153A	↑ 8.0	↑ 24.3	↑ 137.0	(Venkataraman *et al.*, 2002)
E	Y153A	↑ 11.3		↑ 104.3	(Beene *et al.*, 2004)
E	Y153A	↑ 7.0			(Joshi *et al.*, 2006)
E	Y153S	NB		↑ 40.3	(Price & Lummis, 2004)
E	Y153S	NB		↑ 73.0	(Beene *et al.*, 2004)
E	Y153F	↑ 2.9			(Thompson *et al.*, 2005)
E	Y153F	↑ 2.8			(Price & Lummis, 2004)
E	Y153F	↑ 2.8		↑ 19.6	(Beene *et al.*, 2004)
E	Y153F	↑ 6.3			(Joshi *et al.*, 2006)
E	K154A	↑ 7.6	↑ 3.6		(Venkataraman *et al.*, 2002)
Cys	Y167A	0			(Price & Lummis, 2004)
Cys	Y167S	0			(Price & Lummis, 2004)
B	T179A	↑ 10.3			(Thompson *et al.*, 2005)
B	T179S	↑ 1.2			(Thompson *et al.*, 2005)
B	T181A	↓ 2.5			(Thompson *et al.*, 2005)
B	T181S	↑ 1.9			(Thompson *et al.*, 2005)
B	S182A	↑ 3.2			(Thompson *et al.*, 2005)
B	S182T	↑ 5.8			(Thompson *et al.*, 2005)
B	W183A	NB			(Thompson *et al.*, 2005)
B	W183S	NB		NR	(Spier & Lummis, 2000)
B	W183Y	NB			(Thompson *et al.*, 2005)
B	W183Y	NB		↑ 92.4	(Spier & Lummis, 2000)
B	L184A	↑ 13.2			(Thompson *et al.*, 2005)
B	L184A	↑ 4.9			(Joshi *et al.*, 2006)
B	L184I	↑ 2.3			(Thompson *et al.*, 2005)
B	H185A	NB			(Joshi *et al.*, 2006)
B	H185Y	↑ 5.1			(Joshi *et al.*, 2006)
B	T186A	↑ 2.4			(Joshi *et al.*, 2006)
B	I187A	↑ 3.5			(Joshi *et al.*, 2006)
B	Q188A	↑ 1.5			(Joshi *et al.*, 2006)
B	D189A	↑ 22.9			(Joshi *et al.*, 2006)
β8	I192A	↑ 5.8			(Thompson *et al.*, 2006)
β8	I192L	↑ 1.9			(Thompson *et al.*, 2006)
β8	T193A	↑ 3.8			(Thompson *et al.*, 2006)
β8	T193S	↑ 3.6			(Thompson *et al.*, 2006)
β8	S193T			↑ 2.8	(Zhang *et al.*, 2007)
β8	L194A	↑ 7.8			(Thompson *et al.*, 2006)
β8	L194I	↑ 2.4			(Thompson *et al.*, 2006)

m5-HT$_{3A}$Rs mutants: continued from previous page.

APPENDIX: Mutations to the m5-HT$_{3A}$R

Loop	Mutant	Granisetron Kd/Ki Fold change	5-HT Ki Fold Change	EC_{50} Fold Change	Reference
F	W195A	↑ 16.4			(Thompson *et al.*, 2005)
F	W195A	↑ 8.6			(Thompson *et al.*, 2006)
F	W195Y	↑ 28.1			(Thompson *et al.*, 2005)
F	W195Y	↑ 51.2		↑ 3.9	(Spier & Lummis, 2000)
F	W195S	↑ 7.9		↑ 9	(Spier & Lummis, 2000)
F	L195W			0	(Jensen *et al.*, 2006)
F	R196A	↑ 10.9			(Thompson *et al.*, 2006)
F	R196K	↑ 4.4			(Thompson *et al.*, 2006)
F	S197A	↑1.0			(Thompson *et al.*, 2006)
F	S197T	↑ 3.1			(Thompson *et al.*, 2006)
F	L197S			↑ 1.91	(Zhang *et al.*, 2007)
F	P198A	↓ 2			(Thompson *et al.*, 2006)
F	P198H	↑ 6.2			(Thompson *et al.*, 2006)
F	E199A	↓ 2.5			(Thompson *et al.*, 2006)
F	E199D	↑ 1.5			(Thompson *et al.*, 2006)
F	E200A	↓ 2			(Thompson *et al.*, 2006)
F	E200D	↑ 3.7			(Thompson *et al.*, 2006)
F	V201A	↑ 2.1			(Thompson *et al.*, 2005)
F	V201R	↑ 2.2			(Thompson *et al.*, 2005)
F	V201A	↑ 1.2			(Thompson *et al.*, 2006)
F	V201L	↑ 3.9			(Thompson *et al.*, 2006)
F	R202A	0			(Thompson *et al.*, 2005)
F	R202A	↓ 1.6			(Thompson *et al.*, 2006)
F	R202K	↓ 2.5			(Thompson *et al.*, 2005)
F	R202K	↓ 3.3			(Thompson *et al.*, 2006)
F	S203A	↓ 3.3			(Thompson *et al.*, 2005)
F	S203A	↓ 10			(Thompson *et al.*, 2006)
F	S203T	↓1.3			(Thompson *et al.*, 2005)
F	S203T	↓ 5			(Thompson *et al.*, 2006)
F	D204A	NB			(Thompson *et al.*, 2006)
F	D204E	0			(Thompson *et al.*, 2006)
F	D204N	↓ 1.3			(Thompson *et al.*, 2006)
F	K205A	↑ 13.9			(Thompson *et al.*, 2006)
F	K205R	↑ 1.2			(Thompson *et al.*, 2006)
F	K205M	↓ 1.3			(Thompson *et al.*, 2006)
F	R205K			↑ 4.1	(Zhang *et al.*, 2007)
F	S206A	↑ 5.4			(Thompson *et al.*, 2005)
F	S206A	↑ 3.2			(Thompson *et al.*, 2006)
F	S206T	↑ 14.2			(Thompson *et al.*, 2005)
F	S206T	↑ 3.0			(Thompson *et al.*, 2006)
F	I207A	↑ 1.3			(Thompson *et al.*, 2005)
F	I207A	↓ 1.4			(Thompson *et al.*, 2006)
F	I207L	↑ 2.0			(Thompson *et al.*, 2005)
F	I207L	↑ 1.1			(Thompson *et al.*, 2006)
F	V207I			↑ 4.2	(Zhang *et al.*, 2007)

m5-HT$_{3A}$Rs mutants: continued from previous page.

APPENDIX: Mutations to the m5-HT$_{3A}$R

Loop	Mutant	Granisetron Kd/Ki Fold change	5-HT Ki Fold Change	EC_{50} Fold Change	Reference
β9	F208A	↓ 5			(Thompson *et al.*, 2006)
β9	F208Y	↑ 1.7			(Thompson *et al.*, 2006)
β9	I209A	↑ 1.1			(Thompson *et al.*, 2006)
β9	I209L	↑ 1.5			(Thompson *et al.*, 2006)
β9	M209I			↑ 2.6	(Zhang *et al.*, 2007)
β9	N210A	↓ 2.5			(Thompson *et al.*, 2006)
β9	N210Q	↑ 1.5			(Thompson *et al.*, 2006)
β9	Q211A	↓ 1.25			(Thompson *et al.*, 2006)
β9	Q211N	↑ 1.8			(Thompson *et al.*, 2006)
β9	G212A	↓ 1.43			(Thompson *et al.*, 2006)
β9	G212N	↓ 1.43			(Thompson *et al.*, 2006)
β9	G218E			↑ 1.4	(Zhang *et al.*, 2007)
β9	L220F			↑ 2.0	(Zhang *et al.*, 2007)
C	E225A	↑ 4.3	↑ 10.6	↑ 3.2	(Suryanarayanan *et al.*, 2005)
C	E225Q	↑ 4.3		↑ 3.6	(Schreiter *et al.*, 2003)*
C	E225D	↑ 7.9		↑ 10	(Schreiter *et al.*, 2003)*
C	F226A	↓ 1.7			(Thompson *et al.*, 2005)
C	F226A	↑ 1.4	↑ 203.8	NR	(Suryanarayanan *et al.*, 2005)
C	F226Y	↑ 2.1	↑ 185.6	↑ 7.4	(Suryanarayanan *et al.*, 2005)
C	F226Y	↑ 1.8			(Thompson *et al.*, 2005)
C	I228A	↑ 4.5			(Thompson *et al.*, 2005)
C	I228N	0			(Thompson *et al.*, 2005)
C	I228A	↑ 4.7	↑ 235.6	↑ 10.0	(Suryanarayanan *et al.*, 2005)
C	D229A	↑ 12.3			(Thompson *et al.*, 2005)
C	D229A	↑ 8.3	↑ 138.8	↑ 12.6	(Suryanarayanan *et al.*, 2005)
C	D229E	↓ 1.25			(Thompson *et al.*, 2005)
C	E229D	NB			(Thompson *et al.*, 2005)
C	I230A	0			(Thompson *et al.*, 2005)
C	I230N	↑ 5.5			(Thompson *et al.*, 2005)
C	S233A	NB	NB	NR	(Suryanarayanan *et al.*, 2005)
C	S233T	↑ 2.1	↑ 4.1	↓ 1.4	(Suryanarayanan *et al.*, 2005)
C	Y234A	NB			(Thompson *et al.*, 2005)
C	Y234A	NB		NR	(Price & Lummis, 2004)
C	Y234A	NB		↑ 96.8	(Beene *et al.*, 2004)
C	Y234A	NB	NB	NR	(Suryanarayanan *et al.*, 2005)
C	Y234S	NB		NR	(Price & Lummis, 2004)
C	Y234S	NB		↑ 67.8	(Beene *et al.*, 2004)
C	Y234F	↑ 4.1			(Price & Lummis, 2004)
C	Y234F	↑ 4.1			(Thompson *et al.*, 2005)
C	Y234F	↑ 4.1		↑ 8.2	(Beene *et al.*, 2004)
C	Y234F	↑ 11.4	187.5	↑ 2.7	(Suryanarayanan *et al.*, 2005)
C	E236A	↑ 2.6			(Thompson *et al.*, 2005)
C	E236D	↑ 2.3			(Thompson *et al.*, 2005)
C	E236Q	↑ 8.6		↑ 21	(Schreiter *et al.*, 2003)*
C	E236D	NB		↑ 9524	(Schreiter *et al.*, 2003)*
C	K238A	0			(Thompson *et al.*, 2005)
C	K238R	↑ 2.6			(Thompson *et al.*, 2005)
C	Y240A	↓ 3.3			(Price & Lummis, 2004)
C	Y240S	↓ 3.3			(Price & Lummis, 2004)

m5-HT$_{3A}$Rs mutants: continued from previous page.